

ÉCOLE DOCTORALE DES SCIENCES CHIMIQUES

Laboratoire de Bioimagerie et Pathologies – UMR 7021

THÈSE présentée par :

Nina MELNYCHUK

soutenue le : **6 novembre 2019**

pour obtenir le grade de : **Docteur de l'université de Strasbourg**
Discipline/ Spécialité : Chimie/ Chimie moléculaire - chimie supramoléculaire

**Synthèse de nanoparticules organiques
fluorescentes pour la détection de
biomolécules**

THÈSE dirigée par :

M. KLYMCHENKO Andrey

Directeur de recherches CNRS, Université de Strasbourg

RAPPORTEURS :

M. HILDEBRANDT Niko

Professeur, Université Paris-Sud, Université de Rouen Normandie

Mme. LADAVIERE Catherine

Directrice de recherches CNRS, Université de Lyon

AUTRES MEMBRES DU JURY :

M. ZUBER Guy

Directeur de recherches CNRS, Université de Strasbourg

ACKNOWLEDGEMENTS

I would like to express my deepest appreciation to everyone who supported me during these three years of my PhD study. Foremost, I am deeply grateful to my supervisor Dr. Andrey Klymchenko for his guidance during my PhD study. His support and immense knowledge helped me to go through difficulties and finally complete with success my PhD projects. I am grateful to Prof. Yves Mely for welcoming me for my Master internship and further as a PhD student in the Lab. I would like to express my gratitude to Prof. Vasyl Pivovarenko, who introduced me to the fluorescent probes, and without whom my arrival to Strasbourg would not have been possible.

I am particularly grateful to jury members Prof. Niko Hildebrandt, Dr. Catherine Ladaviere and Dr. Guy Zuber for accepting the invitation to evaluate this work.

I am grateful to everyone with whom I had pleasure to work in our “Nanochemistry and Bioimaging Team”, to colleagues from UMR 7021 and to staff of the Faculty of Pharmacy. I am grateful to Dr. Philippe Chabert for his help in translation of part of this thesis in French, to Dr. Andreas Reisch for his help with polymer chemistry, to Dr. Mayeul Collot for his pieces of advice in organic synthesis and to Dr. Jurga Valanciunaite for her help with microscopy and FCS setups. I want to address special thanks to Dr. Nicolas Humbert for teaching me fluorescence spectroscopy techniques, for his help and support in any situation and for encouraging me to speak French. Many thanks to Dr. Pascal Dider, Dr. Frederic Przybilla and Dr. Eleonor Real for their help. I want to thank PACSI team for all the analysis and Corinne Ruhlmann from the FRISBI platform for help in conducting experiments.

I am grateful to Postdocs and PhD students with whom I had a pleasure to collaborate during different projects. I want to thank Dr. Kateryna Trofymchuk and Dr. Bohdan Andreiuk for introducing me to our ultrabright nanoparticles. Also, I want to thank Dr. Ashokkumar and Sylvie Egloff for their contribution to the projects that had been included in this thesis.

Special thanks to Marlyse Wernert and Ingrid Barthel for their help and availability. Many thanks to Dr. Guy Duportail for his help with French burocracie.

I want to thank all my friends in Strasbourg and Ukraine for their support and time that we have spent together. I was really blessed to meet such good friends as Rajhans and Sasha during my stay in Strasbourg. Thank you for our trips and time that we spent together. I want to thank Lesia for welcoming me for the first time in Strasbourg, for her support and bits of advice during my PhD study. Many thanks to my labmates Kyong, Alex, Caterina, Dima, Taras, Liliana, Redouane, Mari for our discussion, barbeques and all the fun that we had together.

I am grateful for the never-ending support of the members of my family. I am especially grateful for the love, guidance, and support of my parents. Thank you for your encouragement to reach new heights and to be a better person.

This work was done with the financial support of ERC Consolidator Grant BrightSens 648528. I am grateful to UMR7021 for providing access to instruments and Ecole doctorale des Sciences Chimiques for my PhD formations.

Nina MELNYCHUK

CONTENTS

Acknowledgements	1
Contents.....	3
List of abbreviations	5
Part 1. Bibliographical overview	7
1.1 Fluorescence spectroscopy and microscopy.....	7
Basics of Fluorescence	7
Förster Resonance Energy Transfer (FRET)	10
Single-molecule spectroscopy and microscopy	12
Labels for single-molecule experiments	17
1.2 Amplification principles and DNA detection.....	19
Molecular multiplication techniques.....	20
Signal amplification via plasmonics.....	23
Amplification with light-harvesting nanomaterials.....	29
1.3 FRET in nanomaterials for biosensing	32
FRET in inorganic nanoparticles	33
FRET in conjugated polymers and conjugated polymer nanoparticles.....	38
FRET in dye-based nanomaterials.....	42
1.4 Surface modification of nanoparticles.....	53
Methods for non-covalent attachment of ligand to nanoparticles surface.....	54
Methods for covalent attachment of the ligand to nanoparticle surface	55
Polymer nanoparticle-DNA conjugates	58
Aim of the PhD thesis.....	61
Part 2. Results and discussions	62
2.1 Investigation of methods that lead to surface functionalized dye-loaded polymeric nanoparticles	62
Introduction	62
Post-functionalization of polymeric nanoparticles	63
Pre-modification of the polymer	69
Cellular experiments	72

Conclusions	73
2.2 Development of DNA-functionalized nanoparticles for ultrasensitive detection of nucleic acids	75
Article 1. DNA-Functionalized Dye-Loaded Polymeric Nanoparticles: Ultrabright FRET Platform for Amplified Detection of Nucleic Acids	79
2.3 Development of nanoprobe with single-molecule sensitivity towards nucleic acid target	80
Article 2 (Manuscript). Light-harvesting nanoparticle probes for FRET-based detection of oligonucleotides with single-molecule sensitivity	85
Part 3. Conclusions and perspectives	86
Part 4. Materials and methods	89
4.1 Materials	89
4.2 Methods	90
Nanoparticle Preparation	90
Protocol for reaction and purification of NPs with Sulfo-Cy5(DBCO)	90
General protocol for nanoprobe synthesis	90
Detection of survivin nucleic acid target	91
Molecular Probe Preparation	92
Nanoparticle characterization	92
Photobleaching of nanoparticles in solution	93
Transmission electron microscopy (TEM)	93
Fluorescence Microscopy	93
Cellular experiments	96
4.3 Chemical synthesis	96
Synthesis of linkers	96
Synthesis of dyes	99
Synthesis of polymers	100
NMR and mass spectra	106
Résumé de la thèse en français	119
References	130
List of publications	137
List of conferences	138

LIST OF ABBREVIATIONS

AE	antenna effect
AgNP	silver nanoparticles
AIE	aggregation induced emission
AuNPs	gold nanoparticles
BHQ	black hole quencher
Boc	<i>tert</i> -butyloxycarbonyl protecting group
BODIPY	boron-dipyrromethene
BSA	bovine serum albumin
CP	conjugated polymer
CPN	conjugated polymer nanoparticle
CT-DNA	deoxyribonucleic acid sodium salt from calf thymus
CuAAC	Cu(I)-mediated azide-alkyne cycloaddition
Cy3	cyanine 3
Cy5	cyanine 5
Cy5.5	cyanine 5.5
DBCO	dibenzocyclooctyne
DCM	dichloromethane
DIPEA	N,N-diisopropylethylamine
DLS	dynamic light scattering
DMF	N,N-dimethylformamide
DNA	deoxyribonucleic acid
ECL	electrochemiluminescence
EDTA	ethylenediaminetetraacetic acid
EET	excitation energy transfer
FBS	fetal bovine serum
FCS	fluorescence correlations spectroscopy
Fmoc	fluorenylmethyloxycarbonyl protecting group
FRET	förster resonance energy transfer
HBTU	hexafluorophosphate benzotriazole tetramethyl uronium
HOBT	hydroxybenzotriazole
LOD	limit of detection
mRNA	messenger RNA
NA	nucleic acid

NIR	near infrared
NP	nanoparticle
NSET	surface energy transfer
PALM	photo-activated localization microscopy
PAMAM	polyamidoamine
PB	phosphate buffer
PBS	phosphate-buffered saline
PCR	polymerase chain reaction
Pdot	polymer dot
PEG	polyethylene glycol
PEMA-MA	poly(ethyl methacrylate-co-methacrylic acid)
PET	photoinduced electron transfer
PLGA	poly(D,L-lactic-co-glycolic acid)
PluS NPs	pluronic silica nanoparticles
PMMA	polymethylmethacrylate
PMMA-MA	poly(methyl methacrylate-co-methacrylic acid)
PNA	peptide nucleic acid
PNIPAM	poly(N-isopropylacrylamide)
QDs	quantum dots
QY	quantum yield
RhB	Rhodamine B
RNA	ribonucleic acid
RT-PCR	reverse transcription polymerase chain reaction
SiNPs	silica nanoparticles
smFRET	single-molecule Förster resonance energy transfer
SNA	spherical nucleic acid
SPR	surface plasmon resonance
ssDNA	single strand deoxyribonucleic acid
STORM	stochastic optical reconstruction microscopy
TAMRA	carboxytetramethylrhodamine
TCS	target competitive sequence
TEM	transmission electron microscopy
TFA	trifluoroacetic acid
TIRF	total internal reflection fluorescence
UCNPs	upconversion nanoparticles

PART 1. BIBLIOGRAPHICAL OVERVIEW

1.1 Fluorescence spectroscopy and microscopy

Fluorescence-based techniques are indispensable tools in studies of biological processes.¹ Fluorescence spectroscopy allows examination and analysis of different ligand-receptor, peptide-peptide, peptide–nucleic acid and ligand–lipid interactions. Fluorescence microscopy permits us to visualize and follow these fundamental intermolecular interactions up to a single-molecule level. It would not have been possible to obtain all current knowledge about cellular organization and processes without exploring the fluorescence phenomenon.

Basics of Fluorescence

Fluorescence is the emission of light quanta by a molecule (*fluorophore*) after its primal electronic excitation in a light-absorption process. More precisely this phenomenon can be described by using the Jablonski diagram² (Fig.1.1A). S_0 is a molecule's singlet ground state. The absorption of light quanta occurs from the ground state and the fluorophore is usually excited to the vibrational levels of the higher singlet states S_1 or S_2 . Then the molecule rapidly relaxes to the lowest vibrational level of S_1 (*internal conversion*). After that several scenarios are possible: molecule can return to the ground state through non-radiative decay (*without light emission*) or with emission of light quanta (*fluorescence*). Another possibility is intersystem crossing (S_1 - T_1), when the molecule undergoes spin conversion to the first triplet state T_1 . Emission from T_1 is called *phosphorescence*. Typically, molecules with heavy atoms such as bromide or iodide are phosphorescent.

Analyzing the Jablonski diagram, one can notice that the fluorescence emission has lower energy than light absorption due to internal conversion energy losses, so it is shifted towards the longer wavelength. The red shift between maximum of absorbance and maximum of fluorescence called a *Stokes shift* (Fig.1.1B). Another general property of fluorescence is that the emission spectrum does not depend on excitation wavelength (*Kasha's rule*).

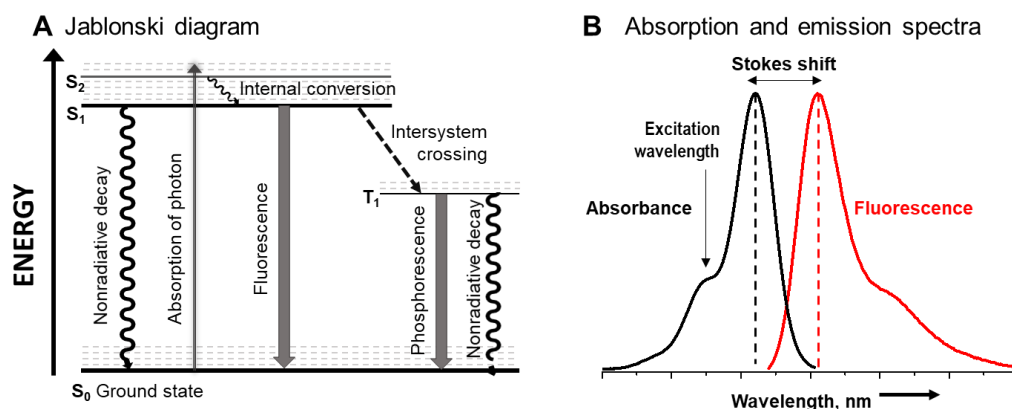


Fig.1.1. Principles of fluorescence. A) Jablonski diagram. B) Representative of absorbance and emission spectra. Adopted from ref. ²

Fluorophore, mentioned above, is the fluorescent molecule that can re-emit light after its excitation. Fluorophores can occur naturally, e.g. fluorescent proteins, enzyme co-factors, etc., or they are synthetic organic molecules and called as fluorescent dyes. All organic fluorophores have structure similarity: they are planar aromatic molecules with an extensive π -electronic system (Fig.1.2). The extent of a π -electron system (degree of conjugation) leads to the lower energy of S_1 state and, therefore, to a red shift of the absorption and corresponding emission spectra. The planar structure is necessary to stabilize the S_1 excited state of the molecule and return to the ground state through fluorescence avoiding the non-radiative decay.³

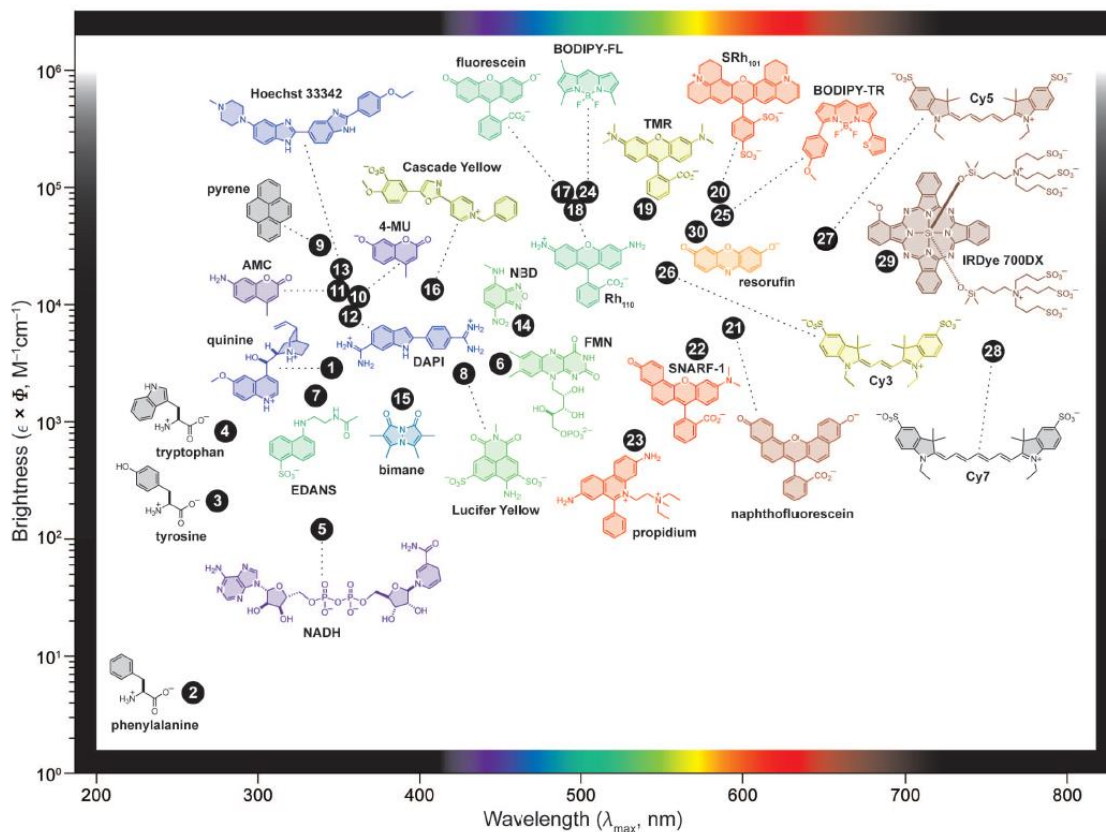


Fig.1.2. Examples of fluorescent dyes. Adopted from ref. ⁴

Every fluorescent dye (material) is characterized by its molar extinction coefficient and the fluorescence quantum yield.

Molar extinction coefficient (ϵ , $M^{-1} \text{ cm}^{-1}$) describes the ability of the molecule to absorb light at a given wavelength. The absorbance A measured at any wavelength is proportional to the concentration C (*Molar*) and the path length l (*cm*) in a sample (Beer-Lambert law). Here, ϵ is a proportional coefficient, which is characteristic to every molecule:

$$A = \epsilon \times C \times l$$

Fluorescence quantum yield (QY), Φ , is defined as the ratio of the number of emitted photons to the whole number of the absorbed photons.

$$\Phi = \frac{\Gamma}{\Gamma + k_{nr}}$$

where Γ is the emissive rate constant of the fluorophore and k_{nr} is the non-radiative decay rate constant to S_0 . The total brightness of the molecule is defined as a product of multiplication $\epsilon \times \Phi$.

Fluorescence quantum yield corresponds to the intensity of light which certain dye emits at a given excitation intensity. Primarily, it depends on the structure of the dyes, but it can be drastically changed by the dye's environment. It means that the change of the molecular environment provokes the change of fluorescence intensity, and the fluorescent dye can be used to recognize this environment. The fluorescent molecules or supramolecular structures that by change of their fluorescent parameters can provide the information about their molecular surroundings are called as *fluorescent probes*. For example, a molecule can be non-fluorescent in a buffer (low quantum yield) but rapidly gain its fluorescence in a viscous environment (high quantum yield). This is the simplest example of *intensity based-molecular sensor*.⁵

The change of polarity of the molecular environment can provoke the shift in both absorption and emission spectra. This phenomenon called *solvatochromism*, and compounds that undergo it are *solvatochromic*. Both bathochromic (red) shift and hypsochromic (blue) shift with the increase of solvent polarity can appear. The solvatochromism found its use in biological research to study bulk and local polarity in macrosystems (membranes, etc.), or even the conformation and binding of proteins.⁶

Two other fundamental parameters of fluorescence that can be used in fluorescence sensing are fluorescence lifetime and fluorescence anisotropy, which can provide information about fluorophore separately or together in time-resolved anisotropy technique.⁷

Fluorescence lifetime (τ) defined by the average time that the fluorophore spends on its excited state before to return to the ground state.

$$\tau = \frac{1}{\Gamma + k_{nr}}$$

In terms of sensing, the fluorescence lifetime determines the time available for the fluorophore to interact or diffuse in its environment. It does not depend upon the fluorophore concentration, but the fluorescence decay is characteristic of the fluorophore and its environment. Moreover, the decays do not depend on emission wavelength, they are also not sensitive to the optical parameters of the instrument. This makes fluorescence lifetime a valuable parameter for sensing.

Fluorescence anisotropy (r) measurement indicates the change of a molecule orientation in space, with respect to the time between the absorption and emission events. Upon excitation with polarized light, only the selected fluorophores are excited whose absorption transition dipole

is parallel to the electric vector of excitation. Further emission occurs with the light polarized along a fixed axis in the fluorophore.

$$r = \frac{I_{\parallel} - I_{\perp}}{I_{\parallel} + 2I_{\perp}}$$

where I_{\parallel} and I_{\perp} are the fluorescence intensities of vertically (\parallel) and horizontally (\perp) polarized emissions, when the sample is excited with vertically polarized light.

Losses between absorption and emission, in this case, happen due to rotational diffusion, because of the displacement of the emission dipole of the fluorophore. The molecules rotate freely in fluid solution, but when the fluorophore is in rigid media or bound to the macromolecule the rotational diffusion decreases. That is how anisotropy can provide valuable information about the rigidity of fluorophore environment, e.g. fluidity of the biomembrane, and, therefore, they are widely used in biochemical applications of fluorescence. The anisotropy measurements are also used to measure different biomolecules associations and for immunoassays of various substances.

Förster Resonance Energy Transfer (FRET)

Förster Resonance Energy Transfer (FRET) is a non-radiative process by which energy is transferred via long-range dipole-dipole interactions from a donor molecule in an excited electronic state to an acceptor molecule (Fig.1.3A). The choice of FRET pair molecules depends on its principal requirement, that the emission band of the donor must overlap the absorption band of the acceptor (Fig.1.3B). Moreover, the best FRET donor would have high quantum yield and acceptor – high extinction coefficient.⁸

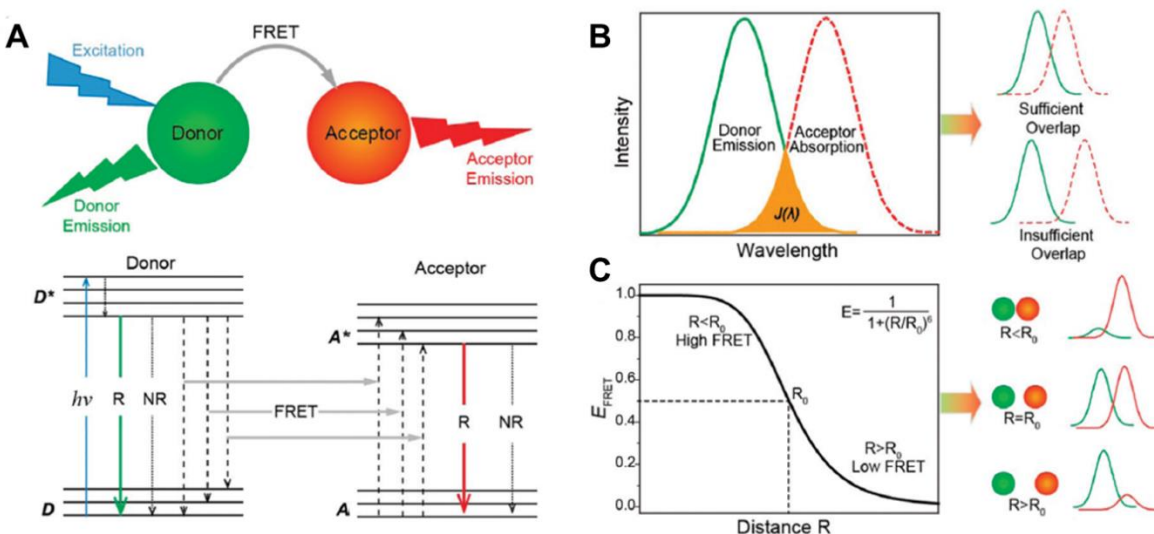


Fig.1.3. FRET concept. A) Schematic representation of energy transfer between two optical entities. B) Spectral overlap $J(\lambda)$ between acceptor's emission and donor's absorption. C) Dependency of FRET efficiency on the distance between the donor-acceptor pair. Adopted from ref. ⁹

FRET is one of the most important tools to investigate molecular interactions because of its two crucial conditions:

- ✓ There is a limited distance of 0.5-10 nm between donor and acceptor when FRET can occur. *Förster radius* (R_0) – is a distance at which the FRET efficiency is 50%, and its typically 2-6 nm. The Förster distance in Å is given by

$$R_0 = 0.211 (\kappa^2 n^4 Q_D J(\lambda))^{1/6}$$

where κ^2 is the orientation factor, n is the refractive index, Q_D is the quantum yield of the donor and $J(\lambda)$ is the overlap integral, which expresses the degree of overlap between the donor emission and acceptor absorption.

- ✓ The donor and acceptor are coupled through dipole-dipole interactions so that the relative orientation of the transition dipole plays a role in the efficiency of the energy transfer. The orientation factor κ^2 is given by

$$\kappa^2 = (\cos\theta_T - 3\cos\theta_D\cos\theta_A)^2$$

where θ_T is an angle between the emission transition dipole of the donor and the transition absorption dipole of the acceptor, θ_D and θ_A are the angles between these dipoles and the vector joining the donor and the acceptor.

This factor can range from 0 to 4, depending upon the relative orientation of the donor and acceptor, but generally, it is assumed to be 2/3 for randomly oriented molecules. However, if the dipoles are oriented perpendicularly to one another, $\kappa^2 = 0$, which results to an error in Förster radius calculation. The favorable orientation for energy transfer is when dipoles are head-to-tail parallel ($\kappa^2 = 4$).

Mathematically, the rate constant of the energy transfer ($k_T(r)$) is a simple function of the distance in between the dye's pair (R):

$$k_T(r) = \frac{1}{\tau_D} \left(\frac{R_0}{r}\right)^6$$

where τ_D is the decay time of the donor in the absence of acceptor, and r is the donor-acceptor distance. From this equation is evident that the rate of FRET is proportional to r^{-6} .

The FRET efficiency (E) is defined as the fraction of the photons absorbed by the donor which are transferred to acceptor:

$$E = \frac{k_T(r)}{\tau_D^{-1} + k_T(r)}$$

Combining FRET efficiency and the rate constant of the energy transfer equations:

$$E = \frac{1}{1 + (r/R_0)^6} = \frac{R_0^6}{R_0^6 + r^6}$$

As demonstrated on Fig.1.3C, when $R_0 \gg r$, FRET is very efficient and in case of $r \gg R_0$, FRET is very low, so that for both of these cases a distinction between different distances within this

portion by FRET changes becomes extremely difficult. It is important to adjust FRET pair so that $r \approx R_0$, so that change of FRET efficiency can be used for biosensing applications.

In practice, FRET efficiency is measured as the ratio of the relative fluorescence intensity (I), lifetime (τ) or QY(Φ) of the donor in the absence (subscript D) and in the presence (subscript D-A) of the acceptor¹⁰:

$$E = 1 - \frac{I_{D-A}}{I_D} = 1 - \frac{\tau_{D-A}}{\tau_D} = 1 - \frac{\Phi_{D-A}}{\Phi_D}$$

Another important parameter that is typically used in FRET-application is a FRET ratio. Usually, fluorescence intensities of donor and acceptor are measured simultaneously, and the ratio of intensities of acceptor (I_A) to donor (I_D) upon donor excitation determines as FRET ratio.

$$\text{FRET ratio} = \frac{I_A}{I_D}$$

In ratiometric measurements, it is often used as a relative FRET ratio, which is determined by the ratio of the intensity of acceptor to the sum of acceptor and donor intensities via donor excitation.

$$\text{relative FRET ratio} = \frac{I_A}{I_D + I_A}$$

The relative method is used mainly for qualitative purposes.

Single-molecule spectroscopy and microscopy

The highest level of sensitivity fluorescence-based detection is the observation of a single molecule.² The measurements in the cuvette give information about a large number of molecules since the fluorescence spectrum represents the average state of fluorophores ensemble. The primary spectroscopy technique that allows to detect single molecules is the fluorescence correlations spectroscopy (FCS) (Fig.1.4).¹¹ FCS is performed in solution using freely diffusing molecules. It is based on the analysis of time-dependent intensity fluctuations that are the result of fluorophore diffusion into a laser-focused spot. If the fluorophore diffuses fast inside the focused light beam, the burst of emitted photons is short. By the correlation analysis of the time-dependent emission, one can determine the diffusion coefficient of the fluorophore. The wide variety of process can cause the intensity fluctuations, like translation and rotational diffusions, ligand-macromolecule binding or excited-state reactions. Hence the FCS has been used to study the diffusion of the labeled proteins, DNA hybridizations, and protein interactions.¹² FCS is the powerful technique in the nanoparticles analyzes, as it can give information about the size, concentration and relative brightness of the system.¹³

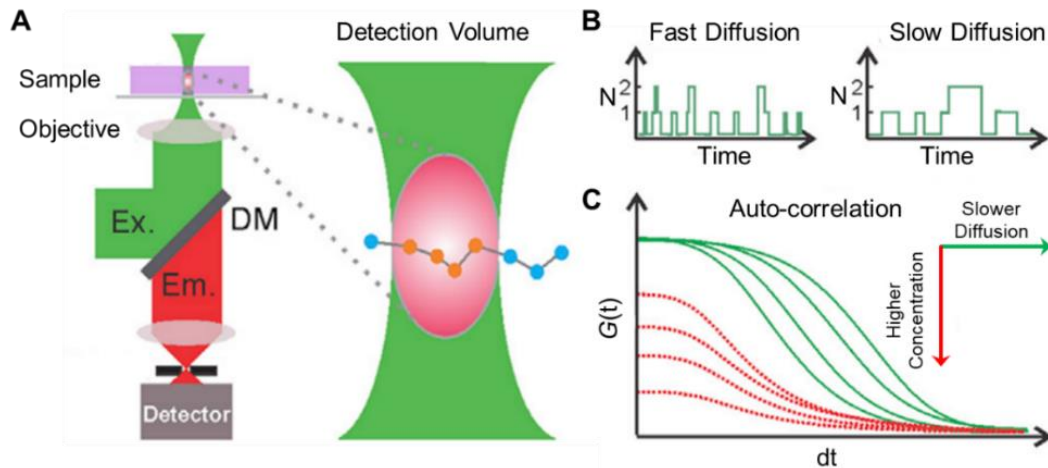


Fig.1.4. FCS principle. A) Typical confocal FCS optical layout and the observation volume. B) Fluorescence fluctuation curves for fast and slow diffusion. C) Auto-correlation curves for varied molecular concentrations and diffusion properties of a single-component system. Adopted from ref.¹¹

The actual following of the processes at the single-molecule level is possible with the single-molecule imaging techniques.¹⁴ Single-molecule microscopy revolutionized the scientific world since it can provide new insights into the biological processes. The different single-molecule techniques allow studying the interactions of individual molecules, their diffusion in cells and precise localization in cell compartments. It is also important to mention the background issues connected with single-molecule imaging. The key problem is the background noise which might come from unwanted sources or detector dark counts. To detect a single molecule, one must respect a sufficient signal to noise ratio. The source of background noises could be the residual emission from the optical parts or excitation source in the red-shifted spectral range. Also, the impurities inside the sample or media can emit strong residual signal. Hence, specific sample preparation and microscope set up are required to obtain relevant results from the single-molecule experiments.¹⁵

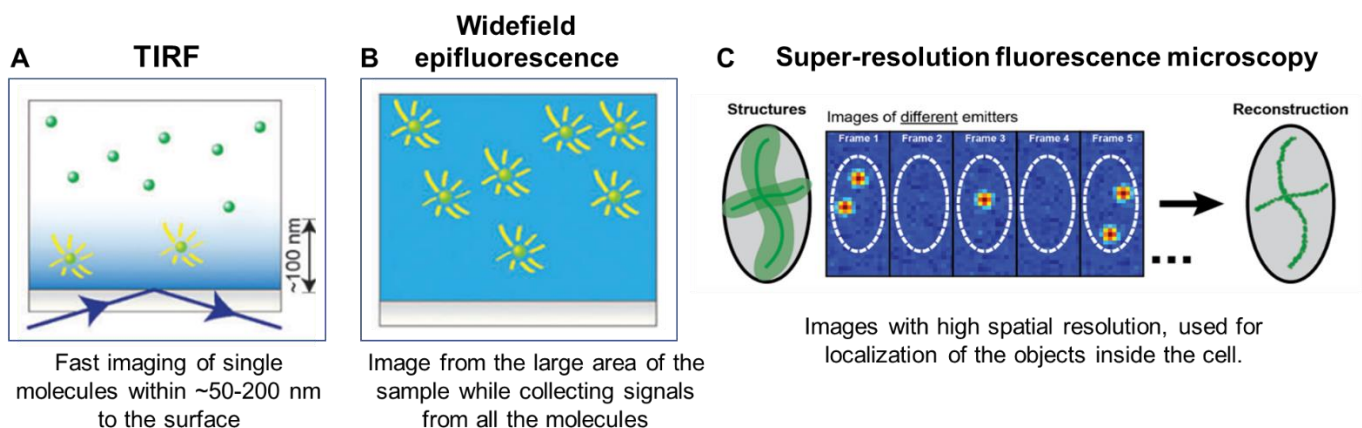


Fig.1.5. Single-molecule techniques. Schematic illustrations of A) TIRF, B) wide-field epifluorescence, C) super-resolution fluorescence microscopy. Adopted from ref. ^{14,15}

Total Internal Reflection Fluorescence (TIRF) microscopy¹⁶ is the most commonly used technique to follow a single molecule. The technique exploits the distance-dependent exponential decay of evanescent waves when the coverslip is illuminated with a laser beam at an incident angle greater than the critical angle of reflection (Fig.1.5A). The efficient excitation of fluorescence is achieved only on a distance 50–200 nm deep into the specimen. Therefore, the background fluorescence from molecules out of focus is reduced. This increase in the signal-to-noise ratio allows the detection of weakly fluorescent molecules. The limitation of this technique is that only the small zone within the cell's area is illuminated.

Traditional fluorescence microscopy with wide-field configuration can be used when there is a small number of single molecules since it excites fluorescence through the whole sample.¹⁷ As a result, the molecules that are not in the focal plane still emit light that contributes to the background fluorescence (Fig.1.5B). This decreases the signal-to-noise ratio, which prevents wide-field microscopy to achieve the single-molecule resolution with a high number of molecules present in the imaging volume. In order to see the single-molecule emission in epifluorescence, it is necessary to have a low number of molecules, which does not move very fast, and the labeling must be highly specific with a good signal-to-noise ratio.

The epifluorescence and TIRF mode is used the same way to image individual macromolecules and nanoparticles. Such single particle measurement allows studying the heterogeneity, brightness, photostability and fluorescence behavior of these systems.¹⁸ More complicated single-molecule imaging techniques are used to get the precise localization or co-localization of fluorophores. Super-resolution microscopy allows overcoming the diffraction limit. In super-resolution localization techniques like Photo-Activated Localization Microscopy (PALM)¹⁹ and Stochastic Optical Reconstruction Microscopy (STORM)²⁰ the concepts of photo-activation or photo-conversion are exploited. In brief, small random fractions of fluorophores situated apart from each other are photo-activated at a time. By repeating this process, the set of images with differently positioned fluorophores are collected (Fig.1.5C). Further image treatment leads to a complete reconstruction of the positions of the molecules in the sample down to 10 nm resolution.

But before concluding results from the single-molecule experiment, one should be sure that the signal is actually coming from a single molecule. After labeling the molecule with a fluorescent marker it is necessary to compare its signal to reference intensity obtained from a single molecule. The single-molecule has a distinctive amplitude of the intensity decrease – single-step photobleaching.²¹ The step-wise intensity drop is characteristic for individual fluorophores and was used to count the number of molecules by recording the total number of steps in the intensity change over time. Zhang et al. demonstrated that by labeling RNA molecules with single fluorophore it is possible to count the number of individual RNA molecules

attached to the nanoparticles of protein's complex.²² To perform this experiment the TIRF setup was used (Fig.1.6).

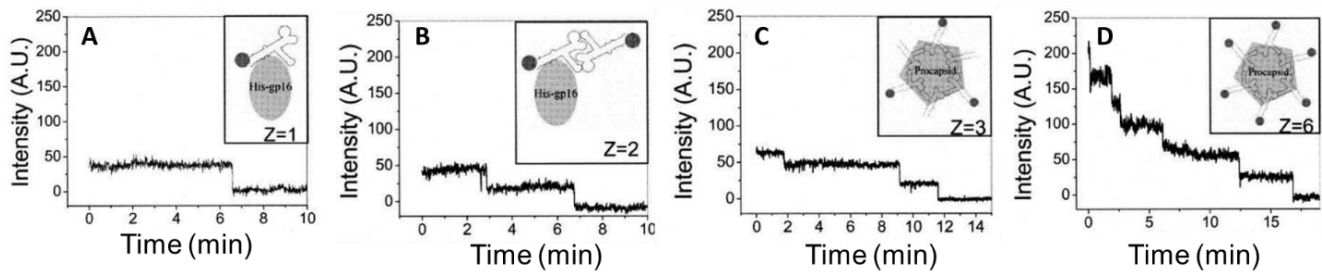


Fig.1.6. Stepwise intensity drop demonstrate photobleaching of individual fluorophores and allows to count the number of labels per nanoparticle. A) 1 label, B) 2 labels, C) 3 labels, D) 6 labels. Adopted from ref.²²

Single-molecule FRET (smFRET)

Single-molecule fluorescence resonance energy is a powerful technique that allows monitoring of the dynamic properties of the individual molecules.²³ The donor and acceptor can be placed either within the same (bio)molecule, so the changes in conformation are measured by the change in emission, or at the specific sites of different molecules, so the appearance of FRET indicates their interaction.¹⁴ smFRET has been broadly used to study conformational states, intramolecular distances, molecular dynamics, and stoichiometries of different biomolecules (Fig.1.7).²⁴

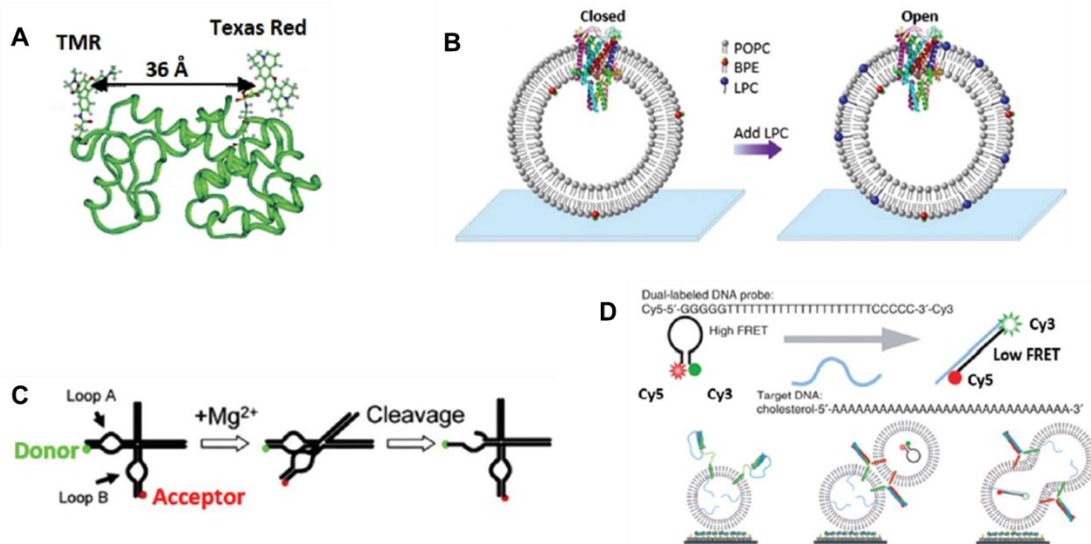


Fig.1.7. Usage of smFRET for studies of biological processes. A) smFRET for investigation of the conformational dynamics of T4 lysozyme. B) smFRET to probe structure and conformational dynamics of ion-channels. C) smFRET to reveal structure and dynamics of nucleic-acids. D) smFRET to study mechanism of vesical fusion by following FRET changes in beacon. Adopted from ref.²⁴

smFRET enables monitoring individual molecules and obtain the dynamic information ranging from milliseconds to minutes.²⁵ The identification of the smFRET is the anti-correlated nature of the donor and acceptor signal, which makes this technique largely stable to instrumental noise and drift. Dye molecules also show transitions to dark states, where acceptor intensity transiently drops to zero or completely photobleaches (Fig.1.8). Typically the smFRET measurements are performed by imaging surface-immobilized molecules with the aid of the TIRF or confocal microscopy.²³

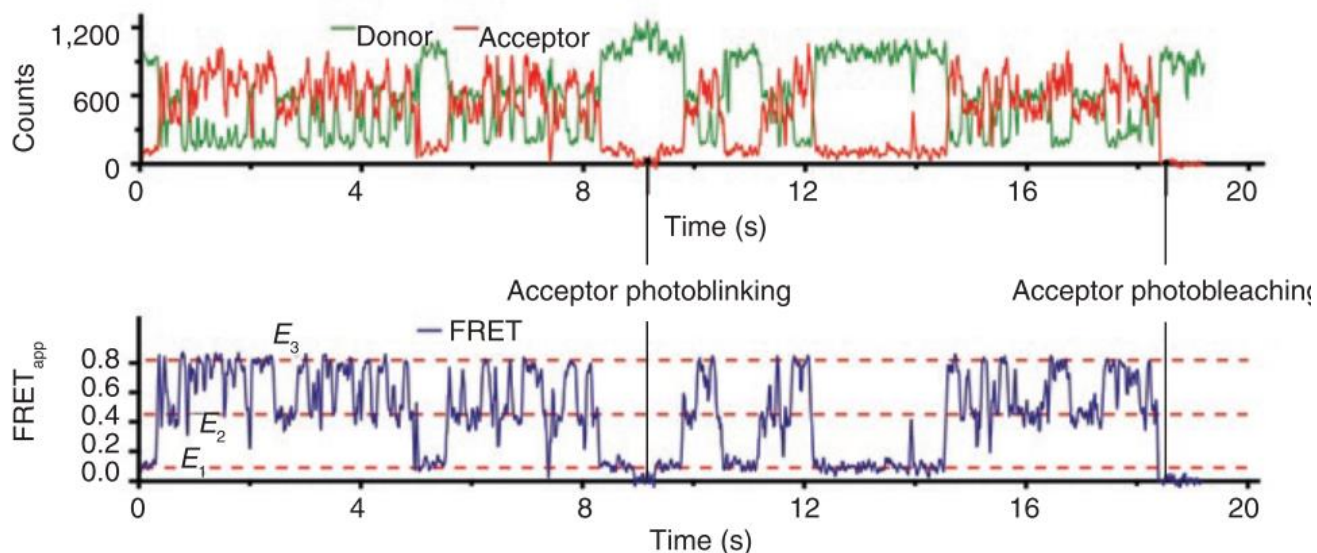


Fig.1.8. Example of a two-color smFRET data. Adopted from ref.²⁵

For every single-molecule imaging technique, the crucial is the choice of a fluorescent marker attached to the molecule of interest. The decisive criteria of the fluorescent markers are high brightness ($\epsilon > 50.000$, $QY > 0.1$), high photostability and minimum interference with the biological function of the target molecule or environment. Additionally, smFRET pair should have a large spectral separation between donor and acceptor emissions and similar detection efficiencies. The correct choice of labels should provide sufficient signal-to-noise ratio (~ 100 total photons need to be detected). The limitation of single-molecule measurements can be fast dye photobleaching caused by reactive oxygen species. Even though oxygen removal reduces photobleaching, but it prolongs the residence time in triplet dark state causing milliseconds fluorescence intermittency. That is why in some applications it is necessary to use the oxygen-scavenging system, like Trolox (vitamin E analog) or β -mercaptoethanol, especially by labeling with Cyanine dyes. Typically, more than 10^5 photons can be collected from single dye molecules before photobleaching. By choosing labels photostability is highly important specifically for single-particle tracking applications.²⁵

Labels for single-molecule experiments

The key to a successful single-molecule experiment is the right choice of label for biomolecules. Usually, for intracellular imaging the genetic approach of labeling with fluorescent protein is less invasive and most common, that's why scientists keep on developing fluorescent proteins with various color and higher brightness. Otherwise, synthetic dyes and fluorescent nanoparticles bring higher brightness and photostability, but require to develop a labeling protocol.¹¹ Especially, when the nanoparticle is used as a marker for the target molecule, it is important to control that one nanoparticle carries one linked molecule. Conventional synthetic dyes used in single-molecule experiments are derivatives of rhodamine, Nile Red, cyanine dyes, and fluorophores from Alexa and ATTO (carbopyronine) families (Fig.1.9).

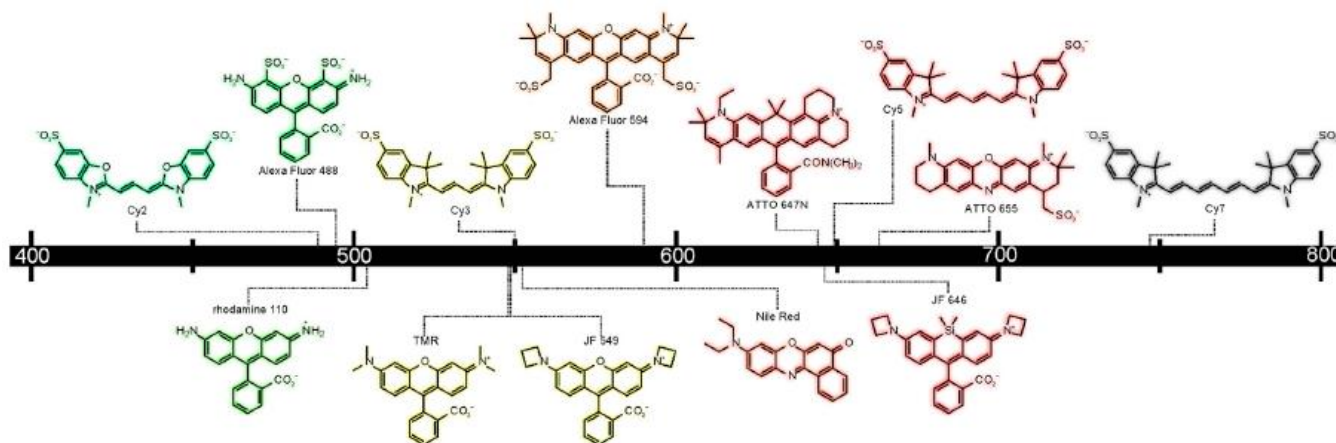


Fig.1.9. Structures and spectral properties of fluorophores useful for single-molecule imaging. Adopted from ref. ¹¹

Implementation of fluorescent nanoparticles in single-molecule labeling is becoming more common, but remains a problem of their size, which can disturb the function of biomolecules, and labeling difficulties of one nanoparticle with single biomolecule.²⁶ Recent developments in the tailored design of nanoscopically sized probes with superior optical properties in compare to dyes allow scientist to explore full capability of nanoparticles in bioimaging (Fig.1.10).²⁷

Quantum dots (QDs) are the most popular among fluorescent nanoparticles for single-particle imaging. With their high brightness and resistance to photobleaching, they own high signal-to-noise ratio which enables usage of a standard epifluorescence microscope for imaging.²⁸ Also, it enables studying the behavior of QD-labeled molecules for an extended duration, but the blinking of QDs complicates data processing. The numerous reports on single quantum dot imaging and single-particle tracking demonstrate their advantages over conventional dyes. For example, the brightness of QDs made it possible to observe a step size of 36 nm of individual myosin V motors with an accuracy of 2 to 3 nm in all three dimensions.²⁹ Upconversion nanoparticles (UCNPs), polymer dots (Pdots) and carbon dots (Cdots) were exploited for single-particle and specifically super-resolution imaging of cellular compartments.²⁷ Pdots and UCNPs

are non-blinking systems, so they were used for single-particle tracking experiments. Cdots exhibit emission blinking, which together with their small size makes them attractive materials for super-resolution localization microscopy techniques. It was demonstrated that 4.5 nm Cdots emit 4 times more photon count per switching event than Cy3 and exhibit great photostability (>30 min).³⁰ For the moment, dye-loaded nanoparticles are not widely used in single-particle applications despite their high brightness (can emit $> 4 \times 10^7$ photons per NP) and for some formulations blinking behavior, necessary for super-resolution imaging.³¹ For example, particles containing aggregation-induced emission chromophores were used in STED imaging of microtubule structures.³²

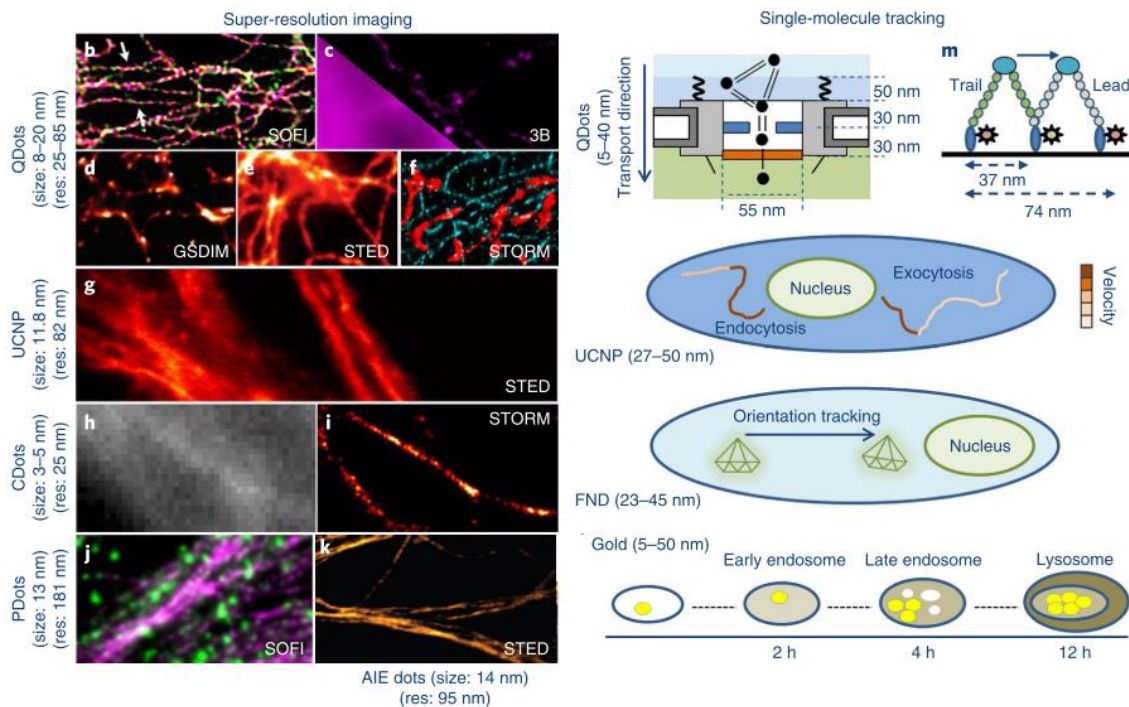


Fig.1.10. Luminescent nanoparticles used in super-resolution microscopy imaging and single-molecule tracking. Adopted from ref.²⁷

Some general drawbacks of the nanoparticles as tools for imaging are cell permeability, toxicity and in some cases surface chemistry.³³ In perspective, design and controlled synthesis of nanoparticles with different sizes, compositions and integrated multifunctionality will offer new superior labels. Together with it, improving the methods of single-molecule imaging enables to develop new improved tools to visualize more processes under the microscope and extend the current knowledge about molecular processes.

1.2 Amplification principles and DNA detection

Amplification is a process whereby a small input signal is transformed into a big output signal with the help of an amplifier.³⁴ Commonly amplifiers are associated with electronic devices, where they are used to increase the power of an electric signal, e.g. audio volume. But living organisms are extensively using amplification concept for their functions such as biosignaling, visual excitation and blood clotting, which are typically achieved through enzyme cascade mechanisms. In living organisms, a signaling molecule (hormone) by interactions with a receptor activates an enzyme, which catalyze the production of multiple signal relay molecules for activations of other enzymes resulting in enzyme cascade. Such amplification occurs within milliseconds.^{35,36}

The amplification concept found its use within many sensing techniques. Very low concentration of molecules is unable to generate a sufficient signal for detection with conventional methods. Here amplification is needed to improve detection protocol and achieve high sensitivity.³⁷ There is a huge demand to detect analytes at low concentrations in many areas of science but particularly within molecular diagnostics. The ability to detect biomarkers with a high sensitivity permits faster diagnosis, which increases the chances of effective treatment.³⁸

DNA is a unique carrier of all our genetic information. RNA plays a key role in each step in gene expression. Due to their functions, nucleic acid (NA) detection assays found their applications in diagnostics, environmental monitoring, food safety evaluations, etc. Currently, NA diagnostics are routinely used in both research and clinical laboratories. Therefore, reports on new or improved nucleic acids detection methods constantly appear. Forensic DNA validation or diagnostics at early stages of disease requires to perform analysis with low amount of NA samples.³⁸

The development of DNA biosensors corresponds to the demand for the development of diagnostic tools such as point-of-care monitoring of treatment and disease progression. A biosensor is a device that combines bio-recognition together with a signal transduction element so that biological component reacts with a target which provokes a response of a signal-generating component.³⁸ In the past decade development of DNA biosensors has been increased, especially the one that uses various signal amplification strategies. The aim of amplification in biosensing is to achieve detectable signals for the lowest possible concentration up to a few target molecules in solution. Incorporation of the amplification element into NA detection is necessary to low limit of detection and achieve the highest level of sensitivity.

The amplification methods could be divided into two principal categories: amplification achieved via molecular multiplication and signal amplification using external amplifier (Fig.1.11).³⁴ Molecular multiplication is a method that involves an increasing number of molecules created after a recognition event. It can be a replication of target molecules prior to detection or replication of labels, which leads to an increase the number of signal-producing

analyte recognition events. Another way is in the recycling of the analyte after the recognition response has been produced. This way target molecule interacts with multiple probes providing a detectable signal. On the other hand, an external amplifier is used to enhance the signal produced by one target-receptor recognition event. This can be achieved either by using macromolecules where one recognition event can trigger a change in the whole structure and produce a strong signal or by using nanostructures with surface plasmon resonance or light-harvesting abilities. There were also developed sensing platforms that unite these two principal approaches: first target is replicated and then detected with an amplified biosensor.³⁹

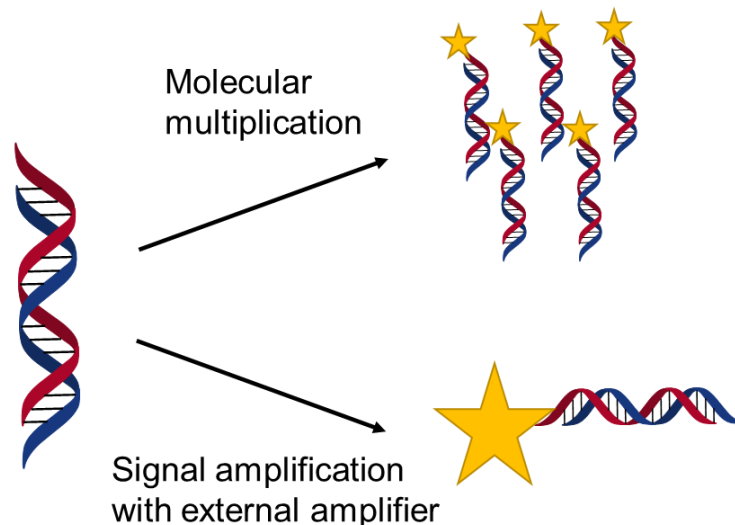


Fig.1.11. Two principle strategies to achieve amplification within DNA-sensing.

Molecular multiplication techniques

All methods of specific nucleic acids detection are based on hybridization: a process whereby complementary strands associate with each other through Watson-Crick base pairing. The hybridization is sequence-specific, and it is used in every DNA technology, including genotyping, gene expression, genetic mapping. It is a fundamental tool in molecular biology.⁴⁰

The golden-standard technique used in DNA detection is polymerase chain reaction (PCR) (Fig.1.12).⁴¹ The idea of the method is to replicate target strands of DNA with the help of enzymes prior to detection. Generally, a method comprised of three steps and performed in thermocycler: (1) double-stranded DNA denaturation at elevated temperatures (90°C), (2) DNA primers annealing at lower temperatures (50-70°C), and (3) polymerase catalyze elongation at a definite temperature. One cycle completes with the appearance of two identical copies of starting DNA and the procedure is repeated until it yields the detectable concentration of the target sequence. Since after each cycle the target is amplified twice, after 30 cycles billions of target copies are produced. Post-PCR steps include analysis of the amplified product and in the classical version of PCR, it is followed by agarose gel electrophoresis.

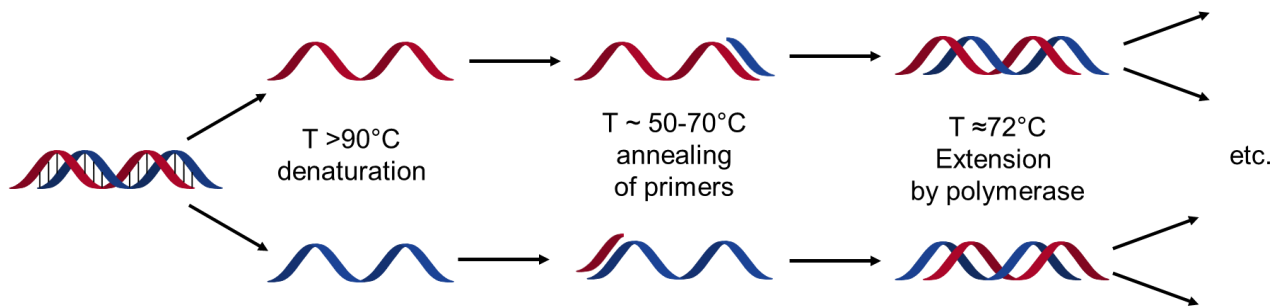


Fig.1.12. Steps of polymerase chain reaction (PCR).

To determine the amount of DNA target the Real-Time quantitative PCR was developed. Target quantification is also necessary to follow PCR performance since it can fail due to DNA degradation, presence of inhibitors or insufficient DNA quantity. Real-time PCR includes basic steps of PCR in combination with fluorescent detection to monitor the reaction with the use of fluorophore, which can be DNA binding dye (SYBR Green) or fluorescent probe. Among specific fluorescent probes most used are hydrolysis probes (TaqMan 5' nuclease assay), hybridization probes and molecular beacons (Fig.1.13).⁴²

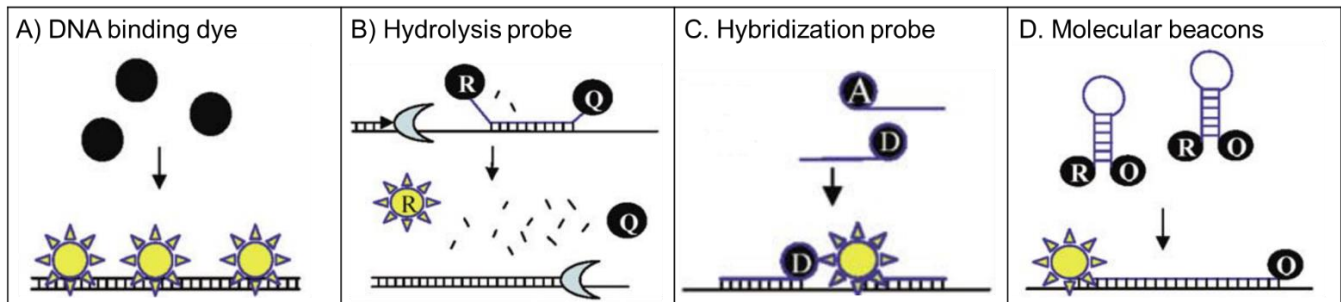


Fig.1.13. Methods of DNA quantification in qPCR. Schematic illustration of DNA quantification using A) binding of specific DNA intercalator, B) hydrolysis probe, C) hybridization probe, D) molecular beacons. Adopted from ref.⁴²

The TaqMan method uses a sequence labeled with a fluorescent dye and a quencher on opposite sides of a probe, so the emission of the dye is quenched. The probe is designed to hybridize in the DNA target region of interest, typically between two PCR primers. During polymerization, the Taq polymerase with its 5'-3' exonuclease activity cleaves the probe so the dye is released and no longer quenched. This way, the fluorescence signal increase with the accumulation of the cleaved dye during the exponential stages of the PCR. In hybridization methods, two sequence-specific probes that bind adjacent to each other in a head-to-tail arrangement are used. One probe is labeled at 3' end with a donor dye, another is labeled at 5' end with an acceptor dye so that FRET appears when they are bound to the target sequence. The molecular beacons are hairpin shaped single-stranded structures, which consist of a loop (region complementary to the target) and a stem (short region of 5-7 base pairs on both ends on the loop, complementary to each other). Stem is labeled at its ends with a fluorophore and a

quencher. In the presence of a target, molecular beacons hybridize with it so the stem separates and fluorescence signal appears. Fluorescence intensity is monitored during each cycle of PCR.

As an alternative to PCR which uses thermal cycler, there were developed isothermal amplification methods, where one temperature is used for the entire amplification process.⁴³ These methods were applied to immunoassays, which allowed sensitive detection of protein through the labeling of an antibody with oligonucleotide. The four major isothermal amplification methods are rolling circle amplification (RCA) (Fig.1.14A), strand displacement amplification (SDA), helicase-dependent amplification (HDA) and recombinase polymerase amplification (RPA). Isothermal amplification was observed to have better resistance towards inhibitors in crude samples compared to PCR. However, now enzyme-free nucleic acid amplification strategies are gaining their popularity due to low-cost and simple handling. Hybridization chain reaction is a non-enzymatic molecular replication strategy that involves two DNA hairpin structures that coexist in solution until selectively triggered by the target (Fig.1.14B).⁴⁴ Once analyte is present in solution, two strands DNA react with one another in an alternating end-to-end manner. Labeling both ends of the hairpin structure with pyrene enables a switch-on fluorescent DNA derivative.

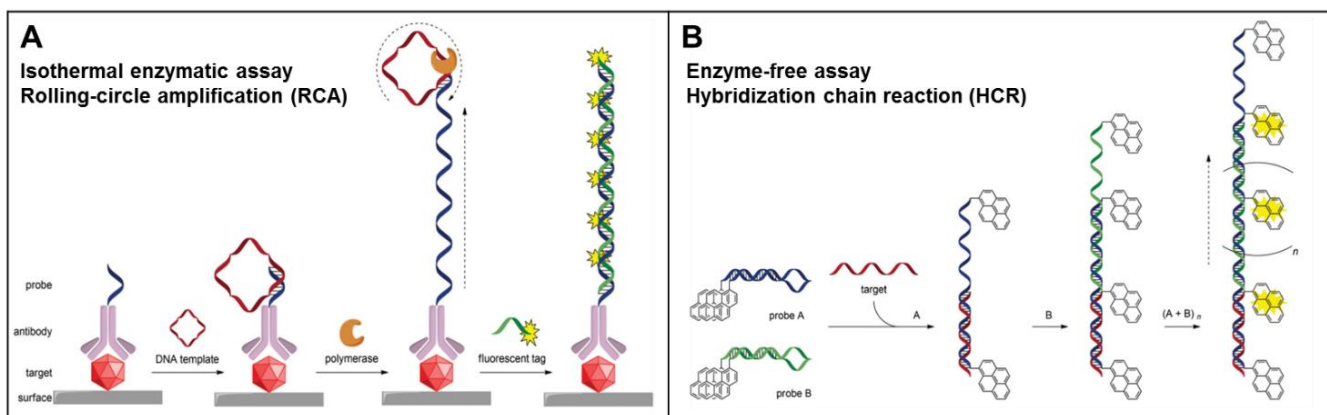


Fig.1.14. Amplification via molecular multiplication. A) Isothermal enzymatic assay: rolling-circle amplification and B) enzyme-free assay: hybridization chain reaction. Adopted from ref.³⁴

Reverse transcription polymerase chain reaction (RT-PCR) is commonly used to detect RNA molecules, such as mRNA, pre-mRNA or noncoding RNAs (Fig.1.15).^{45,46} The first step of reverse transcription (RT) is needed to generate cDNA copy from a target RNA molecule. The RT process involves synthetic oligonucleotide as a primer (e.g. oligo(dT)₁₅₋₁₈) and enzyme reverse transcriptase. In case of miRNA, stem-loop RT primers are used to replace linear primers employed for mRNA reverse transcription.⁴⁷ After cDNA is generated, the PCR or qPCR is performed to amplify and quantify the product.

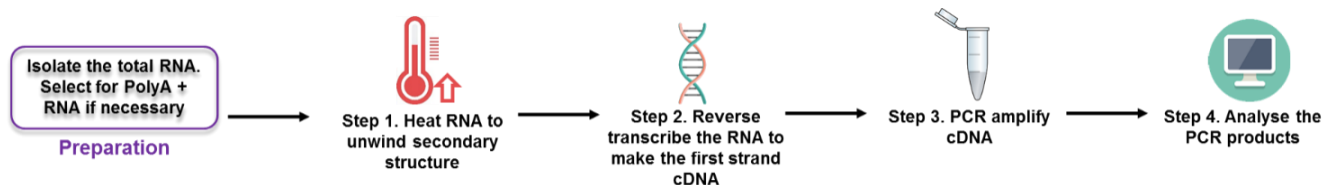


Fig.1.15. Basic outline of the steps for RNA detection with RT-PCR. Adopted from ref.⁴⁶

Other amplification strategies described for DNA are applied also for RNA detection. But for both types of nucleic acids PCR is most widely used in clinical diagnostics.⁴¹ Despite the fact that PCR and its derivatives are the “gold-label” in NA detection, yet it suffers from reproducibility issues and sensitivity towards contaminations. It requires also expensive materials and instrumentations, well-trained staff for its performance.⁴⁸ Other methods of isothermal amplification are developed, but multiplexed analysis of samples and fast, accurate quantification of target are yet difficult. To forward the field, it is necessary to develop platforms for rapid, quantitative and specific NA detection with the ability of multiplex analyses. The advances in nanomaterials could be a solution for this major goal.⁴⁹

Signal amplification via plasmonics

Nobel metal nanoparticles display a property known as localized surface plasmon resonance (SPR), which arises from coherent non-propagating oscillation of surface plasmon, induced by strong resonant interaction between electromagnetic radiations and localized surface charges of plasmonic nanostructures. This unique light-matter interaction creates a plasmonic nanoantenna, which can modulate the optical properties of nearby placed chromophores. Different metal-enhanced optical responses have been reported, including metal-enhanced fluorescence, surface-enhanced Raman scattering, and various nonlinear optical responses.⁵⁰ Interesting, that the energy transfer from plasmon nanostructure to nearby fluorophore could result either in enhancing of fluorescence or in its quenching. When SPR bands overlap with the fluorophore absorption spectrum, FRET induces enhanced plasmon-to-fluorophore energy transfer, resulting in an increase of fluorescence intensity. If the LSPR energy matches with the fluorophore emission, which situated closer than 5 nm to a nanoparticle, FRET results in fluorescence quenching due to the large plasmon absorption cross-section. At longer distances, the effect of FRET becomes insignificant, and overlap of fluorophores emission spectrum with SPR band provokes enhancement of emission due to strong local near field, so-called hot spots, generated by neighboring plasmonic nanostructures.⁵¹ Gold, silver, and graphene nanomaterials are widely-used for plasmon-enhanced sensing.⁵²

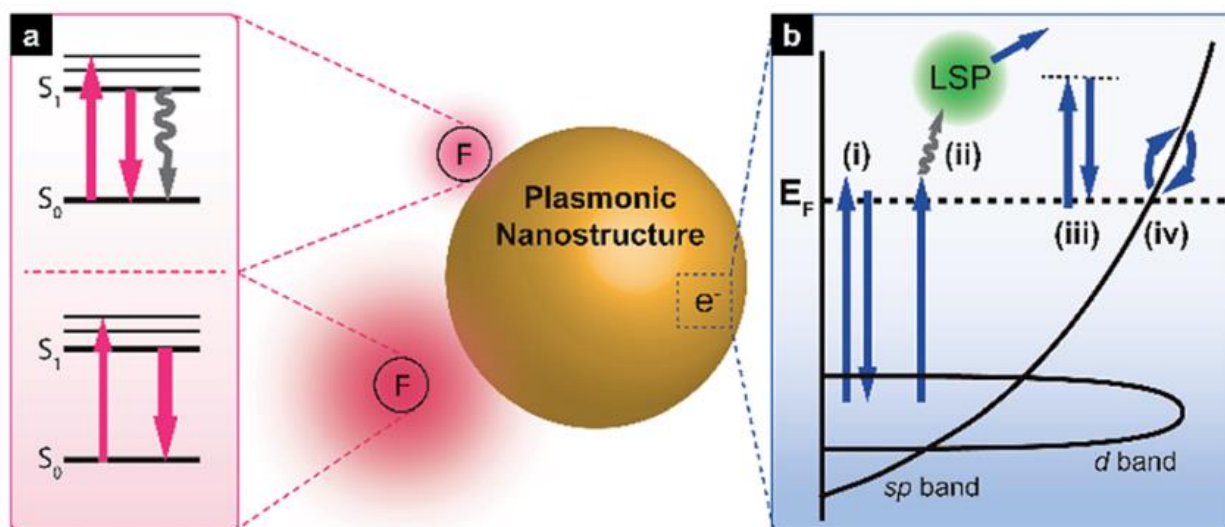


Fig.1.16. Schematic illustration of controlling and enhancing fluorescence emission with plasmonic nanostructures. A) Jablonski diagram illustrating fluorescence signal changes when emitters are close to or at a short distance from plasmonic nanoparticles. B) Simplified band diagram of gold showing a possible electronic transition for direct photoluminescence. Adopted from ref.⁵¹

Plasmonic nanoantennas are especially interesting as the strategies to enhance the single-molecule fluorescence sensing. The technical difficulty is to create a nanometer gap size in order to place the chromophore at a fixed distance to a plasmonic NP or in the hot spot between two or more particles. One way is to fabricate antennas by electron or ion-beam lithography. Wenger et coll. introduced 'antenna-in-box' platform based on a gap-antenna inside a nanoaperture (Fig.1.17A), which allowed to reduce fluorescence background and 1,100-fold fluorescence signal enhancement for Alexa Fluor 647 (initially reduced quantum yield to 8%).⁵³ In another report, with 'gold bowties' plasmonic nanoantennas fabricated using electron-beam lithography (Fig.1.17B). Moerner et coll. achieved the enhancement of single molecule's fluorescence up to a factor of 1340 for NIR dye with an initially low quantum efficiency ($\eta_0=2.5\%$).⁵⁴ To avoid nanofabrication using lithography, there was proposed a method of drying the droplets containing the colloidal suspension of AuNPs that provided the self-assembled dimers with a nanometer gap (Fig.1.17C). Following this approach Wenger et coll. obtained a dimer of 80 nm gold nanoparticles with 6 nm gap. Using this gap-antenna they obtained 70 zL detection volume and achieved 600-fold fluorescence enhancement for Alexa Fluor 647 (with initial quenched quantum yield of 8%).⁵⁵

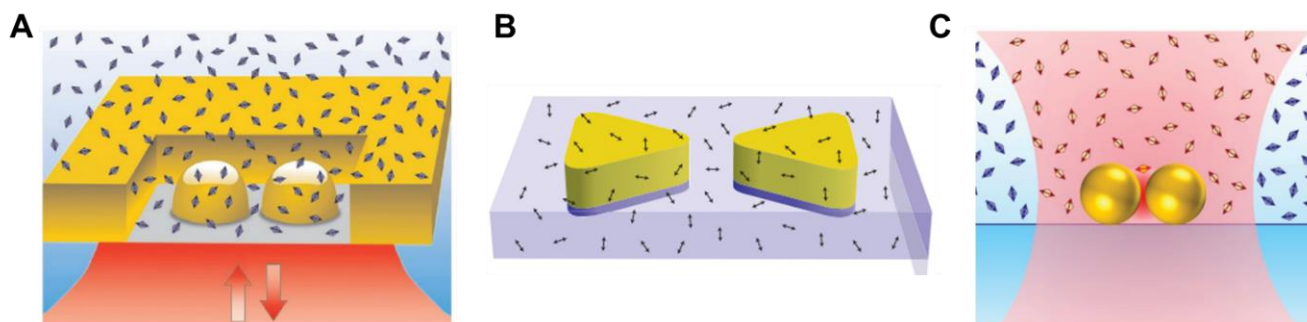


Fig.1.17. Approaches for plasmonic gap-nanoantenna construction. A) 'Antenna-in-box' platform. B) 'Gold bowties' plasmonic nanoantenna. C) Dimer of AuNPs. Adopted from ref. ^{53,54,55}

More controlled way to achieve controlled distance is attaching the plasmon nanostructure and a chromophore to the oligonucleotide. In this case, particularly interesting is DNA origami: discrete DNA nanostructure with long ssDNA scaffold strands, which is used as nanoruler due to its programmable structure. Owing to a possibility of nanometer precision, DNA origami was exploited to assemble several types of NPs (AuNPs, AgNPs, QDs) with controlled distance. Tinnefeld group fabricated a system by incorporating two relatively large AuNPs (100 nm) with a distance of 23 nm onto a DNA origami, which eventually created a plasmonic hot spot and placed an ATTO647N between them (Fig.1.18A). They observed dye emission enhancement up to 117 times.⁵⁶ Afterwards, the same group demonstrated the amplified detection of a specific nucleic acid target with the use of DNA origami-based optical antenna (Fig.1.18B).⁵⁷ For target recognition, the fluorescence-quenching hairpin was placed on DNA-origami together with a silver nanoparticle within a programmed distance. In the presence of the target, its hybridization to hairpin and break of secondary structure provoked emission appearance. The dye on the end of opened hairpin structure is then placed close to silver nanoparticle and exposed to a higher electric field resulting in 7.3-fold fluorescence enhancement. The authors were able to detect 1 nM of DNA and RNA target in human serum with the ability to distinguish a target molecule from a sequence containing two mismatches.

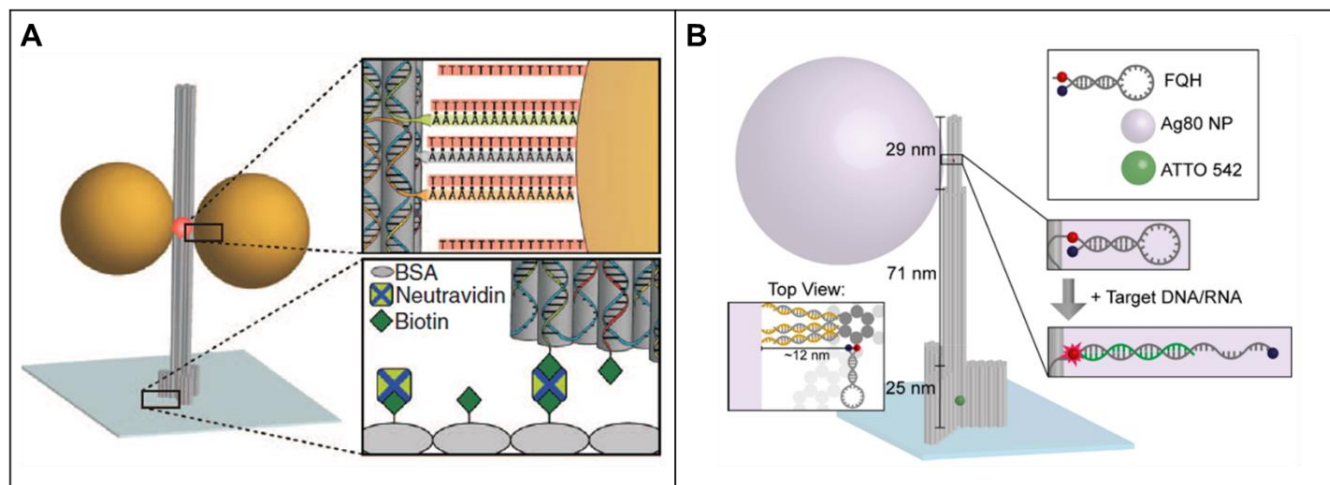


Fig.1.18. DNA origami gold NPs A) Sketch of the DNA origami pillar with two Au NPs forming a dimer. The dye (red sphere) is located between the NPs within the central bundle of the pillar. (Upper right inset) Binding of the NP to the DNA origami structure through three capturing strands. (Lower right inset). Adopted from ref. ⁵⁶ B) DNA-based fluorescence-quenching hairpin (FQH) is used for the detection of Zika-specific DNA. Adopted from ref. ⁵⁷

Metal-enhanced fluorescence is particularly interesting as a result of its ability to improve sensing techniques by amplifying the recognition response. Free colloidal nanoparticles were exploited for the development of a plasmon-enhanced fluorescence probe. Lu et al. developed a nanosensor for the detection of adenosine-5'-triphosphate (ATP) based on core-shell Ag@SiO₂ nanoparticle (Fig.1.19A).⁵⁸ In their design Cy5-labeled aptamer was immobilized onto the surface of the nanoparticles via hybridization with the complementary DNA, grafted on NP, showing a 32-fold enhancement compared to free-standing Cy5 in solution. The presence of ATP led to the detachment of the aptamer and decrease of Cy5 emission. The sensor exhibited a linear response from 0 to 0.5 mM with a LOD of 8 μ M. More efficient detection was achieved with the application of plasmon-enhanced fluorescence in coupled nanostructures for DNA detection.⁵⁰ Zhu et al. attached DNA linked Cy5 to gold nanostructure, so that its fluorescence was quenched through energy transfer, but upon coupling interaction with various metal NPs fluorescence of Cy5 was turned on (Fig.1.19B). By screening of several coupled nanostructures, authors found that with the use of Au@Ag core-shell NPs 100-fold enhancement of fluorescence compared to quenched Cy5-AuNPs and 5-fold enhancement compared to unquenched free Cy5 molecules were obtained. Based on these results, the authors designed a simple turn-on platform for selective detection of a DNA target with a limit of detection of 3.1 pM.

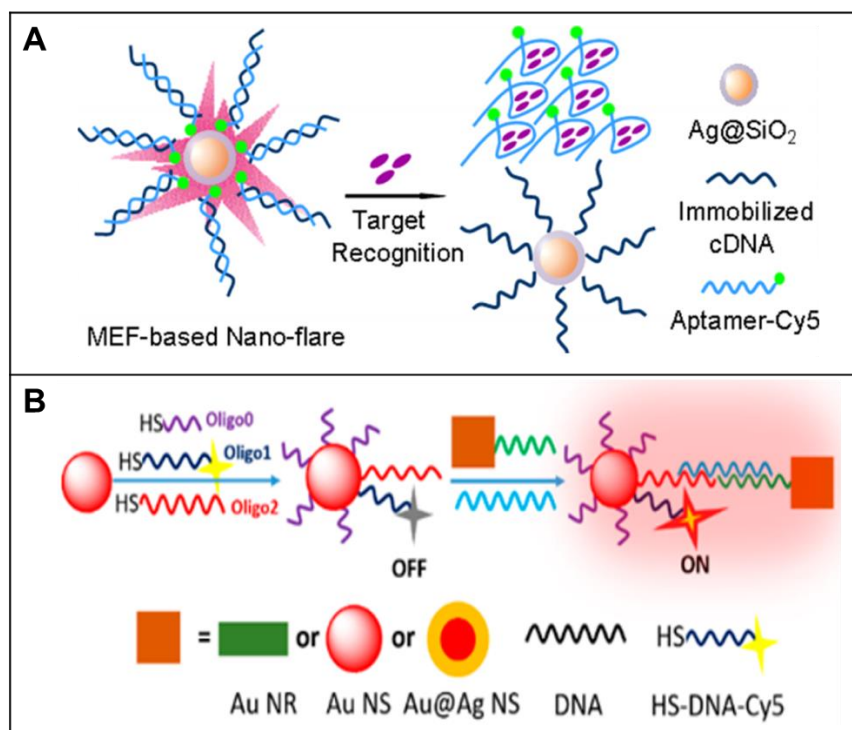


Fig.1.19. Plasmon-enhanced fluorescence sensing. A) Preparation of MEF-based core-shell Ag@SiO₂ nanoflares and ATP detection Adopted from ref. ⁵⁸ B) Coupled nanostructures and its application for DNA detection. Adopted from ref. ⁵⁰

Besides the enhancement of fluorescence emission, the plasmon nanostructures can enhance FRET efficiency due to the effect of plasmon amplification of electric fields inside the nanoscale assembly. The plasmon-assisted FRET process is faster and more long-range.⁵⁹ Lakowicz et al. reported that for a system, where donor-labeled oligonucleotide bound to a single silver nanoparticle and hybridized with an acceptor-labeled complementary oligonucleotide, the FRET radius increased from 8.3 to 13 nm and FRET rate was 21 times faster than that of unbound system.⁶⁰

Based on this phenomenon, a number of FRET-based systems was obtained with improved sensitivity.⁶¹ For example Zhao et al. presented the AgNP plasmonic enhanced FRET strategy for the imaging of protein-specific sialylation on the cell surface.⁶² In their design, AgNP was modified with an aptamer, which is hybridized with a Cy3 labeled DNA sequences applied as the donor, so that distance between AgNP and Cy3 is tuned by the length of oligonucleotide (Fig.1.20). The target monosaccharide was labeled with the Cy5 (FRET acceptor). Binding of aptamer to the target resulted in the plasmonic enhanced FRET-fluorescence of Cy5. Authors demonstrated that in FRET images, the AgNP enhanced FRET signal was *ca.* two times stronger than that in the absence of AgNP. FRET efficiencies were 21% and 37% in the absence and presence of AgNPs, respectively.

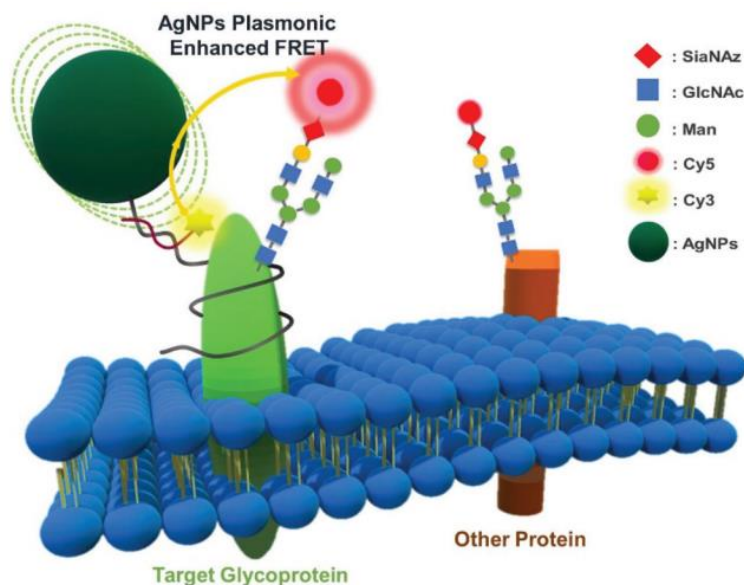


Fig.1.20. Schematic illustration of Ag nanoparticle enhanced FRET imaging for protein-specific sialylation on the cell surface. Adopted from ref.⁶²

Very interesting results were obtained when the nanostructures were involved as FRET donor and acceptor. The increase of Förster radius by 70% together with 12.5-fold enhancement of FRET efficiency with a 173-fold increase of a FRET rate was obtained for the energy transfer from conjugated polymer to a fluorescent core-shell NP with a silver core.⁶³ Boudreau et coll. made a photophysical study on a plasmon-enhanced FRET from conjugated polymer to fluorescent multilayer Ag@SiO₂@SiO₂+FITC core-shell nanoparticles and discovered that in the presence of metal core, Förster distance increased from 5 to 8.5 nm, FRET efficiency enhanced from 4 to 50% and FRET rate increased more than 2 times.⁶⁴ Lunz et al. demonstrated the 80-fold FRET rate increase and doubling of Förster radius from 3.9 to 7.9 nm in the multilayer acceptor QD–AuNP–donor QD sandwich structure compared to the same structure without AuNP.⁶³ In another study, experiments with CdSe/ZnS QD donors and acceptors deposited on top of silver NPs demonstrated 21.2-fold acceptor emission enhancement in comparison to the structure without metal NPs. Hu et al. studied DNA hairpin dynamics by combining plasmonic AuNPs with single-molecule FRET technique.⁶⁵ First, the authors studied the single-molecule fluorescence signal of Cy3 and Cy5 via direct excitation (in the absence of FRET) and discovered the increase of signal by factor 5.1 and 3.7, respectively, on a distance of 10 nm from AuNP (diameter 70 nm). However, authors observed the decrease of smFRET efficiency in the presence of AuNP for closed hairpin, which was explained by larger fluorescence enhancement for the donor (Cy3) than that for the acceptor (Cy5) in the presence of AuNPs. Also, they concluded that DNA hairpin dynamics remain unperturbed by AuNPs with a diameter of 50 and 70 nm.

The fluorescence amplification through plasmonic nanostructures provides great potential for biosensing applications, but the lack of standardization, complicated techniques, and expensive materials creates complications for its usage in clinical diagnostics.⁶⁶

Amplification with light-harvesting nanomaterials

Light-harvesting relies on a process of electronic energy transfer: by excitation of an assembly of molecules, which situated close to each other, the electronic excitation energy is transferred within networks of chromophores to acceptor.³⁶ Nature uses the efficient capture and transfer of solar energy in photosynthesis. The plant leaves contain chromophores that are bound in light-harvesting complexes. They absorb solar energy, which is transferred via light-harvesting proteins to a reaction center. Such a remarkable process inspired scientists for the development of artificial antenna systems at nanoscale mode.⁶⁷ The key criteria for an efficient antenna system are very high molar extinction coefficient, excellent photostability and the ability to transfer energy. This means, that artificial nanoantenna should be able to harvest and transfer energy to an acceptor component with high efficiency. Considering these issues, artificial light-harvesting systems were designed based on dendrimers, porphyrin-based nanostructures, conjugated polymer nanoparticles, organic-inorganic nanocomposites, organogels, biopolymer assemblies, QDs and metallic nanoparticles (Fig.1.21). Recently our group reported the light-harvesting nanoantenna based on dye-loaded polymer nanoparticles.⁶⁸ The fundamental understanding of energy transfer process and nanomaterial design with tailored properties would allow converting light-harvesting systems into ultrasensitive biosensors.

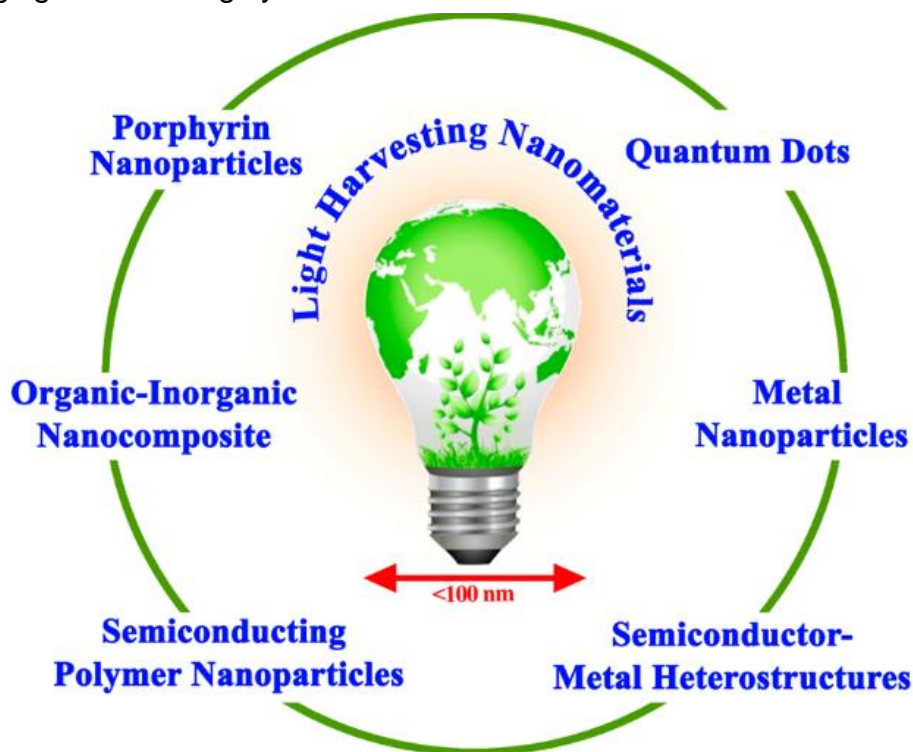


Fig.1.21. Light-harvesting nanoscale systems. Adopted from ref.⁶⁷

Dendrimers are well-defined tree-like structures, which consists of a core, branching units, and peripheral functionalities. The multiple surface functional groups render dendrimers the ability to attach numerous signal tags, this way to enhance the signal output by recognition event.⁶⁹ For example, Wand et al. reported an amplified fluorescent sensing platform for nucleic acids, proteins, and cells based on a dye-intercalated DNA dendrimer probe (G_3SG) integrated with electrospun nanofibers (NFs) (Fig.1.22A).⁷⁰ In this assay, NFs were modified with capture DNA and the 3rd generation DNA dendrimer was prepared and intercalated with SYBR Green I dye. The target hybridization with capture leads to further sandwich complex formation with the G_3SG -labeled DNA reporter on the NF membrane surface and strong fluorescence signal amplification. The authors demonstrated sensitive detection of 20 pM of a β -thalassemia gene fragment. In other work, Divsar and coll. developed electrochemiluminescent (ECL) biosensor for the detection of DNA by using QDs–dendrimer nanocomposites for signal amplification (Fig.1.22B).⁷¹ Authors immobilized on AuNPs modified glassy carbon electrode molecular beacon DNA probe, which loop was opened target recognition and the nanocomposite of QDs-PAMAM dendrimer was attached to free end of DNA probe. The QDs-nanocomposite generated a strong ECL related to target DNA in the presence of $S_2O_8^{2-}$ ion as coreactant with sensitivity of 2.5 aM of the target.

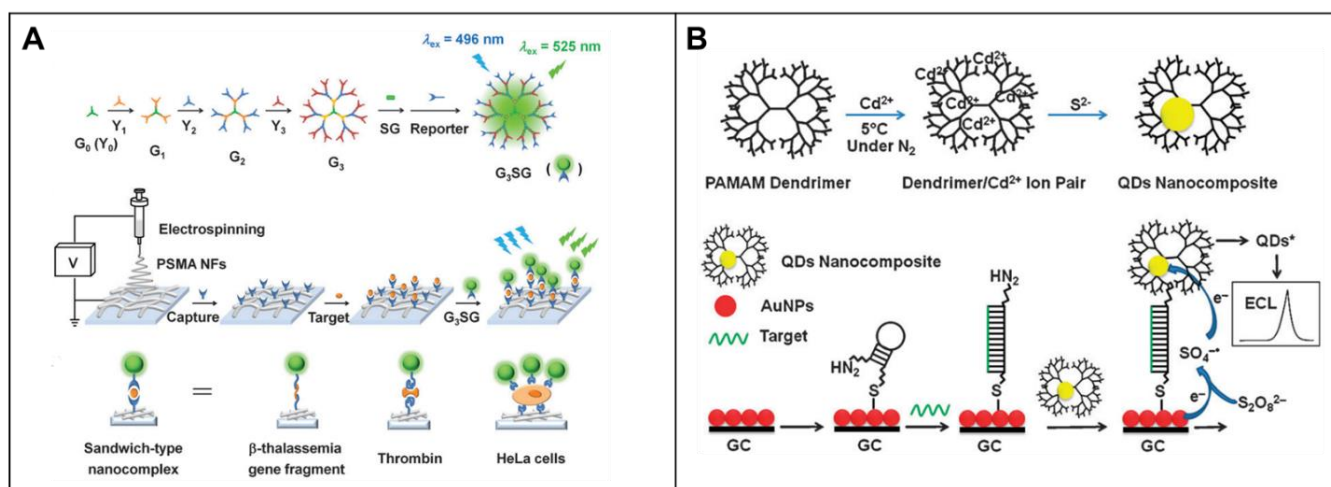


Fig.1.22. Usage of dendrimers for signal amplification. A) Amplified fluorescent sensing platform based on dye-intercalated DNA dendrimer probe (G_3SG) integrated with electrospun nanofibers. Adopted from ref.⁷⁰ B) ECL sensing platform using QDs–dendrimer nanocomposite as label. Adopted from ref.⁷¹

Dendrimers mimic natural light-harvesting systems in which by incorporation of peripheral chromophores, energy is captured and further transferred to the core. The well-designed light-harvesting dendrimer system can serve as the basis for solar energy conversion and photoinduced electron transfer (PET) between units of a dendrimer.⁶⁹ But the development of light-harvesting biosensors based on dendrimers is rather difficult because it is needed to incorporate capture elements in the core, which complicates detection. Other supramolecular

scaffolds have been used to arrange donors and acceptor in order to achieve efficient energy transfer. For example, Xu et al. reported light-harvesting platform based on macrocyclic amphiphiles (calixarenes), with encapsulated donor (1-anilino-8-naphthalenesulfonate) into calixarene cavity and entrapped acceptor (4,7-bis(thien-2-yl)-2,1,3-benzothiadiazole) into the hydrophobic bilayer (Fig.1.23).⁷² Authors demonstrated the energy-transfer efficiency up to 85% by mixing donor and acceptor at a molar ratio of 10:1. The antenna effect (amplification of the acceptor emission) achieved for this ratio was 4.5.

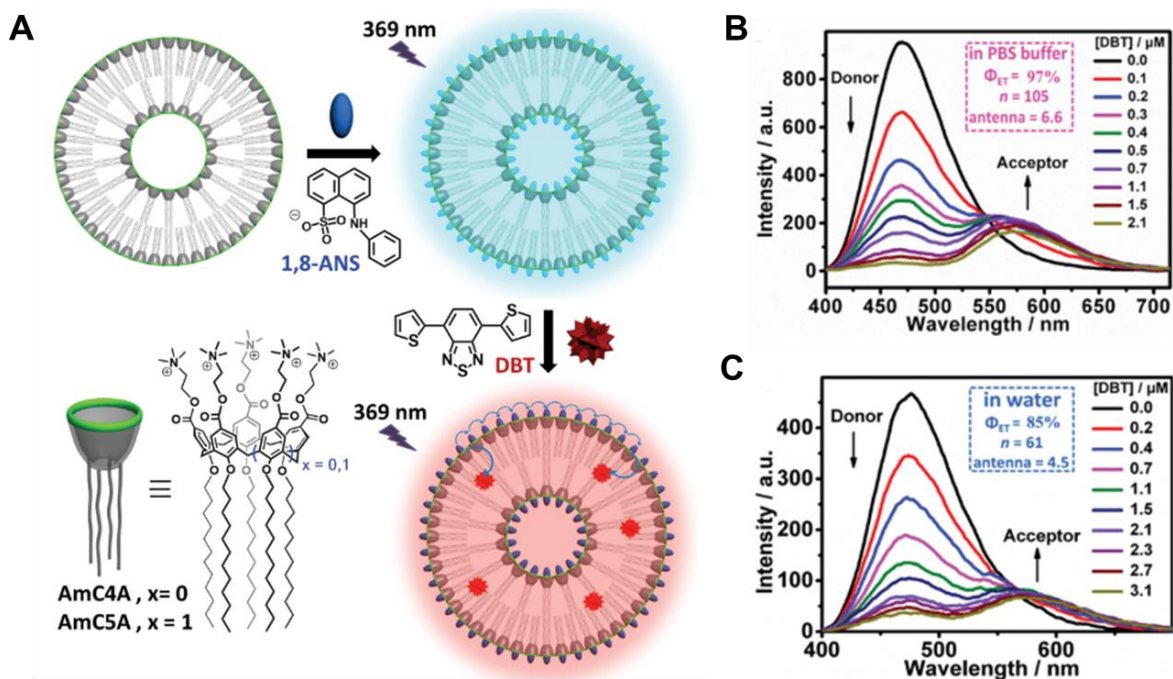


Fig.1.23. Light-harvesting platform based on calixarene. A) Scheme of synthesis and chemical structures. Fluorescent spectra of nanoantenna structure with increasing concentration of acceptor B) in PBS buffer, C) in water. Adopted from ref.⁷²

The basics of the light-harvesting process is energy transfer within molecules, which is achieved by the means of FRET. The ways to achieve amplified FRET in luminescent nanomaterials will be discussed in the next section of this manuscript.

1.3 FRET in nanomaterials for biosensing

Due to its versatility, the field of FRET applications is constantly increasing over the last years (Fig. 1.24).⁷³ The specific conditions of energy transfer allow designing a variety of FRET sensors by exploiting processes that lead to a decrease or increase of FRET efficiency (Fig.1.25).⁹

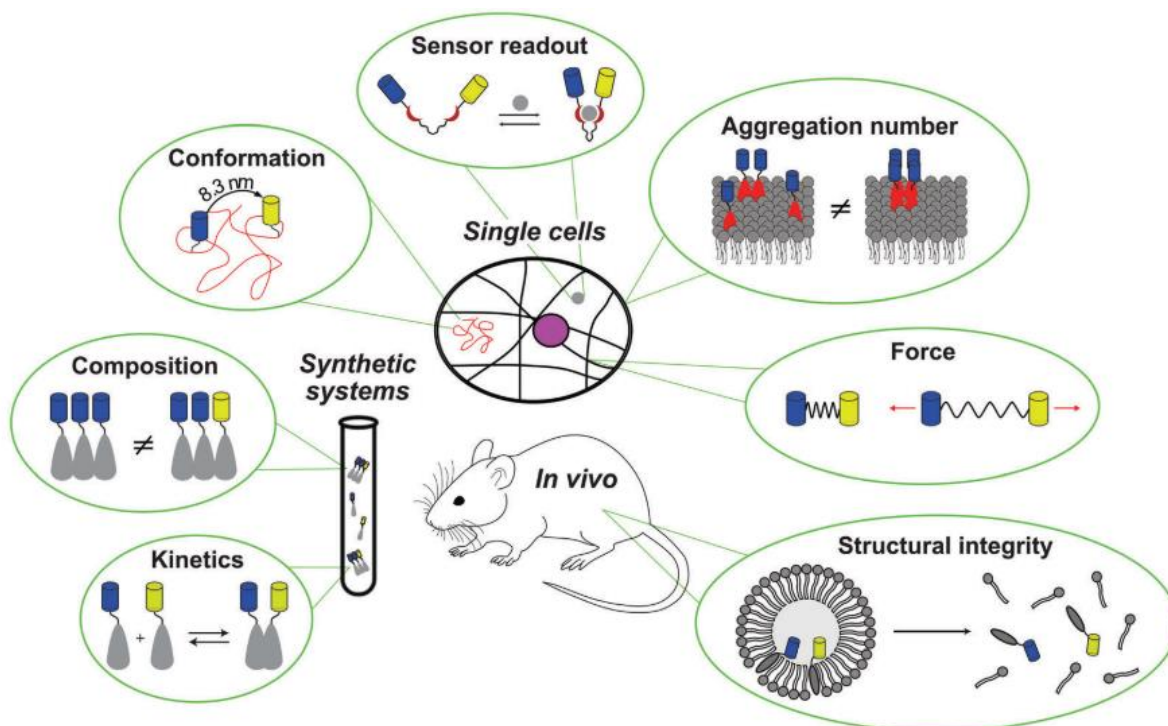


Fig.1.24. Versatility of FRET sensors in different aspects of supramolecular systems: kinetics, aggregate composition, molecular conformation, sensor incitement, aggregation number (using homo-FRET), applied force, and structural integrity. Adopted from ref. ⁷⁴

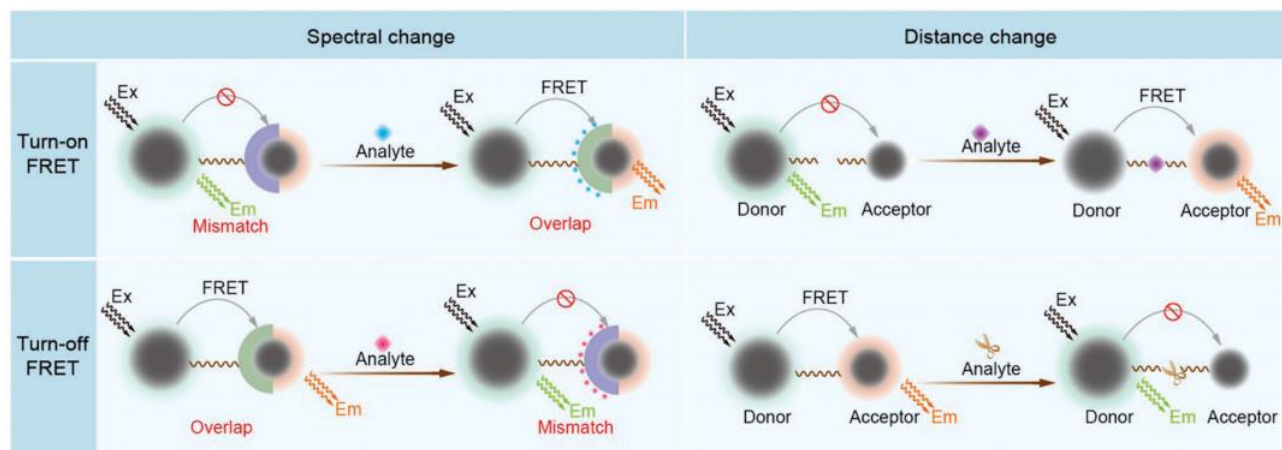


Fig.1.25. General designs for FRET-based biosensing systems. Adopted from ref. ⁹

Currently, the majority of donor and acceptor materials used in FRET applications are organic dyes. Since dye molecules are small, they would not interrupt principle functions of biomolecules, and with FRET it is easy to follow the interaction between the sites of protein or deoxyribonucleic

acid (DNA) molecules. FRET assays are extensively used in the studies which include structure and conformational changes of proteins and DNA. But since it is difficult to deliver the biomolecular sensor directly into the live cell, they can be genetically encoded, allowing the preparation of FRET-based probes directly inside the cells.⁷⁵ With the fast development of new fluorescent proteins of different colors, it became possible to use FRET to monitor the biomolecular interactions in different cell compartments.

With regard to limitations of organic dyes (weak signal and poor photobleaching resistance)⁵, fluorescent nanoparticles with their high brightness, photostability and multifunctionality are more and more frequently exploited in FRET applications.⁷⁶ Different FRET-assays were developed with the use of nanoparticles, among which most investigated are systems based on quantum dots (QDs)¹⁰, upconversion nanoparticles (UCNPs)⁷⁷ and gold nanoparticles (AuNPs).⁷⁸ For FRET-biosensing applications the use of nanoparticles has an advantage over molecular probes in terms of multifunctionality: nanoparticles act not only as effective FRET donors or acceptors (quenchers) but also their surface can be additionally modified with other ligands for specific target recognition.⁷⁹ The potential analytes of interest are nucleic acids, proteins, toxins, metabolites, drugs, microbes, and other pathogens.

Nanomaterials demonstrated their ability to amplify target signal in FRET assays and were used to improve biomolecules detection.³⁷

FRET in inorganic nanoparticles

Quantum dots are luminescent semiconductor nanocrystals with a small size of 1 to 20 nm. The best available QD fluorophores for biological applications consist of CdSe core and layer of ZnS coat, which passivates the core surface and produces a significant improvement in the photoluminescent yield.⁸⁰ They are typically used as FRET donors since they have narrow emission, broad absorption spectrum and large molar extinction coefficients (10^5 - 10^6 M⁻¹ cm⁻¹).⁸¹ This feature allows them to act as nanoantenna for FRET systems by transferring excitation energy to acceptor and enhancing its signal in compare to FRET systems with only organic dyes.¹⁰ Moreover, because of the broad excitation band, the mixture of QDs donors at a single wavelength can be excited which permits the multiplexed FRET applications.⁸² The main issue limiting QDs application is the toxicity of Cd²⁺ and Pb²⁺ ions, but the coating shell can improve their biocompatibility.

QDs can be modified with a variety of biomolecules, including antibodies, proteins, and nucleic acids. One of the first FRET-sensors based on QD-protein assemblies were presented by Medinitz et coll.⁸³ In this work, authors designed two types of sensors for maltose by initially assemble QD with a maltose-binding protein (MPB) via supramolecular interactions. In one configuration of a nanosensor, the dark quencher is conjugated in the binding site of the MBP, which results in FRET-quenching of QD fluorescence, while binding of maltose replaces quencher and restores QD fluorescence (Fig.1.26A). In the second configuration, sensor

assembly consists of QD coupled with Cy3-labelled MBP bound to β -cyclodextrin-Cy3.5, ensuring two-step FRET, where binding of maltose removes Cy3.5-conjugate and changes emission profile (Fig.1.26B). This primarily work demonstrated that biologically compatible QDs can act as FRET donors in recognition-based quantitative sensing.

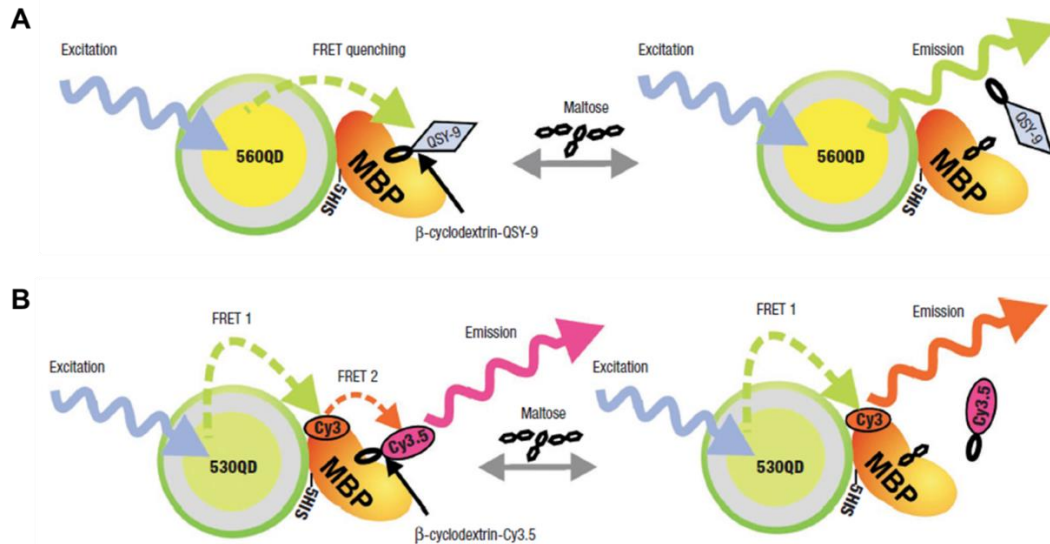


Fig.1.26. QD-protein assemblies as FRET sensors. A) Schematic function of nanosensor with turn-on emission of QD. B) Schematic function of nanosensor with FRET modular function. Adopted from ref. ⁸³

The number of FRET assays for nucleic acids detection was developed using QDs.⁸⁴ For example, Su et al. reported a “signal-off” FRET-based strategy for microRNA and DNA detection based on QDs (Fig.1.27).⁸⁵ In this approach single strand capture DNA is attached to QD and by addition of the target sequence, the emission of QDs is quenched by an organic quencher (BHQ₂). Such a nanosensor demonstrated high sensitivity and a low limit of detection (10 fM).

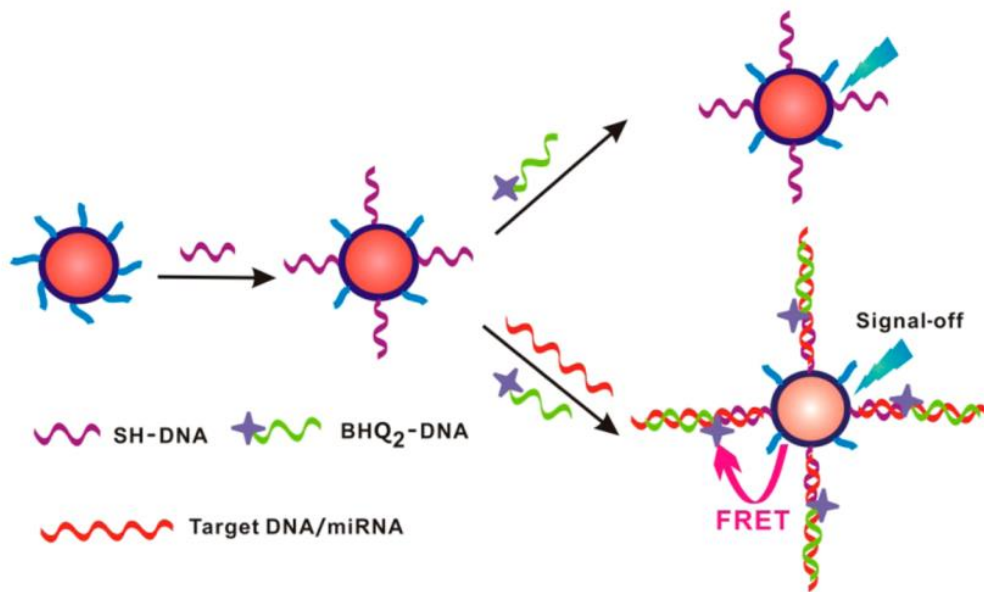


Fig.1.27. Detection of microRNA with sensor based on QDs. Adopted from ref. ⁸⁵

The use of QDs as FRET donors increases sensitivity of FRET assays and allows detection of nucleic acid targets with up to picomolar range without molecular multiplication.¹⁰ Zhang et al. demonstrated the way to achieve a higher sensitivity of DNA detection with the use of QDs linked to several DNA probes to capture DNA targets (Fig.1.28A).⁸⁶ QDs is a FRET donor and a concentrator that amplifies the target signal by confining several targets in a nanoscale domain. In the proposed design, the DNA target hybridized with two reporters labeled with biotin and FRET-acceptor, so that several sandwiched hybrids are then captured by a single QD through biotin–streptavidin binding. This way appearance of acceptor emission indicates the presence of target oligonucleotide and authors were able to detect in with LOD of 4.8 fM at a single particle level in comparison to 0.48 pM for molecular beacons. Hildebrandt et coll. proposed a single-step assay for miRNA quantification at low concentration with the use of single time-gated (TG)-FRET donor-acceptor pair (Fig.1.28B).⁸⁷ As FRET donor Tb-complex was used, and, as FRET-acceptor, the authors compared a dye (Cy5.5) and a quantum dot. QD with its superior photostability provided higher signal and order of color-multiplexing. Also, a large surface of QD was exploited for the conjugation of multiple biomolecules. The authors were able to simultaneously detect and quantify two different miRNAs at nanomolar concentrations.

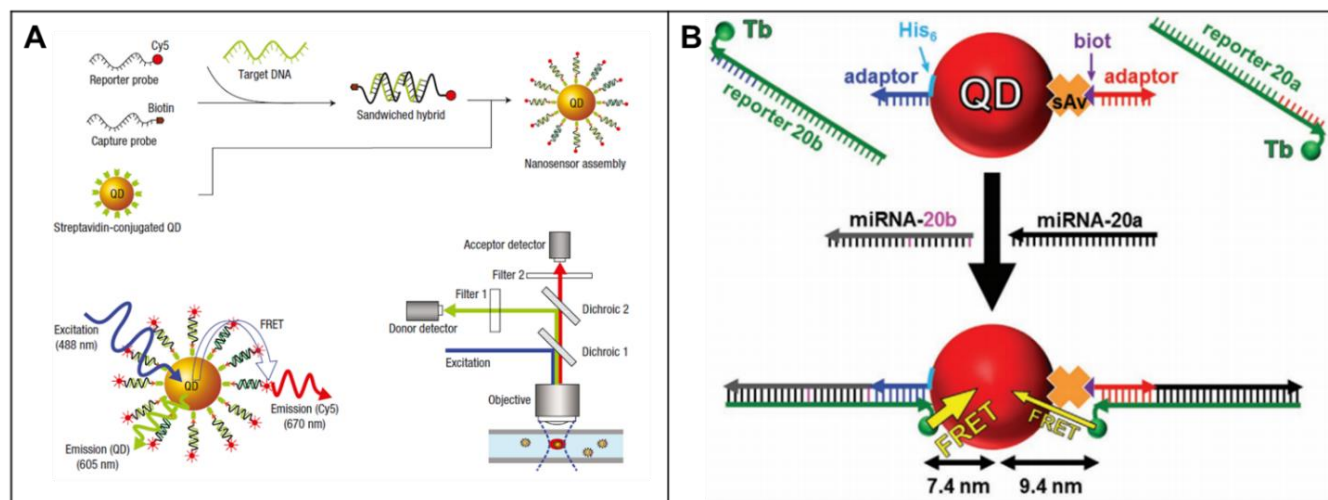


Fig.1.28. Single QD-based FRET-assays for sensitive DNA detection. A) Schematic representation of DNA detection using single QD. Adopted from ref.⁸⁶ B) Illustration of QD-based TG-FRET sensor for the specific quantification of two miRNAs. Adopted from ref.⁸⁷

The other type of NPs, which are used as donors in FRET applications are upconversion nanoparticles.⁷⁷ UCNPs can convert near-infrared radiation into visible light via nonlinear optical processes. This makes them a good alternative to traditional fluorophores because NIR light is far from excitation of other molecules, UCNPs have narrow emission peak, low toxicity, and good chemical stability. In FRET assays UCNPs should be coupled with downconverting acceptor molecule. For example, Huang et coll. developed a DNA-sensor by exploiting energy transfer from UCNP to an acceptor molecule attached to the reporter DNA (Fig.1.29).⁸⁸ Authors demonstrated a linear response to the target in the concentration range of 10-50 nM.

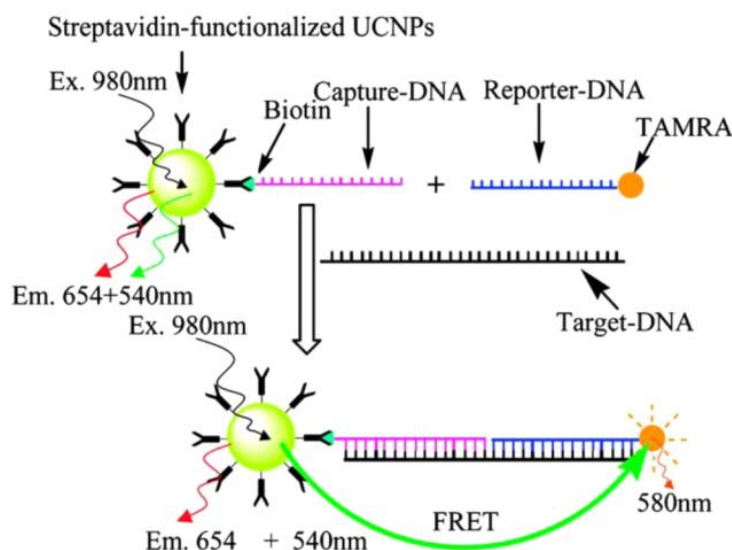


Fig.1.29. Schematic illustration of the DNA-sensor system by manipulating the distance between UCNP and target DNA. Adopted from ref. ⁸⁸

Moreover, UCNPs also enhance the detection assays with efficient energy transfer. Song et al. reported a novel complex of NaYF₄:Yb,Tm UCNPs and TiO₂ inverse opal photonic crystals for responsive sensing of avidin, where upconverting nanocrystal have ~43-fold enhanced luminescence in comparing with normal emission intensity (Fig.1.30A).⁸⁹ This allowed development a nanosensor for avidin with a low detection limit (48 pmol). In other work, reported by Laurenti et al. the sensitive miRNA detection was achieved by exploiting the interactions between ssDNA-functionalized UCNPs and graphene quantum dots. In the absence of a complementary miRNA sequence, the ssDNA-functionalized UCNPs interact with the graphene quantum dots, leading to 25-fold enhancement of the upconversion emission (Fig.1.30B).⁹⁰ By adding the target miRNA sequences, the hybridization process yields dsDNA on the surface of the UCNPs, which hinders interaction with the graphene quantum dots and reduces the emission intensity. Thus, LOD of 10 fM was achieved.

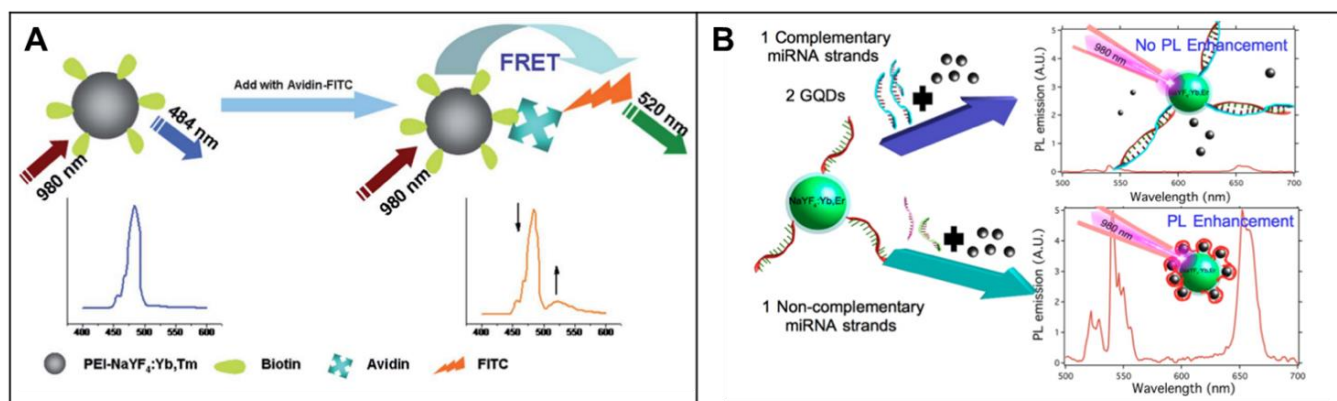


Fig.1.30. UCNPs-based enhanced detection assays. A) FRET detection of avidin by employing upconverting nanocrystal as the donor and FITC as an acceptor. Adopted from ref. ⁸⁹ B) Sensing platform for miRNA detection based on enhanced upconversion emission with graphene quantum dots. Adopted from ref. ⁹⁰

Gold nanoparticles are non-luminescent and, in contrast to QDs and UCNPs, are used as FRET acceptors (dark quenchers).⁶⁶ AuNPs hold unique properties of surface plasmon resonance phenomenon (see above), size- and shape tunable absorption spectrum and high fluorescence quenching capability of a wide range of organic fluorophores. AuNPs are nontoxic and found a variety of biological applications.⁹¹ Countless researchers had contributed to the development of sensors based on AuNPs. Remarkably, a great variety of NA nanoprobe have been developed based on AuNPs.⁸⁴ The Mirkin group demonstrated the use of densely coated DNA functionalized AuNPs (so-called spherical nucleic acid, SNA) as a probe for detection and knocking down of intracellular mRNA^{92,93,94}. They named probes as nanoflares, where 13 nm AuNPs are covered with 20-base DNA recognition domain for specific mRNA. These DNAs are hybridized with the short 12-base oligonucleotides labeled with Cy5, so that dye is situated near the surface of the nanoparticles and quenched via surface energy transfer (NSET). In the presence of the target mRNA, the short sequences are released via strand displacement and Cy5 restores its fluorescence. This way the strong fluorescence signal was detected while incubation of nanoflares with cells expressing a high level of target mRNA transcript of oncogene survivin. Also, the same group demonstrated multiplexed nanoflare assay with different dyes capable of simultaneous detection of two mRNA at once (Fig.1.31).⁹⁵ Regarding their performance, there are a few drawbacks of these systems. Firstly, it is a false-positive signal due to cleavage of the thiol bond by glutathione or protein binding which would lead to flare release. Secondly, the signal intensity-based sensing is affected by the drifts of light source, detectors and by the local distribution of probes. In this respect, Wang and colleagues developed FRET nanoflares, where they follow the appearance of FRET-acceptor signal after flare displacement.⁹⁶

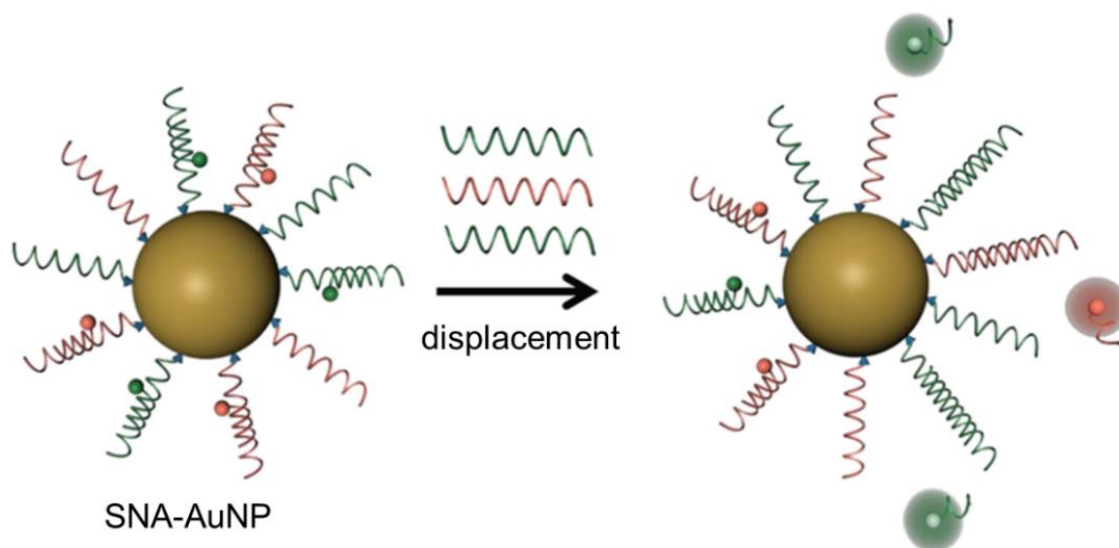


Fig.1.31. Schematic representation of two different nucleic acids target detection by multiplexed nanoflares based on SNA-AuNP. Adopted from ref.⁹⁵

FRET in conjugated polymers and conjugated polymer nanoparticles

Conjugated polymers are macromolecules based on π -conjugated structural units.⁹⁷ In this system, each subunit acts as a chromophore due to electron delocalization. Typically, CPs have broad absorption spectra due to the inhomogeneity of chromophore units. CPs exhibit light-harvesting ability and efficient energy transfer, since excitons can migrate along the polymer backbone, a process that has been described as the “molecular wire effect”. Pairing CPs with suitable acceptor allows to obtain effective sensing and photosensitizing platforms. Multifunctionalized CPs could be converted into conjugated polymer nanoparticles (CPNs) via miniemulsion or reprecipitation methods from corresponding polymer.⁹⁸ This way CPNs have tuneable properties, less toxicity and a possibility of surface modification. The size of nanoparticles varies from 5-10 nm diameter in case of a few polymer chains up to 800 nm for hydrophobic polymers. Same as polymers, CPNs exhibit energy transfer abilities, which was used for biosensor applications.

In these cases, sensor dye and reference dye are loaded in nanoparticle or linked to its surface and a ratiometric signal is obtained by the response of the sensor to an analyte.⁹⁹ For example, Chan et al. reported poly(2,5-di(3',7'-dimethyloctyl)phenylene-1,4-ethynylene) polymer dots (Pdot) as a platform for FRET-based pH nanoprobes (Fig.1.32).¹⁰⁰ Polymer dots are fluorescent nanodots consisting of semiconductor polymer and prepared by either emulsion polymerization or nanoprecipitation.³³

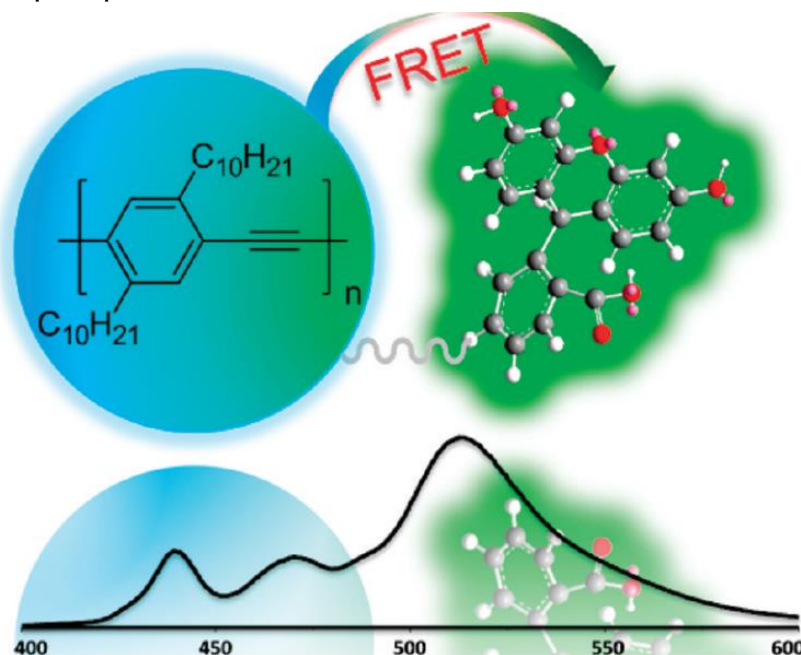


Fig.1.32. Pdot-fluorescein conjugate as FRET-based pH sensor. Authors conjugated Pdot to pH sensitive dye molecule (fluorescein) to obtain highly efficient FRET from Pdot to dye. Adopted from ref. ¹⁰⁰

Frausto et al. proposed a FRET-based ratiometric fluorescent probe for the detection of singlet oxygen ($^1\text{O}_2$) with the use of dye (DA-TMT) doped conjugated polymer nanoparticles

(Fig.1.33).¹⁰¹ Without $^1\text{O}_2$ exposure, via excitation of conjugated polymer it transfers energy to the DA-TMT inside the nanoparticle. But since DA-TMT is sensitive towards singlet oxygen, via $^1\text{O}_2$ exposure it forms a peroxide which is no more fluorescent, so the FRET-signal is diminished. The authors demonstrated a fast ratiometric response to $^1\text{O}_2$ with the use of nanomolar concentration of nanoprobles.

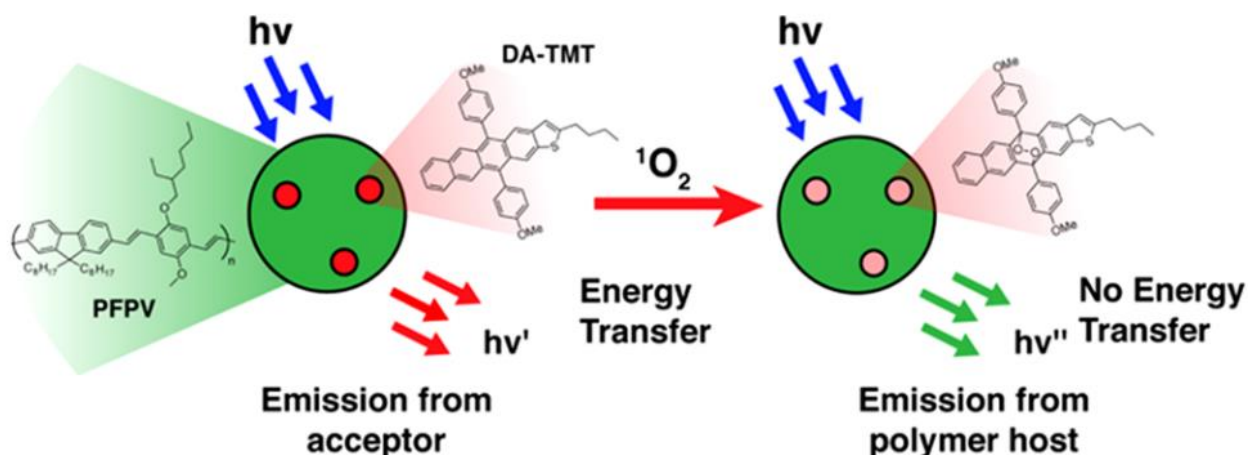


Fig.1.33. Ratiometric singlet oxygen detection using dye-doped conjugated polymer nanoparticles. Adopted from ref.¹⁰¹

Both conjugated polymers and nanoparticles were used for amplified DNA sensing. For DNA recognition CPs are designed to contain charged groups as cationic quaternary ammonium incorporated into side chains of the polymer. This way they bind with negatively charged oligonucleotide via non-specific electrostatic interactions. By designing a sensor with a suitable acceptor, an amplified FRET signal could be achieved bringing high sensitivity towards target biomolecule.¹⁰² One of the first applications was demonstrated by Bazan and coll., where polycationic CPs were paired with a probe peptide nucleic acid (PNA) labeled with fluorescein as FRET acceptor (Fig. 1.34A).¹⁰³ In the absence of the target, no FRET signal was observed, because PNA is neutral and do not interact with CPs. In the presence of the target, the PNA was hybridized with it, gained negative charge and bound to the polymer. CPs excitation provided fluorescein emission >25 times higher than that obtained by the direct excitation of the dye. This allowed 10 pM concentration of DNA target detection with a standard fluorometer. Further Leclerc et coll. reported assay for specific detection of nucleic acids at the zeptomole level based on "Triplex" formation of DNA with a conjugated polymer (Fig.1.34B).¹⁰⁴ In this method positively charged polymer changes its conformation upon binding with ssDNA molecule and the target nucleic acid, which leads to an increase and shift in its fluorescence emission spectrum. The limit of detection was ~ 310 molecules or 0.54×10^{-21} mol in an effective volume of 150 μL .

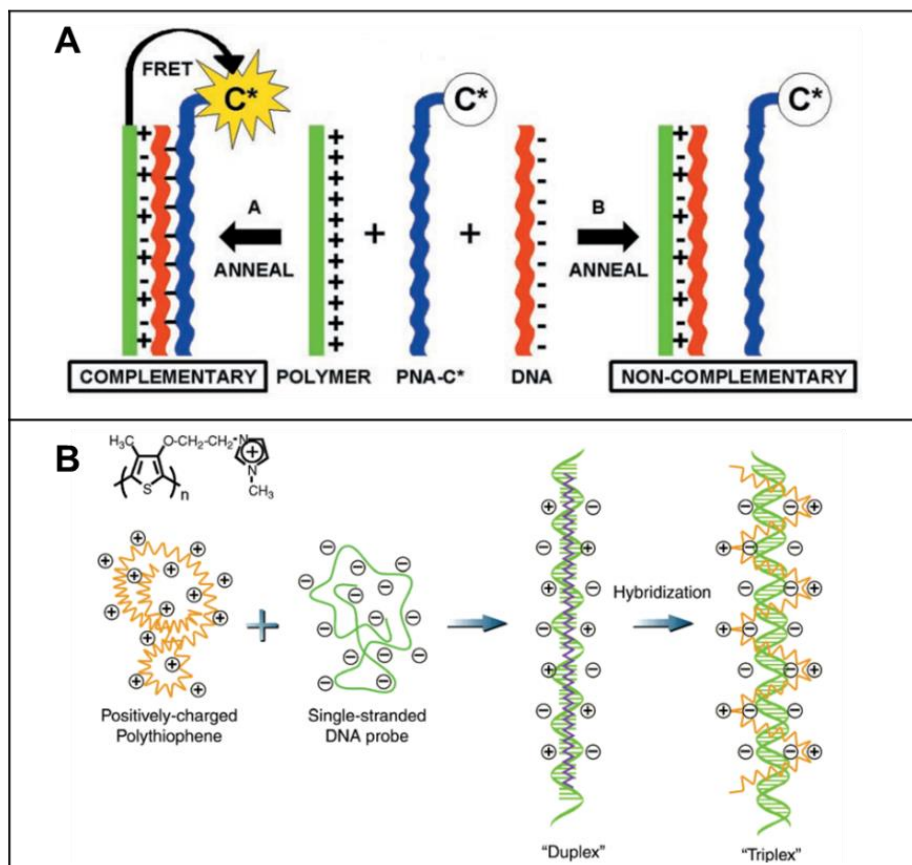


Fig.1.34. Amplified DNA detection with the use of conjugated polymers. A) Scheme of detection of ssDNA with a cationic polymer and specific PNA optical reporter. Adopted from ref.¹⁰³ B) Schematic description of the formation of the conjugated polymer/single-stranded nucleic acid duplex and the conjugated polymer/hybridized nucleic acid triplex. Adopted from ref.¹⁰⁴

CPNs were also used for the development of FRET-based NA biosensors. Bao et al. demonstrated selective ssDNA detection in serum with CPNs.¹⁰⁵ Nanoparticles were formulated so that carboxylic function was exposed on the surface of NPs, which allowed further coupling with amine-functionalized capture DNA sequence (Fig.1.35A). Covalent DNA-modified NPs exhibited excellent photostability in various buffers. In the presence of target DNA, a sequence-specific fluorescence response was achieved by adding PicoGreen as the DNA intercalator and FRET acceptor. The fluorescence signal of PicoGreen was amplified more than 19 times through FRET compared to the direct excitation of the dye. The authors demonstrated selectivity of the probe towards mismatches and sensitivity towards 2 nM of DNA target in serum. Boudreau and coll. developed plasmonic biosensors combining the cationic conjugated polymer and luminescent Ag@silica multilayer dye-doped nanoparticles (NPs) grafted with single-stranded DNA probes (Fig.1.35B).¹⁰⁶ Upon target hybridization with DNA-probe, the conjugated polymer becomes luminescent and its excitation allows following the FRET to an acceptor molecule immobilized in the outer layer of the NPs. The metallic core's plasmon enhances energy transfer efficiency, so this way it amplifies the optical signal generated by DNA hybridization events. The authors obtained the enhancement factor of 8 by comparing the fluorescence intensity of

acceptor with and without Ag core. Obtained biosensors were applied for the rapid identification of the SRY gene extracted from the blood with a detection limit of 10^5 ssDNA per mL (0.2 fM) without chemical amplification.

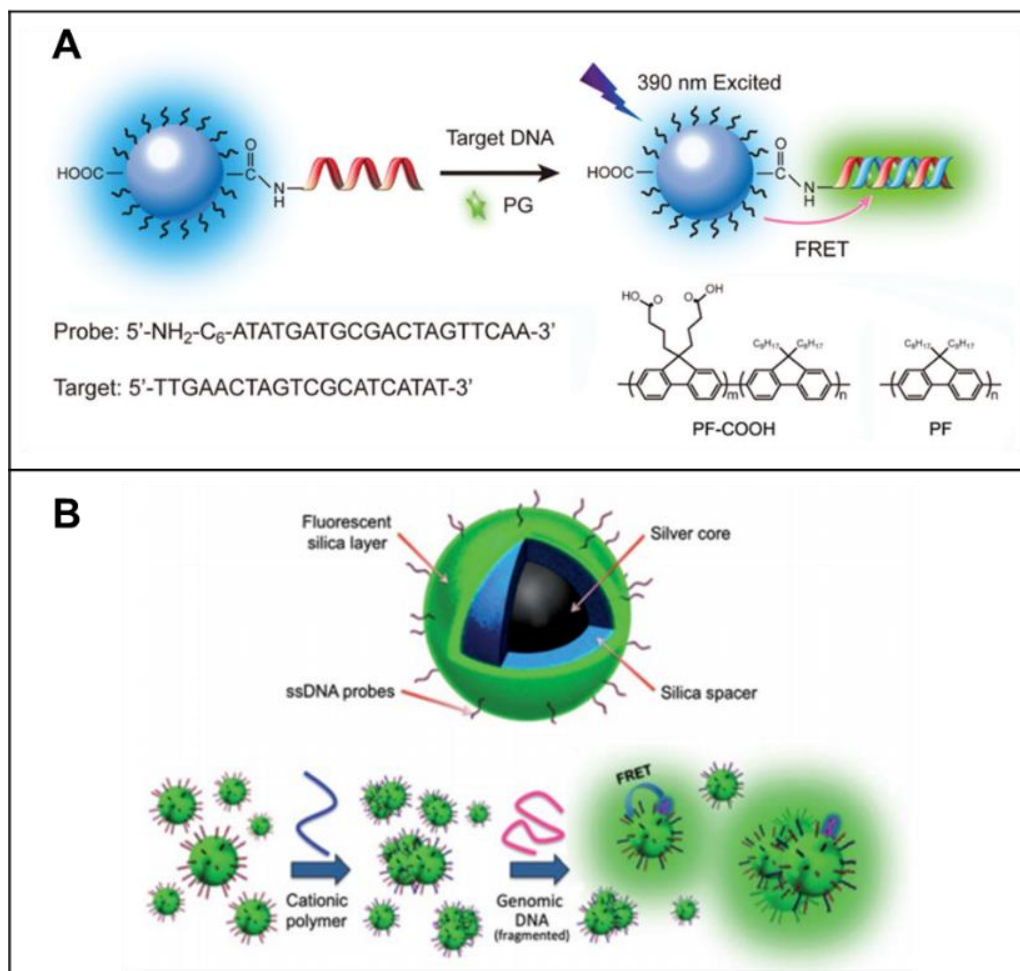


Fig.1.35. DNA detection using nanoparticles with conjugated polymer. A) Schematic illustration of the DNA probe based on CPNs. Adopted from ref.¹⁰⁵ B) Biosensor for DNA detection made of cationic polymer grafted on multi-layer core-shell nanoparticle. Adopted from ref.¹⁰⁶

Y. Wang and Bin Liu demonstrated a hybridization detection approach, where cationic polymer provided over 110-fold signal amplification for silica nanoparticles based assay.¹⁰⁷ They immobilized DNA-capture sequences on silica NPs and placed it in solution, where fluorescein-labeled DNA-target or mismatched sequences were added (Fig. 1.36). Target sequences would hybridize with a capture sequence and bring chromophore close to the surface of nanoparticles. Then the mixture was washed, so the non-binding sequences are removed and conjugated polymer was added. The CP here acts as an energy donor and non-specifically binds to double-strand DNA, which allows FRET to a chromophore (acceptor) attached to DNA-target. Such probe design led to an efficient energy transfer and strong signal amplification resulting in a low

detection limit of 10 pM concentration of DNAs target, which was possible to detect with a standard fluorometer.

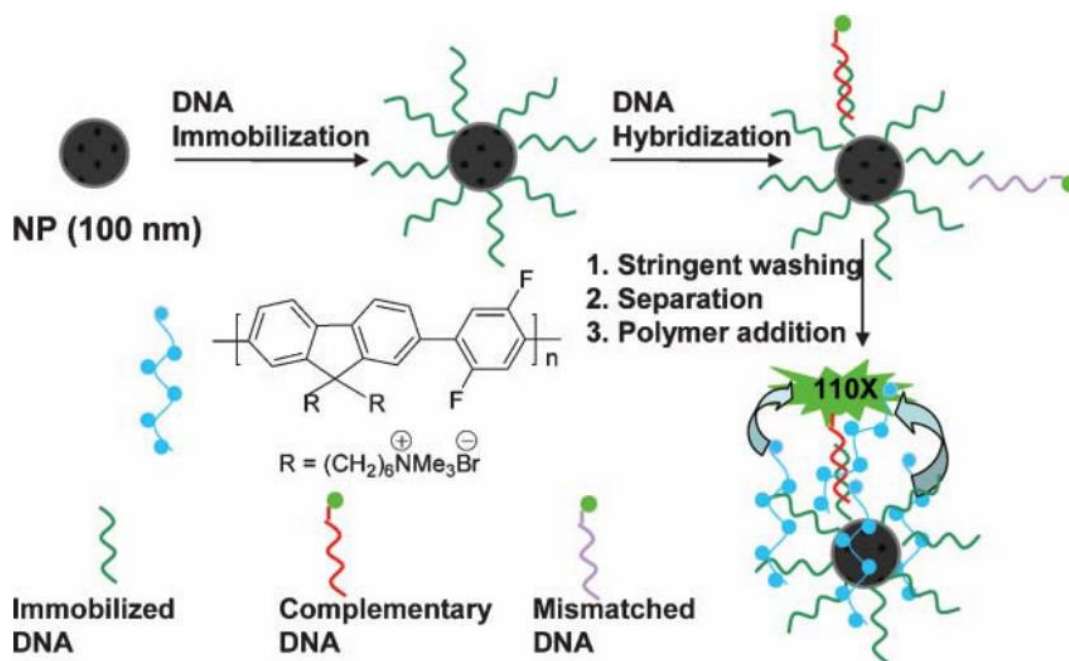


Fig.1.36. Cationic polymer-assisted Si-NPs based DNA assay. Adopted from ref. ¹⁰⁷

In this chapter, I have summarized basic DNA amplification methods and biosensors that use fluorescence response. For the moment, amplification strategies that employ molecular multiplication (PCR) are mainly applied for nucleic acid detection in clinical diagnostics and remain standards for research applications. There is still a lack of DNA biosensors that include external signal amplifiers and can be used for fast and reliable nucleic acid detection. Such a newly designed DNA amplified biosensor has the potential to revolutionize the diagnostic devices and provide methods for highly sensitive, specific, time and cost-effective detection and quantification of disease biomarkers.

FRET in dye-based nanomaterials

Dye-loaded silica NPs

Dye-doped nanoparticles typically act as FRET-donors in FRET-sensing applications.¹⁰⁸ Mesoporous silica nanoparticles (SiNPs) loaded with fluorescent dyes attracted great interest because of their tunable size, low cytotoxicity, and excellent cell imaging capability.³³ The surface chemistry for silica nanoparticles is well-investigated, which facilitates their use as sensors.¹⁰⁹

Dye-doped silica nanoparticles are a worthwhile nanocontainer, which permits fast and efficient energy transfer among dyes confined inside it.¹¹⁰ Moreover, some dyes doped inside silica nanoparticles demonstrate cooperative behavior, which means that the excitation energy

can be distributed within several donor dyes by means of homo-FRET and eventually directed towards the fastest energy transfer pathways. The rates of energy transfer can be adjusted by changing the distance between the dyes and their spectral properties. This leads to cooperative behavior, where the change in the status of one dye can resonate on many (up to all) other dyes in the nanosystem. So the single event (i.e. binding to the analyte) is signaled by the response of many dyes simultaneously, which is the reason for dye-doped nanostructures to undergo strong amplification effects, similar to that in conjugated polymers (Fig.1.37).

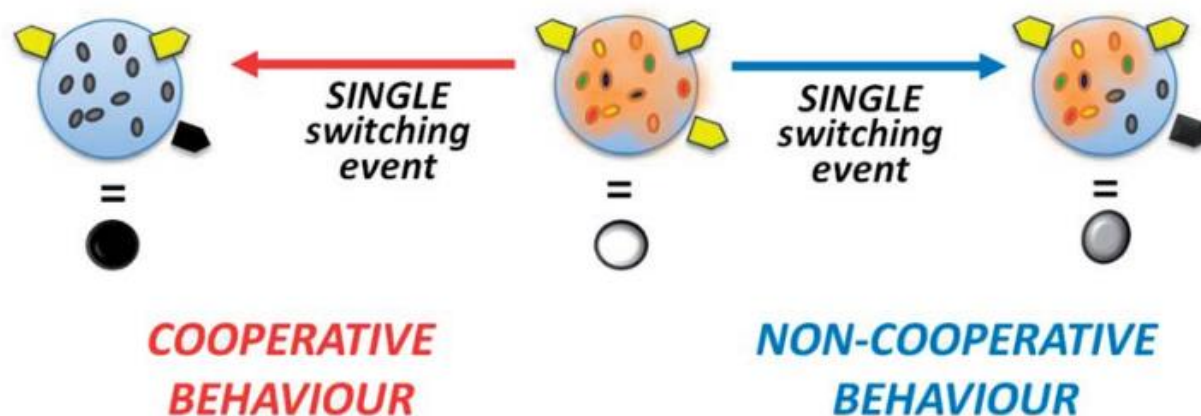


Fig.1.37. Schematic illustration of cooperative and non-cooperative effects in dye-doped nanostructures. Adopted from ref.¹¹⁰

Pluronic silica nanoparticles (PluS NPs) reported by a group of Prodi is an example of the system with cooperative behavior.¹⁰⁹ PluS NPs are obtained by a direct micelles-assisted method, using Pluronic F127 (polyethyleneglycol–polypropylene oxide–polyethyleneglycol (PEG–PPO–PEG) amphiphilic structure) as a surfactant. PluS NPs have a silica core of about 10 nm and an overall hydrodynamic diameter of 25 nm. The embedded fluorescent dyes in nanoparticle structure are homogeneously distributed and have high local concentration, which leads to efficient homo-FRET and finally high efficient one-step FRET from donor to acceptor. It was experimentally demonstrated,¹¹⁰ that in case of PluS NPs doped with ~4.5 dyes on average (covalently linked to the silica core), the excitation energy is distributed over at least 4 dyes, i.e. on almost all of the embedded dyes (Fig. 1.38). Also, for PluS NPs embedded with 10 rhodamine B dyes (donors), the presence of single cyanine dye (acceptor) per NP resulted in strong quenching (~90%) of the fluorescence of rhodamines.

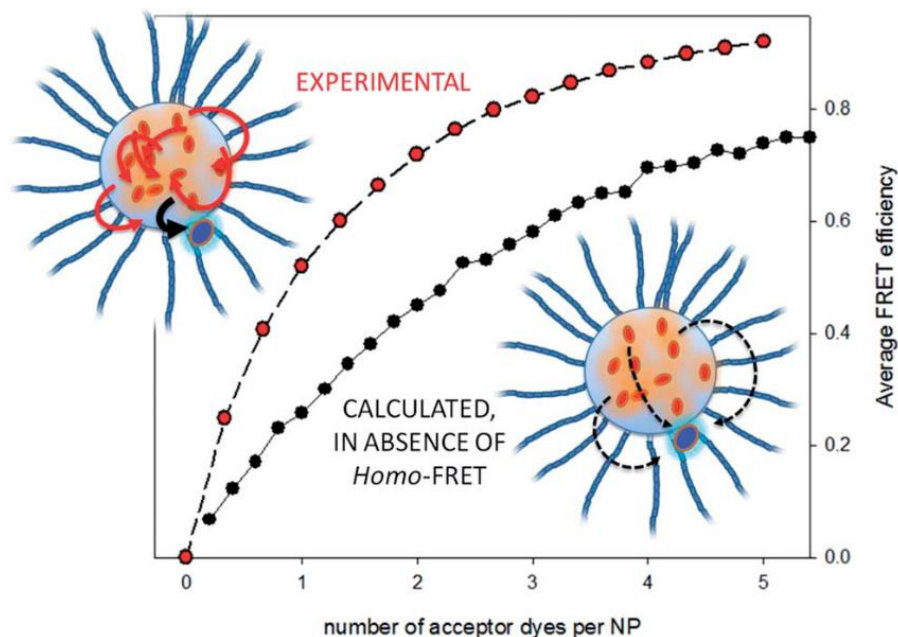


Fig.1.38. Experimental FRET efficiency (red dots) vs simulated average FRET efficiency (black dots). No homo-FRET between donors is considered in the simulations. Each point represents the average FRET efficiency for a set of 1000 NPs containing 10 donor dyes on average embedded in a 5.5 nm radius core, and an increasing number of acceptor dyes hosted in a very thin shell (0.2 nm). Adopted from ref.¹¹⁰

Rampazzo et al. reported the application of Plus NPs doped with coumarin dyes as the fluorescence sensor with amplified response to Cu^+ (Fig.1.39).¹¹¹ BODIPY-based sensor was hosted in the shell NPs, in stoichiometric ratio NP : dye = 1:1. Complex formation of BODIPY-sensor with Cu^+ increased the molar extinction coefficient of the BODIPY, which resulted in increased efficiency of energy transfer ($\sim 80\%$) from the ten coumarin dyes to a single acceptor sensor covalently linked to the shell of NPs. Compare with the free sensor, the energy transfer from nanoparticles provided 35% of emission enhancement at the same concentration of BODIPY.

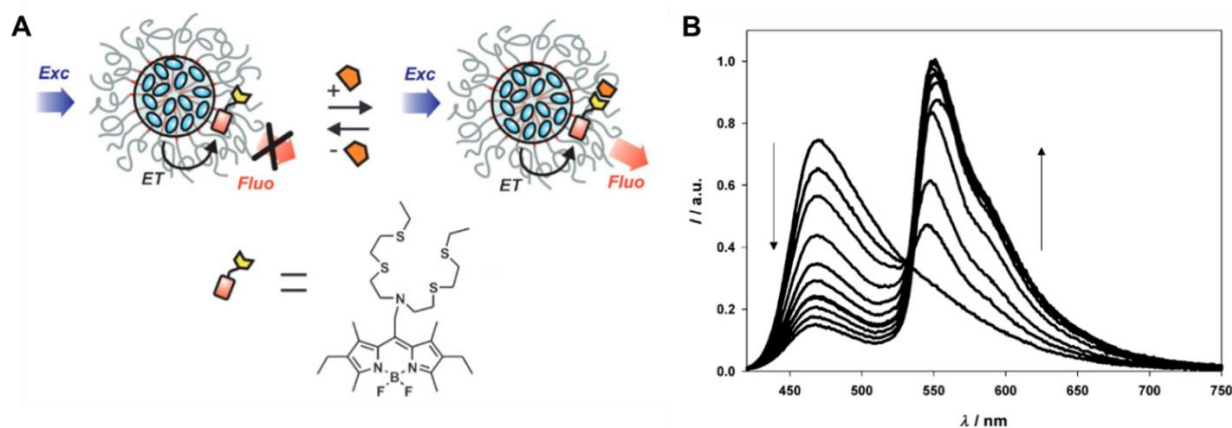


Fig.1.39. Fluorescent sensor based on PlusNPs with amplified response. A) Schematic illustration of the Cu^+ sensing mechanism. B) Fluorescence spectra of nanoparticle aqueous solution upon the addition of increasing amounts of chemosensor. Adopted from ref.¹¹¹

In another example, Gao et al. reported FRET-sensor based on fluorescein-doped silica nanoparticles as donors and AuNPs as acceptors for DNA detection (Fig.1.40).¹¹² In this assay capture sequence is attached to AuNPs and hybridize with short sequence attached to SiNPs, ensuring energy transfer between SiNPs and AuNPs, so that via excitation of SiNPs emission is quenched. In the presence of a target DNA sequence, it hybridizes with AuNPs-oligonucleotide, which leads to realise of SiNPs and fluorescence restores (turn on). The authors demonstrated a linear range response for target DNA in 0-35 nM range with a detection limit (3σ) of 3 pM.

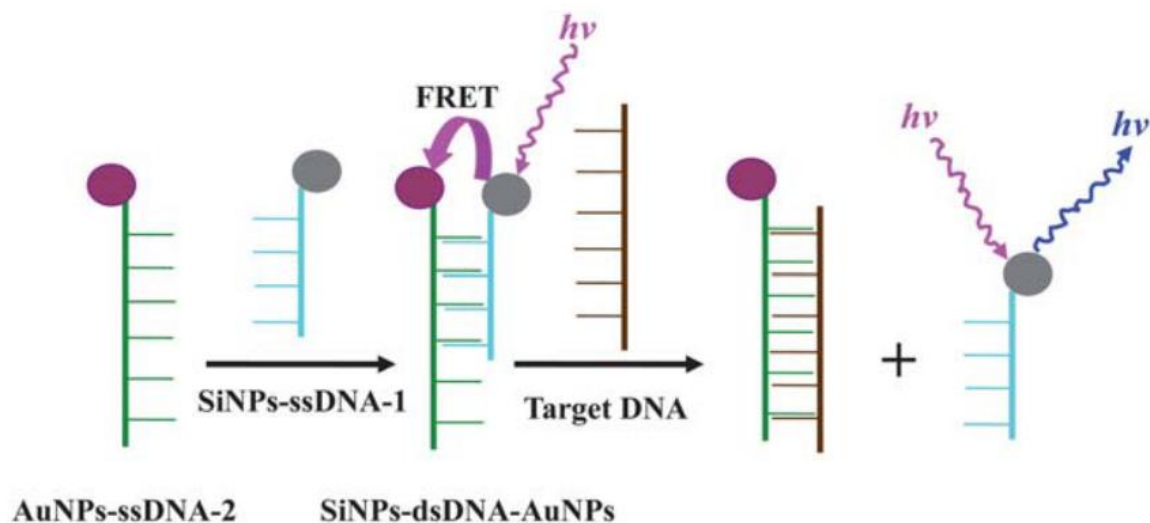


Fig.1.40. Schematic illustration of DNA hybridization detection based on FRET between SiNPs and AuNPs. Adopted from ref. ¹¹²

Aggregation-induced emission nanomaterials

Aggregation-induced emission (AIE) is a phenomenon when the dyes are non-emissive in an isolated molecular state but gained their emission in forms of aggregates.¹¹³ As, the concept of AIE hints to put chromophores together to gain their emission^{114,115}, placing the acceptor molecules close enough to AIE-donors would lead to energy transfer. But the accurate nanoantenna design requires controlled donor to acceptor ratio and their proper arrangement within the nanostructure. One way is an encapsulation of AIE-donors and acceptor molecules inside polymer nanoparticles.¹¹⁶ Here co-encapsulation of AIE-chromophores (AIE-genes) with NIR775 demonstrated 47-fold higher emission intensity by excitation via FRET (510 nm) than upon its direct excitation (710 nm).¹¹⁷ In another example, co-encapsulation of two AIE-genes (donor and acceptor) inside poly(styrene)-b-poly(methacrylic acid) nanoparticles demonstrated 99% of energy transfer and 8-fold amplification of acceptor emission.¹¹⁸

One more way to achieve nanoantennas with high amplification efficiencies is by using of supramolecular assemblies with incorporated AIE chromophores. Liu et al. reported a light-harvesting system, where supramolecular assembly of sulfato- β -cyclodextrin and oligo(phenylenevinylene) derivative (AIE-molecule) acts as a donor and Nile Red, loaded inside

this assembly via hydrophobic interactions, acts as acceptor (Fig.1.41A).¹¹⁹ The authors demonstrated that such system shows energy transfer efficiency of 72% and the antenna effect was calculated to be 32.5 at a donor/acceptor ratio of 125:1. In another report, Wang et al. fabricated light-harvesting system based on the supramolecular self-assembly of a pillar[6]arene (WP6) with a salicylaldehyde azine derivative, which acts as donor, and fluorescence dyes, either Nile Red or Eosin Y (acceptors), loaded within the hydrophobic interior of the obtained nanoparticles (Fig.1.41B).¹²⁰ The systems with Nile Red demonstrated energy transfer efficiency of 55% for the molar ratio of donor/acceptor 150:1, and antenna effect of 25.4, while the system with Eosin Y demonstrated energy transfer efficiency of 42% for the molar ratio of donor/acceptor 200:1, and antenna effect of 28.

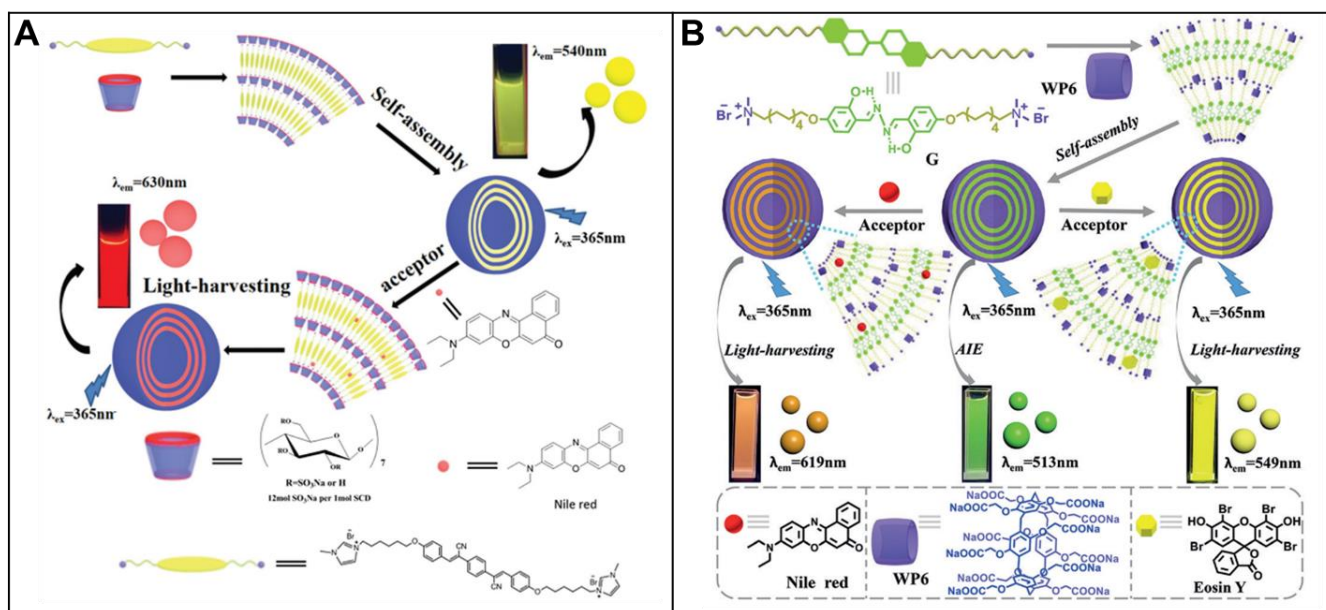


Fig.1.41. Supramolecular assemblies incorporated with AIE-genes. Construction of light-harvesting systems based on A) self-assembly of sulfato- β -cyclodextrin and oligo(phenylenevinylene) derivative with encapsulated Nile Red. Adopted from ref.¹¹⁹ B) Self-assembly of pillar[6]arene with a salicylaldehyde azine derivative and loaded Nile Red or Eosin Y. Adopted from ref.¹²⁰

Aggregation in the confined nanospace leads to systems with high energy transfer efficiency. Li et al. reported an artificial light-harvesting system entrapped in a cross-linked reverse vesicle (Fig.1.42A).¹²¹ In this system, the amphiphile formed the reverse micelles and AIE-genes (donor and acceptor) were entrapped inside it. The further cross-link of micelles and removing the organic solvent led to the placement of AIE-genes in confined space. The quantum yield of donor increased from 0.002 in chloroform to 0.42 in water, and energy transfer efficiency reached 95% at a donor/acceptor ratio of 100:1 with antenna effect of 35. In the most recent report, Tang and coll. made artificial light-harvesting systems based on a conjugated polymeric supramolecular network, which was built from the self-assembly of a pillar[5]arene-based conjugated polymeric host (CPH), that contained AIE-active units (tetraphenylethylene moieties, donors) and conjugated ditopic guests (diketopyrrolopyrrole or anthracene derivatives, acceptors)

(Fig.1.42B).¹²² In this design guests are binding to the cavity of a host, which prevents them from self-quenching and ensures efficient energy transfer. The highest antenna effect of 35.9 was achieved for the system dissolved in *c*-hexane, while in the solid film the antenna effect (AE) was 90.4 for the donor/acceptor ratio of 1000:1.

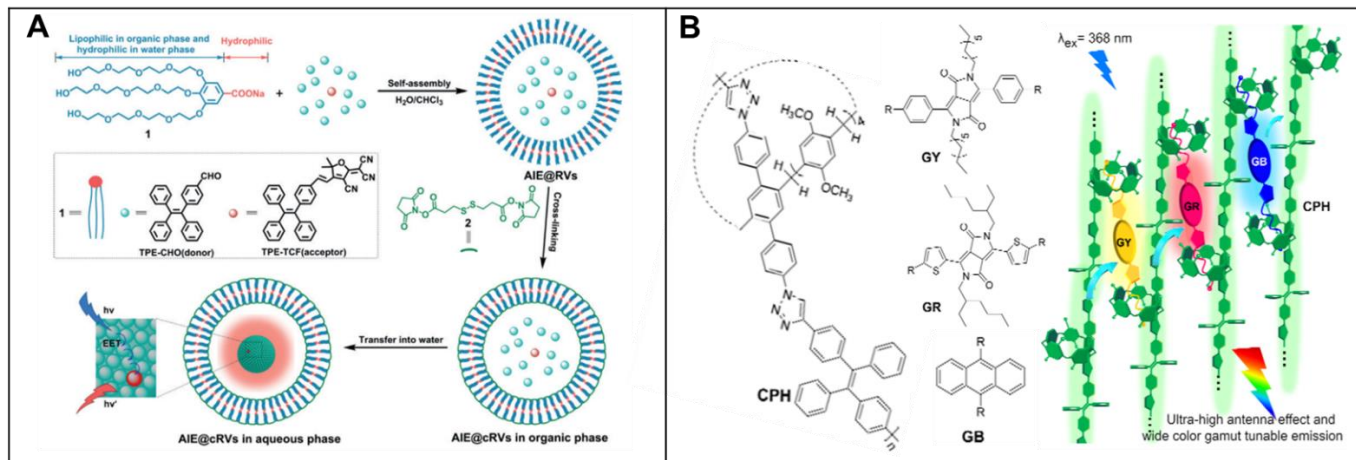


Fig.1.42. Construction of artificial light-harvesting nanoantennas (chemical structure of components) from A) AIE-genes entrapped in cross-linked micelles. Adopted from ref.¹²¹ B) Conjugated polymeric supramolecular network built from the self-assembly of a pillar[5]arene-based conjugated polymeric host (CPH) and conjugated ditopic guests (GY, GR or GB). Adopted from ref.¹²²

FRET in polymeric nanoparticles

Synthetic polymer-based NPs represent an important tool for drug or gene delivery since they are water-soluble, stable in a biological environment, capable of control drug release and biodegradable.¹²³ Polymer nanoparticles loaded with fluorescence dyes are superior bright fluorophores if they overcome aggregation-caused quenching, which could be achieved by few strategies: dye modification with bulky side groups, use of bulky hydrophobic counterions or aggregation-induced emission.⁹⁹ A large number of fluorophores in a small space makes their absorption coefficient $\epsilon > 10^7 \text{ M}^{-1} \text{ cm}^{-1}$ for 100 dyes with $\epsilon > 10^5 \text{ M}^{-1} \text{ cm}^{-1}$ each, which in case of high quantum yield and photostability overcome the limit of brightness of conventional dye molecules and fluorescent proteins. Thus polymer nanoparticles are attractive as bright fluorescent labels since their surface can be modified with a ligand and they can be loaded with dyes of different colors.¹²⁴

Polymer nanoparticles can be loaded with several dyes at a time, so that FRET between the dyes inside the nanoparticles can be used to learn their stability, monitor drug release and obtain systems with emission largely shifted to near-infrared region in comparison to excitation wavelength.⁹⁹ Such FRET systems with large Stokes shift reduce background autofluorescence for *in vivo* applications. Wagh et al. reported a series of nanoparticles for multicolor and multiplex imaging using a single excitation wavelength (Fig.1.43).¹²⁵ Authors encapsulated biocompatible poly(D,L-lactic-co-glycolic acid) (PLGA) and polyethylene glycol nanoparticles with a combination of fluorophores and by excitation observed multiple FRET cascade events. By

conjugation of such nanoparticles with ligands, they were applied to differentiate cancer cells in a mixture of cells *in vitro* and *in vivo*.

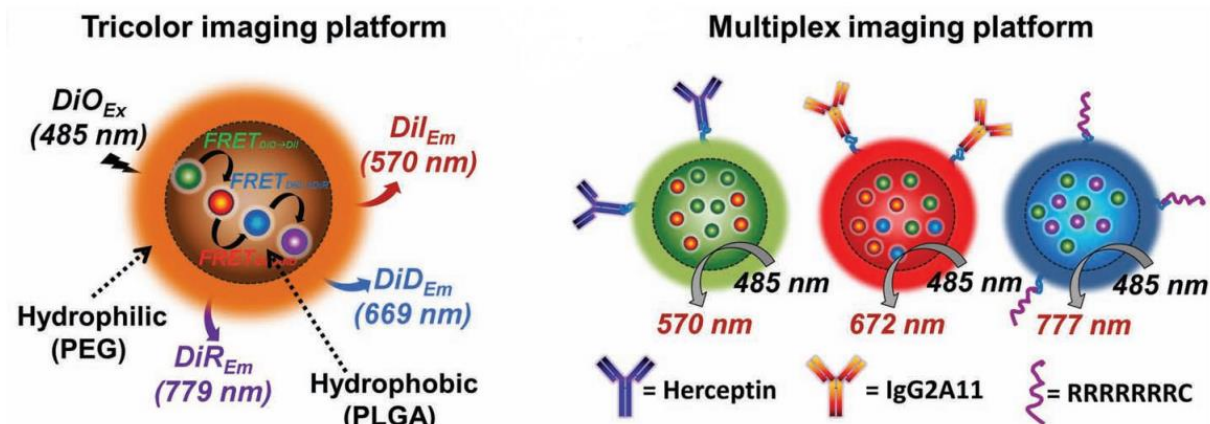


Fig.1.43. Schematic representation of nanoparticles designed for multicolor and multiplex imaging using one excitation wavelength. Adopted from ref.¹²⁵

The other way to obtain FRET inside polymer nanoparticles is to combine FRET-pair chromophores by their incorporation into the polymer structure. Here an interesting example is AIE-polymers. AIE polymers are obtained by incorporation of AIE molecules into a polymer chain and they demonstrate an additional advantage over small molecules since free rotation of AIE segments is restricted, which induce enhanced emission. By self-assembling of amphiphilic polymers or dispersion of hydrophobic polymers into the buffer the AIE nanoparticles can be obtained with tunable emission, tunable size, and strong fluorescence. AIE nanoparticles demonstrated their application for *in vivo* and *in vitro* imaging, gene delivery and sensors for small molecules. Wang et al. proposed conjugated polymer with color-tunable AIE behavior by adjusting their intramolecular FRET pairs as drug carriers (Fig.1.44)¹²⁶. They demonstrated that by placing one or two FRET pairs into the conjugated polymer, the color of AIE fluorescence can be changed from green to red.

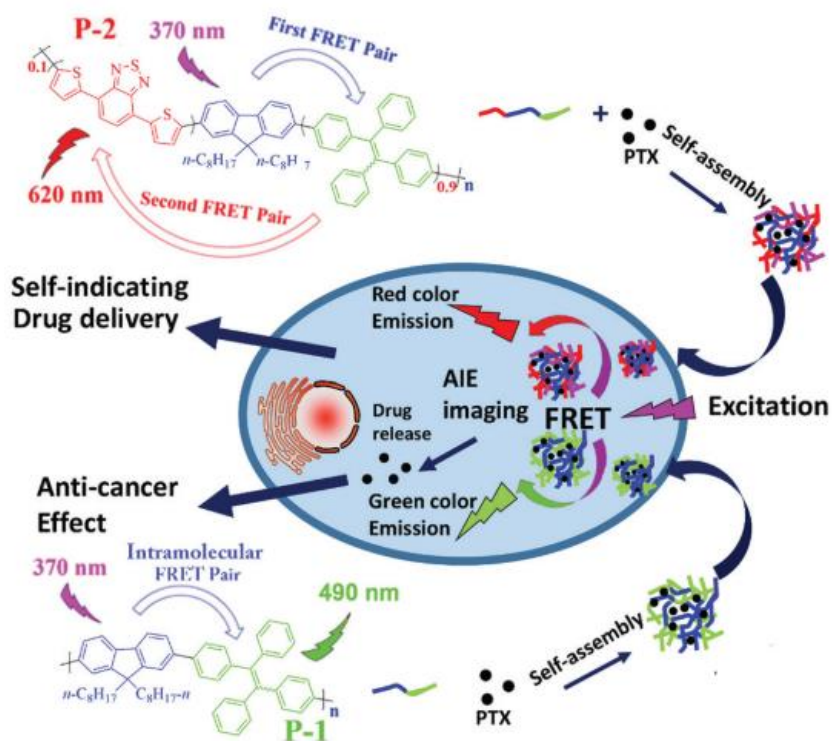


Fig.1.44. Color-tunable AIE-active NPs as drug carriers via adjusting intra- molecular FRET pairs. Adopted from ref.¹¹³

Generally, dye-loaded polymer nanoparticles are not yet well exploited as FRET biosensors in comparison to other nanomaterials like QDs, AuNPs, and UCNPs.⁹⁹ Nevertheless, some reports on FRET sensors for oxygen species, pH, temperature change and analytes as Cu(II) based on polymer nanoparticles are available.¹²⁷ Valanne et al. reported a dual-step FRET-based assay for the primary screening of caspase-3 inhibitors (Fig.1.13).¹²⁸ It is based on inter- and intramolecular FRET between fluorescent polymer europium(III)-chelate-doped nanoparticles and the two terminal labels in a caspase-3-specific substrate. In the absence of a target caspase-3 inhibitor, the emission is weak, because of dual-step FRET quenching technology that includes nanoparticle as a primary donor, Alexa 680, that is a primary acceptor and secondary donor and BlackBerry Quencher 650, which is secondary acceptor. In the presence of target protein, the substrate is hydrolyzed and fluorescence of Alexa is restored.

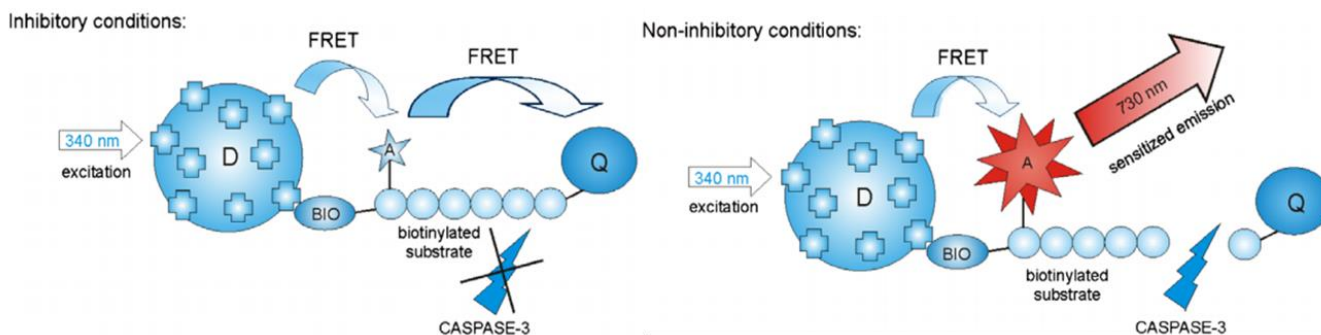


Fig.1.45. Dual-step FRET quenching assay for screening of caspase-3 inhibitors. Adopted from ref.¹²⁸

Doping of dyes inside the polymer nanoparticles lead to similar processes of energy transfer and development of artificial light-harvesting nanoantennas. Bhattacharyya et al. found that self-assembled molecular arrangement of quaterthiophene molecules inside 40 nm PMMA nanoparticles is an efficient light-absorbing antenna material.¹²⁹ By encapsulation quaterthiophene together with Nile Red dye molecules, the antenna effect was 3.2 (Fig.1.44A). Su et al. developed photoswitchable fluorescent NPs based on a diarylethene (DAE) benzothiadiazole (BTD) dyad (Fig.1.44B).¹³⁰ They were able to load 7000 dyad molecules inside 20 nm NPs and achieve superior brightness, which was 100 times higher than most common quantum dots. Moreover, the intermolecular FRET process between the fluorescent units and the photochromic moieties in their closed-form within the NPs created 'giant amplification of fluorescence photoswitching'. They calculated that 420 ± 20 molecules were quenched by a single switching event.

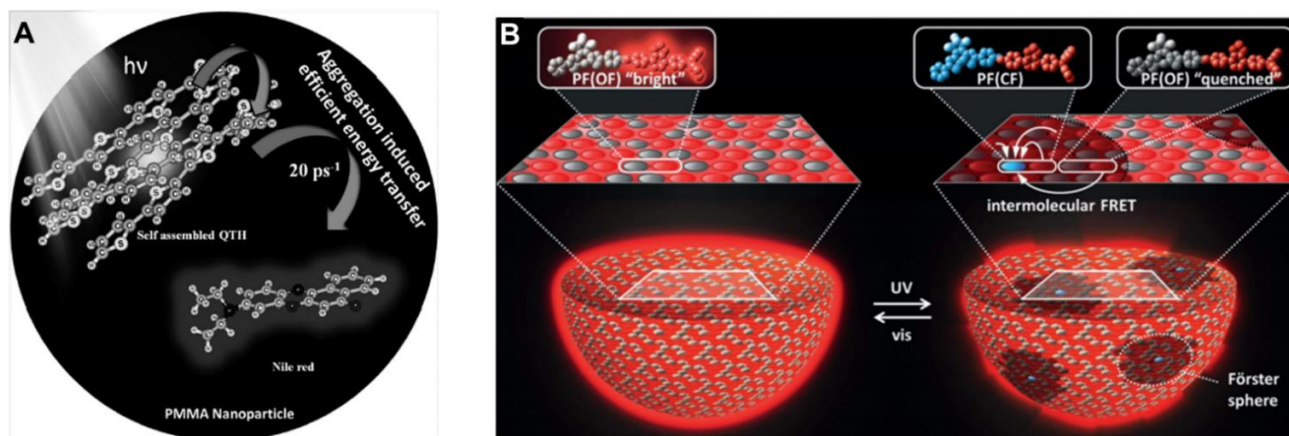


Fig.1.46. Artificial light-harvesting nanoantennas based on polymer nanoparticles. A) Schematic representation of the energy-transfer process from self-assembled quaterthiophene to Nile Red inside PMMA NPs. Adopted from ref. ¹²⁹ B) Illustration of the FRET-induced "giant amplification of fluorescence photoswitching" in NPs. Adopted from ref. ¹³⁰

Sensors based on polymer nanoparticles with efficient energy transfer were also reported. Larpent and co-workers propose FRET-sensor for Cu^{2+} ions based on fluorescent polymer nanoparticles with a copper-selective ligand (cyclam) attached to their surface. ¹³¹ Two fluorophores 9,10-diphenyl-anthracene (donor) and pyrromethene PM567 (acceptor) were embedded within the polymer core of 16 nm polystyrene nanoparticles (Fig.1.45). Authors marked, that FRET efficiency was 80% and 9-fold amplification was observed in the absence of copper. When the copper was present, it attached to the ligand creating quenchers (second acceptors) on the nanoparticle surface, resulting only in the emission of the donor. Nanosensors demonstrated linear response for copper concentration ranging from 10^{-8} to 10^{-5} mol L^{-1} with LOD of 20 nM.

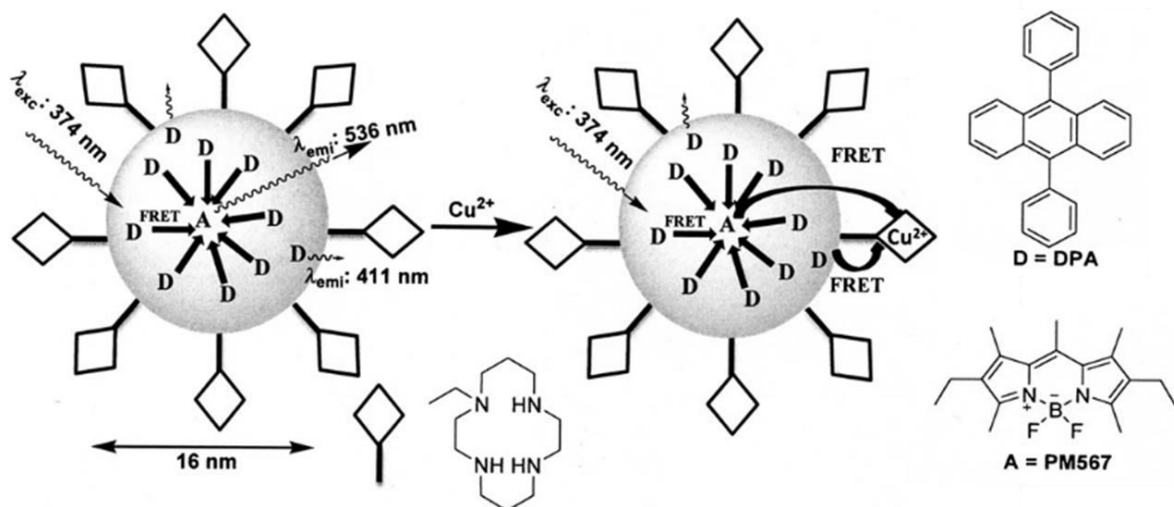


Fig.1.47. Schematic illustration of Cu^{2+} detection with polystyrene core-shell nanoparticles coated with a copper-selective ligand and embedded within the polymer core donor (D) and acceptor (A). Adopted from ref.¹³¹

Finally, our group introduced a concept of fluorescent polymeric nanoparticles, loaded with a cationic dye and a bulky counterion.³¹ The latter serves as a spacer minimizing aggregation and self-quenching of cationic rhodamine dyes (Fig.1.46A). The size of these NPs can be tuned from 10 to 50 nm by the nature of the polymer.^{132,133} Owing to high loading of NPs with dye/counterion pairs with minimal self-quenching these NPs were 10-100-fold brighter than quantum dots of comparable size. In addition to rhodamine, cyanine dyes can also be encapsulated with the help of bulky counterion, generating NPs of any desired color. The latter were applied multi-color barcoding of live cells and their long-term tracking in vitro and in vivo (Fig.1.46B).¹³⁴

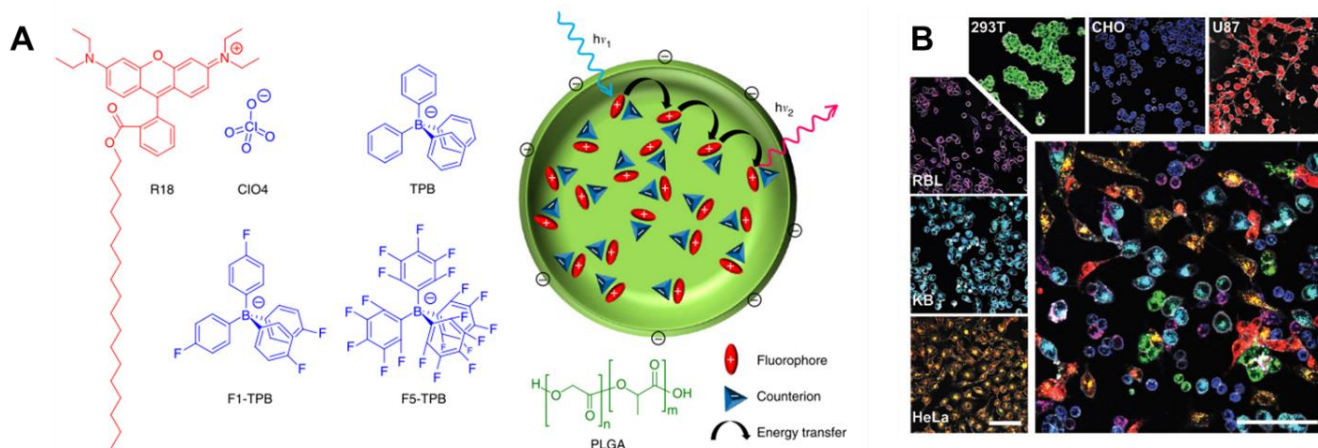


Fig.1.48. Dye-loaded polymer nanoparticles. A) Design of dye-loaded polymer nanoparticle using PLGA polymer with rhodamine B octadecyl ester and counterions. Adopted from ref.³¹ B) Confocal images of 6 cell types and a mixture of 7 co-cultured cell populations, incubated with dye-loaded polymer nanoparticles containing different dye-composition. Adopted from ref.¹³⁴

Importantly, our group recently discovered that the efficient energy transfer within donor dyes inside the nanoparticle could generate a giant light-harvesting antenna for amplifying the fluorescence emission of a single acceptor (Fig.1.47).⁶⁸ The nanoparticle of 65 nm in size are based on PMMA-MA polymer matrix and could encapsulate >10,000 donor dyes at 30 wt % loading corresponding to local dye concentration of ~ 500 mM. At this concentration, the average dye-to-dye distance is estimated to be 1-1.5 nm. Due to such small inter-dye distance, the excitation energy transfer is favored in the femtosecond range with a fast component below 30 fs. Together with a high quantum yield of donor dyes the nanoparticle efficiently transfers its excitation energy to a single acceptor placed stochastically within the nanoparticle at 10,000 to 1 donor/acceptor ratio resulting in ~30% FRET efficiency and antenna effect of ~1,000. In this case, a single acceptor has comparable brightness to the nanoparticles in the absence of the acceptor. Fascinatingly, bleaching of a single acceptor molecule was often followed by a one-step recovery of donor emission. The giant amplification enables the single-molecule detection at remarkably low excitation power, that are >10,000-fold lower than in typical single-molecule measurements. For acceptor absorbed at the surface of nanoparticles, the amplification was reached up to 200-fold. This means that obtained nanoparticles could be used as building blocks for biosensors with single-molecule sensitivity. For this application, the surface chemistry of dye-loaded nanoparticles should be developed, and the homogeneity of nanoparticles should be improved.

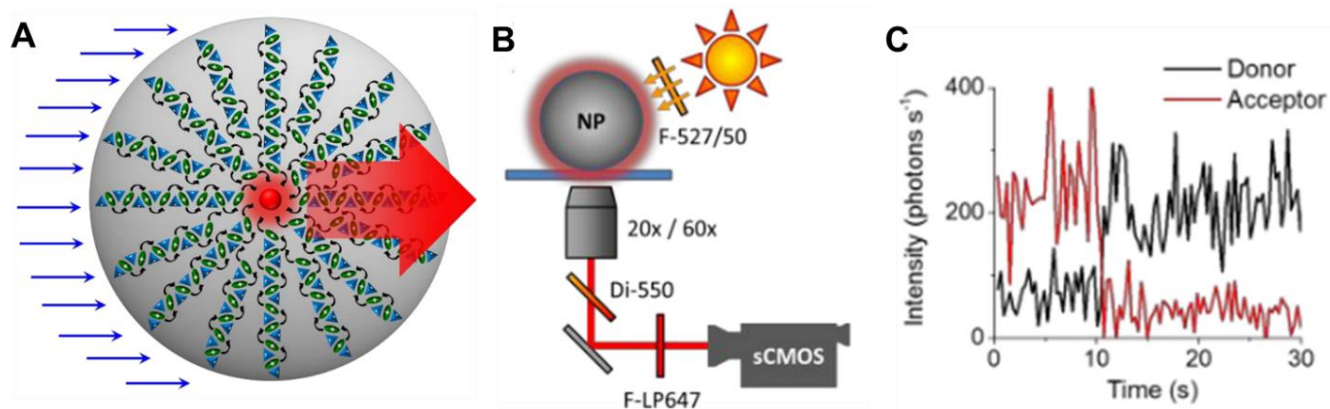


Fig.1.49. Giant light-harvesting nanoantenna for single-molecule detection at ambient light. A) Schematic presentation of the giant light-harvesting nanoantenna concept inside polymer nanoparticle, B) scheme of experimental setup using excitation that mimics direct sunlight, C) representative single-particle trace. Adopted from ref. ⁶⁸

1.4 Surface modification of nanoparticles

The key requirement for nanoparticles to be used as specific sensors, nanocarriers or fluorescent labels in bioimaging is a possibility to modify them with a capture molecule, like an antibody, receptor-ligand, oligonucleotide, etc. Moreover, surface modifications are also necessary to ensure the biocompatibility of nanoparticles, minimize non-specific interactions and make them cell-permeable.⁷⁹

The surface chemistry of nanoparticles obviously depends on their nature. In general, nanoparticles are modified in two steps: first is a surface activation and second is conjugation with ligands or surface protecting molecules (e.g. PEG).³³ Introduction of the functional groups to the surface of nanoparticles depends on ligand conjugation strategies as well as on the nature of nanomaterial.¹³⁵ For example, in the case of golden nanoparticles, alkane thiols are the common surface capping ligands. Generally, for inorganic nanoparticles surface functionalization with hydrophilic ligands through encapsulation, silica or polymer coating, or ligand exchange is necessary before their further reaction with capture molecules. In the case of silica nanoparticles, the different reactive functional groups can be introduced during the co-condensation process during their preparation.¹⁰⁹ For polymer nanoparticles there is also a vast variety of functional groups since they could be directly inserted in the polymer composition.

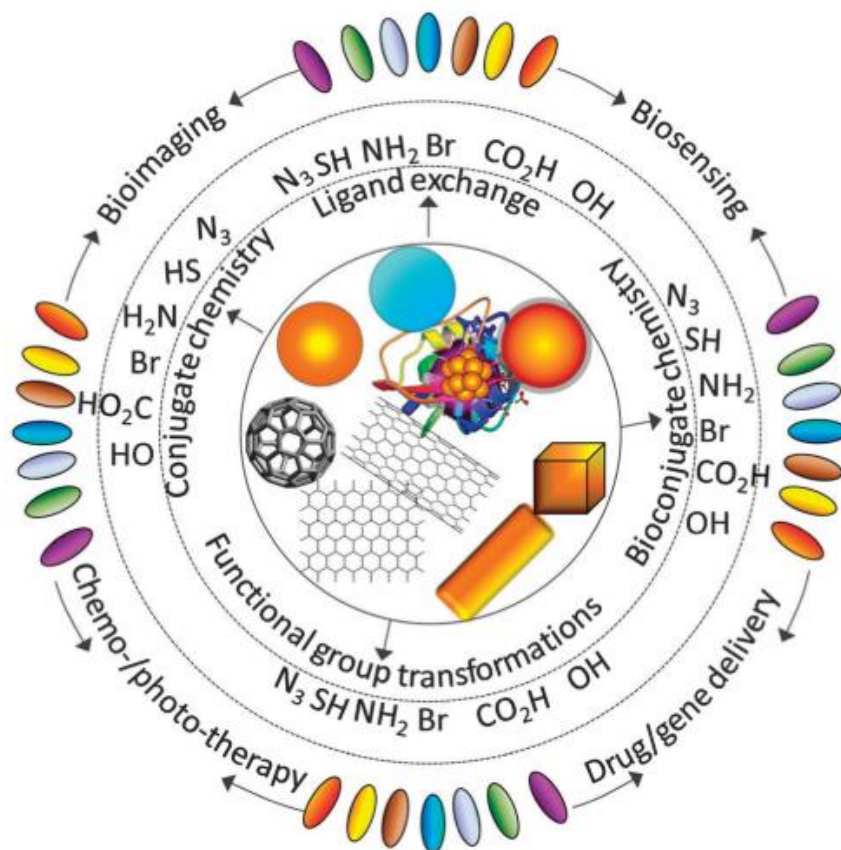


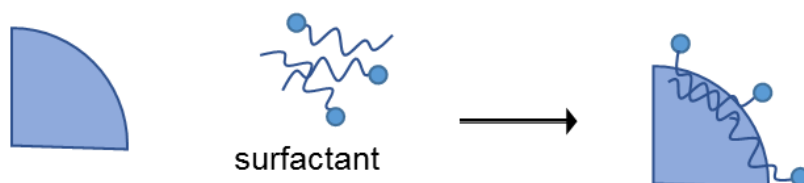
Fig.1.50. Examples of nanomaterials and their functional groups for biological applications. Adopted from ref.¹³⁵

The choice of the conjugation strategy (anchor ligand on the surface of the nanoparticles) depends on the properties of both systems (nanoparticle and ligand) as their size, available functional groups, chemical composition and further application of the obtained conjugate. The same conjugation strategies can be also used to cover nanoparticles with stabilizing molecules like PEG, zwitterionic molecules, glycans, etc. to preserve nanoparticle stability and integrity in biological fluids.

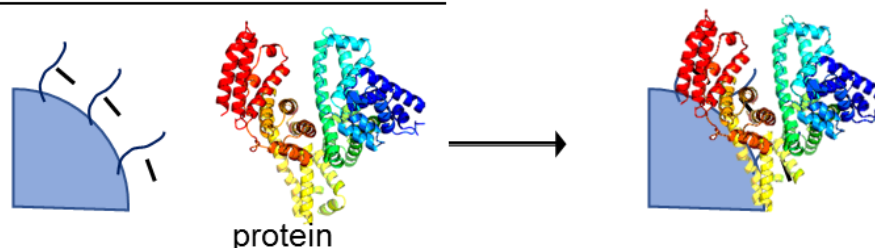
Methods for non-covalent attachment of ligand to nanoparticles surface

In general, all conjugation strategies can be divided into two types: noncovalent and covalent approaches. To noncovalent attachments belong non-specific absorption of molecules to the nanoparticle surface, electrostatic interactions and specific host-guest interactions (Fig.1.51).¹³⁶

1. non-specific absorption



2. electrostatic interactions



3. specific ligand-receptor interactions (e.g. biotin-avidin)

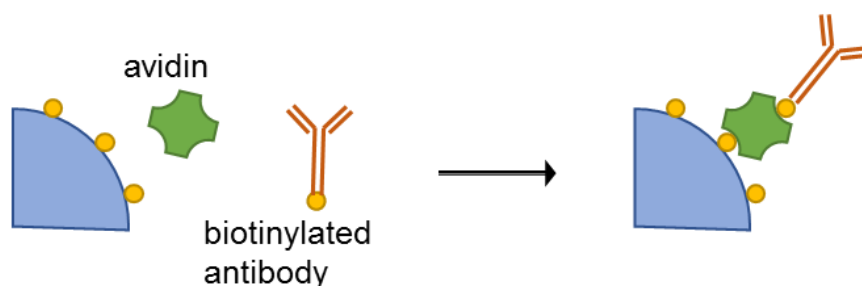


Fig.1.51. Representation of noncovalent attachments.

For nanoparticles, which have a hydrophobic surface after the formulation, the further covering with PEG bearing surfactants Tween 80 or Pluronic F127 is necessary to render them stable in salt media and prevent their interactions with serum proteins.¹³⁷ But since its non-covalent approach, it is not excluded that these surfactants would fall off from nanoparticles in biological media. Therefore, better approaches are either covalent linkage or a straightforward formulation of nanoparticles with a PEG shell.

Electrostatic attachment relies on interactions between oppositely charged species, and it strongly depends on ionic strength, pH and concentration of reagents. The negatively charged nanoparticles bind with positively charged proteins, e.g. BSA has been electrostatically immobilized on native or silanol-derivatized iron oxide NPs without observing protein denaturation.¹³⁸ Analogously, positively charged nanoparticles could be conjugated also with proteins and nucleic acids. Poly(ethyleneimine) (PEI) and poly(lysine) have been grafted to Au, silica and carbon NPs to provide the positively charged substrate for further attachment of oligonucleotides. These complexes with oligonucleotides were further employed as vectors for gene silencing.¹³⁹

Supramolecular host-guest binding is used in numerous biological applications. Biotin-avidin system is the strongest known non-covalent interaction with an association constant (K_a) 10^{15} M^{-1} . There is a huge amount of commercial materials available with different functions for biotin and avidin, which makes them easily applicable to bind to various molecules.¹⁴⁰ Therefore, researchers keep on using biotin-avidin interactions for biorecognition applications and it is routinely used at the initial development stage to demonstrate the “proof-of-concept”. Among all applications, it is a very popular method to attach the antibodies or DNA on the surface of nanoparticles. In the case of polymer nanoparticles, it is possible to incorporate the biotinylated “monomer” unit prior to nanoparticle formulation. Since avidin protein has four binding sites, the biotinylated biomolecule is crosslinked with the nanoparticle via an avidin intermediary. For example, using this method the transferrin was attached to PLA-PEG paclitaxel loaded nanoparticles for targeted drug delivery to brain tumor cells.¹⁴¹

Methods for covalent attachment of the ligand to nanoparticle surface

The covalent modification approach leads to a stable covalent bond formation between the nanoparticle and the ligand. The choice of the type of reaction would depend not only on the availability of both nanoparticle and ligand functional groups but also on reaction conditions and further reaction product purification. For most peptides and proteins, amino acid residues are targeted for conjugation: the ϵ -amino groups on lysine side chains, the N-terminal primary amines, the cysteine thiol, and the carboxyl groups on aspartic acid, glutamic acid or the C-terminus.¹³⁶ The nucleic acids typically provide ribose sugars, phosphates. However, for synthetic proteins and oligonucleotides, there is a possibility to insert site-specifically functional groups including azides, alkynes, carboxyl, thiols, amines, etc. Most typical conjugation reactions are listed in the Fig.1.52.

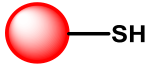
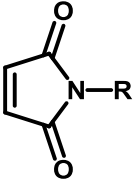
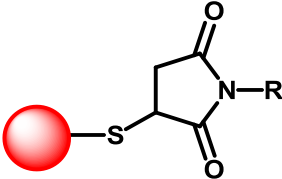
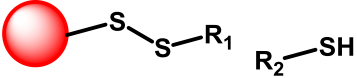
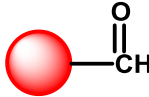
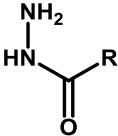
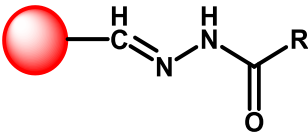
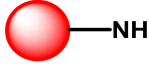
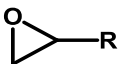
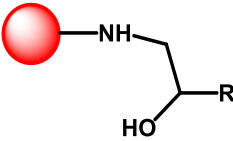
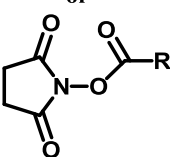
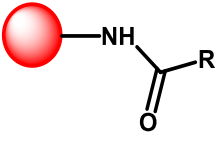
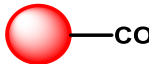
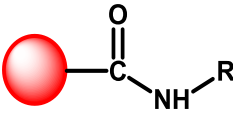
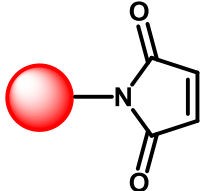
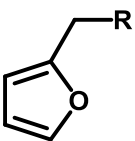
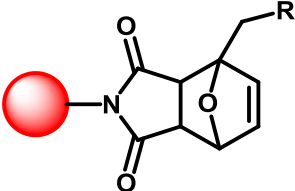
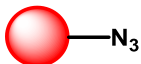
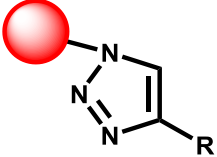
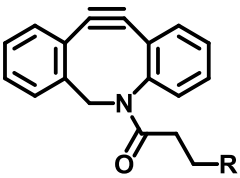
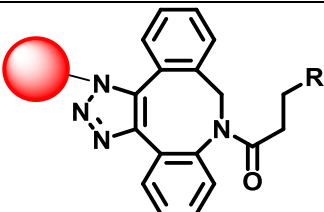
NPs	Ligand	Product: NP-ligand	Type of reaction
			Michael Addition
	$R_1-S-S-R_2$		Thiol exchange
			Hydrazone formation
			Epoxide opening
	$HOOC-R$ or 		Amide bond formation
	H_2N-R		
			Diels-Alder reaction
	$\equiv R$		Cu-catalysed click-reaction
			Cu-free click reaction

Fig.1.52. Selected NP functionalization chemistries.

When attaching biomolecules to nanoparticles or their labeling with the dye, it is necessary to be sure that reaction is selective towards desired reaction groups and do not lead to denaturation of protein or degradation of oligonucleotides. That is why the important concept in bioconjugation chemistry is bioorthogonality.^{142,143} Reactions are considered biorthogonal when the two reactive functional groups are highly chemoselective and do not react with other functional groups present in biological systems. The development of biorthogonal chemistry was driven by the desire of selective functionalization of target molecules inside the cells and tissues. Therefore, biorthogonal reactions should proceed in water at near-neutral pH between 25 and 37 °C, and should not involve cytotoxic reagents or by-products.

Practically biorthogonal chemistry is a subclass of “click”-chemistry, which recently gained its popularity. The reaction considers as “click” if it is i) modular, ii) high yield, iii) wide in scope, iv) produce nontoxic by-products. The “click” reactions include certain cycloadditions, nucleophilic substitutions, nonaldol carbonyl formations, and epoxidations. The most popular “click” reaction is the Huisgen 1,3-dipolar cycloaddition of azide and alkyne to form 1,2,3-triazoles.¹⁴⁴ It requires Cu(I) as a catalyst, which usually *in situ* generated from CuSO₄ and ascorbic acid, and commonly referred to Cu(I)-mediated [3+2] azide-alkyne cycloaddition (CuAAC). Despite the fact that CuAAC is widely used for conjugations, the metal’s toxicity limits its usage in living systems. The other way to increase the reaction rate without a catalyst is to use the ring-strained alkynes.¹⁴⁵ For cyclooctyne the bond angle of the sp-hybridized alkynes is 160°, which is distorted towards the transition state of the cycloaddition reaction, resulting in dramatic reaction acceleration without any catalyst. Bertozzi and coworkers had evaluated the cyclooctyne derivatives which undergo cycloaddition with azides with much vastly accelerated kinetics than linear azides (Fig.1.53).¹⁴⁶ Then, Boons group demonstrated that functionalized derivatives of dibenzocyclooctyne (DBCO) enhance reaction kinetics.¹⁴⁷ These molecules can be readily synthesized with various derivatives at aryl positions to enhance their solubility. So far, many other cyclooctyne derivatives have been synthesized and used as reagents for biorthogonal reactions in biological applications. For example, Bertozzi showed that the cyclooctynes were able to selectively label cells that had metabolically incorporated azidosugars onto their surface as glycoproteins.¹⁴² Due to the growing popularity of Cu-free “click” chemistry, there are numerous commercial available cyclooctyne derivatives with different functional moieties for conjugations.

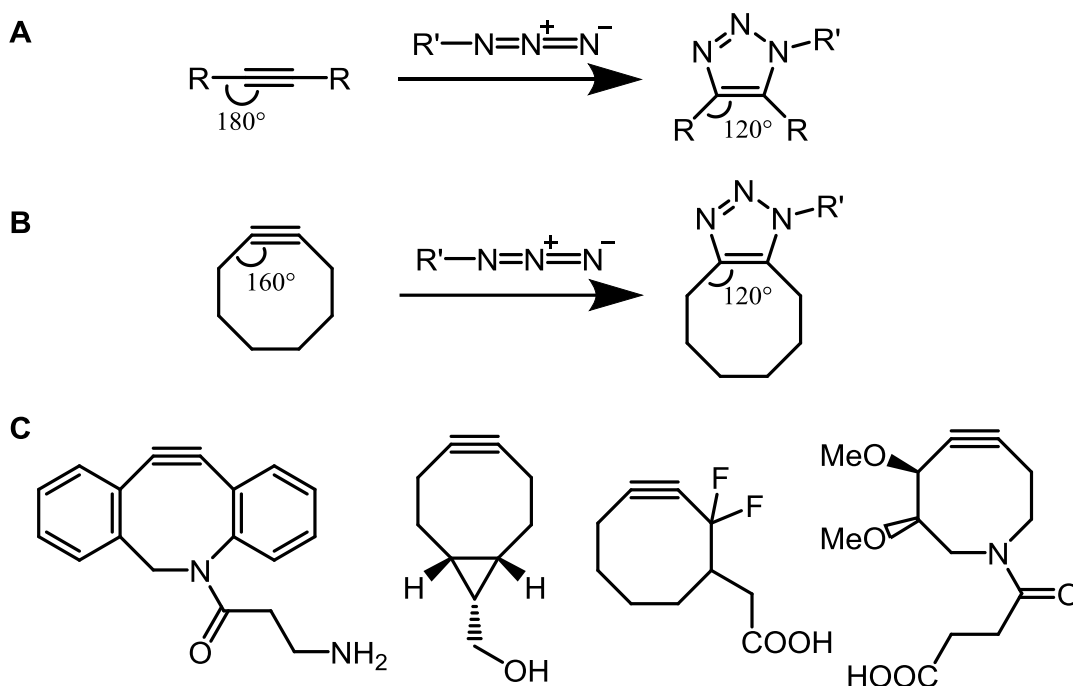


Fig.1.53. A comparison of bond angles between A) linear alkynes and triazoles, B) strained cyclooctyne and its corresponding triazole product, C) cyclooctyne reagents for copper-free “click” reaction. Adopted from ref.¹⁴²

Polymer nanoparticle-DNA conjugates

The coupling of nucleic acids and nanoparticles creates new composite materials that unite their both properties and could be used for diverse applications including biosensing, target imaging, diagnostics, cellular delivery, etc. It was already synthesized the composite of oligonucleotides with AuNP, QDs, AgNP, UCNPs, carbon nanomaterials, micelles, magnetic, silica, viral and polymer nanoparticles.⁸⁴

For polymer nanoparticles, there are two principal ways to insert the oligonucleotides on the nanoparticles surface: conjugation of oligonucleotides with polymer prior nanoparticle formation or direct conjugation of oligonucleotide with nanoparticles, like in case of AuNPs.¹⁴⁸

The prior modification requires to perform the chemical reaction between the polymer and oligonucleotides, where appears the incompatibility in terms of solubility issues between the hydrophobic polymer and the hydrophilic DNA. But for hydrophilic polymers, it is not a case since the reaction could be performed in an aqueous phase. It was demonstrated that amino-functionalized oligonucleotides react with carboxylic terminated polymers like PEG, poly(N-isopropylacrylamide) (PNIPAM), PLGA and poly(p-phenyleneethynylene) to form an amide bond. Another popular method is conjugation via disulfide bond or Michael addition (Fig.1.52).

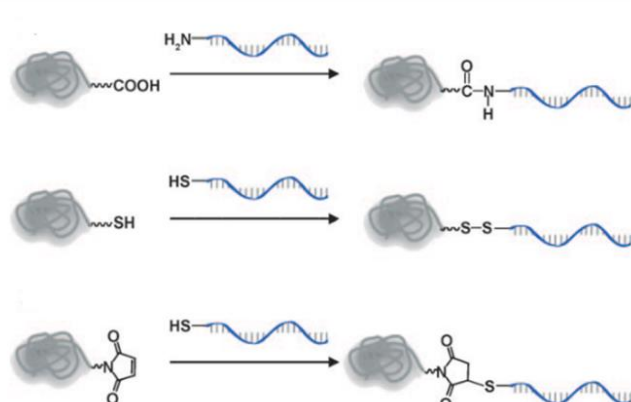
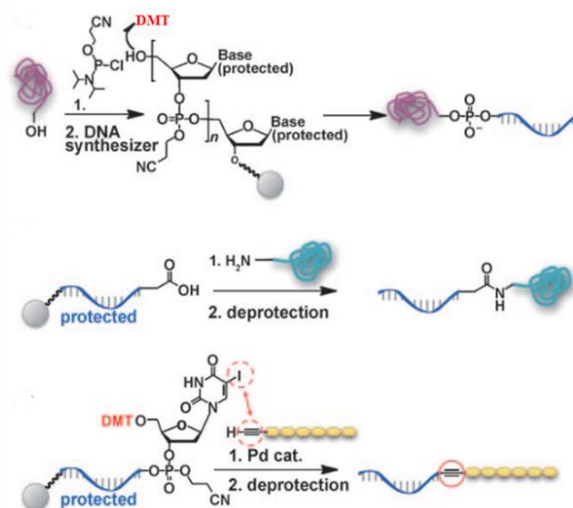
A Coupling methods in solution**B** Coupling reactions on solid support

Fig.1.54. Methods of synthesis of DNA block copolymers. A) Coupling methods in solution including amide coupling, disulfide bond formation and Michael addition. B) Coupling reactions on solid support including phosphoramidite activated coupling to 5'-OH group of DNA, amide coupling and Pd-catalyzed Sonogashira coupling. Adopted from ref. ^{148,149}

Wilks and O'Reilly investigated DNA covalent conjugation to poly(*N*-isopropylacrylamide) in organic solvents.¹⁵⁰ They checked amide coupling, thiol-ene chemistry and Diels-Alder reaction in *N,N*-dimethylformamide, *N,N*-dimethylacetamide and *N*-methyl-2-pyrrolidone and discovered that first two type of reaction failed to yield significant amounts despite their high efficiency in water in case of hydrophilic polymers. In case of Diels-Alder reaction between norbornene and tetrazine it was possible to follow product formation but yields were still low.

However, hydrophobic polymer-DNA coupling is rather difficult, so the most used strategy for hydrophobic polymers is their grafting onto DNA on a solid support.¹⁴⁹ When DNA is present on a resin the phosphate groups are still protected, so it allows oligonucleotides to be dissolved in organic solvents. DNA diblock copolymers, e.g. DNA-*b*-poly(propylene oxide) was obtained via reaction of DNA detritylated 5'-OH group with activated terminal polymer hydroxyl group with phosphoramidite chloride.¹⁵¹ Similarly, Mirkin group synthesized polystyrene-DNA conjugate on controlled pore glass beads and demonstrated further formation of 16 nm micelles with DNA corona by resuspension of amphiphile in water.¹⁵² But this approach requires expensive DNA-synthesizer equipment so that it is difficult to perform it in a conventional chemical laboratory.

The other concept is a direct modification of nanoparticles with the oligonucleotides. To our knowledge, there are only several examples of direct covalent attachment of DNA to polymer nanoparticles. Nguyen and coll. reported synthesis doxorubicin-loaded polymer organic nanoparticles covered with DNA through direct surface functionalization.¹⁵³ They synthesized block-copolymer which contained PEG-chain with a free carboxylic group exposed to the surface of the nanoparticles and further used for amide coupling with amine-terminated oligonucleotides

(Fig.1.55A). Obtained nanoparticles of 65 ± 5 nm demonstrated excellent stability in cell-culture media and were readily internalized by the cells. In another report, nanoparticles were formulated from PLGA-PEG-N3/PLGA with a size of ~ 50 nm.¹⁵⁴ They were modified with a DBCO-terminus oligonucleotides (20 NA) by copper-free click reaction (Fig.1.55B). In this way, so-called PLGA-SNAs (spherical nucleic acids) were obtained with a size of 65 nm determined by DLS. Authors also demonstrated that these nanoparticles readily enter cells without the use of transfection agents.

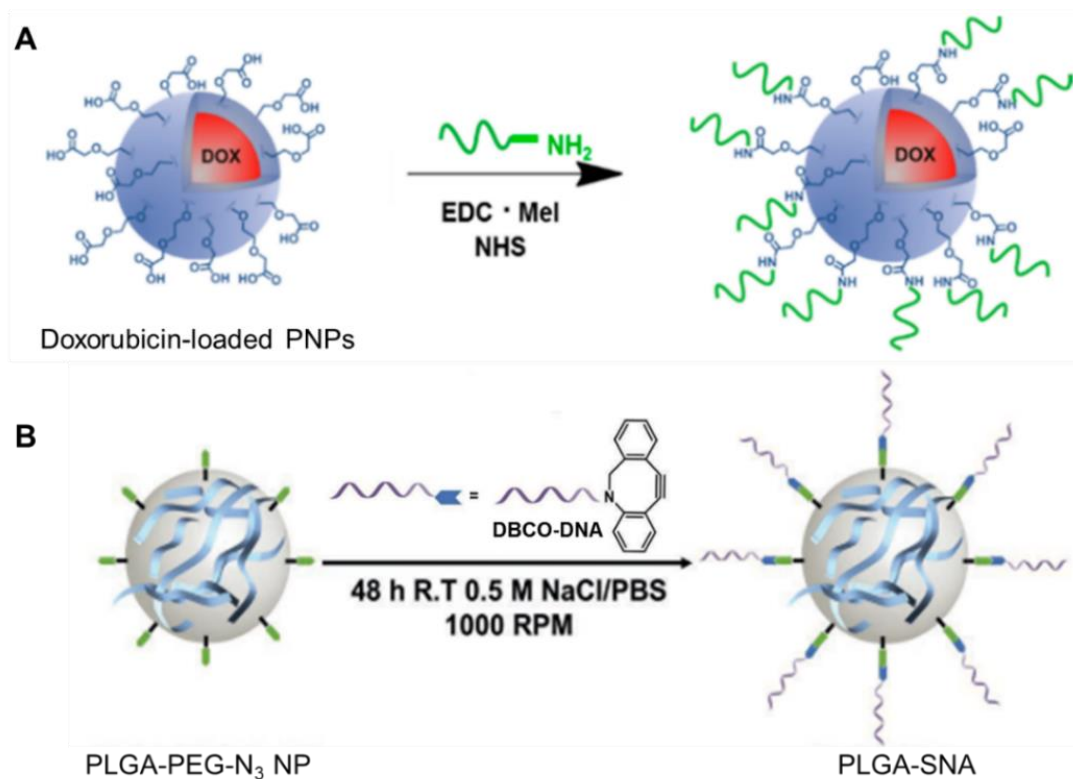


Fig.1.55. Polymer nanoparticle-DNA conjugates by direct surface functionalization. A) Modification via amide coupling of doxorubicin-loaded polymer nanoparticles with DNA.¹⁵³ B) Modification via copper-free click reaction PLGA-PEG-N₃ nanoparticles with DNA.¹⁵⁴

The nanoparticle-DNA conjugates create new composite nanomaterials by uniting properties of both, where polymer nanoparticle could act as a carrier or ultra-bright fluorescent label and the oligonucleotide represents a recognition element. Methods to attach DNA to commercially available hydrophobic polymers are not fully established. Reaction on solid support requires special equipment, while direct surface functionalization is not yet well mastered.

AIM OF THE PHD THESIS

Fluorescent nanoparticles reveal unique optical properties since they are many times brighter than organic dyes or fluorescent proteins. An integration of a biomolecule with a nanoparticle leads to a hybrid nanostructure that combines both their features and results in a new nanomaterial with advanced functionality.

To date, our group developed ultrabright dye-loaded polymeric nanoparticles.³¹ They feature a small size (10-100 nm), which is controlled by the nature of the polymer. The encapsulation of dye with bulky counterion minimizes dye self-quenching and preserves the exceptional brightness of the nanoparticle. It was found that these nanoparticles operate as giant light-harvesting nanoantenna capable to amplify emission of single dye molecules >1000 fold.⁶⁸ Such unique feature enables for the first-time detection of single molecules in ambient light excitation conditions. In order to convert such nanoparticles into nanoprobess for biomolecules, their surface should be functionalized in order to attach a sensor molecule.

The highly important biomarkers in biological research and medical diagnostics are nucleic acids.¹⁵⁵ The demand for diagnostics is an ability to detect the ultralow concentration of nucleic acid target, which requires the use of amplification techniques. PCR is a “golden-label” technique for nucleic acid detection, but it is complex and requires expensive reagents and equipment.⁴⁵ The rapid detection directly from cell lysates without complex purification and PCR amplification would accelerate the research in the field and open the new route to low-cost diagnostics tools and point-of-care tests.

The objectives of my thesis were to develop strategies for the functionalization of polymeric nanoantenna particles with oligonucleotides and to convert these nanoparticles into ultrasensitive nanoprobess for nucleic acids, which respond to a single hybridization with a target nucleic acid molecule by a change of their emission color.

To follow these objectives, a workplan of the thesis consisted of main three steps:

1. To design and synthesize small nanoparticles with large dye content, which contain reactive groups on the surface for further modifications;
2. To graft oligonucleotides to the polymeric nanoparticle surface and develop a nanoprobe for amplified detection of the nucleic acids.
3. To develop a system, where nanoparticle would change its fluorescence color in response to a single target oligonucleotide and apply it for the detection of target nucleic acids in cell lysates.

PART 2. RESULTS AND DISCUSSIONS

2.1 Investigation of methods that lead to surface functionalized dye-loaded polymeric nanoparticles

Introduction

Nanoprobes have major advantages over molecular probes in terms of their multifunctionality: designed size, structure and presence of capture moieties lead to superior performance in comparison with conventional molecular probes.⁷⁹ The key requirement of nanoprobes is their specificity which can be achieved by attaching ligands to nanoparticle surface that would lead to selective recognition of target or molecular environment. There were demonstrated examples of surface modification of polymer nanoparticles by adsorbing proteins or surfactants on their surface, which led both to the stabilization of nanoparticles and their functionalization. But the most of robust nanoprobe design is based on covalent attachment of ligands to the surface. This would eliminate false-positive results, which are consequences of a detachment of ligand adsorbed to the surface of nanoparticle.¹³⁵

Polymeric nanoparticles have advantages over inorganic nanoparticles: the attachment of the ligand can be done either through polymer functionalization prior NPs formulation or through modification of already formulated NPs (Fig. 2.1).

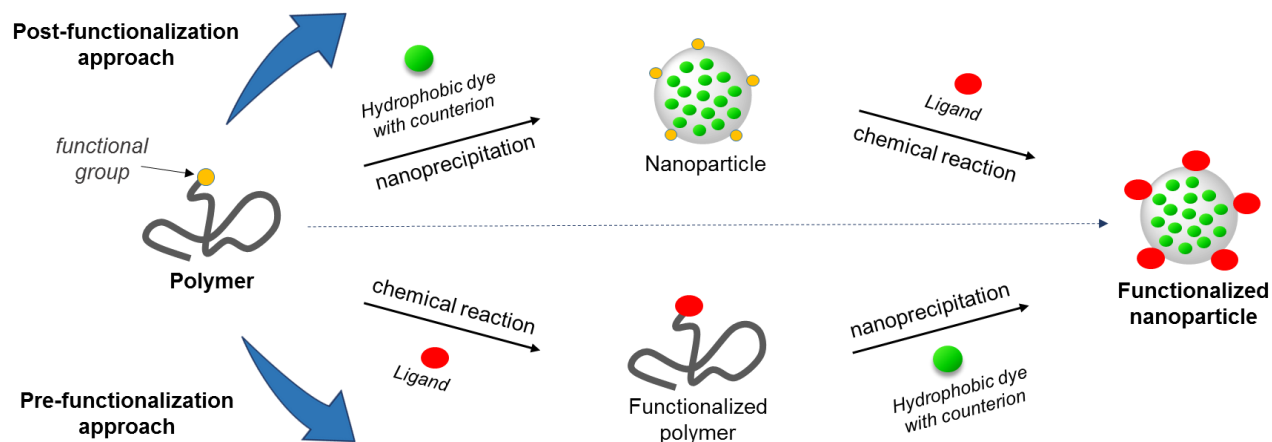


Fig. 2.1. Two principle approaches to obtain functionalized dye-loaded nanoparticles starting from the polymer.

In this part of the project, we investigated two principle approaches that lead to surface functionalized dye-loaded nanoparticles. The first approach was a post-functionalization, where the ligand is attached to the nanoparticle after its formulation. The second approach was a pre-functionalization, where initially ligand was attached to the polymer prior to nanoparticles formulation. Based on the obtained results, we designed the nanoprobes for a reduction environment and demonstrated their performance in cells.

Post-functionalization of polymeric nanoparticles

Firstly, we investigated a post-functionalization approach. As the basis, we chose the PMMA-MA polymer, since it gave small nanoparticles and demonstrated efficient encapsulation of dyes without a leakage.¹³² As the coupling method we selected a copper-free click cycloaddition. It is a two-component, easy-handling reaction¹⁴² and it has already proven its efficiency for coupling of small molecules to nanoparticles.¹⁵⁴ To obtain azide-bearing polymer, we initially synthesized PMMA-N3 by coupling commercial PMMA-MA with 3-azido-1-propamine (Fig 2.2A).

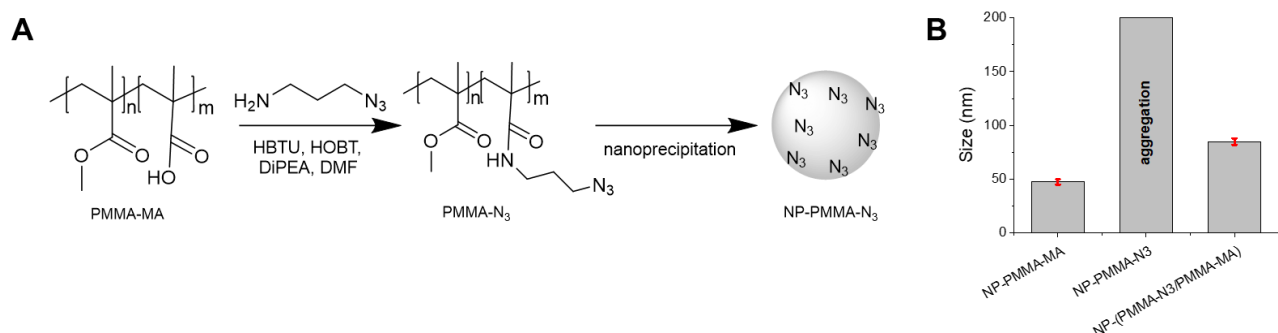


Fig.2.2. Synthesis and characterization of NP-PMMA-N3. A) Scheme of synthesis of PMMA-N3, B) Size by DLS of NP-PMMA-MA, NP-PMMA-N3, NP-(PMMA-MA/PMMA-N3).

However, after nanoprecipitation of an acetonitrile solution of the corresponding polymer into an aqueous buffer (pH 7.4), we failed to obtain small-sized nanoparticles due to the absence of charged groups in the polymer structure (Fig. 2.2B). Then, we nanoprecipitated the mixture of PMMA-MA/PMMA-N3, consisted of equal aliquots of each polymer, but this also led to comparatively large nanoparticles. In both of these systems, azide groups due to their hydrophobicity are hidden inside the polymer matrix and stochastically exposed to the surface of aggregates. Nevertheless, our aim was to obtain the nanoparticles with fully exposed functional azide groups on the surface.

Previous reports from our group demonstrated the role of charge in order to obtain small nanoparticles.¹³² Therefore, to have functional groups on the surface, it should be linked to the charged group, that would pull it out of the polymer matrix during nanoprecipitation. Thus, the commercial PMMA-MA was coupled with a three-functional linker containing (i) carboxyl as a charged group; (ii) azide for further “click” reaction; and (iii) amino group for conjugation with the polymer. As a building block, we chose the biprotected aspartic acid, commonly used for solid-phase peptide synthesis, Fmoc-Asp(OtBu)-OH (Fig.2.3A). Its carboxylic function was modified with 3-chloropropylamine, and then the chlorine was substituted with an azide, which resulted also in Fmoc removal giving the linker Asp(OtBu)-N3. In order to have more charged groups we decided to couple it with two more Fmoc-Asp(OtBu)-OH and obtained second linker Asp3(OtBu)-N3. Then, linkers were coupled with PMMA-MA through an amide bond. The obtained polymers were characterized by H-NMR, where characteristic protons of the polymer and the Boc-group of the linker were identified. Finally, the removal of tert-butyl group in the

presence of TFA resulted in PMMA-AspN₃ and PM-Asp₃N₃ polymers (Fig.2.3B), which was confirmed by NMR.

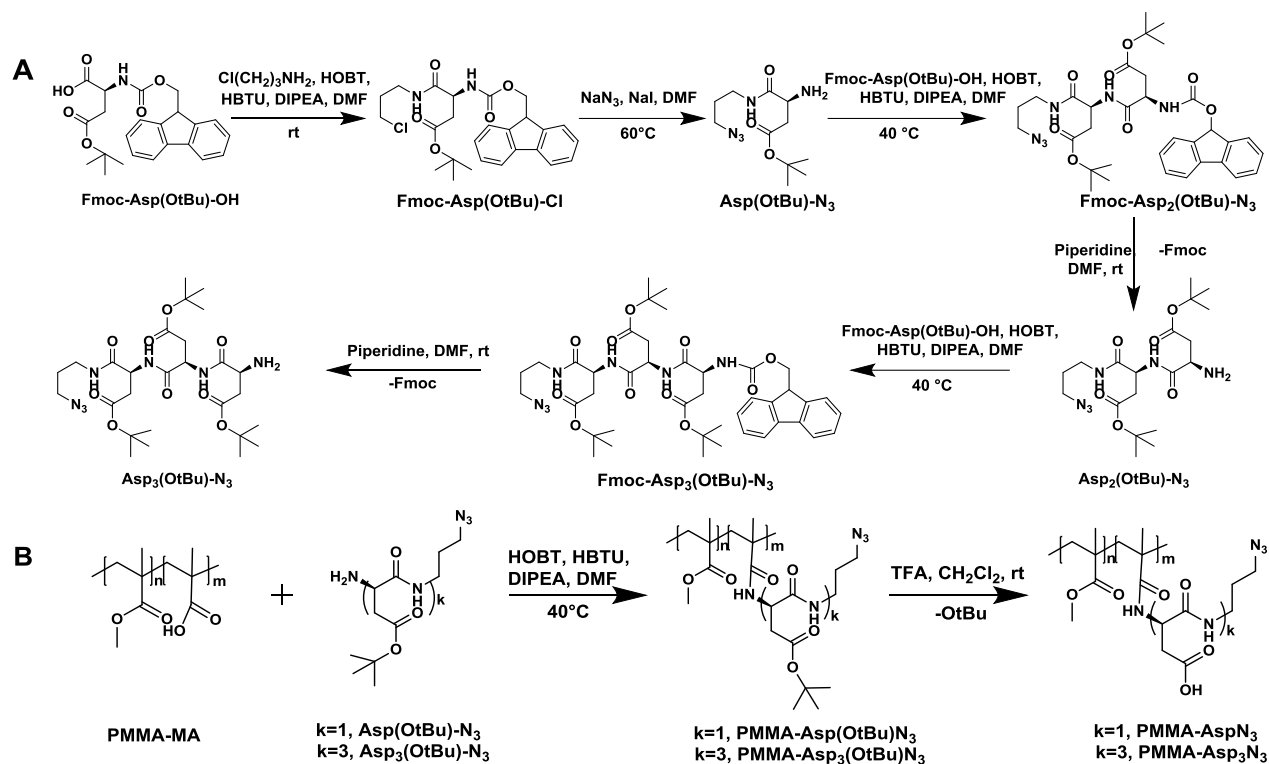


Fig.2.3. Schemes of chemical synthesis A) synthesis of linkers, B) synthesis of polymers.

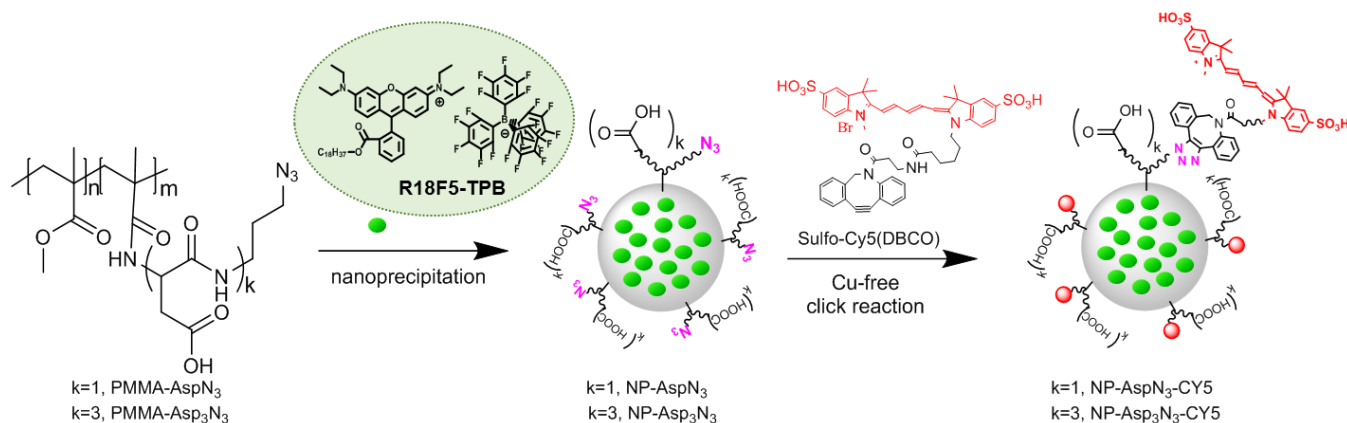


Fig. 2.4. Surface functionalization of nanoparticles.

Nanoparticles were obtained via nanoprecipitation of acetonitrile solution of corresponding polymers with fluorescent dye (R18/F5-TPB, 20 wt% with respect to the polymer) into an aqueous buffer (pH 7.4). To perform a copper-free click reaction we incubated nanoparticles with an excess of Sulfo-Cy5(DBCO) (2 μ M) for 24 h and purified reaction mixture on size exclusion columns (PD10) (Fig. 2.4). In this case, Cy5 acts as FRET-acceptor, while nanoparticle loaded with RhB/F5-TPB is a FRET donor. Size, shape, and polydispersity of NPs before and after

functionalization were studied by DLS and TEM. Both types of NPs containing azides were 30-35 nm, which were even smaller than control PMMA-MA NPs. Also, with higher content of carboxylic groups size of NPs decreased by 3 nm, indicating that the higher charge of polymer contributes to smaller NPs. Moreover, after surface modification with Cy5 dyes the size of functionalized NPs increased by 4 nm (Fig. 2.5A, B). According to absorption spectra, in case of control PMMA-MA NPs, Cy5 dye was completely removed from the reaction mixture by purification with the size exclusion column. In sharp contrast, for NP-AspN3 and NP-Asp3N3, Cy5 signal was present in the absorption spectrum with 5-times higher amount for the first type of NP in comparison to NP-Asp3N3 (Fig. 2.5C, D).

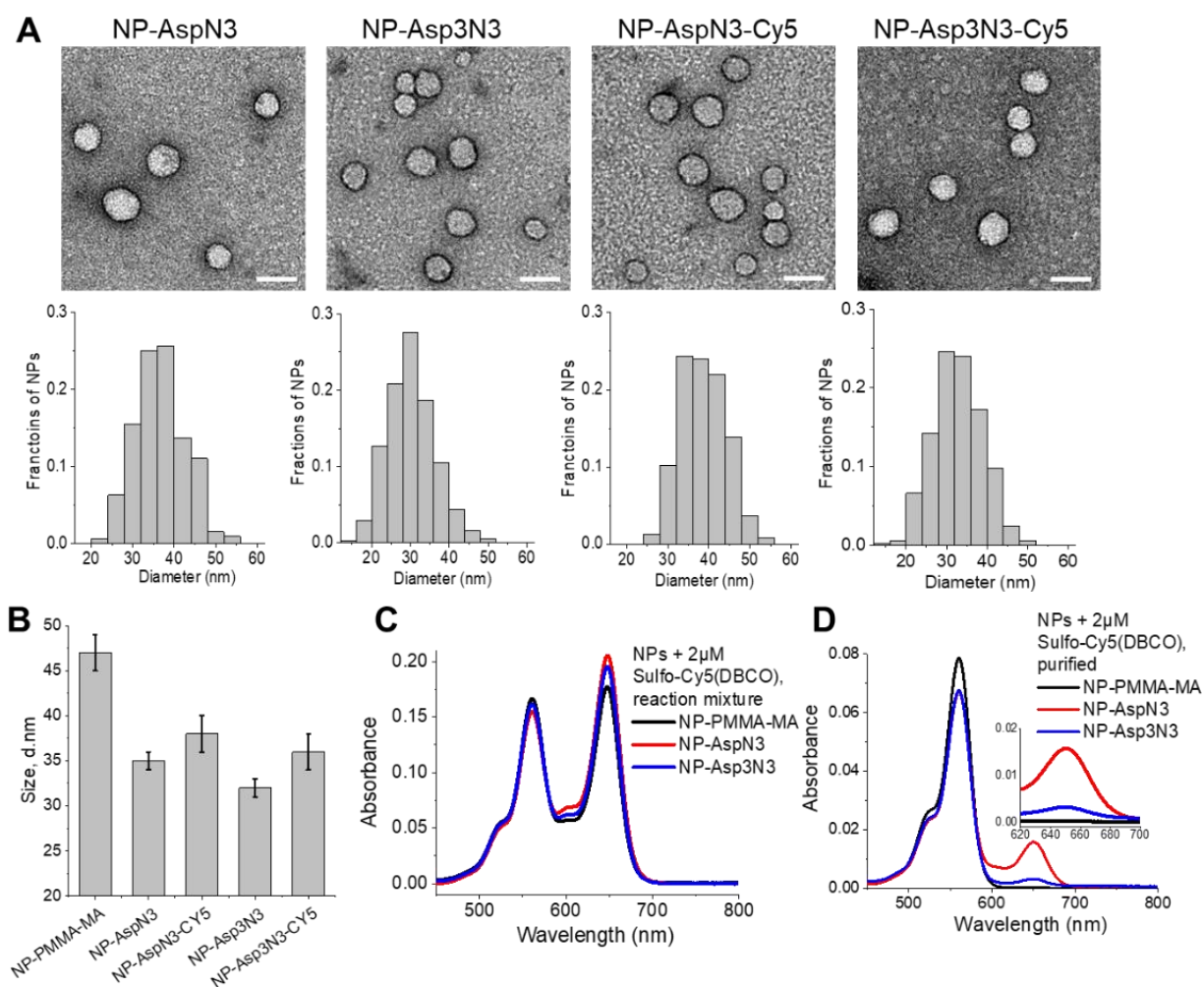


Fig.2.5. Post-functionalization of nanoparticles. A) TEM images and corresponding size distribution statistics (below), scale bar – 50 nm. B) Size by DLS. Absorbance spectra of nanoparticles incubated with 2 μM of Sulfo-Cy5(DBCO) C) reaction mixture D) after purification on size-exclusion column.

Then, fluorescence emission spectra of the obtained systems were measured. For the reaction mixtures before the purification, dual emission corresponding to rhodamine donor (at ~ 580 nm) and FRET acceptor Cy5 (at ~ 670 nm) was observed for all 3 types of NPs, although in case of NP-AspN3 the emission intensity was low. After purification of PMMA-MA NPs, the

Cy5 acceptor signal disappeared, while for azide containing NPs, FRET signal of acceptor was conserved. As absorbance spectra revealed a much higher amount of acceptor dyes in case of NP-AspN3, the low emission intensity is probably a result of excessive functionalization of the NPs surface with Cy5 dyes, leading probably to their self-quenching. (Fig. 2.6). These results suggest that NP-AspN3 is probably more reactive towards Sulfo-Cy5(DBCO) than NP-Asp3N3.

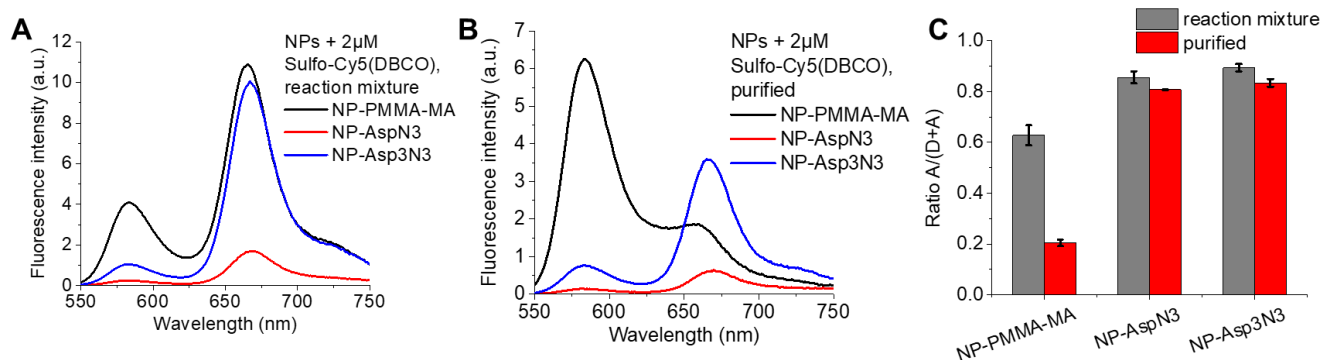


Fig.2.6. Fluorescence emission spectra of nanoparticles incubated with 2 μM of Sulfo-Cy5(DBCO) A) reaction mixture B) after purification on the size-exclusion column. C) FRET ratio $A/(D+A)$ of nanoparticles NP-PMMA-MA, NP-AspN3 and NP-Asp3N3 in the reaction mixture and after purification on size-exclusion column. A and D are the pick intensities of the acceptor (at 665 nm) and the donor (at 580 nm), respectively. Excitation wavelength was 530 nm.

To compare the reactivity of the polymeric NPs we studied the kinetics of their reaction by adding 50 nM of Sulfo-Cy5(DBCO) and monitoring the appearance of the acceptor signal and decrease of the donor signal. The experiment revealed that the NP-AspN3 reacts much faster than NP-Asp3N3. For NP-PMMA-MA the initial non-specific absorbance was observed, with slight quenching of the donor (Fig.2.7).

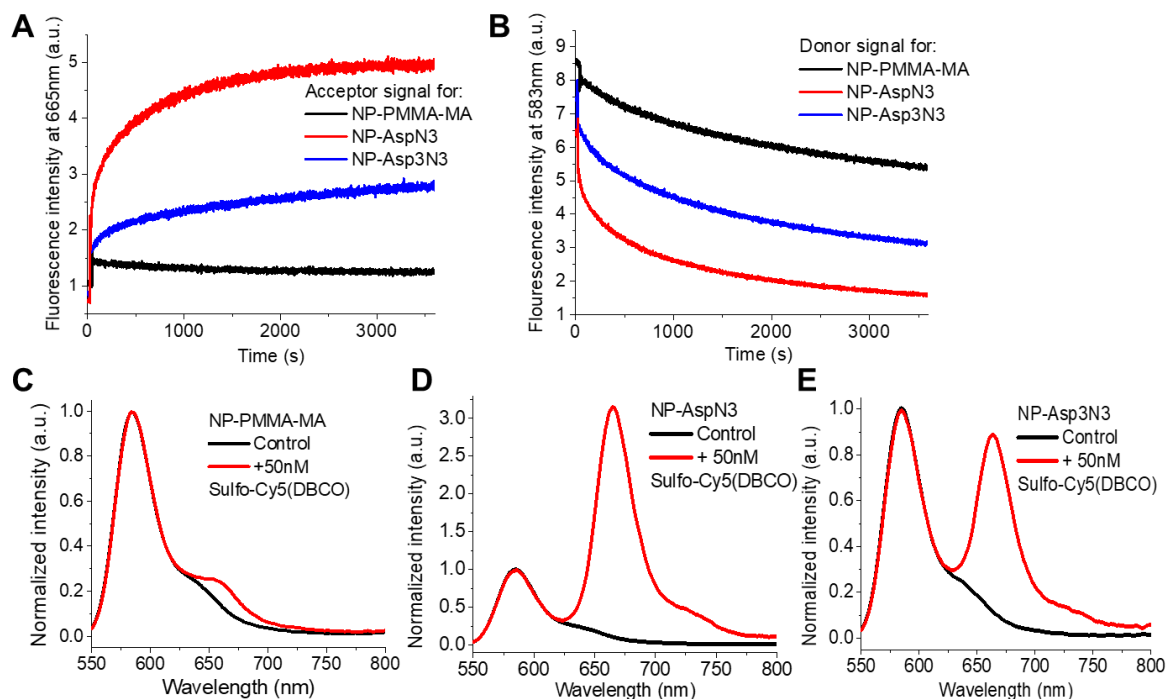


Fig.2.7. Kinetics of the reaction of nanoparticles with 50 nM of Sulfo-Cy5(DBCO) followed by A) acceptor emission at 665nm and B) donor emission at 583 nm. Fluorescence emission spectra of nanoparticles before and after 1 hour after addition of 50 nM of Sulfo-Cy5(DBCO) for C) NP-PMMA-MA, D) NP-AspN3, E) NP-Asp3N3.

We also incubated the nanoparticles with an increasing amount of Sulfo-Cy5(DBCO) and measured emission spectra right after the addition of acceptor and after 24 h of reaction (Fig.2.8). By the addition of 2.4 nmol of Cy5, which corresponds to one acceptor per NP (nanoparticle contains 2000 donors), we did not observe an appearance of FRET band after 24 h. But starting from 24 nmol of Cy5 (10 acceptors per NP), acceptor band appeared and further increased, reaching its maximum at 1 μ M of Sulfo-Cy5(DBCO). Already at low concentrations (0.121 μ M) NP-AspN3 showed a strong FRET signal (A/D ratio) after 5 min incubation, which further increased after 24h. In case of NP-Asp3N3, the FRET signal was weaker especially at short incubation times, while for control PMMA-MA NPs no FRET was observed for both incubation times. Further increase in the concentration significantly increased the FRET signal for NP-Asp3N3, while for NP-AspN3 we observed a decrease of emission intensity after 24h for higher concentrations of the Cy5 dye. We can conclude that, because of high reactivity, NP-AspN3 is able to attach a large number of acceptors to its surface, which causes self-quenching of the Cy5 acceptor. In case of control PMMA-MA NPs, we observed the initial appearance of FRET signal at higher concentrations of acceptor, which did not change after 24 h, so that it corresponds to the non-specific rapid absorption of dye to the nanoparticle surface.

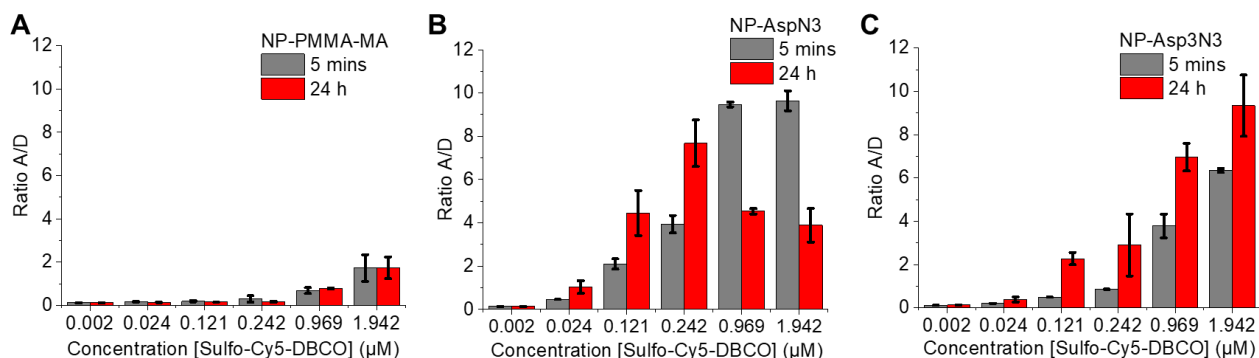


Fig.2.8. FRET ratio A/D of NP-PMMA-MA, NP-AspN3 and NP-Asp3N3 in reaction mixture, measured after 5 mins and 24 h incubation with Sulfo-Cy5(DBCO). A and D are the pick intensities of the acceptor (at 665 nm) and the donor (at 580 nm), respectively. Excitation wavelength was 530 nm.

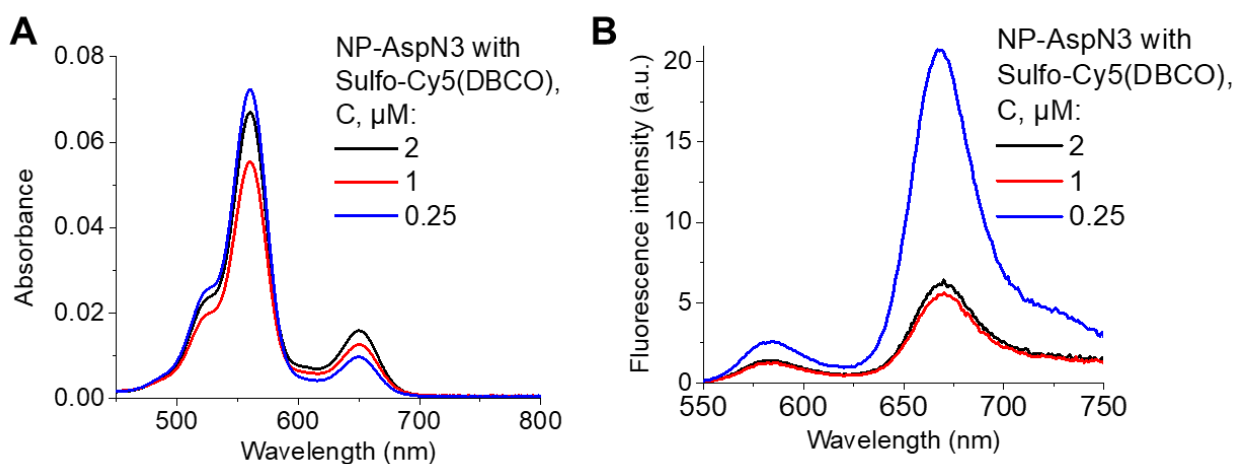


Fig.2.9. A) Absorbance and B) fluorescence emission spectra of NP-AspN3 incubated with 0.25, 1 and 2 μM of Sulfo-Cy5(DBCO) for 24 h and purified on size-exclusion column.

Table 2.1. Compare of reactivity of NP-AspN3 and NP-Asp3N3 with Sulfo-Cy5(DBCO).

Nanoparticles	C (Sulfo-Cy5(DBCO)) in reaction mixture, μM	Number of Acceptors per nanoparticle ¹	Reaction yield ² , %
NP-AspN ₃	0.25	74	7.9
	1	124	13.5
	2	129	14.6
NP-Asp ₃ N ₃	0.25	12	1.3
	1	23	2.6
	2	26	3.1

¹Donor nanoparticle contains 3200 dyes. ²Cacluted for 1 μM concentration of azide groups on the surface of the nanoparticle.

The reaction mixtures with higher concentrations of Cy5 acceptor were purified and the number of acceptors per nanoparticle was calculated from the absorption spectra (Fig. 2.9). Based on the theoretical total amount of azide groups in nanoparticle solution, the reaction yield was calculated and NP-AspN3 appeared to be systematically ~5 times more effective than NP-Asp3N3 (Table 2.1).

Based on the obtained results we concluded that the process of reaction involves first the absorption of Cy5 on the nanoparticle surface and further its covalent attachment. Apparently, in case of NP-AspN3 the repulsion between one carboxylic group and sulfo-groups of Cy5 is not as strong as in case of 3 carboxylic groups and it facilitates the reaction. However, the relatively strong repulsion between 3 carboxylic groups of NP-Asp3N3 and sulfo-groups of Cy5 does not allow Cy5 to absorb on the surface. This makes NP-AspN3 about 5-fold more reactive compared to NP-Asp3N3.

Pre-modification of the polymer

The next step of the project was to study the pre-functionalization approach that leads to surface-functionalized dye-loaded nanoparticles. Here, we needed a way to monitor the exposure of the ligand to the surface of NPs.

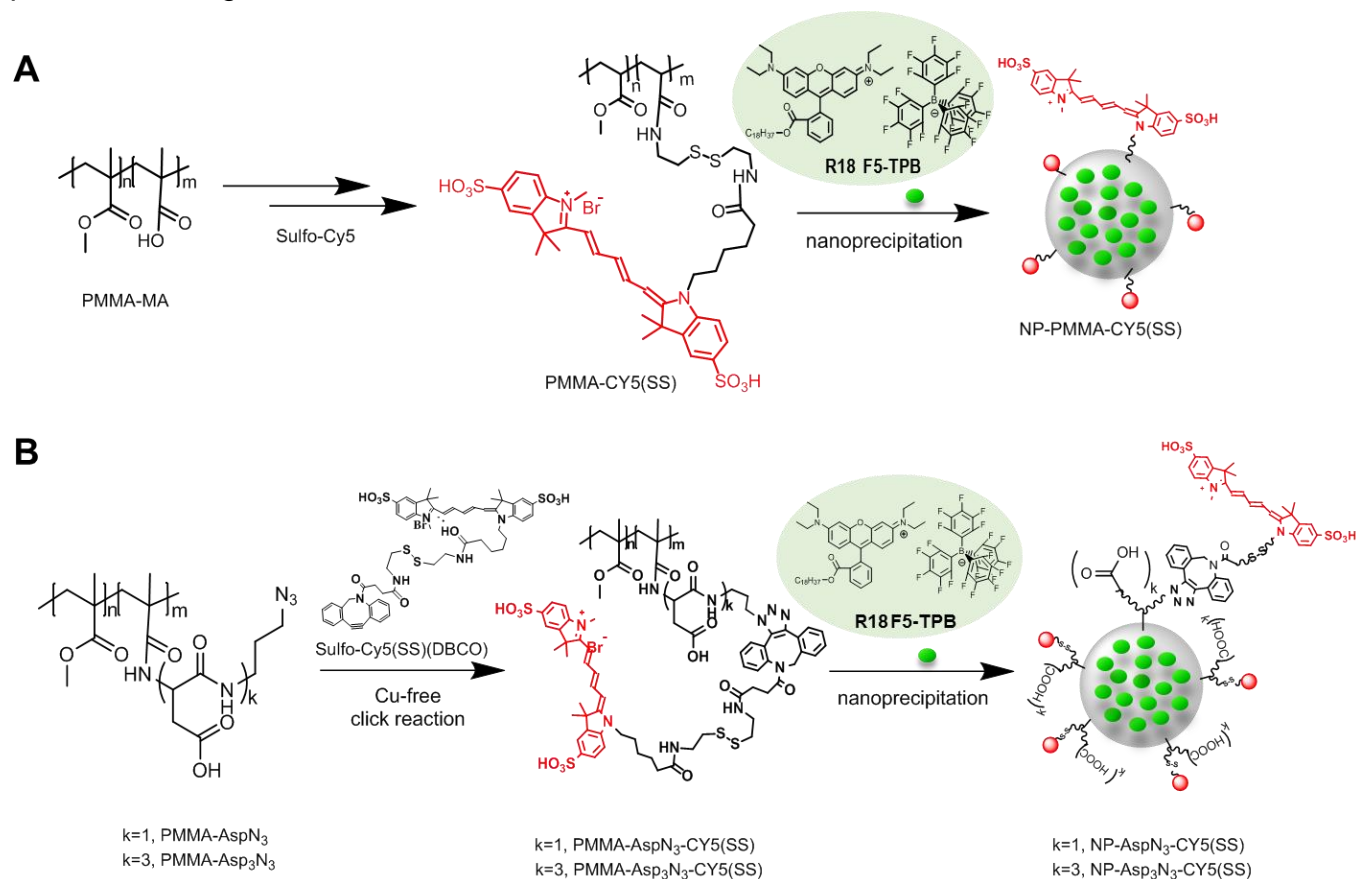


Fig.2.10. Scheme of synthesis NP-PMMA-Cy5(SS), NP-AspN3-Cy5(SS) and NP-Asp3N3-Cy5(SS) via pre-functionalization approach.

To do it, we synthesized the polymers where ligand attached through a cleavable bond – disulfide. PMMA-Cy5(SS) was obtained via a multistep reaction by attaching a linker with disulfide bond to PMMA-MA, and further coupling with Sulfo-Cy5 (Fig.2.10A). PM-AspN3-Cy5(SS) and PM-Asp3N3-Cy5(SS) were obtained through the reaction of corresponding PM-AspN3 and PM-Asp3N3 with Sulfo-Cy5(SS)(DBCO) (Fig.2.10B). The coupling of the dyes of the polymers was confirmed by absorption spectroscopy.

The nanoprecipitation of the polymers functionalized with Cy5 was performed with a varied fraction of corresponding non-labelled polymers (PMMA-MA, PM-AspN3 and PM-Asp3N3), which was expected to tune the statistical number of acceptors per NP. The measurements of size revealed that in case of NP-PMMA-Cy5(SS) and NP-Asp3N3-Cy5(SS) their size increased in 2 nm after acceptor appearance, while in case of NP-AspN3-Cy5(SS) the increase of size was higher (up to 10 nm) (Fig. 2.11A). For all three types of formulated NPs, the increase in the fraction of Cy5-modified polymer increased the Cy5 emission intensity, which was accompanied by the gradual decrease in the donor intensity (for NP-PMMA-Cy5(SS) see Fig. 2.11B), confirming FRET in our NPs. The fluorescence emission spectra demonstrated that the FRET efficiency for the same acceptor:donor ratio is similar for nanoparticles obtained from NP-PMMA-Cy5(SS) and NP-Asp3N3-Cy5(SS), while for NP-AspN3-Cy5(SS), FRET efficiency was generally lower, which might be due to partial aggregation of the system (Fig.2.11B, C).

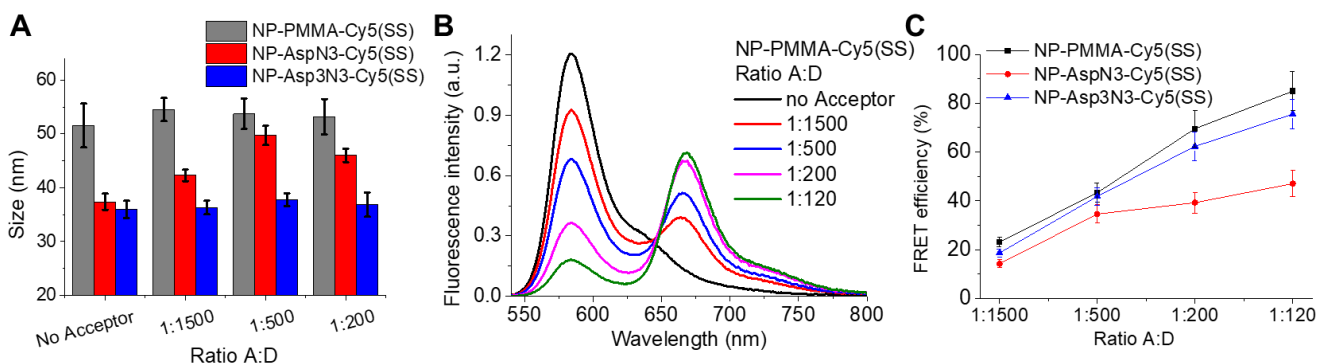


Fig.2.11. A) Size by DLS, B) emission spectra of NP-PMMA-Cy5(SS) with different Acceptor to Donor ratios, C) FRET-efficiency for nanoparticles formulated with different acceptor (A) to donor (D) ratios.

The next step was to verify whether the Cy5 acceptor was really situated on the surface of the nanoparticles after their formulation. To this end, we added a water-soluble thiol-reducing reagent DTT and monitored the changes in the fluorescence spectra of our FRET NPs. We monitored the reduction kinetics by measuring the emission intensity of the donor for NPs with A/D ratio 1/120 and found that the highest difference is achieved by NP-Asp3N3-Cy5(SS), while the modified NP-PMMA-Cy5(SS) demonstrated the lowest change (Fig.2.12A, B).

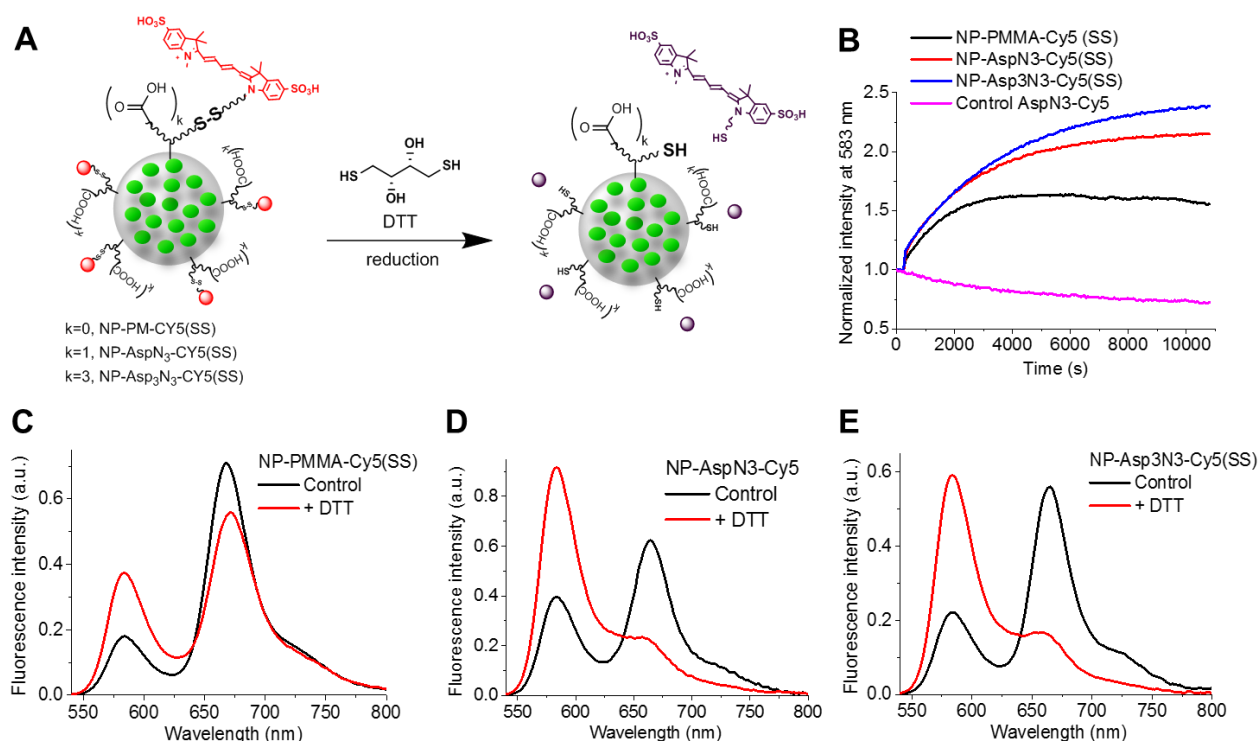


Fig. 2.12. Response of our FRET NPs to a reducing agent DTT. A) Scheme of reduction with DTT. B) Reduction kinetics of NP-PMMA-Cy5(SS), NP-AspN3-Cy5(SS), NP-Asp3N3-Cy5(SS) and AspN3-Cy5(control nanoparticles without disulfide bond) incubated with 30 mM of DTT. Measured emission intensity at 583 nm. Emission spectra of reduction probes before and after 3h of incubation with 30 mM of DTT based on C) NP-PMMA-Cy5(SS), D) NP-AspN3-Cy5(SS), E) NP-Asp3N3-Cy5(SS). Excitation wavelength 530 nm.

Emission spectra after 3 h of incubation with an excess of DTT revealed the nearly complete loss of the FRET signal for NP-AspN3-Cy5(SS) and NP-Asp3N3-Cy5(SS), confirming that the reduction agent cleaved the exposed acceptor from NPs surface (Fig.2.12D, E). However, in the case of polymer NP-PMMA-Cy5(SS), without additional charged group, the dual emission changed moderately, so that the FRET band of Cy5 was still larger than that of the donor (Fig.2.12C). This means that in the latter case the acceptor was probably not exposed well to the surface of the nanoparticles and was inside the nanoparticle, thus shielding the acceptor from the cleavage. In case of control particles without SS bond, the decrease of the donor intensity was observed due to the photobleaching (Fig.2.12B). Obtained results demonstrate that the linker with a charged group is absolutely necessary for the acceptor exposure to the surface of the NP during the nanoprecipitation.

The same type of nanoparticles with a disulfide bond was also synthesized through the pre-functionalization route. It can be noted that the NP-Asp3N3-Cy5(SS) demonstrated better response probably due to better availability of disulfide function (Fig.2.13). Direct excitation of the acceptor confirmed that DTT did not directly influence Cy5 fluorophore (Fig. 2.13B,D), but simply cleaved the disulfide bond. Moreover, the obtained FRET NPs constitute promising

fluorescent ratiometric probes for the reductive environment, which can be of interested for bioimaging.

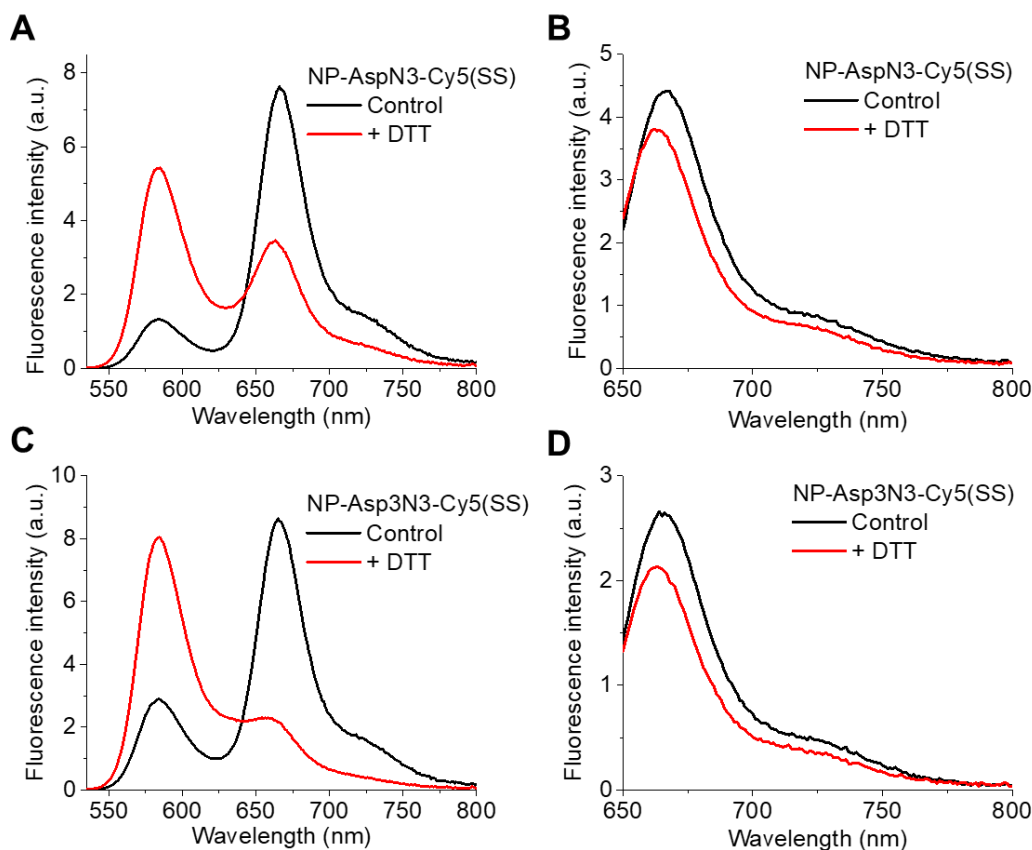


Fig.2.13. Reduction probes obtained via pre-functionalization approach. Fluorescence emission spectra of NP-AspN3-Cy5(SS) and NP-Asp3N3-Cy5(SS), control NPs and after 3h of incubation with 30mM of DTT, obtained via surface modification of NP-AspN3 and NP-Asp3N3 with Sulfo-Cy5(SS)(DBCO) A,C) excitation at 530 nm, B, D) excitation at 640 nm, correspondingly.

Cellular experiments

Fluorescent nanoparticles demonstrated superior sensing properties in comparison to molecular probes due to their higher brightness and photostability.³³ To monitor the reduction environment inside the cells by our FRET NPs we incubated NP-Asp3N3 with the attached Sulfo-Cy5(SS)DBCO obtained through pre-functionalization method since it demonstrated the best result in cuvettes. As a negative control, we also tested FRET NPs, where the acceptor is attached to the surface without a cleavable disulfide bond.

It is known that the living cell exhibit strong reductive potential in the cytosol as well as in endosomes and lysosomes,^{156,157} which should result in the cleavage of disulfide bonds of the internalized NPs. In case of short incubation (20 min at room temperature), both types of FRET NPs showed strong emission at the cell surface observed in both donor and acceptor channels, giving yellow-orange color in the merged images. As the NPs did not have time to get inside the cells, their disulfide was not cleaved and thus their FRET was preserved. After 3 h of incubation

at 37 °C with HeLa cells, the internalization of both reduction probe and control NPs was observed. In case of NP-Asp3N3-Cy5, the relative intensity in the acceptor channel remained high, so that the orange-yellow color in the merged image was preserved. In the case of the nanoprobe with the disulfide bond, the emission in a donor channel was stronger, which resulted in yellow-green color in the merged image (Fig. 2.14). This means that the reduction of the disulfide bond occurred, which resulted in the loss of the acceptor FRET signal.

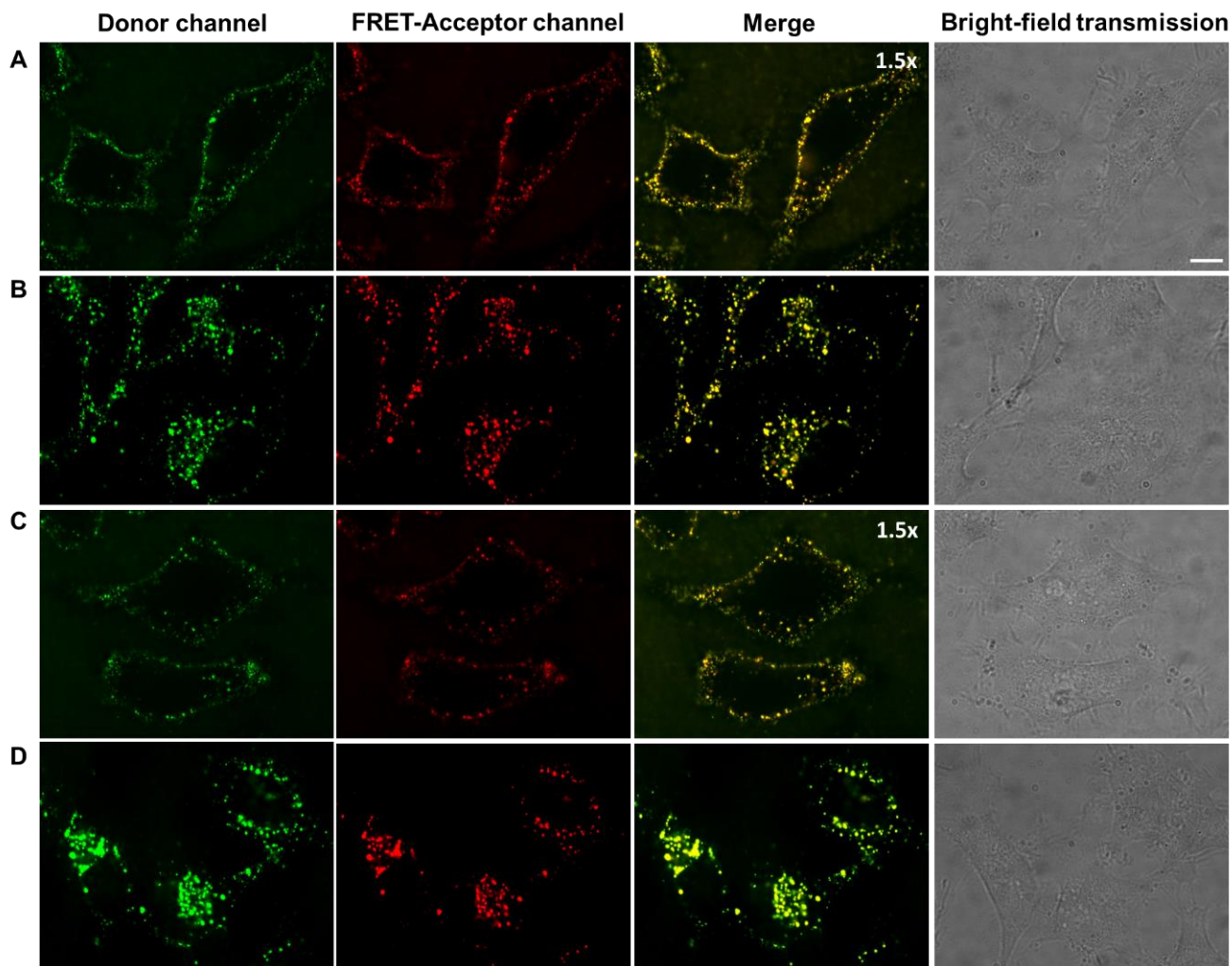


Fig.2.14. Cellular experiments. Fluorescence microscopic images of HeLa cells incubated with NPs (Ratio A:D 1:120) for 20 mins at room temperature (a,c) and for 3 h at 37°C (b,d) containing a,b) NP-Asp3N3-Cy5; c,d) NP-Asp3N3-Cy5(SS). The excitation wavelength was at 532 nm. Signals from the donor and the acceptor were recorded at <640 and >640 nm, respectively. Scale bar is 10 μ m.

These cellular experiments demonstrate the proof of concept for FRET-based sensing of a reductive environment with our polymeric particles in live cells.

Conclusions

In conclusion to this part, a functionalized polymer was developed and two principal approaches for the functionalization of polymer nanoparticles were studied. The first approach was post-functionalization of nanoparticle surface, where ligand was attached to the nanoparticle

after its formulation. The second approach was the pre-functionalization of polymer with a ligand prior to the nanoparticle formulation.

Both methods have their advantages and limits. The straightforward modification of the polymer allows to control number of ligands per NP during the nanoprecipitation and eliminates the purification step. But the type of ligand is limited to the molecules that are soluble in organic solvents in order to be directly attached to the polymer. Since proteins and oligonucleotides have poor solubility in organic solvents, this method is not well adapted for the functionalization of NPs with water-soluble biomolecules. On the other hand, the post-functionalization proceeds in buffer, so that nanoparticles can be functionalized with any water-soluble molecule. But here the number of ligands depends on the reaction yield, so the reaction conditions for the desired number of ligands per NP should be adjusted. Also, the post-functionalization approach includes a purification step.

Our results demonstrated that for each of these two approaches, the choice of the polymer is very important. In the case of post-functionalization nanoparticles, the polymer with one carboxylic group per reactive azide demonstrates faster reaction kinetics than the polymer with three carboxylic groups. The negative charge is absolutely important to prepare small NPs with exposed azide. However, the increase of the negative charge close to azide provokes the repulsion between the polymer and ligand molecules which decelerates the reaction rate. For the polymer pre-functionalization approach, the attached ligand should be enough hydrophilic or to have enough charge to be placed on the nanoparticle surface after nanoprecipitation. Moreover, the more negatively charged linker makes better accessibility of functional moieties in solution. That is why in case of reduction probes, nanoparticles with three carboxylic groups demonstrated better results. Obtained results validate methods for surface functionalization of dye-loaded polymer nanoparticles and suggest their application as advanced FRET-based sensors or labels for biomolecules.

2.2 Development of DNA-functionalized nanoparticles for ultrasensitive detection of nucleic acids

Demand for the detection of biomolecules at ultralow concentrations motivates researches for the development of new biosensors with enhanced sensitivity.⁴⁹ One way is amplification strategies, where the weak signal from the recognition event is converted by amplifiers into one that can be detected by conventional methods.³⁴ In case of nucleic acid, amplification by polymerase chain reaction revolutionized the field and remains the most used technique till nowadays in clinical nucleic acid detection assays.⁴¹ But PCR-based assays are multistep processes, which require a mix of expensive reagent, specific equipment and well-trained staff.⁴⁸ Therefore researchers keep on developing FRET-biosensor that exploit other amplification techniques, among which especially promising is optical amplification.⁷⁸ To this end, conjugated polymers and noble metal nanoparticles were used as optical amplifiers in proposed DNA-detection assays.⁸⁴ However, despite achieved low detection limits, conjugated polymers exhibit non-specific interaction with other biomolecules in solution. The amplification assays for DNA-detection with noble metal nanoparticles require complicated techniques, such as DNA origami.

Recently, our group designed dye-loaded nanoparticles operating as giant light-harvesting nanoantenna that transfers efficiently the energy from >10 000 rhodamine dyes (FRET donors) to few FRET acceptors inside the nanoparticle. The nanoantenna amplifies acceptors emission >1000 fold, which enables following their signal at ambient sunlight excitation conditions.⁶⁸ The aim of this part of my thesis project was to convert this nanoantenna into ultrasensitive nanoprobess for nucleic acid detection based on the surface chemistry described in the previous chapter.

We proposed a design of nanoprobess (Fig.2.15), where dye-loaded polymer nanoparticle (FRET donor) modified on the surface with capture oligonucleotide complementary to a nucleic acid fragment encoding cancer marker survivin (SurC)¹⁵⁸. SurC is hybridized with a short target-competitive sequence bearing FRET acceptor Cy5 (TCS-Cy5), so that the acceptor is localized close to the nanoparticle surface, which ensures good FRET efficiency. Then, the target nucleic acid displaces TCS-Cy5 acceptors and blocks FRET, so that nanoprobe would switch to green emission of nanoparticle. Combination of these two oligonucleotide sequences was originally proposed by Mirkin and co-workers in Nanoflares, which are based on gold NPs.⁹⁵

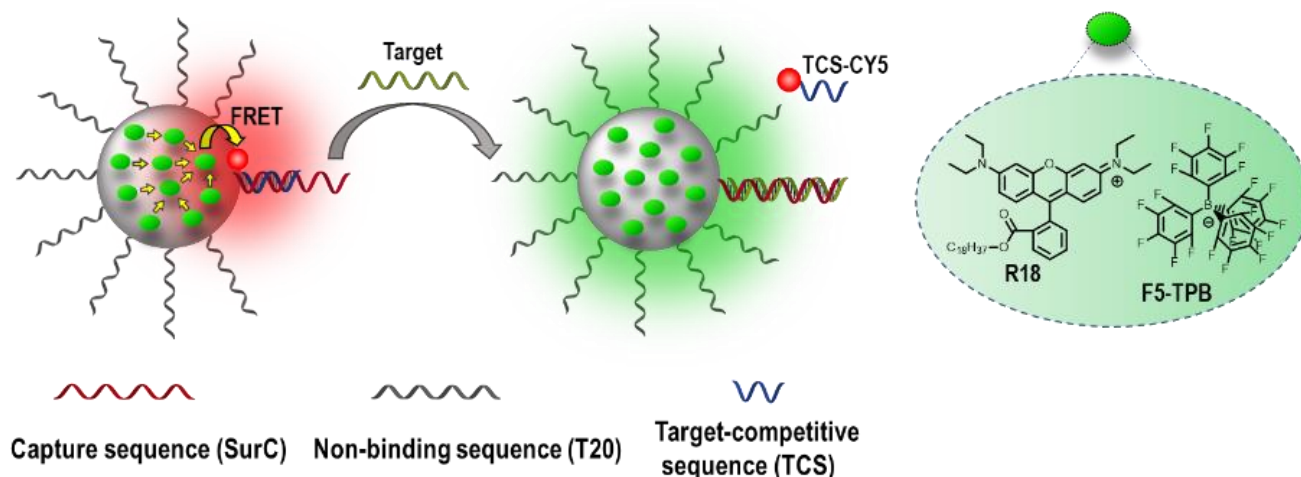


Fig.2.15. Concept of nanoantenna for amplified detection of nucleic acids.

In order to synthesize the nanoprobe, we grafted oligonucleotides to the concentrated NP-Asp-N3 via reaction with DBCO-bearing oligonucleotides SurC-DBCO and T20-DBCO, followed by annealing with shorter oligonucleotide TCS-Cy5 bearing FRET acceptor (Fig. 2.16A). The noncoding sequence T20 was needed to ensure stability and sensitivity of NP-Probe in saline phosphate buffer containing 30 mM NaCl and 12 mM Mg^{2+} , which is necessary for duplex stabilization (Fig. 2.16B). Successful grafting of oligonucleotides demonstrated the presence of Cy5 signal in absorption spectra after purification ($\sim 23 \pm 3$ per NP) and appearance of FRET band in emission spectra (Fig. 2.16C). The power of the obtained nanoantenna amplification approach was demonstrated by comparison of the NP-system with a molecular FRET probe (Cy3-SurC/TCS-Cy5), where SurC conjugate with Cy3 dye was hybridized with TCS-Cy5. For the same FRET acceptor concentration (1 nM of TCS-Cy5), the signal from our NP-Probe was >100-fold higher compared to the molecular probe (Fig. 2.16D). The TCS-Cy5 was hybridized with SurC-modified NPs at the different ratios to demonstrate that hybridization of 3–5 TCS-Cy5 per particle produced a clearly detectable change in the dual emission of the nanoprobe, indicating that just a few molecular recognition events can control emission of ~ 3200 donor dyes inside nanoantenna (Fig. 2.16E). This sensitivity of the nanoantenna-based probes to few hybridization events together with a strong signal amplification phenomenon is of key importance for the detection of the target nucleic acids.

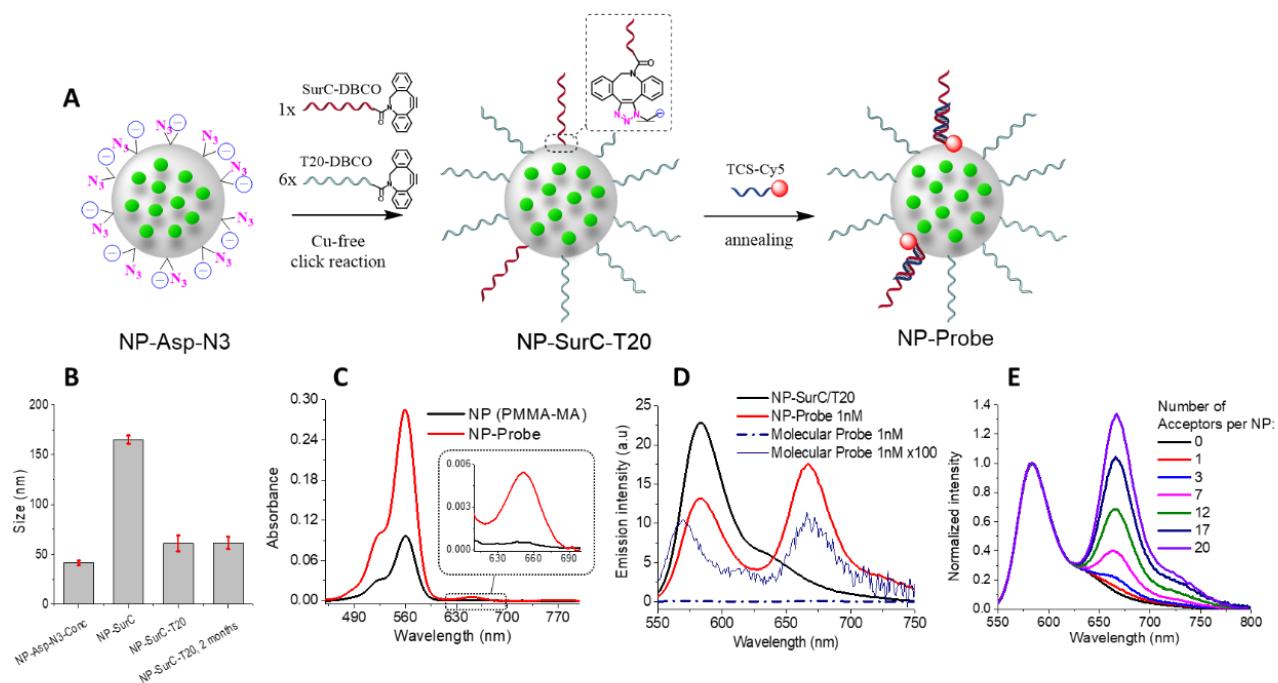


Fig.2.16. A) Scheme of nanoprobe synthesis, B) size by DLS of NP-AspN3 (conc), NP-SurC and NP-SurC-T20 (latter and after 2-month storage). C) Absorbance spectra of control (PMMA-MA) and NP-Probe after reaction with SurC-DBCO and T20-DBCO followed by hybridization with TCS-Cy5 and purification, D) Fluorescence emission spectra of NP-SurC/T20, NP-Probe at 1 nM of TCS-Cy5 and Molecular probe at 1nM of TCS-Cy5 (experimental conditions and 100x). E) Normalized fluorescence spectra of NP-SurC-T20 at different number of hybridized TCS-Cy5 per particle.

In the presence of the nucleic acid target (DNA and RNA) encoding survivin NP-Probe lost FRET signal at 670 nm, in contrast to the control sample without the target. Further incubation of NP-Probe with DNA target mismatches demonstrated good sequence specificity (Fig. 2.17A). We estimated the limit of detection of 5 pM in solution and demonstrated the robustness of the NP-Probe in different biological media (Fig. 2.17B-C). The ultimate test for the nanoprobe was to determine their performance at the single-particle level. Fluorescence microscopy of these NPs immobilized on the glass surface¹⁵⁹, showed homogeneity of their fluorescence intensity (Fig. 2.17D) that was ~100-fold stronger than that of QD605. Incubation with different concentrations of the survivin target showed that nanoprobe is functional at the single-particle level in different biological media with a limit of detection of 0.25 pM (Fig.2.17E-F).

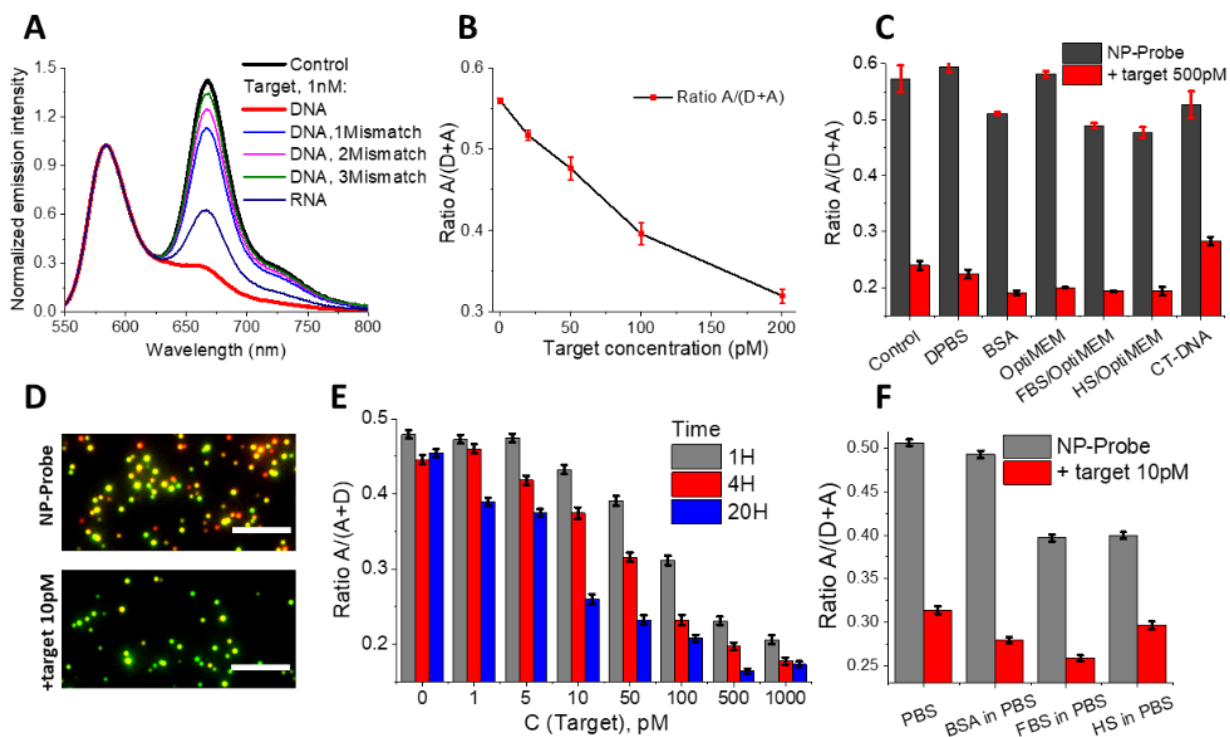


Fig.2.17. A) fluorescent emission spectra of NP-probe after incubation with DNA and RNA target and DNA targets containing 1, 2 and 3 mismatches; B) values of FRET response $A/(D+A)$ of NP-probe after incubations with different amounts of DNA target and C) with 500 pM DNA target in different biological media, D) images of replacement of 10 pM DNA target at the single-particle level, E) ratiometric response of immobilized NP-probe to different concentrations of DNA target at three different incubation times, F) responses of NP-probe 10 pM DNA target after 20h incubations at 4°C in different biological media.

In conclusion to this part, we developed a methodology of chemical functionalization of dye-loaded polymeric NPs with nucleic acids. The obtained probes showed unprecedented properties, such as high brightness, amplification of the nucleic acid detection where FRET from ~3000 donors inside NPs was successfully realized to a few (~20) acceptors at the surface. Thus, we developed an ultrabright platform for amplified FRET-based sensing of nucleic acids.

These results were published in the article: Nina Melnychuk & Andrey S. Klymchenko. DNA-Functionalized Dye-Loaded Polymeric Nanoparticles: Ultrabright FRET Platform for Amplified Detection of Nucleic Acids. *J. Am. Chem. Soc.* 2018, 140, 10856-65. Moreover, a European patent application (18305253.9) was deposited.

A full description of the work can be found in the article enclosed below.

**Article 1. DNA-Functionalized Dye-Loaded Polymeric Nanoparticles:
Ultrabright FRET Platform for Amplified Detection of Nucleic Acids**

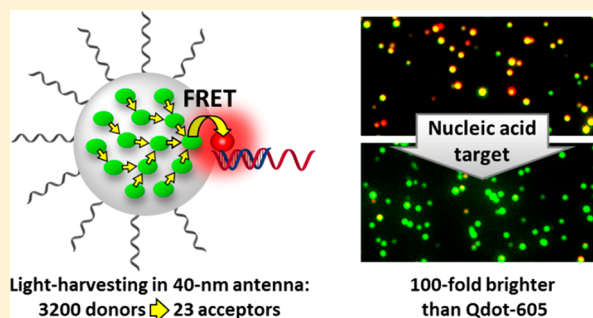
DNA-Functionalized Dye-Loaded Polymeric Nanoparticles: Ultrabright FRET Platform for Amplified Detection of Nucleic Acids

Nina Melnychuk and Andrey S. Klymchenko*¹

Laboratoire de Bioimagerie et Pathologies, UMR 7021 CNRS, Faculté de Pharmacie, Université de Strasbourg, Strasbourg CS 60024, France

Supporting Information

ABSTRACT: Going beyond the limits of optical biosensing motivates exploration of signal amplification strategies that convert a single molecular recognition event into a response equivalent to hundreds of fluorescent dyes. In this respect, Förster Resonance Energy Transfer (FRET) with bright fluorescent nanoparticles (NPs) is an attractive direction, but it is limited by poor efficiency of NPs as FRET donors, because their size is typically much larger than the Förster radius (~ 5 nm). Here, we established FRET-based nanoparticle probes that overcome this fundamental limitation by exploiting a phenomenon of giant light harvesting with thousands of strongly coupled dyes in a polymer matrix. These nanoprobe are based on 40 nm dye-loaded poly(methyl methacrylate-*co*-methacrylic acid) (PMMA-MA) NPs, so-called light-harvesting nanoantennas, which are functionalized at their surface with oligonucleotides. To achieve this functionalization, we developed an original methodology: PMMA-MA was modified with azide/carboxylate bifunctional group that enabled assembly of small polymeric NPs and their further Cu-free click coupling with oligonucleotides. The obtained functionalized nanoantenna behaves as giant energy donor, where hybridization of target nucleic acid (encoding survivin cancer marker) with ~ 23 grafted oligonucleotides/Cy5-acceptors switches on/off FRET from ~ 3200 rhodamine-donors of the nanoantenna, leading to 75-fold signal amplification. In solution and on surfaces at single-particle level, the nanoprobe provides sequence-specific two-color ratiometric response to nucleic acids with limit of detection reaching 0.25 pM. It displays unprecedented brightness for a FRET biosensor: it outperforms analogous FRET-based molecular probe by >2000 -fold and QDot-605 by ~ 100 -fold. The developed concept of amplified sensing will increase orders of magnitude sensitivity of fluorescent probes for biomolecular targets.



INTRODUCTION

The problem of limited brightness of fluorescent dyes¹ in biomolecular sensing stimulated development of amplification mechanisms that convert a single molecular recognition event into a response equivalent to hundreds of fluorescent dyes.² Beyond strategies that multiply (chemically/enzymatically) the number of molecular species,³ concepts of direct amplification of dye emission have been developed. The first one is based on conjugated polymers, where a large number of aromatic unites strongly coupled by π -conjugation can efficiently transfer the excitation energy to a single energy acceptor.⁴ Second one uses plasmonic nanostructures (nanoantennas), where fluorescence of single molecules located in the “hot spots” can be amplified.⁵ Fluorescent nanoparticles (NPs),⁶ such as quantum dots (QDots),⁷ dye-doped silica,⁸ aggregation-induced emission,⁹ conjugated polymer,¹⁰ and dye-loaded polymer¹¹ NPs, being much brighter than organic dyes, are promising scaffolds for fabrication of biosensors with signal amplification. To convert fluorescent NPs into biosensors (nanoprobes), Förster Resonance Energy Transfer (FRET) is generally used, where the particle serves as energy donor, while energy acceptors with target-recognition units are grafted to its surface.¹² However,

to achieve direct signal amplification in this case, efficient FRET from the whole particle to a single acceptor should be achieved, which is a fundamental challenge because the particle size is generally much larger than the Förster radius (~ 5 nm).^{12a-c,13} For instance, in case of QDots, which are probably the most popular NPs for fabrication of biosensors,^{12b} efficient FRET can be obtained only when significant amounts of FRET acceptors (10–50) are attached to their surface through a thinnest possible organic shell.^{12a,14} Dye-loaded polymeric NPs are particularly attractive alternatives to QDots,¹¹ because of their superior brightness,¹⁵ biocompatible/biodegradable matrix, and low cytotoxicity.¹⁶ Very recently, following a concept used by nature in chlorophyll,¹⁷ we designed dye-loaded polymeric NPs operating as giant light-harvesting nanoantenna.¹⁸ Its >10 000 rhodamine dyes, assembled together by bulky counterions within in 60 nm poly(methyl methacrylate-*co*-methacrylic acid) (PMMA-MA)-based nanoparticle, transferred efficiently the energy to few FRET acceptors inside the particle, leading to amplification of their

Received: June 4, 2018

Published: August 1, 2018

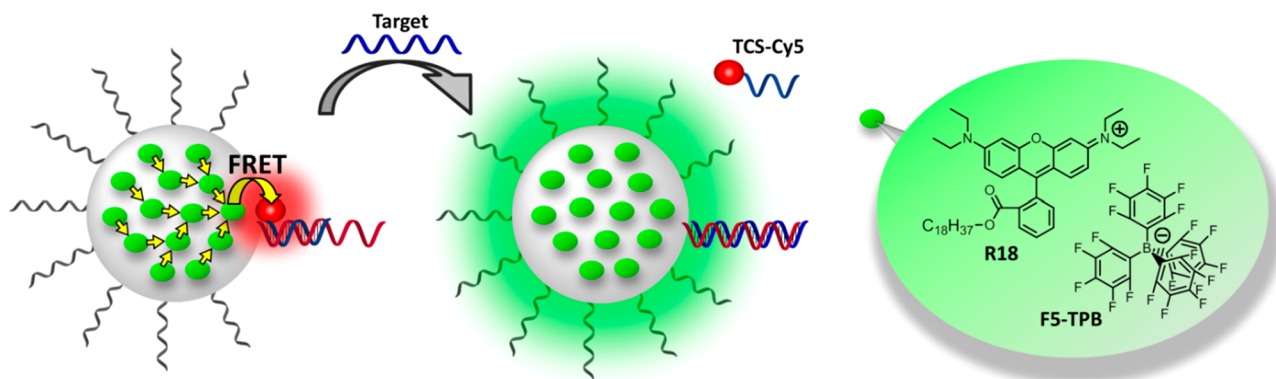


Figure 1. Concept of polymeric nanoantenna for amplified detection of nucleic acids. The dye-loaded nanoparticle is schematically presented, bearing noncoding (in gray) and capture (dark red) oligonucleotides. Yellow arrows schematically show the light-harvesting process toward FRET acceptor at the surface of nanoparticle. Target NA displaces short oligonucleotide with FRET acceptor (TCS-Cy5) from the NP surface, resulting in the FRET loss, so that the emission of the probe switches from red (acceptor) to green (donor). Chemical structures of the rhodamine derivative R18 and its bulky counterion F5-TPB are also shown.

emission >1000-fold. It surpassed plasmonics-based amplification values¹⁹ and enabled first observation of single molecules in sunlight conditions.¹⁸ However, to transform them into probes for biomolecules, the surface chemistry of these unique nanomaterials remains to be developed.

The ubiquitous nature of nucleic acids (NAs) makes them highly important targets for detection in biological research and medical diagnostics.^{6c,20} Their ultralow concentrations in biological samples, below the detection limit of fluorescent molecular probes, require molecular multiplication techniques, notably polymerase chain reaction (PCR), a multistep process that uses complex mixture of reagents, sophisticated equipment and well-trained staff.²¹ Chemists developed variety of fluorescent probes that can detect low concentrations of NAs, up to few pM, but they also use molecular multiplication, based on enzymes^{3b} or hybridization chain reactions.^{3a,22} To achieve direct one-step amplification, without molecular multiplication, cationic conjugated polymers were initially proposed,^{4b} because they can report on sequence specific hybridization improving detection limits down to the 10 pM range.²³ However, their limitations are nonspecific interaction with other NA duplexes and proteins, and strong dependence on the ionic strength.²⁴ Noble metal nanoparticles offered new opportunities in NA detection.^{6c,20e} Very recently, Tinnefeld and co-workers pioneered the amplified detection of NAs based on plasmonics nanoantenna positioned precisely in space with help of DNA origami.²⁵ The amplification achieved was 7.3 on average, although higher values were observed for some NPs. In this respect, our organic nanoantennas are expected to offer new possibilities.

We hypothesize that giant light-harvesting in the organic nanoantenna can be used to establish a concept of amplified FRET-based sensing, where a few nucleic acid hybridization events at the nanoantenna surface can trigger fluorescence response of thousands of dyes. To this end, a methodology of chemical functionalization of the PMMA-MA-based nanoantenna with oligonucleotides has to be developed first. Moreover, to achieve efficient FRET, the size of the nanoantenna particle should be optimal (40–50 nm) and the distance from its surface to the FRET acceptor should be minimized. However, small PMMA-MA-based NPs bearing nucleic acids have not been reported to date. The problem is inefficiency of the direct coupling of hydrophobic polymers

(including PMMA-MA derivatives) with oligonucleotides because of difficulty to solubilize together highly apolar and polar species,²⁶ so that solid phase synthesis is required.^{26a,27} However, the examples of direct modification of polymeric NPs by oligonucleotides are limited to block copolymers containing relatively large hydrophilic units with PEG linkers,²⁸ which is incompatible with our FRET strategy. On the basis of our recent work, showing that a single charge per polymer is sufficient to assemble small NPs by nanoprecipitation,²⁹ we expect that addition of a reactive group next to this charged group will enable preparation of functionalizable nanoantennas.

In the present work, we developed a robust approach to functionalize small (<50 nm) polymeric NPs with oligonucleotides and thus provided the first platform based on dye-loaded organic nanoantennas for amplified sensing of biomolecules. Due to the light-harvesting principle, we achieved efficient FRET from ~3200 donor dyes inside nanoantenna to ~23 acceptors hybridized at the particle surface, leading to average signal amplification of 75. Being ~100-fold brighter than QDot-605, the nanoprobe produce donor/acceptor emission ratio response to just 3–4 NA hybridizations per particle, which makes them the brightest nanoprobe reported to date. The nanoprobe was designed to detect a fragment of nucleic acid encoding survivin protein, an important antiapoptotic cancer marker.³⁰ The obtained nanoprobe operates in solution and on surfaces delivering limit of detection for the NA target of 5 and 0.25 pM, respectively, which is 1000–10 000-fold lower than that achieved using molecular probes. Given the universality of FRET-based detection concept, our functionalizable organic nanoantennas open the route to a broad range of ultrabright probes for amplified detection of biomolecules.

RESULTS AND DISCUSSION

Design of Nanoprobes for Nucleic Acids. In our design, the light-harvesting nanoantenna (FRET donor) is based on poly(methyl methacrylate-*co*-methacrylic acid (PMMA-MA, 1.6% methacrylic acid) NPs loaded with ion pair of hydrophobic rhodamine (R18) with bulky hydrophobic counterion tetrakis(pentafluorophenyl)borate (F5-TPB). The latter serves as spacer between dyes to minimize their aggregation-caused quenching inside NPs^{16a} and ensures ultrafast excitation energy migration required for efficient

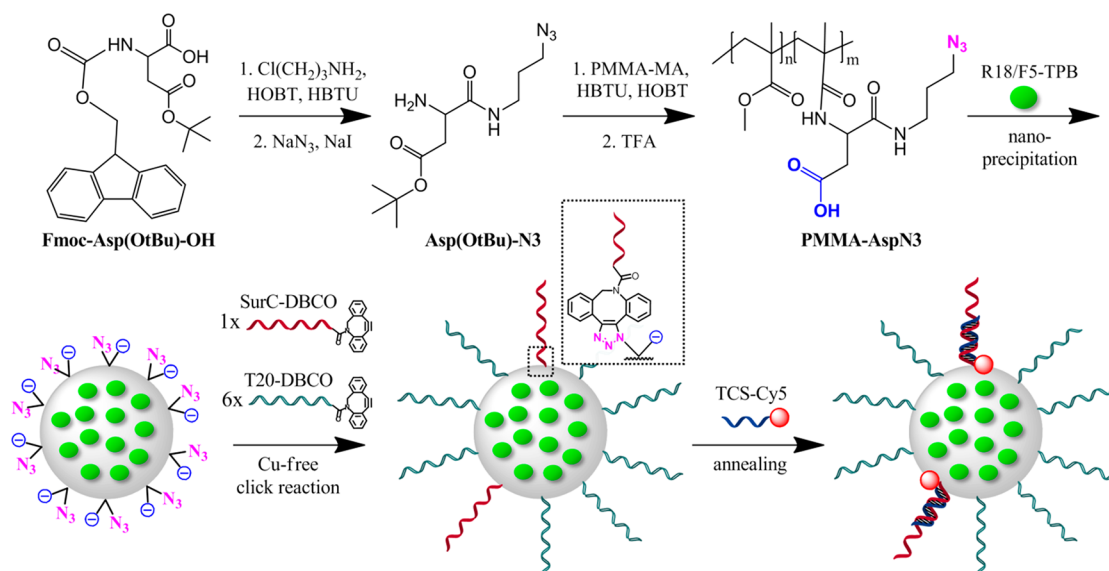


Figure 2. Scheme of synthesis of nanoprobe for nucleic acids. It includes synthesis of linker molecule (Asp(OtBu)-N3), its conjugation to PMMA-MA and deprotection affording target polymer PMMA-AspN3, nanoprecipitation of PMMA-AspN3 to obtain NPs bearing azide groups, DNA grafting to the surface of NPs and hybridization with Cy5-TCS.

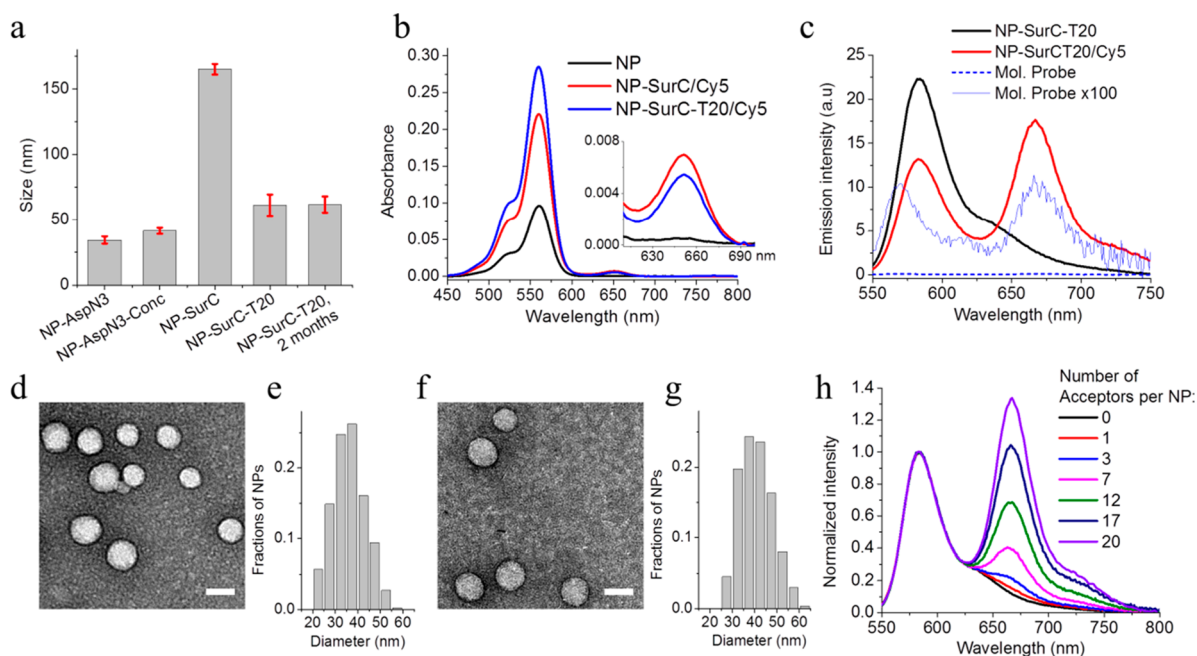


Figure 3. Characterization of DNA conjugates with nanoantenna particles. (a) Size by DLS of NPs bearing the motif AspN3 (NP-AspN3), NPs bearing AspN3 prepared at high concentration (NP-Asp-N3-Conc), NPs bearing AspN3, and target-specific oligonucleotide SurC (NP-SurC), NPs bearing Asp-N3, SurC, and nonspecific oligonucleotide T20 (NP-SurC-T20), and the latter after 2 months storage (NP-SurC-T20, 2 months). (b) Absorption spectra of control PMMA-MA NPs (without azide groups) and NP-AspN3 after reaction with SurC followed by hybridization with TCS-Cy5 (NP and NP-SurC/Cy5, respectively), and NP-AspN3 after reaction with SurC and T20 followed by hybridization with TCS-Cy5 (NP-SurC-T20/Cy5). (c) Fluorescence spectra of NP-SurC-T20 (43 pM) without and with TCS-Cy5 (1 nM) and comparison with spectra of corresponding molecular probe Cy3-SurC/TCS-Cy5 (1 nM) at the same instrumental conditions. For better comparison the latter spectrum was also multiplied 100-fold, showing that it is >100 fold less bright than the NP-probe. TEM images of NP-AspN3 (d) and NP-SurC-T20 (f) and corresponding size distribution statistics (e,g). Scale bar 50 nm. (h) Normalized fluorescence spectra of NP-SurC-T20 at different number of hybridized TCS-Cy5 per particle. Phosphate buffer (20 mM, pH 7.4) with 30 mM of NaCl and 12 mM of MgCl₂ was systematically used. (c,h) Excitation wavelength was 530 nm.

light harvesting (Figure 1).¹⁸ This nanoantenna is modified at the surface with a capture oligonucleotide, complementary to a nucleic acid fragment encoding cancer marker survivin (20mer, SurC). SurC is hybridized with a short target-competitive sequence bearing FRET acceptor Cy5 (12mer, TCS-Cy5), so

that the acceptor is localized close to the nanoantenna surface. Cy5 dye was selected because its absorption spectrum has a good spectral overlap with the emission spectrum of R18/F5-TPB-loaded NPs with a Förster radius of 6.1 nm.¹⁸ Combination of these two oligonucleotides was originally

proposed by Mirkin and co-workers in NanoFlares,^{20e,31} which ensured quenching of dyes located close to gold NPs. In our case, this design is used to induce FRET form nanoantenna to Cy5 acceptor. Here, thousands of rhodamine dyes inside nanoantenna pump the energy to a few Cy5 acceptors at the surface, resulting in strong acceptor (red) emission amplified by the light harvesting (Figure 1). Then, the target nucleic acid displaces TCS-Cy5 acceptors and blocks FRET, so that nanoprobe should switch to green emission of nanoantenna. Importantly, a few hybridization events are expected to switch emission of thousands of dyes, provide this basis for signal amplification. To obtain such a nanoprobe, the primary challenge is to functionalize our polymeric nanoantenna with controlled number of oligonucleotides.

DNA-Modified Polymeric Nanoparticles. In the first approach, we modified the PMMA-MA polymer with an azide group (PMMA-N3), which was further reacted with oligonucleotide bearing dibenzocyclooctyne (DBCO) unit through a Cu-free click cycloaddition.³² The latter was reported to provide efficient coupling without DNA damage.³³ However, this direct coupling failed because we could not find an appropriate solvent to solubilize both polar oligonucleotide and apolar polymer. Moreover, in contrast to PMMA-MA, nanoprecipitation of PMMA-N3 gave only very large aggregates (Figure S1 of the Supporting Information, SI), because the charged carboxylate group, essential for obtaining small NPs,^{18,29} was absent in PMMA-N3. Therefore, we designed a polymer bearing both charged carboxylate and reactive azide groups in close proximity. In addition to formation of small NPs, this charged group can favor the exposure of reactive azide group at the NPs surface (Figure 2). For this purpose, we developed a three-functional linker containing: (i) carboxyl as a charged group; (ii) azide for coupling with the oligonucleotide; and (iii) amino group for conjugation with the polymer (Figure 2). As a building block, we chose the biprotected aspartic acid, commonly used for solid-phase peptide synthesis, Fmoc-Asp(OtBu)-OH. Its carboxylic function was modified with 3-chloropropylamine, and then the chlorine was substituted with an azide, which resulted also in Fmoc removal giving target linker Asp(OtBu)-N3 (Figure 2). The latter was coupled with PMMA-MA through an amide bond. NMR spectra confirmed good yield of the polymer modification. Finally, *tert*-butyl group was removed giving a final polymer (PMMA-AspN3) for preparation of functionalized nanoantennas (Figure 2).

Nanoprecipitation of acetonitrile solution of PMMA-AspN3 polymer with fluorescent dye (R18/F5-TPB) into aqueous buffer (pH 7.4) gave small NPs (35 nm, Figure 3a), highlighting the crucial role of the additional charged carboxylate group. Moreover, with modified nanoprecipitation protocol, concentration of PMMA-AspN3 NPs was further improved ~10-fold (Figure S2), while keeping small particle size (42 nm, Figure 3a). Despite high 30 wt % loading of R18/F5-TPB (e.g., ~ 3200 dyes per 40 nm particle), the fluorescence quantum yield of NPs was very high (47%, Table S1), which renders our nanoantenna particles exceptionally bright.

For grafting oligonucleotides, the obtained concentrated dye-loaded NPs were reacted with DBCO-bearing oligonucleotide SurC-DBCO for 18 h at different temperatures, followed by annealing with shorter oligonucleotide TCS-Cy5 bearing FRET acceptor. The purification of the DNA-conjugated NPs from nonreacted oligonucleotides was achieved by successive

filtrations through 100 kDa filters, as verified by absorption spectroscopy (Figure S3). Fluorescence spectra suggested that at 4 and 20 °C the reaction did not occur, while at 40 °C we observed a clear FRET signal from NPs to hybridized TCS-Cy5, indicating successful conjugation reaction (Figure S4). Moreover, grafting reaction at 40 °C was confirmed by absorption spectroscopy, where the signal of the hybridized TCS-Cy5 was observed in the purified samples, in contrast to negative control based on PMMA-MA NPs without azide group mixed with SurC-DBCO (Figure 3b). The heating at 40 °C is probably necessary in order to increase the probability of collision between DBCO group grafted to oligonucleotide and azide group at the particle surface, in line with relatively slow DBCO/azide reaction kinetics reported recently for other type of polymeric NPs.^{28c} However, in phosphate buffer containing 12 mM Mg²⁺ ions, required for formation of stable duplexes,²⁵ DNA-NPs conjugates (NP-SurC) showed relatively large size (Figure 3a), probably because of partial aggregation of the obtained NPs.

Stability of DNA-NPs conjugates can be improved by increasing number of oligonucleotides per particle, as it was recently shown for NPs built of ring-opening metathesis block copolymers.^{28a} However, to achieve the highest optical amplification through the light-harvesting mechanism, minimal ratio of acceptors to donors should be used,¹⁸ i.e., minimal number of FRET acceptors should be grafted to the particle surface. To address these both issues, our NPs were reacted with a mixture of coding (SurC-DBCO) and noncoding (T20-DBCO) oligonucleotides. According to absorption spectroscopy, addition of T20-DBCO (20 μM) to SurC-DBCO (3 μM) did not inhibit the grafting of SurC to NPs surface (Figure 3b), probably because azide groups of NPs were in excess (26 μM). Fluorescence spectra of these NPs (NP-SurC-T20/Cy5) showed strong emission of the FRET acceptor TCS-Cy5 around 670 nm (Figure 3c). Moreover, the emission maximum of Cy5 shifted to the red and its anisotropy value increased compared to free TCS-Cy5 (Figure S5), confirming the TCS-Cy5/SurC hybridization. These results suggested successful grafting of SurC-DBCO to NPs in the presence of T20-DBCO. Remarkably, NP-SurC-T20/Cy5 particles remained small in phosphate buffer with Mg²⁺ ions and their size did not change even after 2 month incubation in this medium (Figure 3a). Moreover, their emission spectrum with characteristic FRET signal remained practically invariant for this 2 month period (Figure S6). Therefore, grafting excess of noncoding DNA (T20) is essential for stability of our polymeric NPs. In addition, transmission electron microscopy (TEM) confirmed that conjugation of NPs with oligonucleotides did not modify their spherical shape and monodispersity, while their size increased only by ca. 5 nm (Figure 3d-g).

Signal Amplification by Nanoantenna. Our further studies were focused on the most promising NPs bearing both SurC and T20. Their hybridized form with FRET acceptor TCS-Cy5 (NP-SurC-T20/Cy5) was called “NP-probe”. The synthesis of these nanoprobe was repeated four times showing good reproducibility of their size and spectroscopic properties (Table S2). On the basis of the absorption data and the particle size from TEM (41 ± 12 nm) we estimated that 23 ± 3 (s.e.m., *n* = 4) FRET acceptors (TCS-Cy5) were grafted per nanoantenna particle containing 3200 ± 400 donor dyes. In this respect, two outstanding features of NP-probe should be mentioned: (i) high fluorescence quantum yield (46%, Table S1) and (ii) 60 ± 6% FRET efficiency from 3200 donor dyes

inside nanoantenna of 20 nm radius to 23 acceptors at the surface, i.e., through distances far beyond the Förster radius (6.1 nm). This is a highly efficient light-harvesting phenomenon with minimal energy losses, where giant ensemble of donors “pumps” the energy to few acceptors, which implies strong amplification of the acceptor emission (antenna effect). The antenna effect, measured as an intensity ratio of the donor to acceptor in the excitation spectra (Figure S7),³⁴ was 58 ± 1 with high reproducibility for all four preparations (Table S2). This result means that excitation via nanoantenna amplifies acceptor (TCS-Cy5) emission 58-fold. To show the power of our nanoantenna amplification approach, we compared the NP-system with a molecular FRET probe (Cy3-SurC/TCS-Cy5), where SurC conjugate with Cy3 dye was hybridized with TCS-Cy5. The Cy3 dye was chosen because it exhibited similar absorption and emission properties to rhodamine dye used in our NPs (Table S1). Remarkably, for the same FRET acceptor concentration (1 nM of TCS-Cy5), the signal from our NP-probe was >100-fold higher compared to the molecular probe (Figure 3c), in line with the antenna effect values. As the NP-probe concentration in this case was 43 pM, the single NP-probe was >2000-fold brighter than the single molecular probe. Finally, we verified the minimal number of TCS-Cy5 that NP-probe can distinguish by its FRET signal. To this end, TCS-Cy5 was hybridized with SurC-modified NPs at the different ratios (Figure S8). The increase in number of FRET acceptors per NP improved the FRET signal (Figure 3h). Remarkably, hybridization of 3–5 TCS-Cy5 per particle produced clearly detectable change in the dual emission of the nanoprobe, indicating that just a few molecular recognition events can control emission of ~ 3200 donor dyes inside nanoantenna. This unique sensitivity of our nanoantenna-based probes to few hybridization events together with strong signal amplification phenomenon are of key importance for detection of the target nucleic acids.

Detection of Target Nucleic Acids. In the presence of the NA target encoding survivin NP-probe totally lost FRET signal at 670 nm, in contrast to the control sample without the target (Figure 4a). Importantly, the response is ratiometric, displaying >5-fold change in the A/D intensity ratio. This result shows that the target sequence displaced FRET acceptor TCS-Cy5 at NPs surface, thus stopping FRET. Moreover, the response of NP-probe decreased drastically already for a single mismatch in the target sequence, which was located in the middle of the region corresponding to the target-competitive sequence. Second and third mismatches further deteriorated the response to the oligonucleotide (Figures 4a as S9), showing very good sequence-specificity of the NP-probe. We further verified the importance of the Mg^{2+} ions in the response of NP-probe. Remarkably, below 12 mM of Mg^{2+} , NP-probe showed a decrease in the FRET signal after 3 h incubation without the target (Figure S10a), confirming that 12 mM concentration of Mg^{2+} ensures stability of the duplex between the capture sequence and TCS-Cy5. Importantly, the response of NP-probe to the target also decreased at lower Mg^{2+} concentrations (Figure S10), indicating that Mg^{2+} could also assist the displacement of TCS-Cy5 by the target sequence. Therefore, 12 mM concentration of Mg^{2+} was systematically used in all further experiments. Then, the NP-probe diluted to TCS-Cy5 concentration of 10 pM (i.e., ~ 0.4 pM NP-probe) was tested in growing concentrations of NA target. The relative intensity of the FRET acceptor, expressed as semiempirical parameter of FRET efficiency, $A/(A + D)$,³⁵

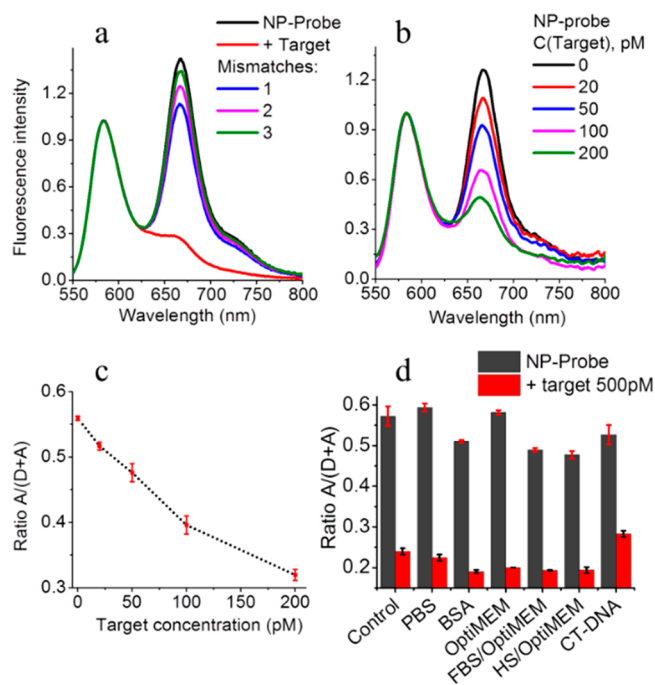


Figure 4. Response of nanoprobe to the nucleic acid target. (a) Fluorescence spectra of NP-probe (100 pM of TCS-Cy5) after incubation for 20 h at 4 °C without and with survivin NA target (1 nM). Targets containing 1, 2, and 3 mismatches were tested at the same conditions. Fluorescence spectra (b) and values of FRET response $A/(A + D)$ (c) of NP-Probe after incubation with target at different concentrations. A and D are the pick intensities of the acceptor (at 665 nm) and the donor (at 580 nm), respectively. Concentration of the NP-probe corresponds to 10 pM of TCS-Cy5. Phosphate buffer (20 mM, pH 7.4) with 30 mM of NaCl and 12 mM of $MgCl_2$ was systematically used. (d) FRET response of the NP-probe (100 pM of TCS-Cy5) to the NA target (500 pM) in different biological media (concentration of Mg^{2+} was adjusted to 12 mM): Control (20 mM phosphate buffer with 30 mM of NaCl), PBS, BSA (0.5 mg/mL in PBS), OptiMEM, FBS (inactivated, 10% in OptiMEM), Human Serum (inactivated, 10% in OptiMEM), and DNA from calf thymus (CT-DNA, heat denatured, 10 μ g/mL in PBS). (c,d) Error bars are standard deviation of the mean ($n = 3$). Excitation wavelength was 530 nm.

gradually decreased in the concentration range of the NA target from 20 to 200 pM (Figure 4b,c). The estimated limit of detection (LOD) was 5 pM, which is remarkably low for a standard fluorometer. Then, we checked whether our nanoprobe is operational in different biological media. In all studied media, namely phosphate buffered saline (PBS), PBS with bovine serum albumin (BSA), Opti-MEM (cell culture medium without serum), Opti-MEM with fetal bovine serum (FBS), and Opti-MEM with human serum, the probe showed robust ratiometric response to the NA target: decrease in the relative intensity of the acceptor emission (Figure 4d). Moreover, the probe preserved the response in the excess of the denatured calf thymus DNA, which served as model of random NA sequence. Thus, our NP-probe is compatible with highly complex media containing variety of biomolecules, including proteins and NAs.

Evaluation of NP-Probe at the Single-Particle Level.

The ultimate test for the performance of the nanoprobe is to verify whether it can operate at the level of single particle. To this end we modified the glass surface with A20 sequence, which is complementary to that of noncoding T20 sequence of

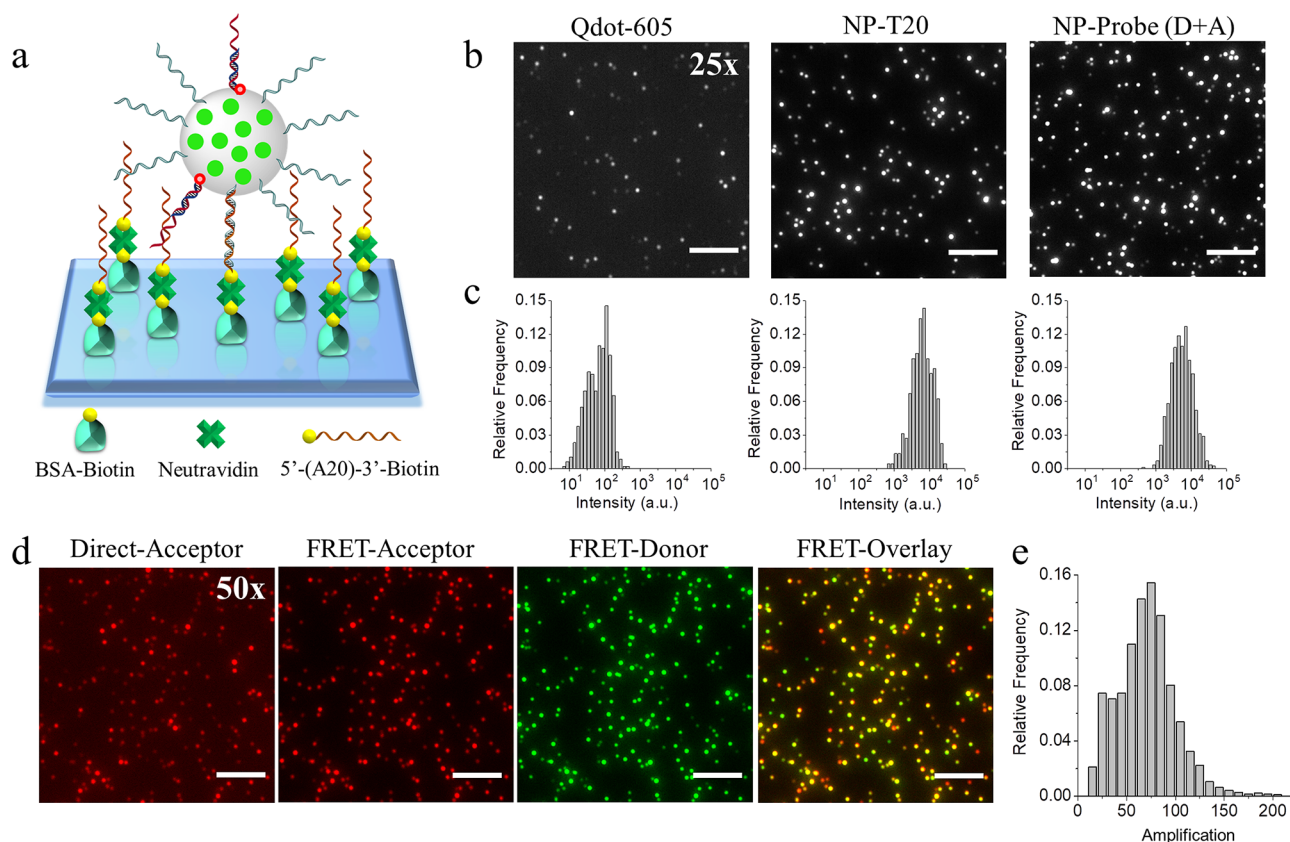


Figure 5. Single-particle imaging of immobilized nanoprobes. (a) Scheme of nanoprobes immobilization on glass surface modified with BSA-biotin, neutravidin, and A20-biotin. The interaction with the surface occurs due to hybridization of A20-biotin with T20 of NP. (b) Wide-field fluorescence microscopy of the immobilized NPs: quantum dots (QDot-605) excited at 470 nm, control NP-T20 and nanoprobe (sum of donor and acceptor channels is shown). To obtain comparable signals excitation power density for QDot-605 was 25-fold higher than that for NP-T20 and nanoprobe: 14 vs 0.56 W cm^{-2} , respectively. (c) Histogram of single-particle intensity distribution for these three types of NPs. At least 1000 NPs were analyzed in each case. (d) Wide-field microscopy images of the nanoprobe at the acceptor (direct excitation at 640 nm), antenna-amplified acceptor (FRET-Acceptor), donor (FRET-donor), and merged FRET-Acceptor and donor channels (at the same intensity scale). The excitation of nanoprobe (FRET-Donor and FRET-Acceptor) was at 550 nm with excitation power density 0.4 W cm^{-2} , while direct excitation of acceptor was done at 640 nm using 50-fold higher power density (20 W cm^{-2}). Signals from FRET-Donor and FRET-Acceptor were recorded at <640 and >640 nm, respectively. Integration time was systematically 200 ms. (b,d) Scale bar, $5 \mu\text{m}$. (e) Amplification of FRET-Acceptor emission (antenna effect) by the nanoprobe at the single-particle level presented as a distribution histogram. At least 1500 NPs were analyzed.

our NP-probe (Figure 5a). After incubation with the NP-probe fluorescent particles were clearly seen displaying remarkable homogeneity of their fluorescence intensity (Figure 5b,c). Importantly, the overall (donor + acceptor) intensity recorded per NP-probe was similar to that for control NP-T20 (without acceptor), being ~ 100 -fold higher compared to QDot-605 excited at optimal (470 nm) wavelength (Figure 5b,c, Table S3). This unprecedented brightness for a FRET biosensor is explained by high overall fluorescence quantum yield of NP-probe (46%) and ~ 3200 rhodamine dyes inside nanoantenna with total molar extinction coefficient of $\sim 3.2 \times 10^8 \text{ M}^{-1}\text{cm}^{-1}$ at 550 nm (vs $1.1 \times 10^6 \text{ M}^{-1}\text{cm}^{-1}$ for QDot-605 at 488 nm) that serve as giant ensemble of energy donors.

To evaluate FRET signal at the single particle level, the images of NPs were recorded simultaneously at the green (donor) and red (acceptor) channels. It can be seen that NP-probe showed similar intensities at these two channels and appeared mostly yellow in the overlay (Figure 5d), whereas control NP-T20 showed signal only in the donor channel (Figure 6a). These results provide clear evidence that, after immobilization at the surface, our NP-probe preserved strong FRET, as in the spectroscopy measurements (Figure 3c). Then, to evaluate antenna effect at the single-particle level, we

compared emission of the acceptor excited via nanoantenna (at 550 nm) vs that directly excited at 640 nm. Remarkably, 50-fold higher excitation power density (irradiance) at 640 nm was required to achieve emission intensity comparable to that excited at 550 nm (Figure 5d). Quantitative image analysis revealed 75 ± 30 fold amplification of acceptor emission (Figure 5e), in line with the spectroscopic data in solution. We should note that this is the first report where this high amplification is reported at the single particle level for a biosensor. Previous reports that used QDot as a FRET donor for NA detection at the single particle level did not exploit light-harvesting concept because a large number of acceptors per particle (~ 50) was required to achieve efficient FRET.^{14b} Indeed, the ratio of extinction coefficients of QDot-605 ($1.1 \times 10^6 \text{ M}^{-1}\text{cm}^{-1}$ at 488 nm) to 50 acceptors ($2.5 \times 10^5 \times 50 = 1.25 \times 10^7 \text{ M}^{-1}\text{cm}^{-1}$) is 0.09, suggesting that excitation through QDot-605 is less efficient than direct excitation of the acceptors. In case of our nanoantenna, the ratio of extinction coefficients of nanoantenna and 23 acceptors at the used excitation wavelengths (550 and 640 nm) is $3.2 \times 10^8 / 4.5 \times 10^6 = 71$, in agreement with the amplification values measured at the single-particle level. The amplification at the single-particle level within a biosensor was reported very recently for

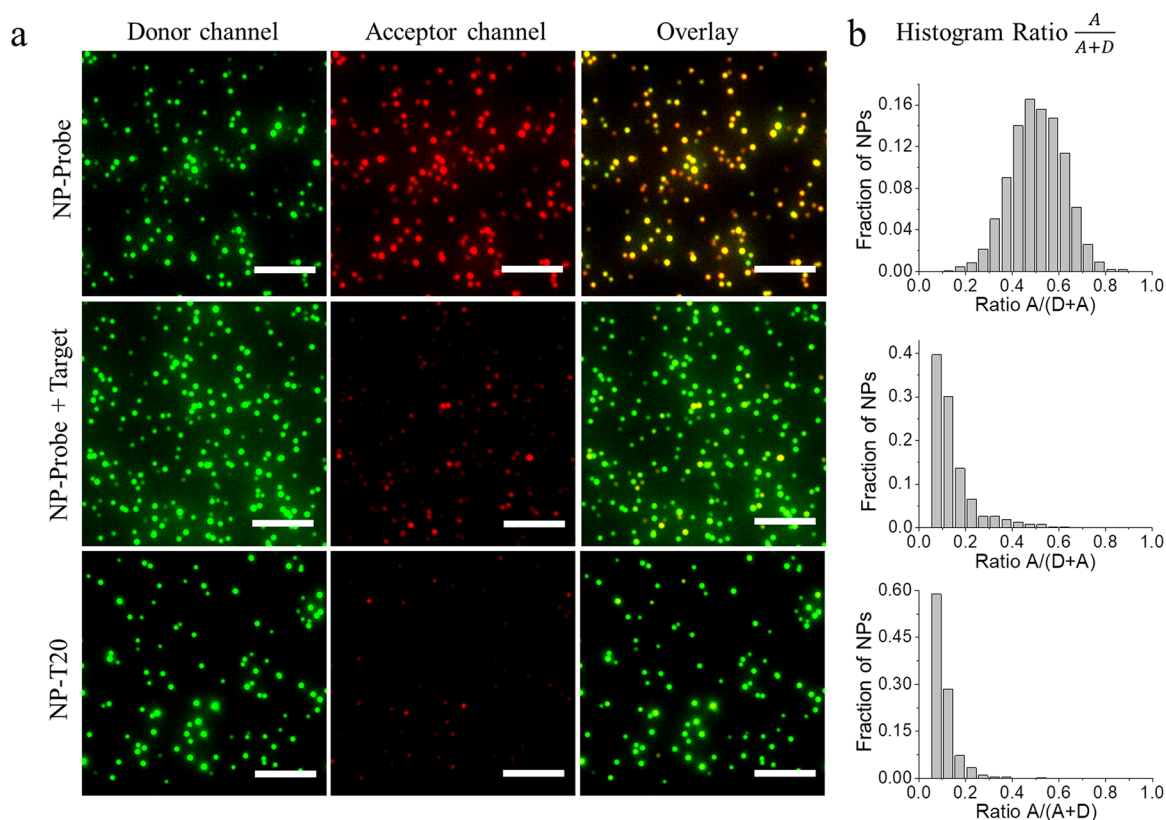


Figure 6. Response of surface-immobilized NP-probe to the NA target at the single-particle level. (a) Wide-field FRET images (donor channel, acceptor channels and overlay) and (b) corresponding histograms of relative FRET efficiency, $A/(A + D)$, of the NP-probe (first row), nanoprobe after incubation with 100 pM survivin NA target for 20 h at 4 °C (second row) and control NP-T20 (third row). All channels are represented at the same intensity scale. The excitation wavelength was at 550 nm with 0.4 W cm^{-2} power density. Signals from the donor and the acceptor were recorded at <640 and >640 nm, respectively. A and D are the integrated densities of the signal from individual particles recorded at the acceptor and the donor channels, respectively. Scale bar, 5 μm .

a plasmonic system using DNA origami, where the average amplification was 7.3.²⁵

Finally, we tested the response of our nanoprobe to the target at the single-particle level (Figure 6). After incubation of immobilized NP-probe with the target the emission in the red channel strongly decreased, in line with our observations by fluorescence spectroscopy. The semiquantitative FRET efficiency parameter, $A/(A + D)$, decreased from 0.48 down to 0.20 (Figure 6b), reaching values close to that for the control NP-T20 without FRET acceptor (0.12). Immobilized NP-probe was able to detect NA target in the concentration range of 1–1000 pM (Figures 7a and S11) with a remarkably low LOD of 0.25 pM (down to 12.5×10^{-18} moles in 50 μL). At low target concentration, the response of NP-probe was significantly improved for longer incubation times (Figure 7a), showing that sensitivity of our system was only limited by the kinetics of hybridization with the target NA. The latter is known to be on the time scale of hours for pM NA concentrations.³⁶ Robust detection of 10 pM NA target at the single-particle level was achieved in the presence of BSA, bovine and human serum (Figures 7b,c and S12), showing potential of our surface-immobilized NP-probe for development of future diagnostics assays. Finally, we should stress that ~ 23 hybridization events at the surface of the single NP-probe (corresponding to the number of TCS-Cy5 per NP) resulted in the color switching of a particle exhibiting the brightness of >3000 rhodamine dyes or ~ 100 QDot-605. This outstanding performance of the developed NP-probe has two important

consequences. First, the observed color switching implies that, at the single particle level, the NP-probe could readily detect just a few copies of the nucleic acid target. Indeed, according to spectroscopy data, hybridization of 3–5 nucleotides can provide detectable change in the FRET signal (Figure 3h). Second, due to the signal amplification produced by light harvesting with >3000 dyes, the target nucleic acids could be detected at very low excitation power density (0.4 W cm^{-2}) of LED in an epi-fluorescence mode, which is >100 fold-lower than required in the single-molecule detection measurements. The use of low power significantly decreases the background noise and makes possible detection of a few copies of nucleic acids using relatively weak and inexpensive light sources and a simple imaging setup.

CONCLUSIONS

Here, we introduce a concept of amplified fluorescence sensing based on giant light-harvesting ensemble of organic dyes in a polymeric nanoparticle (nanoantenna). This nanoantenna serves as superefficient energy donor in a FRET-based nucleic acid detection assay, where a few hybridization events at the surface of the nanoparticle switch on/off energy transfer from thousands of dyes. As chemical modification of small polymeric nanoparticles with oligonucleotides remains a challenge, we developed an original strategy for functionalization of the polymeric nanoantennas. Bifunctional moiety bearing charged carboxylate and azide was grafted to a biocompatible hydrophobic polymer (PMMA-MA), which ensured (i)

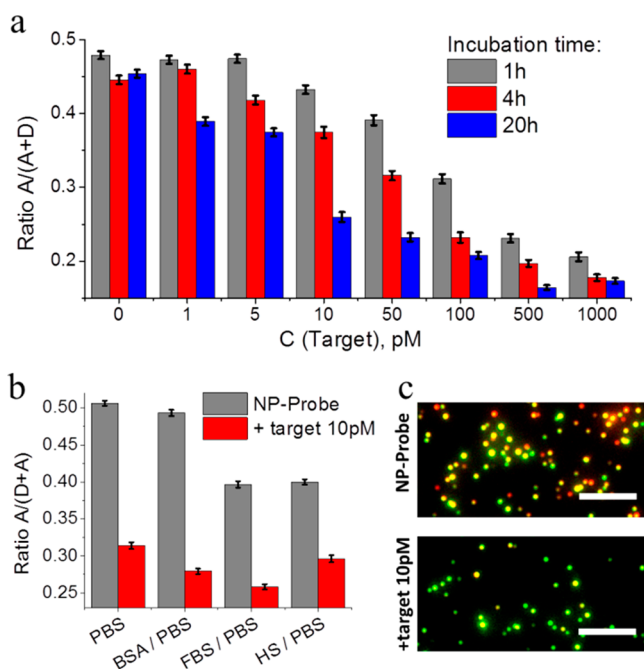


Figure 7. Single-particle evaluation of NP-probe ratiometric response in different conditions. (a) Ratiometric response of the immobilized NP-probe to different concentrations of survivin NA target after three different incubation times: 1 and 4 h at room temperature, and 20 h at 4 °C. (b) Responses of NP-probe 10 pM NA target after 20 h incubation at 4 °C in different biological media: BSA, FBS, and human serum (HS) in PBS. (a,b) The error bars are s.e.m. At least 1000 particles were analyzed for each condition. (c) Example of overlaid images of Donor and Acceptor channels for NP-probe incubated with 10 pM NA target after 20 h incubation at 4 °C. The excitation wavelength was 550 nm with power density of 0.4 W cm⁻²; integration time was 200 ms. Scale bar, 5 μm.

preparation of small nanoparticles (~40 nm) by nanoprecipitation and (ii) effective exposure of the azide group for coupling with oligonucleotides by Cu-free click reaction. Using this strategy, we functionalized the nanoantenna particles with two oligonucleotides simultaneously. The first one is the molecular recognition unit that after hybridization with the target nucleic acid (encoding a fragment of cancer marker survivin) removes the energy acceptor (Cy5 dye) from the nanoantenna surface, triggering the loss of FRET. The second one is a noncoding oligonucleotide, which is found to be essential for nanoparticle stability in biological media. The obtained nanoprobe displays efficient FRET (>60%) from ~3200 rhodamine-based donor dyes of nanoantenna to only 23 Cy5-acceptors. This efficient light-harvesting phenomenon results in the amplification of the acceptor emission (antenna effect) reaching 75. The nanoprobe detects target nucleic acid by changing the ratio of its donor/acceptor intensity ratio and can distinguish down to 3–5 hybridizations at its surface. Our nanoantenna based probe is ~100-fold brighter than quantum dots (QDot-605) and >2000-fold brighter than analogous FRET-based molecular probe. To our knowledge, it is the first nanoparticle-based probe for biomolecules that combines this exceptional brightness and such high signal amplification. The nanoprobe operates in solution and on surfaces at the single-particle level delivering limit of detections of 5 and 0.25 pM, respectively, the latter being limited only by the hybridization kinetics. We expect that the outstanding brightness and amplification characteristics of nanoantenna probes will greatly

simplify detection of nucleic acids with low-cost portable fluorescence detection instruments, which is of highest importance for detection biomolecular markers of diseases in point of care diagnostics. Moreover, our functionalized organic nanoantenna, owing to the exceptional capacity to donate the energy from thousands of donors to few acceptors at its surface, can increase by orders of magnitude brightness of practically any FRET based detection assay.

EXPERIMENTAL SECTION

Oligonucleotides. Lyophilized single strand DNA sequences were purchased from IBA, dissolved in Milli-Q water, aliquoted and stored at -20 °C for further experiments. The oligonucleotide sequences used in this study are shown below. SurC-DBCO, 5'-CCC AGC CTT CCA GCT CCT TGA-(DBCO)-3'; T20-DBCO, 5'-TTT TTT TTT TTT TTT TT-(DBCO)-3'; TCS-Cy5, 5'-(Cy5)-TCA AGG AGC TGG-3'; Target, 5'-CAA GGA GCT GGA AGG CTG GG-3'; single mismatch, 5'-CAA GCA GCT GGA AGG CTG GG-3'; two mismatches, 5'-CAA GCA GCT GGA AGC CTG GG-3'; three mismatches, 5'-CAA GCA GCT CGA AGC CTG GG-3'; A20-Biotin, 5'-(BIO)-AAA AAA AAA AAA AAA AAA AA-3'.

Nanoparticle Preparation. Protocol for diluted NPs: 50 μL of the PMMA-AspN3 polymer solution in acetonitrile (1 mg mL⁻¹ containing R18/F5-TPB at 30 wt % relative to the polymer) were added quickly using a micropipette to 450 μL of 20 mM phosphate buffer, pH 7.4 at 21 °C under shaking (Thermomixer comfort, Eppendorf, 1100 rpm). The particle solution was then quickly diluted 5-fold with the same buffer. For preparation of NPs functionalized with DNA the protocol was modified to increase the NP concentration: 100 μL of the PMMA-AspN3 polymer solution in acetonitrile (2 mg mL⁻¹ with 30 wt % R18/F5-TPB relative to the polymer) were then added quickly using a micropipette to 900 μL of the same buffer under shaking with Thermomixer (1100 rpm). Then, the residues of acetonitrile were evaporated.

NP-Probe Synthesis. Aliquots of DNA (3 μM SurC-DBCO, with or without 20 μM T20-DBCO) were added to 300 μL of nanoparticles (concentration of azide groups were ~26 μM). The reaction was mixed and kept overnight at 40 °C in Thermomixer without shaking protected from light. Then the reaction was cooled down to room temperature. For annealing with TCS-Cy5, the aliquot of TCS-Cy5 in ratio 1:1 with SurC-DBCO was added and mixture was heated to 70 °C in water bath for 3 min. To complete hybridization the reaction was cooled down to room temperature and kept in the dark for 2 h. Then the mixture was diluted with 20 mM phosphate buffer containing 12 mM MgCl₂ and 30 mM NaCl to 4 mL and purified by centrifugation using centrifuge filters (Amicon, 0.5 mL, 100 kDa) on 1000g at 20 °C for 2 min. The procedure of centrifugation was repeated 5 times to remove the nonreacted oligonucleotides. The obtained NP-probes in volume of 1 mL were kept in the dark at 4 °C.

Detection of Survivin Nucleic Acid Target. For detection in solution the NP-Probe was diluted in 20 mM phosphate buffer containing 30 mM NaCl and 12 mM MgCl₂ to a desired concentration (corresponding to TCS-Cy5) and aliquot of target oligonucleotide was added. Before measurements the mixture was incubated in the dark at 4 °C for 20 h, unless specified. For detection of target NA on surfaces, the aliquot of the NA target was added to the LabTek chamber with immobilized NP-Probes. The mixture was kept in the dark at the room temperature for 1 and 4 h incubation or at 4 °C for 20 h incubation.

For NA detection in different biological media, the PBS and OptiMEM were adjusted to 12 mM MgCl₂ concentrations and further used for sample preparations. BSA was diluted to 0.5 mg/mL concentration in PBS. The DNA sodium salt from calf thymus (CT-DNA) was dissolved to concentration of 2 mg/mL in water and kept overnight at 4 °C for complete dissolution. Then, it was heated for 3 min at 90 °C followed by rapid transfer into ice bath. For measurements it was diluted to concentration of 10 μg/mL in PBS. Foetal bovine serum (FBS) and Human Serum were heat-inactivated

by exposing them for 30 min to 56 °C before they were used. After that the FBS and Human Serum were diluted to 10% concentration in OptiMEM. For measurements in solution the NP-Probe was diluted in the corresponding media and the target oligonucleotide was added. Before the measurements were made, the mixtures of NP-Probe with and without target oligonucleotide were incubated in the dark at 4 °C for a given time. For the measurements on the surface, 300 μ L of the media was mixed with aliquot of the target oligonucleotide, and then the mixture was added to the LabTek chamber with immobilized NP-Probes. Prepared mixtures were incubated for 20 h at 4 °C before measurements.

■ ASSOCIATED CONTENT

Supporting Information

The Supporting Information is available free of charge on the ACS Publications website at DOI: 10.1021/jacs.8b05840.

Materials and methods section, supporting tables and figures (PDF)

■ AUTHOR INFORMATION

Corresponding Author

*andrey.klymchenko@unistra.fr

ORCID

Andrey S. Klymchenko: 0000-0002-2423-830X

Notes

The authors declare no competing financial interest.

■ ACKNOWLEDGMENTS

This work was supported by the European Research Council ERC Consolidator grant BrightSens 648528. We thank to C. Ruhlmann from the FRISBI platform for help with the electron microscopy, A. Reisch for fruitful discussions, and J. Valancianaite for reading the manuscript.

■ REFERENCES

- (1) Grimm, J. B.; English, B. P.; Chen, J. J.; Slaughter, J. P.; Zhang, Z. J.; Revyakin, A.; Patel, R.; Macklin, J. J.; Normanno, D.; Singer, R. H.; Lionnet, T.; Lavis, L. D. *Nat. Methods* **2015**, *12*, 244.
- (2) Scrimin, P.; Prins, L. J. *Chem. Soc. Rev.* **2011**, *40*, 4488.
- (3) (a) Choi, H. M. T.; Chang, J. Y.; Trinh, L. A.; Padilla, J. E.; Fraser, S. E.; Pierce, N. A. *Nat. Biotechnol.* **2010**, *28*, 1208. (b) Ali, M. M.; Li, F.; Zhang, Z.; Zhang, K.; Kang, D.-K.; Ankrum, J. A.; Le, X. C.; Zhao, W. *Chem. Soc. Rev.* **2014**, *43*, 3324.
- (4) (a) Thomas, S. W.; Joly, G. D.; Swager, T. M. *Chem. Rev.* **2007**, *107*, 1339. (b) Wu, W. B.; Bazan, G. C.; Liu, B. *Chem.* **2017**, *2*, 760. (c) Rochat, S.; Swager, T. M. *ACS Appl. Mater. Interfaces* **2013**, *5*, 4488. (d) Jiang, Y.; McNeill, J. *Chem. Rev.* **2017**, *117*, 838. (e) Chen, L. H.; McBranch, D. W.; Wang, H. L.; Helgeson, R.; Wudl, F.; Whitten, D. G. *Proc. Natl. Acad. Sci. U. S. A.* **1999**, *96*, 12287.
- (5) (a) Novotny, L.; van Hulst, N. *Nat. Photonics* **2011**, *5*, 83. (b) Acuna, G. P.; Moller, F. M.; Holzmeister, P.; Beater, S.; Lalkens, B.; Tinnefeld, P. *Science* **2012**, *338*, 506. (c) Anker, J. N.; Hall, W. P.; Lyandres, O.; Shah, N. C.; Zhao, J.; Van Duyne, R. P. *Nat. Mater.* **2008**, *7*, 442.
- (6) (a) Howes, P. D.; Chandrawati, R.; Stevens, M. M. *Science* **2014**, *346*, 1247390. (b) Wolfbeis, O. S. *Chem. Soc. Rev.* **2015**, *44*, 4743. (c) Chinen, A. B.; Guan, C. M.; Ferrer, J. R.; Barnaby, S. N.; Merkel, T. J.; Mirkin, C. A. *Chem. Rev.* **2015**, *115*, 10530.
- (7) (a) Alivisatos, P. *Nat. Biotechnol.* **2004**, *22*, 47. (b) Wegner, K. D.; Hildebrandt, N. *Chem. Soc. Rev.* **2015**, *44*, 4792.
- (8) (a) Bonacchi, S.; Genovese, D.; Juris, R.; Montalti, M.; Prodi, L.; Rampazzo, E.; Zaccheroni, N. *Angew. Chem., Int. Ed.* **2011**, *50*, 4056. (b) Lee, J. E.; Lee, N.; Kim, T.; Kim, J.; Hyeon, T. *Acc. Chem. Res.* **2011**, *44*, 893.

- (9) (a) Mei, J.; Leung, N. L. C.; Kwok, R. T. K.; Lam, J. W. Y.; Tang, B. Z. *Chem. Rev.* **2015**, *115*, 11718. (b) Li, K.; Liu, B. *Chem. Soc. Rev.* **2014**, *43*, 6570.
- (10) (a) Wu, C.; Chiu, D. T. *Angew. Chem., Int. Ed.* **2013**, *52*, 3086. (b) Pecher, J.; Mecking, S. *Chem. Rev.* **2010**, *110*, 6260.
- (11) Reisch, A.; Klymchenko, A. S. *Small* **2016**, *12*, 1968.
- (12) (a) Medintz, I. L.; Clapp, A. R.; Mattoussi, H.; Goldman, E. R.; Fisher, B.; Mauro, J. M. *Nat. Mater.* **2003**, *2*, 630. (b) Hildebrandt, N.; Spillmann, C. M.; Algar, W. R.; Pons, T.; Stewart, M. H.; Oh, E.; Susumu, K.; Diaz, S. A.; Delehanty, J. B.; Medintz, I. L. *Chem. Rev.* **2017**, *117*, 536. (c) Sapsford, K. E.; Berti, L.; Medintz, I. L. *Angew. Chem., Int. Ed.* **2006**, *45*, 4562. (d) Clapp, A. R.; Medintz, I. L.; Uyeda, H. T.; Fisher, B. R.; Goldman, E. R.; Bawendi, M. G.; Mattoussi, H. *J. Am. Chem. Soc.* **2005**, *127*, 18212. (e) Boeneman, K.; Mei, B. C.; Dennis, A. M.; Bao, G.; Deschamps, J. R.; Mattoussi, H.; Medintz, I. L. *J. Am. Chem. Soc.* **2009**, *131*, 3828.
- (13) Genovese, D.; Rampazzo, E.; Bonacchi, S.; Montalti, M.; Zaccheroni, N.; Prodi, L. *Nanoscale* **2014**, *6*, 3022.
- (14) (a) Clapp, A. R.; Medintz, I. L.; Mauro, J. M.; Fisher, B. R.; Bawendi, M. G.; Mattoussi, H. *J. Am. Chem. Soc.* **2004**, *126*, 301. (b) Zhang, C. Y.; Yeh, H. C.; Kuroki, M. T.; Wang, T. H. *Nat. Mater.* **2005**, *4*, 826.
- (15) Reisch, A.; Trofymchuk, K.; Runser, A.; Fleith, G.; Rawiso, M.; Klymchenko, A. S. *ACS Appl. Mater. Interfaces* **2017**, *9*, 43030.
- (16) (a) Reisch, A.; Didier, P.; Richert, L.; Oncul, S.; Arntz, Y.; Mely, Y.; Klymchenko, A. S. *Nat. Commun.* **2014**, *5*, 4089. (b) Andreiuk, B.; Reisch, A.; Lindecker, M.; Follain, G.; Peyrieras, N.; Goetz, J. G.; Klymchenko, A. S. *Small* **2017**, *13*, 1701582.
- (17) Scholes, G. D.; Fleming, G. R.; Olaya-Castro, A.; van Grondelle, R. *Nat. Chem.* **2011**, *3*, 763.
- (18) Trofymchuk, K.; Reisch, A.; Didier, P.; Fras, F.; Gilliot, P.; Mely, Y.; Klymchenko, A. S. *Nat. Photonics* **2017**, *11*, 657.
- (19) Puchkova, A.; Vietz, C.; Pibiri, E.; Wunsch, B.; Paz, M. S.; Acuna, G. P.; Tinnefeld, P. *Nano Lett.* **2015**, *15*, 8354.
- (20) (a) Brown, P. O.; Botstein, D. *Nat. Genet.* **1999**, *21*, 33. (b) Tyagi, S. *Nat. Methods* **2009**, *6*, 331. (c) Zheng, J.; Yang, R. H.; Shi, M. L.; Wu, C. C.; Fang, X. H.; Li, Y. H.; Li, J. H.; Tan, W. H. *Chem. Soc. Rev.* **2015**, *44*, 3036. (d) Jung, C.; Ellington, A. D. *Acc. Chem. Res.* **2014**, *47*, 1825. (e) Seferos, D. S.; Giljohann, D. A.; Hill, H. D.; Prigodich, A. E.; Mirkin, C. A. *J. Am. Chem. Soc.* **2007**, *129*, 15477. (f) Cutler, J. I.; Auyeung, E.; Mirkin, C. A. *J. Am. Chem. Soc.* **2012**, *134*, 1376. (g) Labib, M.; Mohamadi, R. M.; Poudineh, M.; Ahmed, S. U.; Ivanov, I.; Huang, C.-L.; Moosavi, M.; Sargent, E. H.; Kelley, S. O. *Nat. Chem.* **2018**, *10*, 489. (h) He, L.; Lu, D. Q.; Liang, H.; Xie, S. T.; Luo, C.; Hu, M. M.; Xu, L. J.; Zhang, X. B.; Tan, W. H. *ACS Nano* **2017**, *11*, 4060.
- (21) Nolan, T.; Hands, R. E.; Bustin, S. A. *Nat. Protoc.* **2006**, *1*, 1559.
- (22) (a) Dirks, R. M.; Pierce, N. A. *Proc. Natl. Acad. Sci. U. S. A.* **2004**, *101*, 15275. (b) Huang, J.; Wang, H.; Yang, X. H.; Quan, K.; Yang, Y. J.; Ying, L.; Xie, N. L.; Ou, M.; Wang, K. M. *Chem. Sci.* **2016**, *7*, 3829. (c) Wu, C. C.; Cansiz, S.; Zhang, L. Q.; Teng, I. T.; Qiu, L. P.; Li, J.; Liu, Y.; Zhou, C. S.; Hu, R.; Zhang, T.; Cui, C.; Cui, L.; Tan, W. H. *J. Am. Chem. Soc.* **2015**, *137*, 4900.
- (23) (a) Gaylord, B. S.; Heeger, A. J.; Bazan, G. C. *Proc. Natl. Acad. Sci. U. S. A.* **2002**, *99*, 10954. (b) Wang, Y. S.; Liu, B. *Chem. Commun.* **2007**, 3553. (c) Dore, K.; Dubus, S.; Ho, H. A.; Levesque, I.; Brunette, M.; Corbeil, G.; Boissinot, M.; Boivin, G.; Bergeron, M. G.; Boudreau, D.; Leclerc, M. *J. Am. Chem. Soc.* **2004**, *126*, 4240.
- (24) Wang, S.; Gaylord, B. S.; Bazan, G. C. *J. Am. Chem. Soc.* **2004**, *126*, 5446.
- (25) Ochmann, S. E.; Vietz, C.; Trofymchuk, K.; Acuna, G. P.; Lalkens, B.; Tinnefeld, P. *Anal. Chem.* **2017**, *89*, 13000.
- (26) (a) Alemdaroglu, F. E.; Herrmann, A. *Org. Biomol. Chem.* **2007**, *5*, 1311. (b) Wilks, T. R.; O'Reilly, R. K. *Sci. Rep.* **2016**, *6*, 39192.
- (27) (a) Watson, K. J.; Park, S. J.; Im, J. H.; Nguyen, S. T.; Mirkin, C. A. *J. Am. Chem. Soc.* **2001**, *123*, 5592. (b) Jia, F.; Lu, X. G.; Tan, X. Y.; Zhang, K. *Chem. Commun.* **2015**, *51*, 7843. (c) Rush, A. M.;

Nelles, D. A.; Blum, A. P.; Barnhill, S. A.; Tatro, E. T.; Yeo, G. W.; Gianneschi, N. C. *J. Am. Chem. Soc.* **2014**, *136*, 7615.

(28) (a) Banga, R. J.; Krovi, S. A.; Narayan, S. P.; Sprangers, A. J.; Liu, G. L.; Mirkin, C. A.; Nguyen, S. T. *Biomacromolecules* **2017**, *18*, 483. (b) Farokhzad, O. C.; Jon, S. Y.; Khademhosseini, A.; Tran, T. N.T.; LaVan, D. A.; Langer, R. *Cancer Res.* **2004**, *64*, 7668. (c) Zhu, S. S.; Xing, H.; Gordiichuk, P.; Park, J.; Mirkin, C. A. *Adv. Mater.* **2018**, *30*, 1707113.

(29) Reisch, A.; Runser, A.; Arntz, Y.; Mely, Y.; Klymchenko, A. S. *ACS Nano* **2015**, *9*, 5104.

(30) Olie, R. A.; Simoes-Wust, A. P.; Baumann, B.; Leech, S. H.; Fabbro, D.; Stahel, R. A.; Zangemeister-Wittke, U. *Cancer Res.* **2000**, *60*, 2805.

(31) (a) Prigodich, A. E.; Randeria, P. S.; Briley, W. E.; Kim, N. J.; Daniel, W. L.; Giljohann, D. A.; Mirkin, C. A. *Anal. Chem.* **2012**, *84*, 2062. (b) Prigodich, A. E.; Seferos, D. S.; Massich, M. D.; Giljohann, D. A.; Lane, B. C.; Mirkin, C. A. *ACS Nano* **2009**, *3*, 2147.

(32) Jewett, J. C.; Bertozzi, C. R. *Chem. Soc. Rev.* **2010**, *39*, 1272.

(33) Lauer, M. H.; Vranken, C.; Deen, J.; Frederickx, W.; Vanderlinden, W.; Wand, N.; Leen, V.; Gehlen, M. H.; Hofkens, J.; Neely, R. K. *Chem. Sci.* **2017**, *8*, 3804.

(34) Woller, J. G.; Hannestad, J. K.; Albinsson, B. *J. Am. Chem. Soc.* **2013**, *135*, 2759.

(35) (a) Søren, P.; Marcus, W. L. *ChemBioChem.* **2012**, *13*, 1990.

(b) Nir, E.; Michalet, X.; Hamadani, K. M.; Laurence, T. A.; Neuhauser, D.; Kovchegov, Y.; Weiss, S. *J. Phys. Chem. B* **2006**, *110*, 22103.

(36) Zhang, J. X.; Fang, J. Z.; Duan, W.; Wu, L. R.; Zhang, A. W.; Dalchau, N.; Yordanov, B.; Petersen, R.; Phillips, A.; Zhang, D. Y. *Nat. Chem.* **2017**, *10*, 91.

Supporting information

DNA- functionalized dye-loaded polymeric nanoparticles: ultrabright FRET platform for amplified detection of nucleic acids

Nina Melnychuk and Andrey S. Klymchenko*

Laboratoire de Bioimagerie et Pathologies, UMR 7021 CNRS, Faculté de Pharmacie, Université de
Strasbourg, France

*e-mail: andrey.klymchenko@unistra.fr

Table of Contents

1. Experimental section	3
1.1. Materials	3
1.2. FRET-based molecular probe preparation	4
1.3. Nanoparticle characterization	4
1.4. Transmission electron microscopy (TEM)	5
1.5. Estimation of number of dyes per particle and the molar extinction coefficient of NP-probe	5
1.6. Fluorescence microscopy	6
1.7. Protocols of synthesis	8
<i>1.7.1. Synthesis of Asp(OtBu)-N3 linker</i>	8
<i>1.7.2. Synthesis of modified PMMA polymers</i>	10
<i>1.7.3 NMR and mass spectra</i>	12
2. Supporting Figures and Tables	17
2.1. Dynamic light scattering	17
2.2. Optical spectroscopy	18
2.3. Single-particle measurements	27
2.4. Tables	31
3. References	33

1. Experimental section

1.1. Materials

Chemical compounds: Poly (methyl methacrylate-co-methacrylic acid) (PMMA-MA, 1.6% methacrylic acid, Mn ~15000, Mw ~34000), 3-chloropropanamine hydrochloride (98%), rhodamine B octadecyl ester perchlorate (>98.0%), lithium tetrakis (pentafluorophenyl)borate ethyl etherate, N,N-dimethylformamide (anhydrous, 98%), N,N-Diisopropylethylamine ($\geq 99\%$), acetonitrile (anhydrous, 99.8%), dichloromethane (anhydrous, $\geq 99.8\%$), 1-Hydroxybenzotriazole ($\geq 97\%$), 3-azido-1-propamine ($\geq 95\%$), BSA-biotin, Deoxyribonucleic acid sodium salt from calf thymus (Type I, fibers), Albumin bovine serum (Fraction V, minimum 96%, lyophilized powder), Amicon Centrifugal filters (0.5mL, 100K) were purchased from Sigma-Aldrich. Citric acid monohydrate ($\geq 99.5\%$), sodium azide (99%), sodium iodide ($\geq 99.5\%$) and trifluoroacetic acid (99%) were purchased from Alfa Aesar. Sulfo-Cyanine3 azide (95%) was purchased from Lumiprobe. Fmoc-Asp(OtBu)-OH was purchased from Activotec. HBTU was purchased from ChemPep Inc. Neutravidin, LabTek chambers (Borosilicate cover glass, eight wells), QDot[®] 605 Streptavidin Conjugate (QDot-605), OptiMEM (Gibco[®]) and FBS (Gibco[®]) were purchased from ThermoFisher Scientific. Illustra NAP Columns (prepacked with Sephadex G-25 DNA Grade) were purchased from GE Healthcare. Human Serum was purchased from hospital and supernatant was stored at -20 °C. Sodium phosphate monobasic (>99.0%, Sigma-Aldrich) and sodium phosphate dibasic dihydrate (>99.0%, Sigma- Aldrich) were used to prepare 20 mM phosphate buffers at pH 7.4. For saline buffer sodium chloride ($\geq 99\%$, Sigma Aldrich) 30 mM and magnesium chloride ($\geq 98\%$, Sigma Aldrich) 12 mM was added to 20 mM phosphate buffer and pH was adjusted with sodium hydroxide 1N solution. Milli-Q water (Millipore) was used in all experiments. For immobilization protocol PBS (without Ca²⁺ and Mg²⁺) was purchased from Lonza.

1.2. FRET-based molecular probe preparation

To 120 μL of 20 mM phosphate buffer containing 50 mM NaCl and 1 mM of EDTA was added 30 μL of SurC-DBCO (400 μM stock in water) and 50 μL of Sulfo-Cyanine3 azide (2 mM stock in water). The mixture was left overnight under shaking (Thermomixer comfort, Eppendorf, 400 rpm) at room temperature. Then, the mixture was purified using disposable columns pre-packed with Sephadex G-25 DNA Grade (illustra NAP Columns, GE Healthcare) and 20 mM phosphate buffer as an eluent. The fractions were collected in 50 μL volumes and the conjugate formation was verified by absorption and fluorescence emission spectra. The 10 μM of conjugate was further mixed with 10 μM of TCS-Cy5 and the mixture was heated for 70 $^{\circ}\text{C}$ in water bath for 3 mins. Finally, it was cooled down to room temperature and kept in the dark for 2 hours before the experiments.

1.3. Nanoparticle characterization

Measurements for the determination of the size of nanoparticles were performed on a Zetasizer Nano ZSP (Malvern Instruments S.A.). The mean value of the diameter of the size distribution per volume was used for analysis. Absorption spectra were recorded on a Cary 4000 scan UV-visible spectrophotometer (Varian), excitation and emission spectra were recorded on a FluoroMax-4 spectrofluorometer (Horiba Jobin Yvon). For standard recording of fluorescence spectra, the excitation wavelength was set to 530 nm. The fluorescence spectra were corrected for detector response and lamp fluctuations. Quantum yields of donor dye in NPs were calculated using Rhodamine 101 in methanol as a reference (QY = 1.0) with an absorbance of 0.01 at 530 nm.¹ QYs of the acceptor were measured using DiD in methanol (QY = 0.33) as a reference.² To calculate FRET efficiency based on fluorescence spectra, a classical equation was used: $E_{\text{FRET}} = 1 - \frac{I_{D-A}}{I_D}$, where I_D is the donor maximum intensity and I_{D-A} is the maximum intensity of the donor in the presence of the acceptor. Amplification factor of the acceptor emission (antenna effect, AE) was expressed as

the ratio of the maximal excitation intensity of the donor to that of the acceptor with correction from the emission of the donor dyes at 690 nm:³

$$AE = \frac{I_{D-FRET}^{ex} - I_D^{ex} * \frac{I_{D-FRET}^{em}}{I_D^{em}}}{I_{A-FRET}^{ex} - I_A^{ex}}$$

Where I_{D-FRET}^{ex} and I_{A-FRET}^{ex} are the maximal excitation intensities of donor and acceptor in NP-Probe, respectively; I_D^{ex} and I_A^{ex} are the excitation intensities at the wavelengths of excitation maximum of donor and acceptor in NP-SurC-T20; I_{D-FRET}^{em} and I_D^{em} maximum emission intensity of donor for NP-Probe and NP-SurC-T20, respectively.

1.4. Transmission electron microscopy (TEM)

Carbon-coated copper-rhodium electron microscopy grids with a 300 mesh (Euromedex, France) were surface treated with a glow discharge in amylamine atmosphere (0.45 mbar, 4 – 4.5 mA, 22 s) in an Elmo glow discharge system (Cordouan Technologies, France). Then, 5 μ L of the solution of NPs at 0.04 g/L were deposited onto the grids and left for 2 min. The grids were then treated for 1 min with a 2% uranyl acetate solution for staining. They were observed with a Philips CM120 transmission electron microscope equipped with a LaB6 filament and operating at 100 kV. Areas covered with nanoparticles of interest were recorded at different magnifications on a Peltier cooled CCD camera (Model 794, Gatan, Pleasanton, CA). Image analysis was performed using the Fiji software.

1.5. Estimation of number of dyes per particle and the molar extinction coefficient of NP-probe

Using the diameter of NPs measured by TEM, we calculated the volume of a nanoparticle in form of sphere. Then, we estimated how many dye molecules are encapsulated per nanoparticle of a given volume. Based on loading of the donor dye into the polymer matrix of NPs (30 wt%), we calculated

the number of moles of the dye per volume of the single particle. The latter value was multiplied by the Avogadro constant giving the estimated number of donor dye molecules per particle (~3200). Then, based on the absorption spectrum of NP-probe (Fig. 3b) and known molar extinction coefficient of R18 dye ($125,000 \text{ M}^{-1}\text{cm}^{-1}$), we estimated the extinction coefficient of the dye at 550 nm ($100,000 \text{ M}^{-1}\text{cm}^{-1}$), corresponding to the excitation wavelength used in microscopy. Then, the total molar extinction coefficient of NP-probe at 550 nm was estimated as $3200 \times 100,000 = 3.2 \times 10^8 \text{ M}^{-1} \text{ cm}^{-1}$. To calculate the number of hybridized TCS-Cy5 per particle, the molar concentration of the donor R18/F5-TPB ($C(\text{donor})$) and the acceptor TCS-Cy5 ($C(\text{acceptor})$) dyes were estimated based on the absorbance of NP-probe at 560 and 650 nm, respectively. Then, the number of TCS-Cy5 per particle was estimated as $3200 \times C(\text{acceptor}) / C(\text{donor})$.

1.6. Fluorescence microscopy

Immobilization of nanoparticles and QDot-605 in LabTek chamber was performed according to previously described protocol.⁴ The LabTek chamber was washed 3 times with PBS followed by incubation with 200 μL of BSA-Biotin (0.5 mg mL^{-1} in BPS) for 5 min. Then, BSA-biotin solution was removed, and the chamber was washed 3 times with 500 μL of PBS. In case of NP-probe immobilization, the chamber was incubated with 200 μL of neutravidin solution (0.5 mg mL^{-1} in BPS) for 5 min and washed 3 times with 500 μL of PBS. Then the chamber was incubated with 200 μL of 1 μM solution of A20-biotin in PBS for 5 min and washed 3 times with 20 mM phosphate buffer containing 12 mM MgCl_2 and NaCl 30mM. Then NP-Probe solution was deposited with proper concentration to achieve desired density and incubated for 1 hour at room temperature in the dark. Before measurements the chamber was washed 2 times with 20 mM phosphate buffer containing 12 mM MgCl_2 and 30 mM NaCl and covered with 200 μL of the same buffer. In case of QDot-605 immobilization, QDot-605 Streptavidin Conjugate (ThermoFisher Scientific) was diluted

to 100 pM concentration in PBS and 300 μL was added to the chamber. After 1 h of incubation, the chamber was washed 3 times with 500 μL of PBS and filled with 200 μL of PBS.

Single-particle measurements were performed in the epi-fluorescence mode using Nikon Ti-E inverted microscope with a 100x objective (Apo TIRF, oil, NA 1.49, Nikon). The excitation was provided by light emitting diodes (SpectraX, Lumencor) at 550 and a 640 nm. The 550-nm light power was set to 0.2 mW at the sample level. The diameter of the wide-field illumination spot was 250 μm, according to a photobleaching test, so that the power density used at 550 nm was 0.4 W cm⁻². For direct excitation of acceptor Cy5, the 640-nm light was used with a power density of 20 W cm⁻². The fluorescence signal was recorded with a Hamamatsu Orca Flash 4 camera. The exposure time was set to 200 ms per image frame. To enable two-color image detection, corresponding to R18/F5-TPB and Cy5 signals, W-VIEW GEMINI image splitting system (Hamamatsu) was used with dichroic 640 nm (Semrock FF640-FDi01-25x36). Single-particle analysis was performed using the Fiji software. Particle locations were detected through a Fiji routine applied to a projection (maximum intensity) of 20 frames. After the automatic background subtraction, the mean intensities of circular regions of interest with a diameter of 8 pixels around the found particle locations were then measured. Average of intensity of NPs was obtained base on the first 3 frames for each channel. At least three image sequences (245 pixel × 245 pixel) per condition were analyzed with, on average, 500-1000 particles per sample.

The amplification factor of the acceptor emission at the single particle level was determined using:

$$AF = \frac{I_A^{550nm}}{I_A^{640nm}} \times \frac{P^{640nm}}{P^{550nm}}$$

Where I_A^{550nm} and I_A^{640nm} are mean intensities of acceptors under excitation at 550 and 640 nm, respectively, and P^{640nm} and P^{550nm} are laser powers at corresponding wavelengths. The

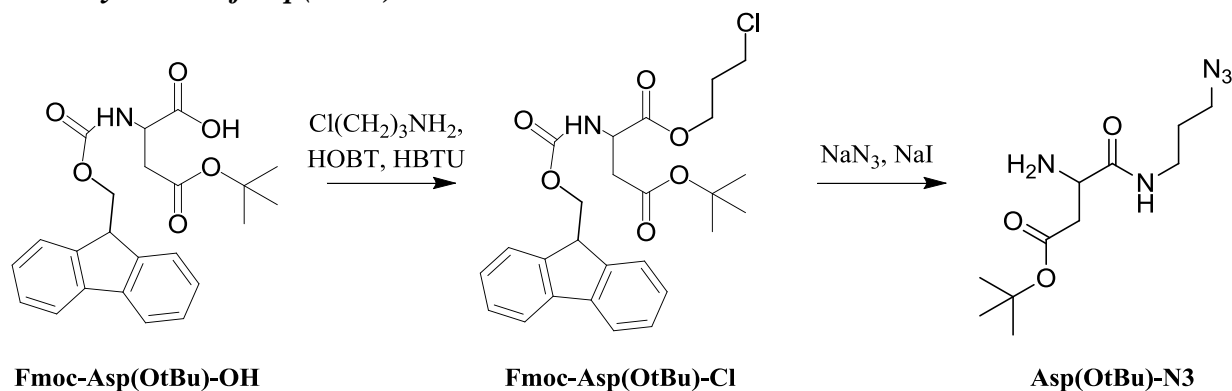
amplification factor indicates how many fold the emission increases when the dye is excited via nanoantenna vs direct dye excitation.

Comparison of single-particle brightness of our NPs vs QDot-605 was done using the same experimental setup. Excitation of nanoantenna particles was done using 550-nm light with power density of 0.56 W cm^{-2} , whereas QDot-605 were excited by 470-nm light with power density of 14 W cm^{-2} .

1.7. Protocols of synthesis

NMR spectra were recorded at 20°C on Bruker Avance III 400MHz spectrometer and chemical shifts were reported as delta scale in ppm relative to CHCl_3 ($\delta = 7.26 \text{ ppm}$) for ^1H NMR and CDCl_3 ($\delta = 77.16 \text{ ppm}$) for ^{13}C NMR. Mass spectra were obtained using an Agilent Q-TOF 6520 mass spectrometer.

1.7.1. Synthesis of Asp(OtBu)-N3 linker



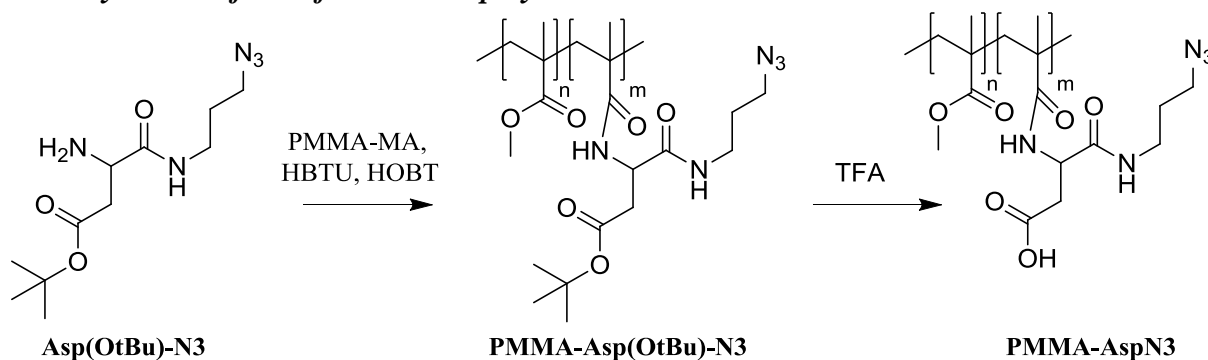
Tert-butyl 3-[(3-chloropropyl) carbamoyl]-3-[[9H-fluoren-9-ylmethoxy]carbonyl]amino] propanoate (Fmoc-Asp(OtBu)-Cl). Fmoc-Asp(OtBu)-OH (1 eq 6 mmol 2.47 g), HBTU (1.2 eq 7.2 mmol 2.73 g) and HOBt (1.3 eq 7.8 mmol 1.05 g) were dissolved in 30 mL of anhydrous N,N-

dimethylformamide. After complete dissolution the N,N-diisopropylethylamine (3 eq 18 mmol 2.97 mL) was added to the stirring mixture under argon at room temperature and after 15 min 3-chloropropanamine hydrochloride (1 eq 6 mmol 0.78 g) was added. The reaction was stirred for 24 h and completion of the reaction was checked by TLC (DCM/MeOH 98/2). The solvent was evaporated under reduced pressure, the residue was diluted with water and precipitate was collected. The crude product was washed with solution of citric acid, followed by solution of sodium bicarbonate. After the crude product was purified by column chromatography (DCM/MeOH 98/2), the product was obtained as pale-yellow solid (2.3 g 80% yield). ^1H NMR (400 MHz, CDCl_3) δ , ppm: 1.46 (s, 9 H), 1.98 (quin, $J=6.30$ Hz, 2 H), 2.60 (dd, $J=16.75$, 6.24 Hz, 1 H), 2.95 (br d, $J=15.16$ Hz, 1 H), 3.45 (m, 2 H), 3.56 (br t, $J=6.24$ Hz, 2 H), 4.23 (m, 1 H), 4.36 - 4.60 (m, 3 H), 5.93 (br s, 1 H), 6.59 (br s, 1 H), 7.27 - 7.36 (m, 2 H), 7.42 (t, $J=7.50$ Hz, 2 H), 7.60 (d, $J=7.34$ Hz, 2 H), 7.78 (d, $J=7.58$ Hz, 2 H). ^{13}C NMR (101 MHz, CDCl_3) δ , ppm: 28.00, 31.92, 37.07, 37.35, 42.16, 47.13, 51.12, 67.07, 81.88, 120.01, 124.93, 127.01, 127.05, 127.74, 141.28, 143.58, 143.63, 156.02, 170.71, 171.20. . HR/LC/MS for $\text{C}_{26}\text{H}_{31}\text{ClN}_2\text{O}_5$ m/z (M+) calc 487.19943, found 487.19706.

Tert-butyl 3-amino-4-((3-azidopropyl)amino)-4-oxobutanoate (Asp(OtBu)-N3). Fmoc-Asp-Cl (1 eq 3 mmol 1.5 g), sodium azide (5 eq 15.4 mmol 1 g) and sodium iodide (1 eq 3 mmol 0.47 g) were dissolved in anhydrous N,N-dimethylformamide (20 mL) and stirred under Ar overnight at 60 °C. Then, the solvent was evaporated, the residue was extracted with water/DCM and washed twice with brine. The crude product was purified by column chromatography (DCM/MeOH 94/6). By LCMS and NMR was observed Fmoc deprotected Asp(OtBu)-N3 as pale-yellow oil (460 mg 55% yield). ^1H NMR (400 MHz, CDCl_3) δ , ppm: 1.46 (s, 9 H), 1.65 (m, 2 H), 1.81 (quin, $J=6.72$ Hz, 2 H) 2.57 (dd, $J=16.63$, 8.07 Hz, 1 H) 2.8 - 2.85 (m, 1 H) 3.29 - 3.44 (m, 4 H) 3.63 (dd, $J=8.07$, 3.67 Hz, 1 H), 7.57 (br s, 1 H). ^{13}C NMR (101 MHz, CDCl_3) δ ppm 28.08, 28.89, 36.65, 40.52, 49.20,

52.02, 81.15, 171.24, 173.71. HR/LC/MS for $C_{11}H_{21}N_5O_3$ m/z (M+) calc 272.17226, found 272.17153.

1.7.2. Synthesis of modified PMMA polymers



PMMA-Asp(OtBu)-N3. The PMMA-MA (1 eq of COOH groups, 0.06 mmol, 400 mg) was dissolved in anhydrous N,N-dimethylformamide (5 mL). To this solution HBTU (3 eq, 0.183 mmol, 70 mg), HOBT (4 eq, 0.24 mmol, 33 mg) and N,N-diisopropylethylamine (10 eq 0.61 mmol 0.1 mL) was added. The mixture was stirred for 15 min and after Asp(OtBu)-N3 (3 eq 0.183 mmol 50 mg) was added. The reaction was stirred overnight at room temperature under argon. The solvent was evaporated under reduced pressure and residue was dissolved in minimum of acetonitrile and precipitated with methanol. The precipitate was washed with methanol, redissolved in acetonitrile and reprecipitated twice in methanol. After drying under a vacuum, product was obtained as a white solid – 220 mg, yield 55%. ^1H NMR (400 MHz, CDCl_3) δ , ppm: 0.85 (br s, 2 H), 1.02 (br s, 1 H), 1.18 - 1.29 (m, 0.31 H), 1.46 (br s, 0.29 H), 1.65 (br s, 1H), 1.74 - 2.11 (m, 2 H), 3.60 (br s, 3 H). (Degree of modification was 82%, calculated from BOC signal in NMR spectra).

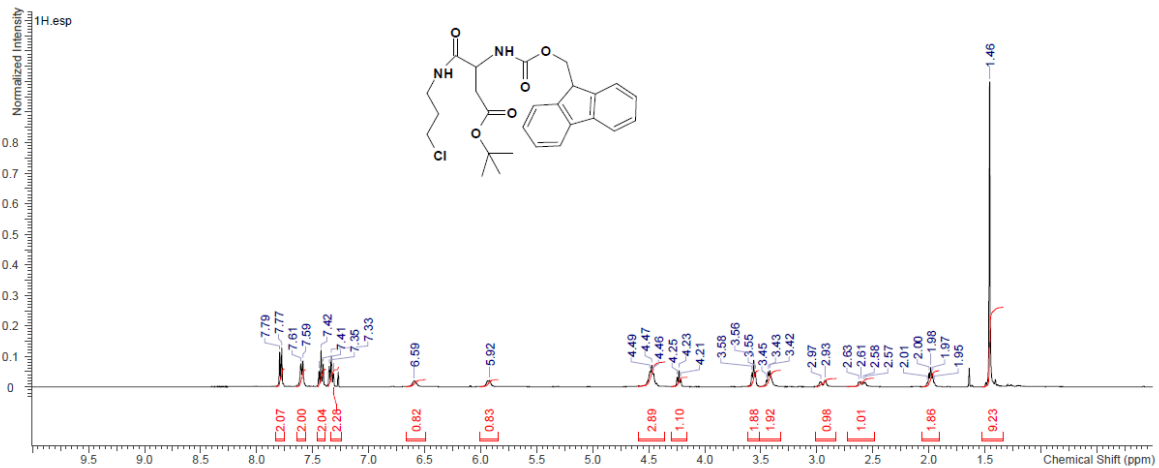
PMMA-AspN3. PMMA-Asp(OtBu)-N3 (200 mg) was dissolved in anhydrous dichloromethane (5 mL) and 2 mL of trifluoroacetic acid was added. The mixture was stirred for 3 h. Then solvents were evaporated under reduced pressure. Acetonitrile was added to the residue and evaporation was repeated several times until the absence of the trifluoroacetic acid. Then the product was precipitated

in methanol and filtrated. After drying under vacuum, the product was obtained as a white solid – 160 mg, yield 80%. ¹H NMR (400 MHz, CDCl₃) δ, ppm: 0.78 - 1.11 (m, 2 H), 0.94 - 1.11 (m, 1 H), 1.24 (br s, 0.30 H), 1.45 (br s, 0.37 H), 1.72 - 2.15 (m, 2 H), 3.60 (br s, 3 H).

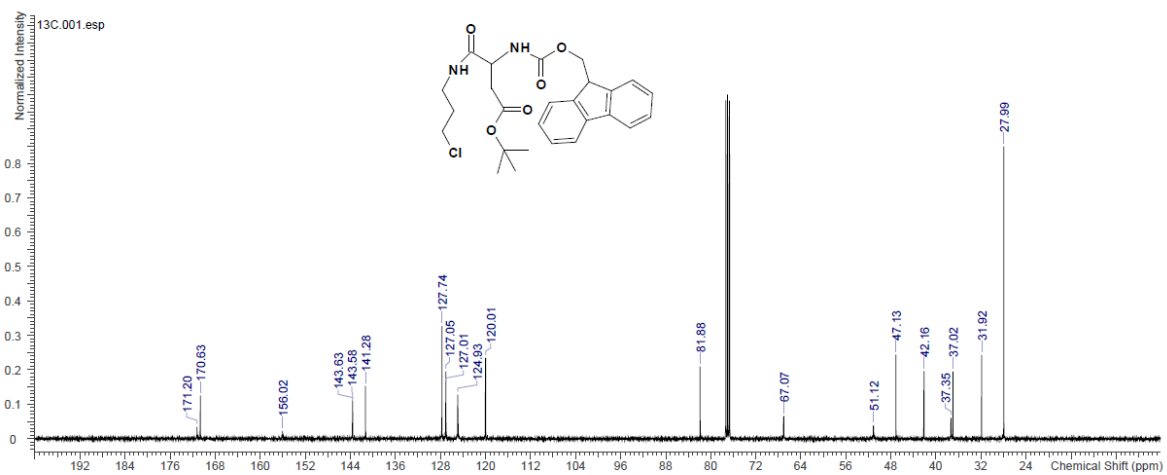
PMMA-N3. The PMMA-MA (1eq of COOH groups, 0.03 mmol, 250mg) was dissolved in anhydrous N,N-dimethylformamide (5 ml). To this solution HBTU (3eq, 0.098 mmol, 38 mg), HOBt (3.3 eq, 0.109 mmol, 15 mg) and N,N-diisopropylethylamine (10eq, 0.33mmol, 0.054mL) was added. The mixture was stirred for 15 min and after 3-azido-1-propamine (3eq, 0.098 mmol, 10mg) was added. The reaction was stirred overnight at room temperature under argon. The solvent was evaporated under reduced pressure and residue was dissolved in minimum of acetonitrile and precipitate with methanol. The precipitate was washed with methanol, redissolved in acetonitrile and reprecipitated twice in methanol. After drying under a vacuum, product was obtained as a white solid – 130 mg, yield 52%. ¹H NMR (400 MHz, CDCl₃) δ, ppm: 0.84 (br s, 2 H), 1.02 (br s, 1 H), 1.19 - 1.28 (m, 0.31 H), 1.44 (m, 0.29 H), 1.79 - 2.07 (m, 2 H), 3.60 (br s, 3 H).

Rhodamine B octadecyl ester trakis(penta-fluorophenyl)borate (R18/F5) was synthesized by ion exchange and purified by column chromatography as described previously.⁵

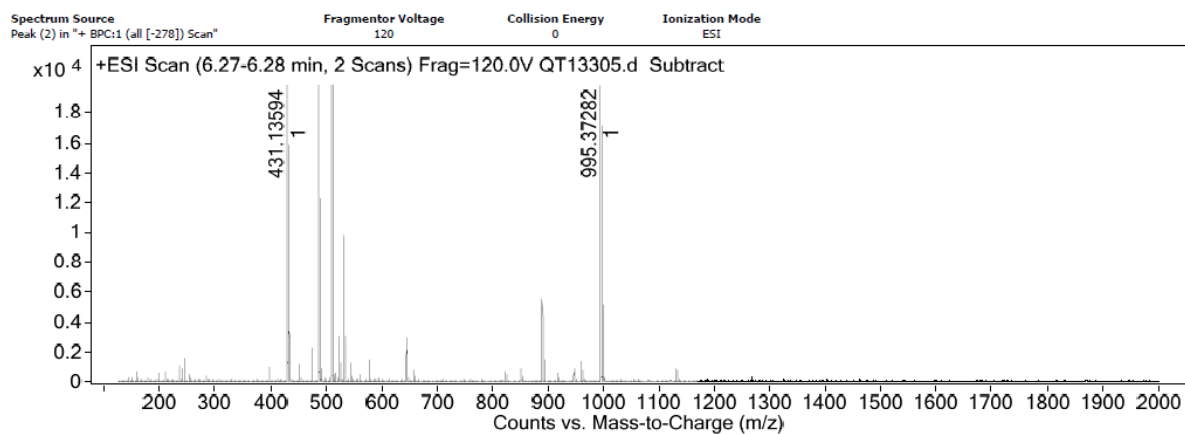
1.7.3 NMR and mass spectra



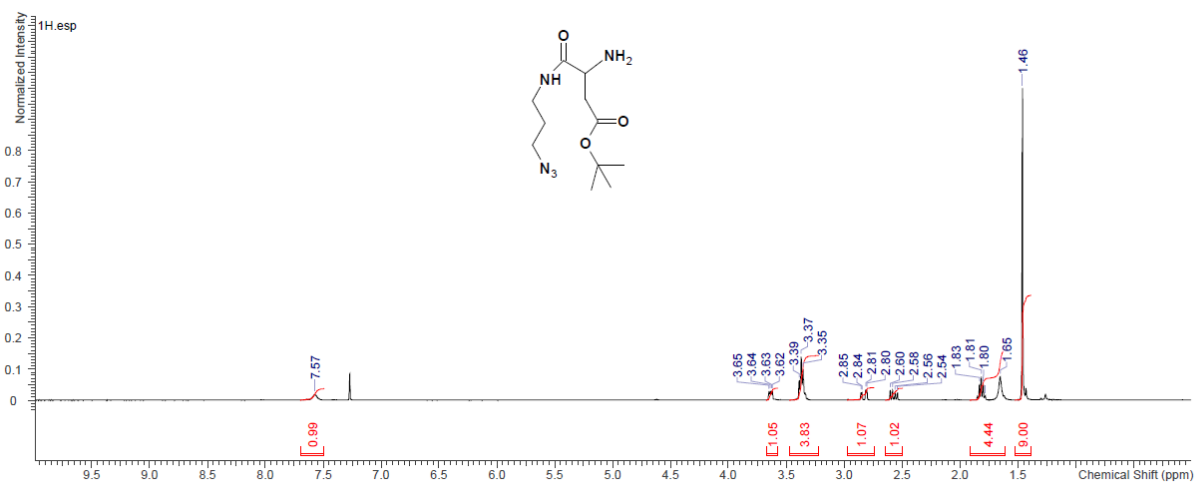
¹H NMR spectrum of Fmoc-Asp(OtBu)-Cl.



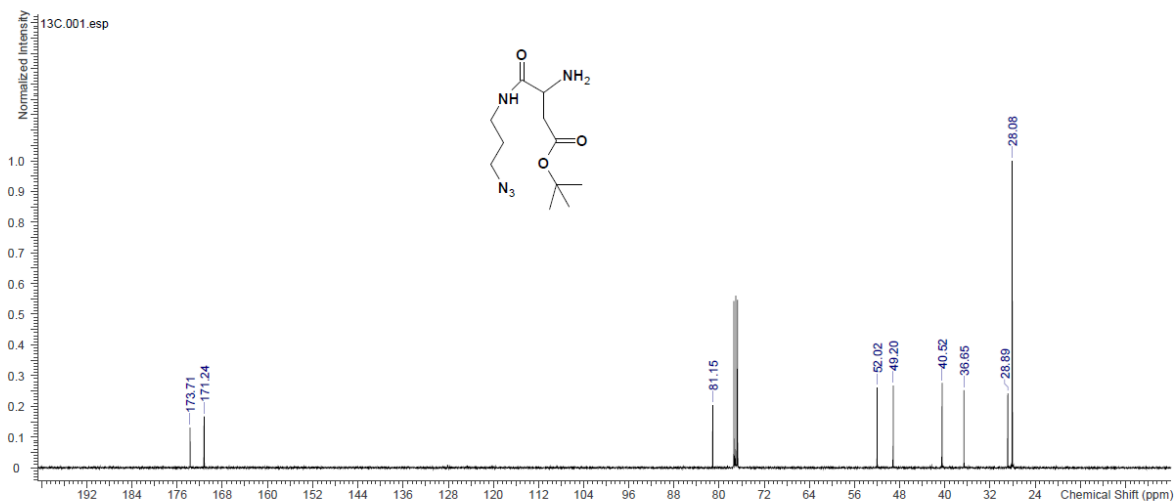
¹³C NMR spectrum of Fmoc-Asp(OtBu)-Cl.



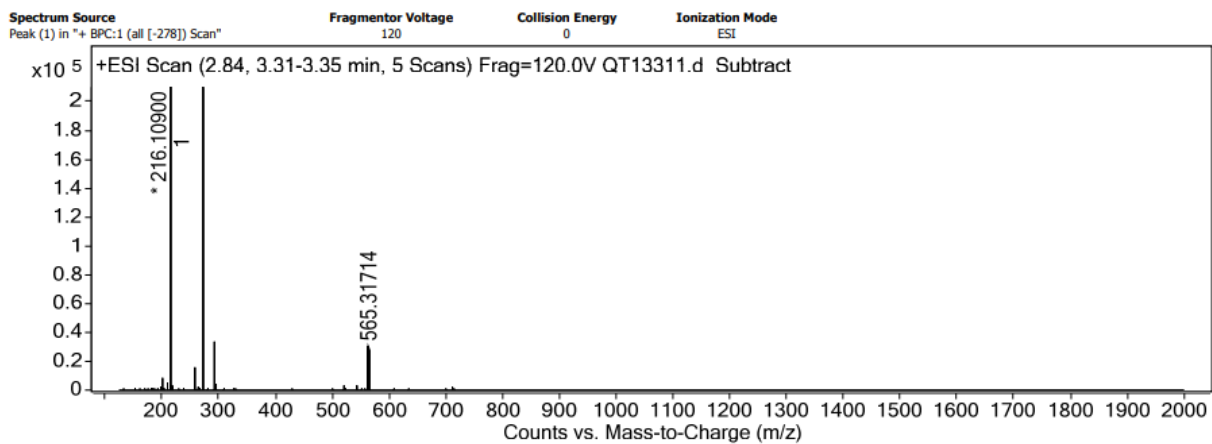
Mass spectrum of Fmoc-Asp(OtBu)-Cl.



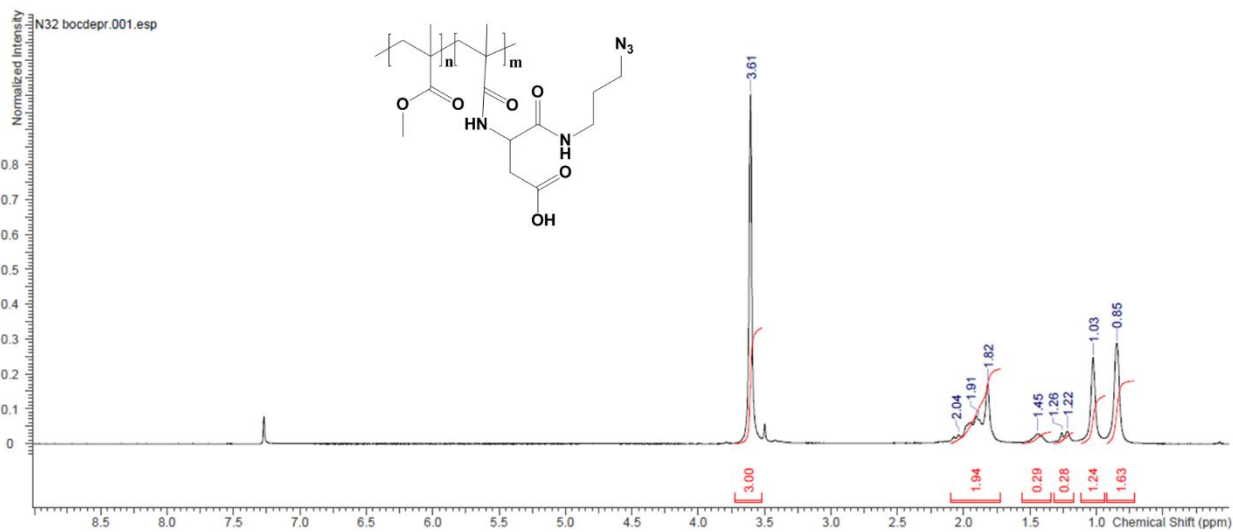
¹H NMR spectrum of Asp(OtBu)-N3.



^{13}C NMR spectrum of Asp(OtBu)-N3.



Mass spectrum of Asp(OtBu)-N3.



¹H NMR spectrum of PMMA-AspN3.

2. Supporting Figures and Tables

2.1. Dynamic light scattering

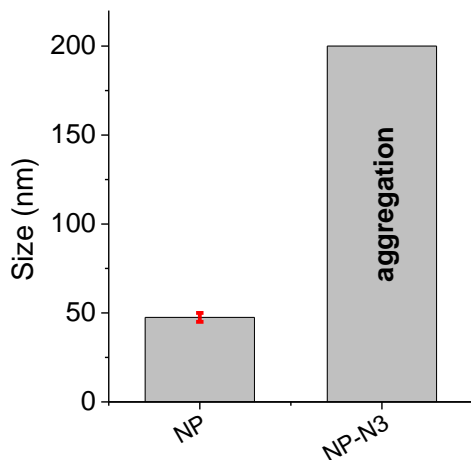


Figure S1. Size of NPs prepared from PMMA polymers with and without carboxyl group. Hydrodynamic diameter by DLS of NPs made from non-modified PMMA-MA (NP) and PMMA-MA with azide moiety grafted to the carboxyl group of the polymer (NP-N3). Absence of charged carboxyl group in the latter polymer leads to aggregation of polymer after nanoprecipitation in phosphate buffer, in contrast to parent PMMA-MA. Error is standard deviation of the mean ($n = 3$).

2.2. Optical spectroscopy

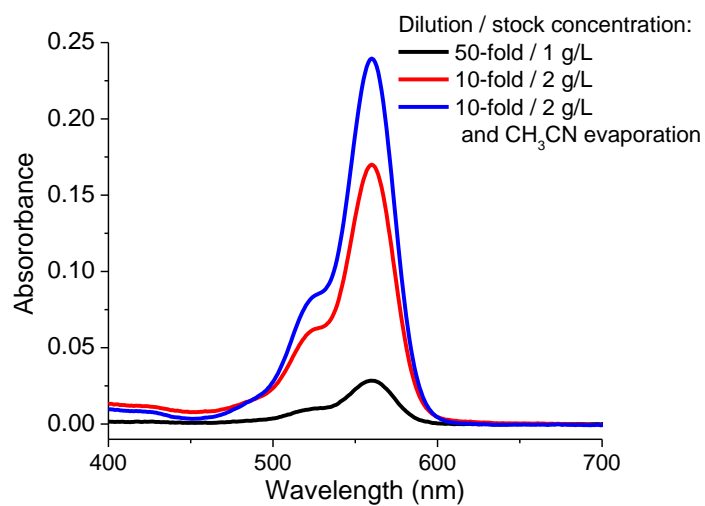


Figure S2. Absorption spectra of NPs prepared from PMMA-AspN3 polymer (NP-AspN3) using different protocols. Nanoprecipitation of more concentrated solution of polymer with lower dilution (10-fold) in phosphate buffer, followed by acetonitrile evaporation, provides more concentrated samples of NPs.

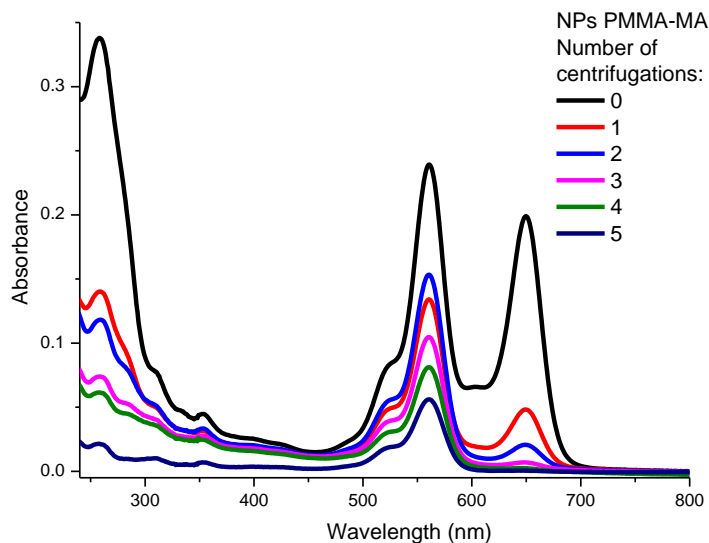


Figure S3. Purification by ultrafiltration of NPs from non-reacted oligonucleotides (SurC-DBCO hybridized with TCS-Cy5) monitored by absorption spectra. Control PMMA-MA NPs (without azide groups) were incubated with SurC-DBCO for 20 h at 40 °C, followed by hybridization with TCS-Cy5. Absorption spectra are presented at different steps of purification by ultrafiltration with centrifugal filters.

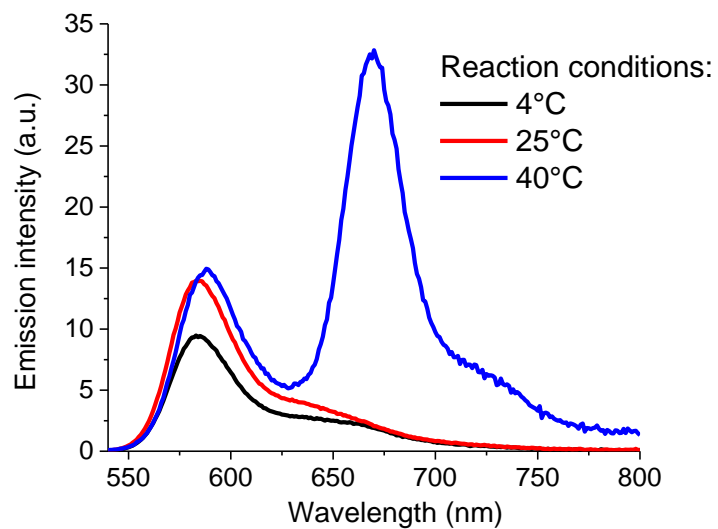


Figure S4. Monitoring grafting of oligonucleotides at different temperatures using FRET. Fluorescence emission spectra of NP-AspN3 after reaction with SurC (10 μ M) and hybridization with TCS-Cy5 at different temperature conditions followed by purification by ultrafiltration. Excitation wavelength was 530 nm.

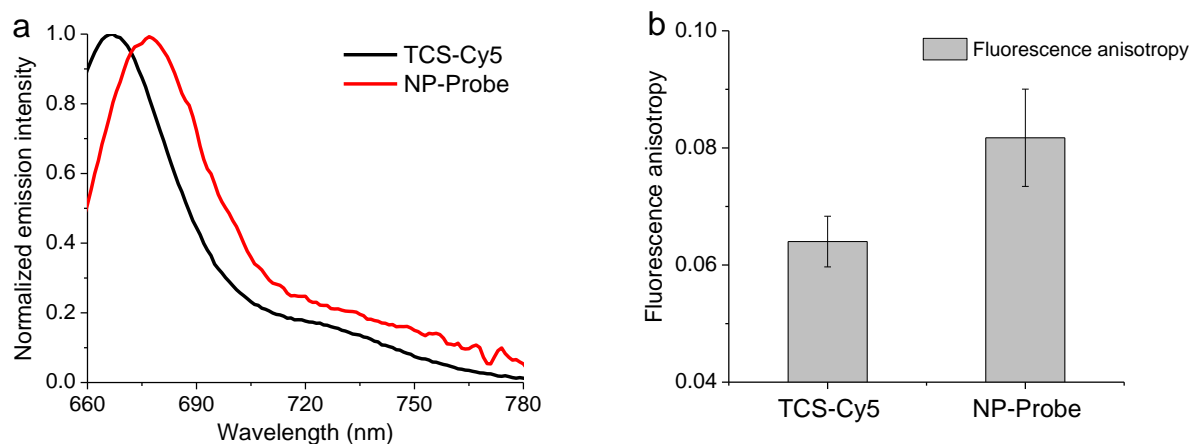


Figure S5. Evidences for hybridization of TCS-Cy5 with SurC grafted to nanoantenna. (a) Fluorescence emission spectra (excitation at 640 nm) of TCS-Cy5 along (50 nM) and in the NP-Probe. (b) Fluorescence anisotropy values of Cy5-dye in TCS-Cy5 along and in the NP-Probe (excitation at 640 nm, emission at 665 nm). Anisotropy values: 0.0640 ± 0.0043 for TCS-Cy5 and 0.0817 ± 0.0083 for NP-Probe. Error is standard deviation of the mean ($n = 3$).

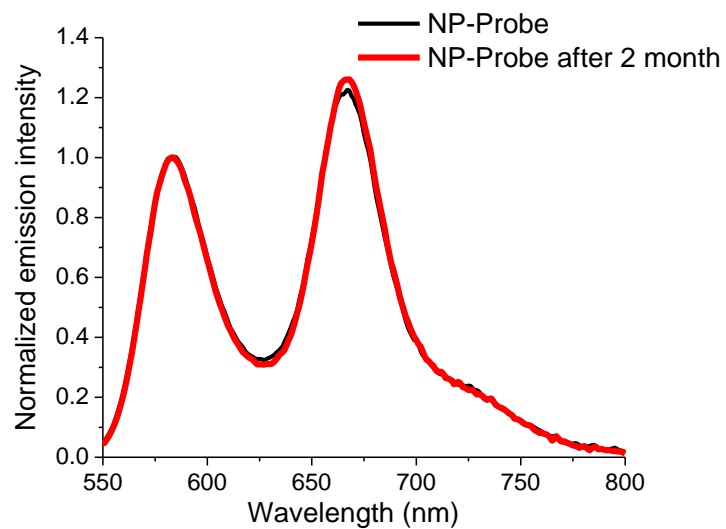


Figure S6. Stability of NP-probe over time. Fluorescence emission spectra of NP-Probe immediately after preparation and after 2 months storage in the dark at 4 °C. Phosphate buffer (20 mM) with 30 mM NaCl and 12 mM of MgCl₂ was used. Excitation wavelength was 530 nm.

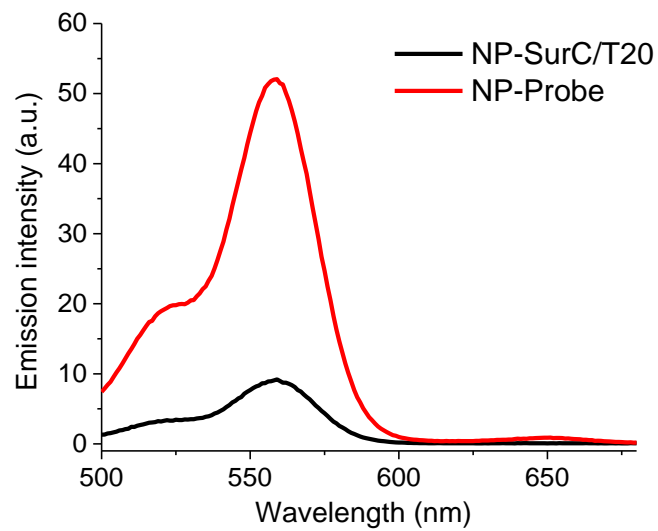


Figure S7. Fluorescence excitation spectra of NP-SurC-T20 and NP-Probe. Emission wavelength was 690 nm.

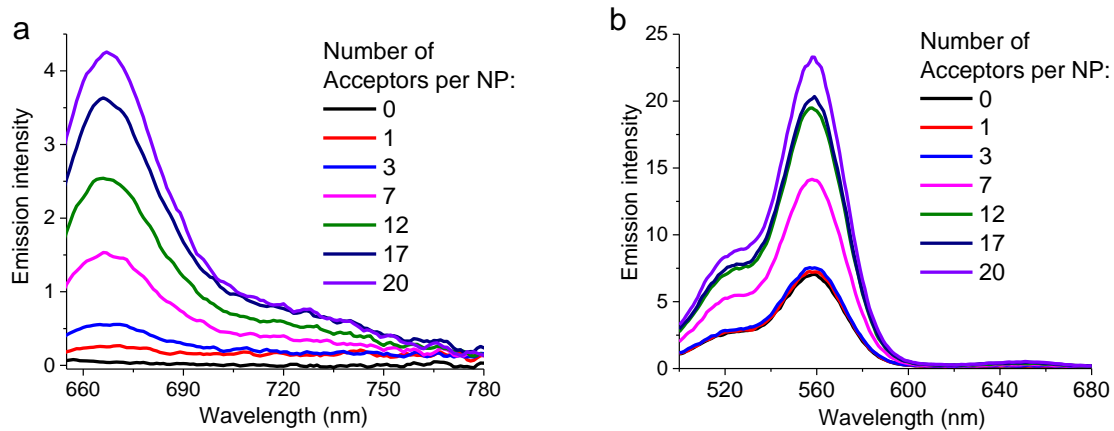


Figure S8. Characterization of NP-probes bearing different number of TCS-Cy5 per particle. (a) Fluorescence emission spectra of the acceptor of NP-Probes under direct excitation at 640 nm. (b) Fluorescence excitation spectra of NP-Probes. Emission was detected at 690 nm.

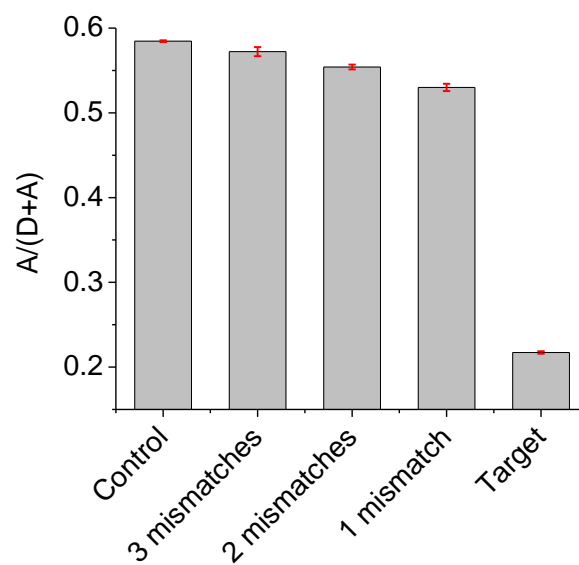


Figure S9. Sequence-specificity of the NP-probe. Ratiometric response of NP-Probe (200 pM TCS-Cy5) and 1 nM of oligonucleotide in 20 mM phosphate buffer containing 30 mM NaCl and 12 mM MgCl₂. Before measurements the mixture was incubated for 20 h at 4 °C. Error is standard deviation of the mean (n = 3).

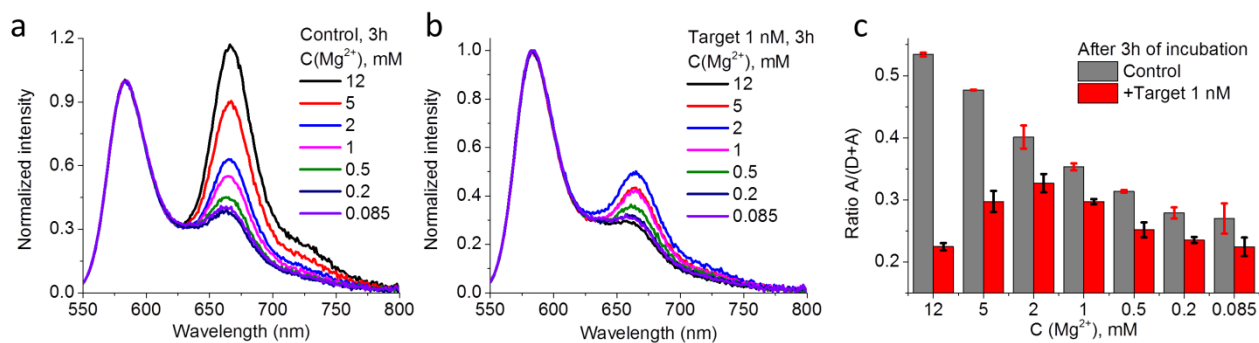
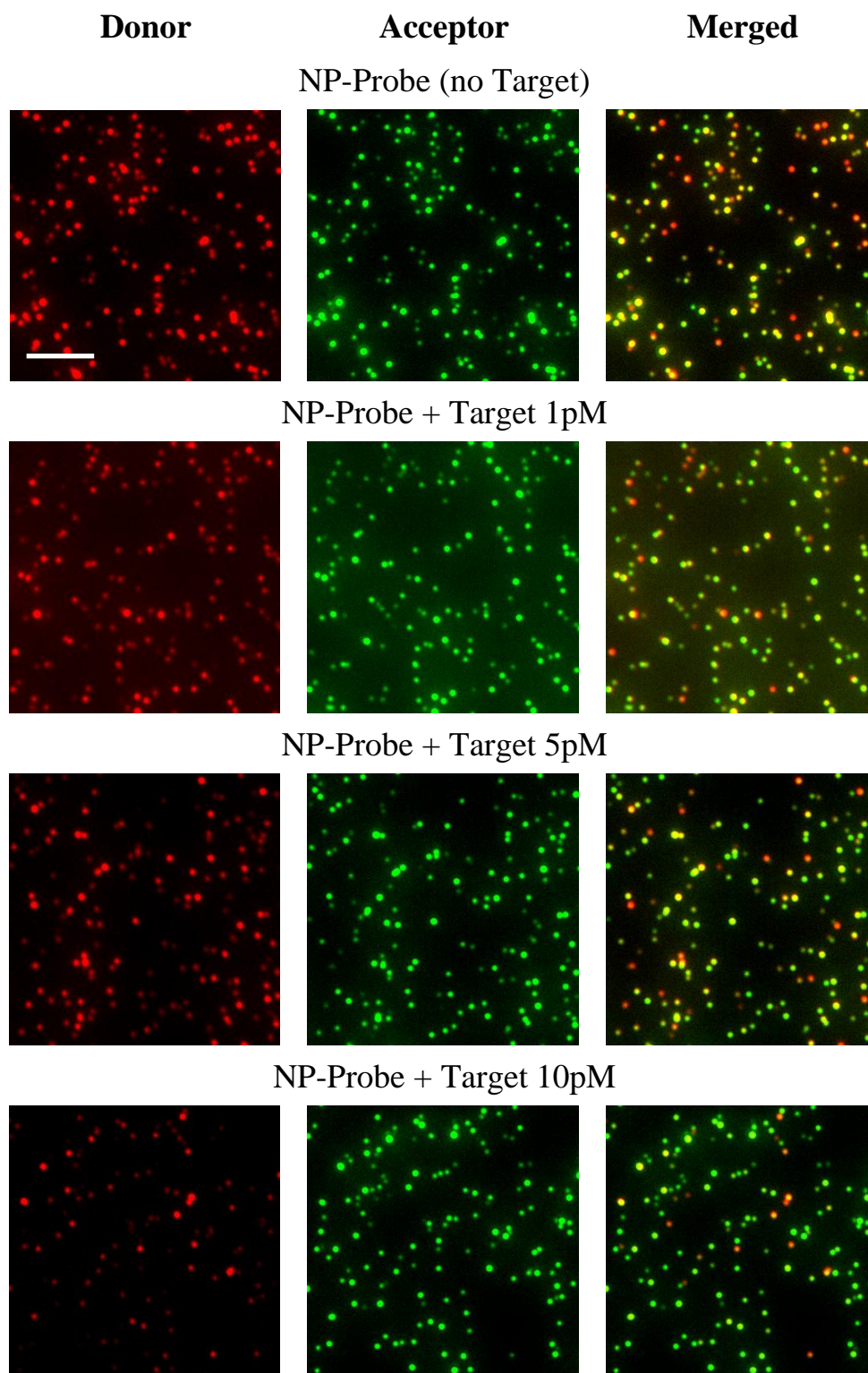


Figure S10. Effect of magnesium ions on the fluorescence response of NP-probe. (a,b) Fluorescence spectra of NP-probe (100 pM of TCS-Cy5, 5 pM of NPs) after incubation with the target for 3h without and with 1 nM survivin NA target in 20 mM phosphate buffer (pH 7.4) with 30mM NaCl and different concentrations of MgCl₂. Excitation wavelength was 530 nm. (c) FRET-based response of NP-probe to survivin NA target at different concentrations of MgCl₂. Error bars are standard deviation of the mean (n = 3).

2.3. Single-particle measurements



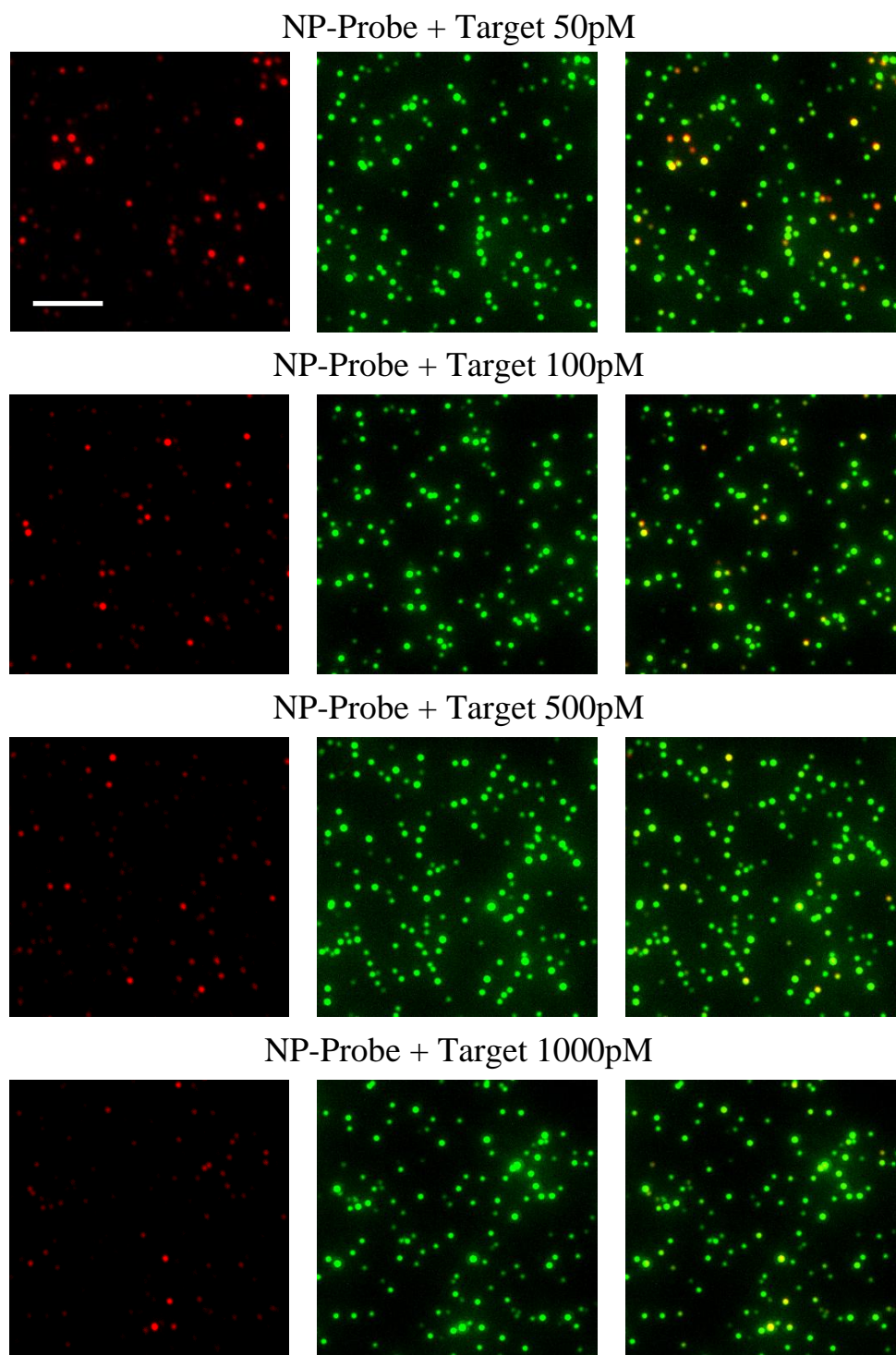


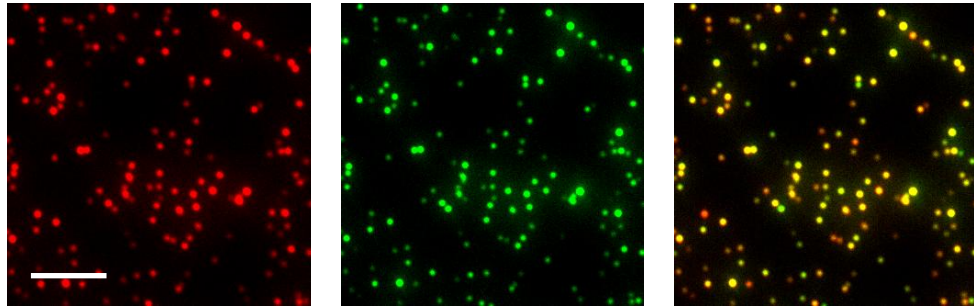
Figure S11. Response of NP-probe to survivin NA target at the single particle level. Wide-field fluorescence microscopy images of the immobilized NP-Probe after 24h incubation with different concentrations of survivin NA target. Both donor and acceptor channels are presented at the same intensity. Scale bar, 5 μM . All images are of the same size. The excitation wavelength was at 550 nm with 0.4 W cm^{-2} power density. Signals from FRET-Donor and FRET-Acceptor were recorded at <640 and >640 nm, respectively.

Donor

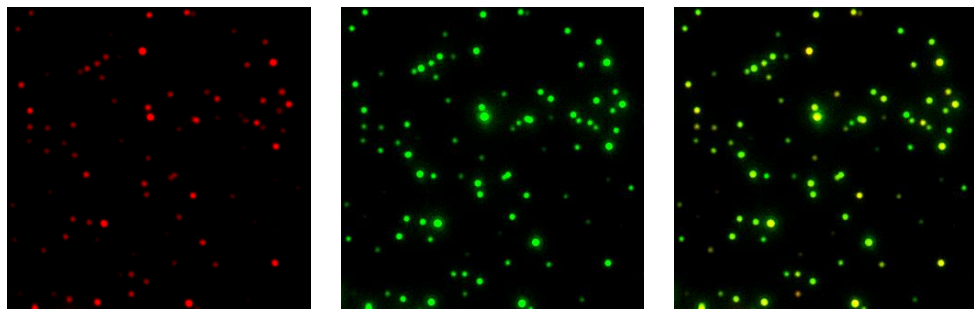
Acceptor

Merged

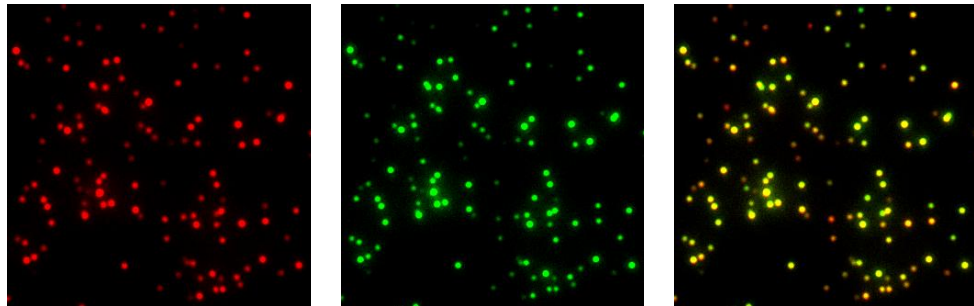
NP-Probe in PBS



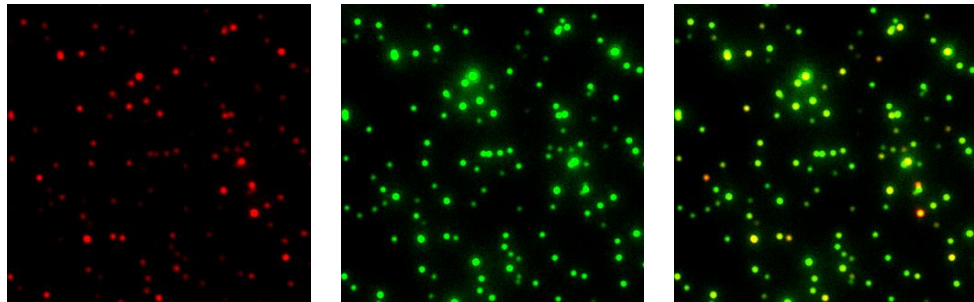
NP-Probe + Target 10 pM in PBS



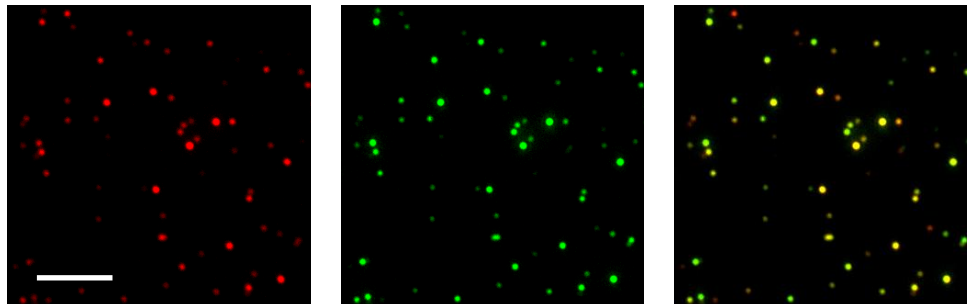
NP-Probe in BSA (1 mg/mL in PBS)



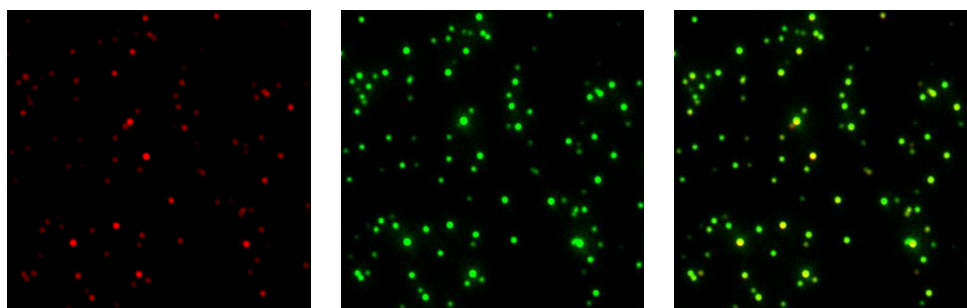
NP-Probe + Target 10pM in BSA (1 mg/mL in PBS)



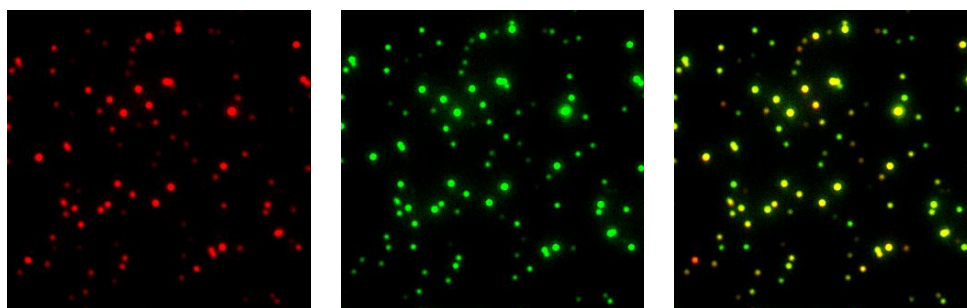
NP-Probe in 10% of FBS in PBS



NP-Probe + Target 10 pM in 10% of FBS in PBS



NP-Probe in 10% of Human Serum in PBS



NP-Probe + Target 10 pM in 10% of Human Serum in PBS

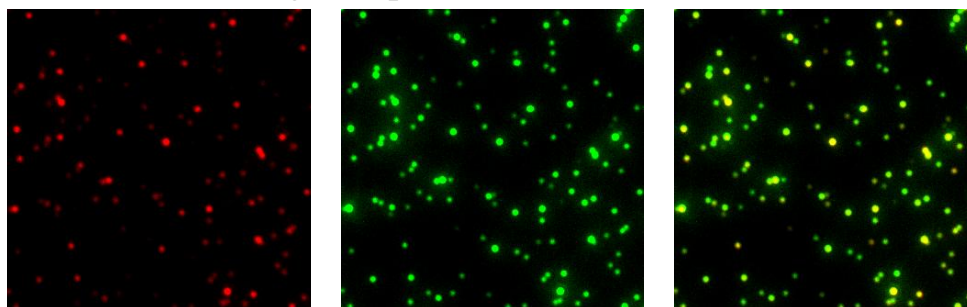


Figure S12. Response of NP-probe to survivin NA target at the single particle level. Wide-field fluorescence microscopy images of the immobilized NP-Probe after 24 h incubation without and with the NA target (10 pM) in different biological media. Both donor and acceptor channels are presented at the same intensity. Scale bar, 5 μM . All images are of the same size. The excitation wavelength was at 550 nm with 0.4 W cm^{-2} power density. Signals from FRET-Donor and FRET-Acceptor were recorded at <640 and >640 nm, respectively.

2.4. Tables

Table S1. Fluorescence quantum yields (QY) of studied systems.

Sample	QY (%)
NP-AspN3 (donor) ^a	47±1
NP-probe (donor + acceptor) ^b	46±1
Cy3-SurC (donor) ^c	31±2
TCS-Cy5 (acceptor) ^d	32±2

^a Sample prepared according to 10-fold dilution protocol. ^b QY corresponds to the total emission of both donor and acceptor, measured using the integral for the entire emission spectrum of NP-probe (550 – 800 nm range). ^{a,b,c} QY was measured using rhodamine101 in ethanol as a reference (QY = 100%). ^d QY of TCS-Cy5 was measured by direct excitation at 630 nm of NP-Probe and comparison with DiD in MeOH as a reference (QY = 33%). Error are standard deviation of the mean (n = 2).

Table S2. Size, composition and light-harvesting properties of the NPs-DNA conjugate prepared four times.^a

Sample	Diameter (nm) by DLS ^c	Ratio D/A	A per NP	FRET efficiency, (%)	AE
1	71.8±2.5	143	20.1	42.3	58.2
2	60.2±2.3	117	25.7	66.9	56.7
3	61.4±3.1	190	15.8	65.1	58.2
4	52±1.3	101	29.6	66.8	57.3
Average ^b	61±4	138±20	23±3	60±6	58±1

^a Statistics by volume was used in DLS data; Ratio D/A is the molar donor-acceptor ratio; A per NP is the number of acceptors per particle; AE is antenna effect. ^b Average values are shown together with s.e.m. (n = 4). ^c Despite variations in the DLS data, the average size by TEM was relatively stable (41±12 nm), where the error is the half width at half maximum of the size distribution (number of particles analysed >500). A per NP – 3200 (Number of Donors in NPs with size 40 nm) divided by Ratio D/A.

Table S3. Comparison of brightness QDot-605, NP-T20 (donor channel) and NP-probe (sum of acceptor and donor channels).^a

Sample	Excitation wavelength (nm)	Excitation power density (W cm^{-2})	Average intensity (a.u)	Median intensity (a.u.)	s.e.m.
QDot 605	470	14	2050	1770	60
NPs-T20	550	0.56	7720	6380	350
NP-probe (D+A)	550	0.56	7120	5490	190

^a >500 particles were analysed in total per each sample.

3. References

- (1) Karstens, T.; Kobs, K. *J. Phys. Chem.* **1980**, *84*, 1871.
- (2) Texier, I.; Goutayer, M.; Da Silva, A.; Guyon, L.; Djaker, N.; Josserand, V.; Neumann, E.; Bibette, J.; Vinet, F. *J. Biomed. Opt.* **2009**, *14*, 054005.
- (3) Trofymchuk, K.; Reisch, A.; Didier, P.; Fras, F.; Gilliot, P.; Mely, Y.; Klymchenko, A. S. *Nat. Photonics* **2017**, *11*, 657.
- (4) Schmied, J. J.; Raab, M.; Forthmann, C.; Pibiri, E.; Wunsch, B.; Dammeyer, T.; Tinnefeld, P. *Nat. Protoc.* **2014**, *9*, 1367.
- (5) Reisch, A.; Didier, P.; Richert, L.; Oncul, S.; Arntz, Y.; Mely, Y.; Klymchenko, A. S. *Nat. Commun.* **2014**, *5*, 4089.

2.3 Development of nanoprobe with single-molecule sensitivity towards nucleic acid target

A single-molecule sensitivity is an ultimate goal in biosensing and biomedical diagnostics.² The next step of my PhD project was focused on development of a system where the single hybridization event at the surface of the nanoparticle would switch on/off energy transfer from thousands of dyes inside the nanoantenna. Despite the excellent performance of nanoantenna-based nucleic acid detection assay described in a previous chapter, to obtain such nanoprobe with a single-molecule sensitivity it was necessary to redesign it, in particular, the donor particle and the acceptor dye.

The original Cy5 acceptor dye appeared to have poor photostability at the single-molecule level when thousands of dyes transferred their energy to 23 acceptors. In order to find the photostable dye, which is an absolute must for a single acceptor-based nanoprobe, we performed a screening of possible acceptors in the nanoprobe approach (Fig.2.18A). We checked 3 families of commercially available dyes: Cy, DY and ATTO with different polarities, charge and absorption/emission wavelengths. A series of nanoprobe with 10 different acceptors were synthesized and we discovered that only positively or neutrally charged fluorophores appropriate for hybridization of their TCS oligonucleotide and corresponding FRET signal (Fig.2.18B-C). Then, we compared the photostability of ATTO and Cy dye families at the single-particle level and found that ATTO647N and ATTO665 are far more photostable in the nanoprobe context than Cy5 or Cy5.5 dyes (Fig. 2.18D). As the replacement of Cy5, we chose the ATTO665 dye due to its exceptional photostability and better spectral resolution of its emission band from the donor emission band which is favorable for the ratiometric detection.

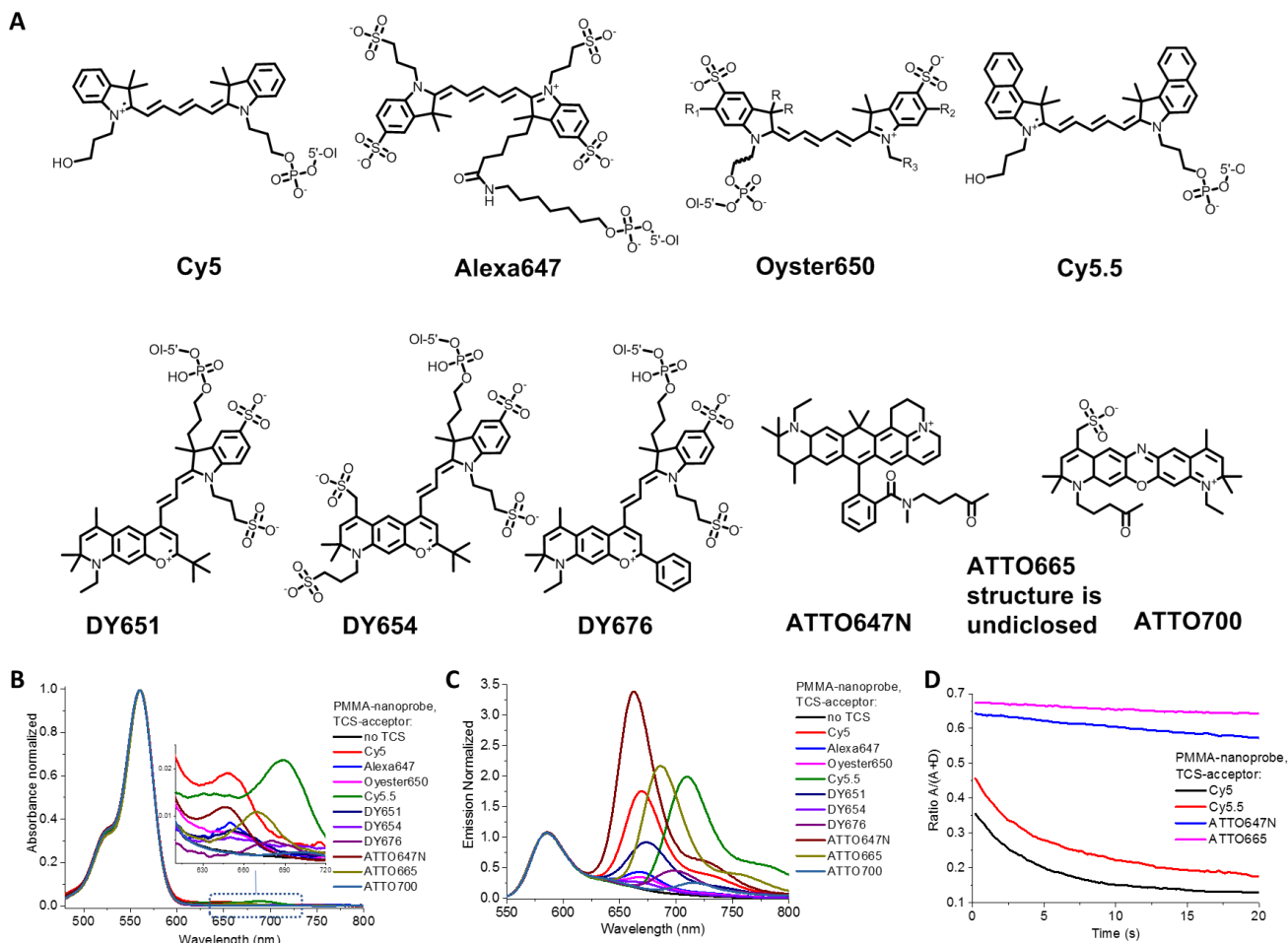


Fig.2.18. Acceptor screening. A) Chemical structure of dyes conjugated with TCS and used as FRET-acceptors, B) Absorbance spectra and C) Normalized fluorescence spectra of nanoprobe formulations with different TCS-acceptors. Excitation wavelength was 530 nm. D) Photobleaching curves of nanoprobe formulations immobilized on the glass surface formulated with TCS-CY5, TCS-Cy5.5, ATTO647N and ATTO665. Excitation was at 550 nm with power density 0.41 W cm^{-2} .

Our previous results demonstrated that the nanoantenna of 40 nm can distinguish 3-5 hybridization events on the surface. Therefore, we aimed to decrease the size of the nanoantenna. To this end, we performed the nanoprecipitation PMMA-AspN3 polymer at the higher pH and obtained the nanoprobe of lower size (32 nm) and then functionalized them with the lower number of acceptors per particle (4). Obtained results showed that FRET efficiency was not sufficient so that further decrease of the size was required. Therefore, we synthesized polymers PMMA-AspN3 with 5 mol% of methacrylic acid groups in the polymer compared to 1.6% in the original polymer. We found that the obtained NPs (PMMA-AspN3) were much smaller in size (~16 nm) and exhibited excellent FRET to 1-2 acceptors, but they were poorly photostable. Therefore, we synthesized the polymer based on poly(ethyl methacrylate-co-methacrylic acid) (PEMA-MA) with 5 mol% of methacrylic acid (PEMA-AspN3) (Fig. 2.19A). The

obtained NPs from this polymer exhibited very high homogeneity, small size of 18 nm (Fig. 2.19B) and much higher photostability at the single-particle level compared to corresponding PMMA-AspN3. In order to obtain higher brightness and amplification of the acceptor signal, we increased the loading of PEMA-AspN3 NPs to 50 wt% of the dye.

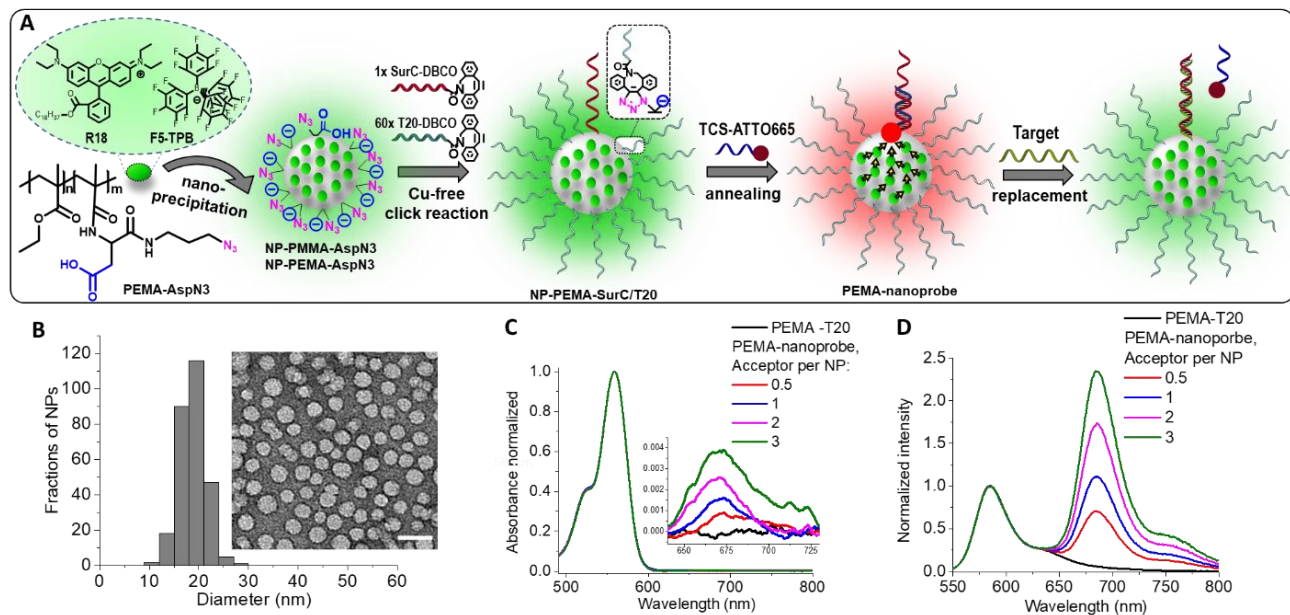


Fig.2.19. Synthesis and characterization of PEMA-nanoprobes. A) Scheme synthesis of nanoprobe with a single TCS-ATTO665 and its response to the Target. B) TEM images and size distribution statistics for NP-PEMA-AspN3. C) Absorption spectra and D) normalized fluorescence spectra of PEMA-nanoprobe hybridized with 0 (PEMA-T20) and 0.3, 1 and 2 TCS-ATTO665.

Formulated nanoprobes with PEMA-AspN3, bearing oligonucleotides and statistically single acceptor ATTO665 exhibited extraordinary results: both high fluorescence quantum yield (46%) and high FRET efficiency (51%) through the distance far beyond the Förster radius (6.65 nm vs 20 nm particle size). The amplification of the acceptor emission (antenna effect), measured from the excitation spectra, was 208 ± 17 . To verify the presence of the single acceptor on the nanoantenna we immobilized nanoparticles and analyzed their traces by excitation at 550 nm (Fig. 2.20A). The single-step switch on/off of acceptor/donor in nanoparticle demonstrated the modification with a single acceptor at least in 50% of nanoparticles (Fig. 2.20C). The presence of a single acceptor in these nanoprobes was confirmed by the analysis of emission traces of acceptor by its direct excitation at 640 nm laser (Fig.2.20D). Moreover, the antenna effect at the single-particle level was 257 ± 30 (Fig. 2.20B). Remarkably, using these NPs, we were able to detect single hybridized oligonucleotide labeled with the acceptor at ambient sunlight-like excitation conditions.

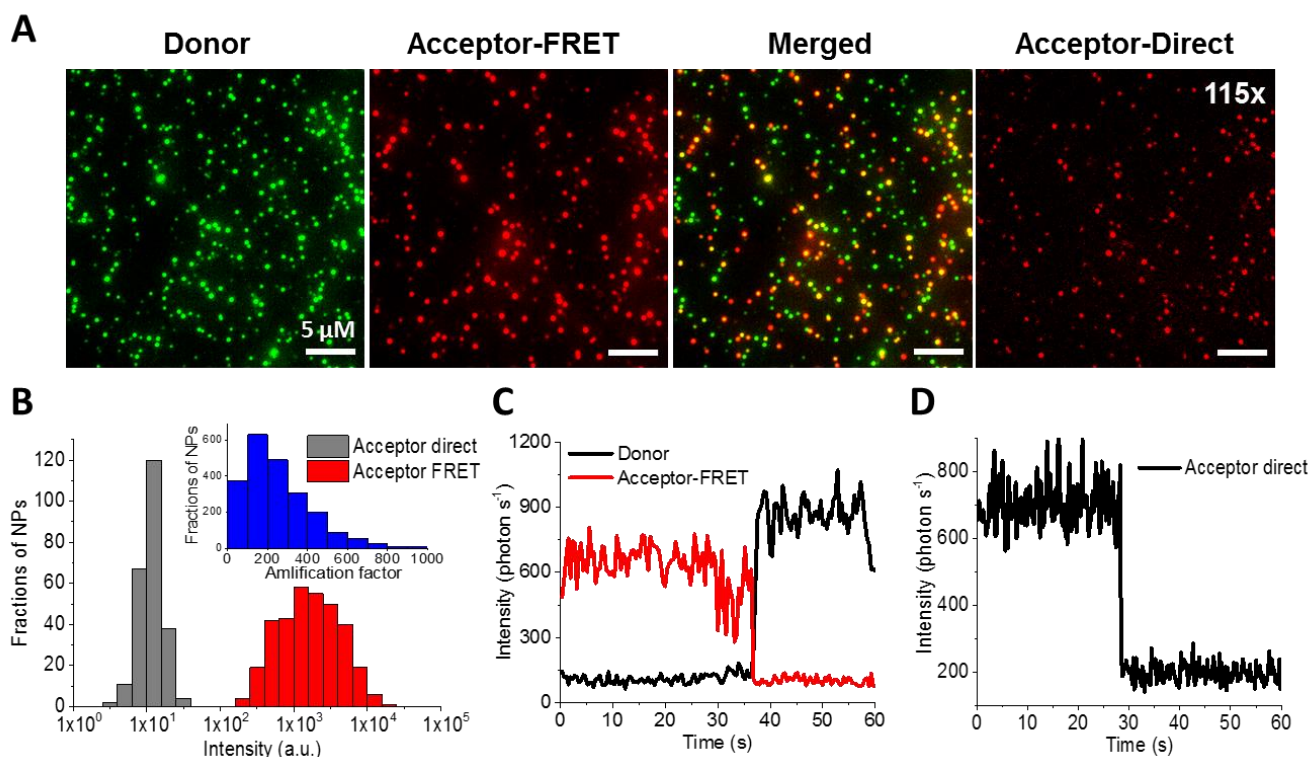


Fig.2.20. Characterization of PEMA-nanoprobes at the single-particle level. A) Wide-field fluorescence microscopy of the immobilized PEMA-nanoprobe: donor, antenna-amplified acceptor, merged FRET-acceptor and donor (excitation wavelength was 550 nm with power density 0.24 W cm^{-2}) and direct excitation of acceptor at 640 nm with power density 27.65 W cm^{-2} . Signals from Donor and FRET-Acceptor were recorded at <640 and >640 nm, respectively. Integration time was 400 ms. B) Histogram of single-particle intensity distribution for acceptor through direct excitation and nanoantenna energy transfer. A smaller graph represents a distribution histogram of amplification of FRET-Acceptor emission (antenna effect) by the nanoprobe at the single-particle level. At least 2000 NPs were analyzed in each case. Examples of intensity curves of C) nanoprobes through FRET and D) direct excitation of acceptor on TIRF setup with power density 24.69 W cm^{-2} .

The obtained system opened a new way for “digital” detection of nucleic acids (Fig. 2.21A). Since the single hybridization event can switch the color of nanoparticle, it means that one nucleic acid molecule corresponds to one nanoparticle. We imaged the same immobilized nanoprobes at ambient sunlight-like excitation power before and after incubation with DNA and RNA targets for one hour at room temperature. This way by following the single-particle hybridization event we were able practically to calculate the number of nucleic acids targets hybridized to the nanoparticles, which decreased the theoretical limit of detection down to the single hybridization (Fig. 2.21B).

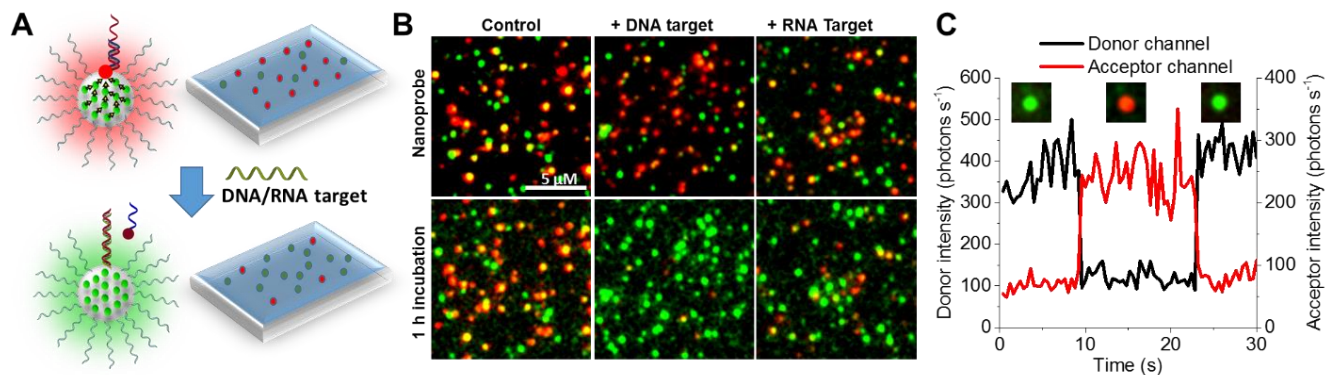


Fig.2.21. Detection of oligonucleotides and their hybridization with single-molecule sensitivity. Concept of digital detection. (A) Schematic presentation of digital detection of single oligonucleotides. (B) Wide-field FRET images (merged) without and with 100 pM of DNA and RNA targets. The excitation wavelength was 550 nm, 60x oil objective with power density 0.036 W cm^{-2} . Integration time was 1 s. (C) Intensity traces of donor (black) and acceptor (red) of a single nanoprobe with addition of TCS-ATTO665 of 12NA and corresponding two-color merged images of the same single particle. The excitation wavelength was 550 nm, 100x oil objective with power density 0.24 W cm^{-2} . Integration time was 400 ms.

The final test was the direct imaging of the single hybridization event under the microscope. During the imaging, we added the TCS-ATTO665 and by recording the acceptor signal, we were able to follow a direct hybridization event of a single oligonucleotide. The single-step intensity trace proved the appearance of single acceptors, which was followed by the bleaching of the single acceptor on the nanoparticle surface (Fig. 2.21C). Such exceptional ability of our developed nanoantenna to donate the energy from a thousand donors to a single acceptor enabled unprecedented direct observation of single oligonucleotide hybridization event under a simple epi-microscope at the excitation powers equivalent to ambient sunlight conditions. Overall, through the rational design of the nanoprobe, the main objective of my thesis was achieved, where the developed NPs enabled detection of individual molecules of nucleic acids.

A full description of the work can be found in the manuscript enclosed below.

Article 2 (Manuscript). Light-harvesting nanoparticle probes for FRET-based detection of oligonucleotides with single-molecule sensitivity.

Light-harvesting nanoparticle probes for FRET-based detection of oligonucleotides with single-molecule sensitivity

Nina Melnychuk, Sylvie Egloff, Anne Runser, Andreas Reisch and Andrey S. Klymchenko*

Abstract: Bright luminescent nanoparticles (NPs) can drastically increase the sensitivity of Förster resonance energy transfer (FRET) assays for detection of biomolecular markers, such as DNA and RNA. However, existing luminescent NPs, including quantum dots (Qdots), are unable to undergo efficient FRET to a single acceptor because their size is far beyond the Förster radius. To overcome this fundamental problem, we have developed a 20-nm DNA-functionalized light-harvesting nanoantenna particles, built of specially designed hydrophobic charged polymer poly(ethyl methacrylate-co-methacrylic acid), encapsulating ~1000 strongly coupled and highly emissive rhodamine dyes with their bulky counterion. This is the first nanomaterial exhibiting >50% FRET efficiency to a single acceptor (ATTO665) at the particle surface, being 87-fold brighter than QDots605 (52% quantum yield and $10^8 \text{ M}^{-1} \text{ cm}^{-1}$ extinction coefficient). The obtained FRET nanoprobe enable single-molecule detection of short DNA and RNA, encoding a cancer marker, and imaging single hybridization events by a simple epi-fluorescence microscope with ultra-low excitation power close to ambient sunlight.

Introduction

Detection of biomolecular targets, such as nucleic acids, with single-molecule sensitivity is an ultimate goal in biosensing and biomedical diagnostics.^[1] In optical detection of single molecules, the limited brightness of organic dyes, having molar absorption coefficients below $300,000 \text{ M}^{-1} \text{ cm}^{-1}$ and quantum yields below unity,^[2] imposes the use of very high excitation powers ($\sim 1 \text{ kW cm}^{-2}$) and minimized detection volumes,^[1a, 3] in order to achieve good signal-to-background ratio. Plasmonic nanomaterials can address this problem by enhancing emission of single dyes in the hot spots,^[1h, 4] in particular between two gold nanoparticles with strictly respected distances.^[3b] This sophisticated system based on DNA origami enabled up to 100-300-fold signal amplification of single molecules,^[3b, 5] however, so far, the reported biosensor for nucleic acids based on this concept can amplify the signal by 7-fold on the average.^[6]

A promising amplification approach is to use bright luminescent nanoparticles^[7] as energy donors that pump excitation energy to a single dye molecule by Förster Resonance Energy Transfer (FRET).^[8] However, nanoparticles are generally not efficient FRET donors, because their diameter is generally far beyond the Förster radius (R_0).^[9] Indeed, in case of quantum dots (QDots),

10-50 acceptor molecules are needed to ensure efficient FRET.^[10] Similar large number of acceptors are also needed to ensure FRET from UCNPs^[11] and dye-doped silica NPs.^[12] One way to go beyond the Förster radius is to use light-harvesting nanomaterials^[13] where the strongly coupled energy donors communicate through excitation energy migration,^[14] which allows transporting the energy through long distances up to the FRET acceptor. Previous works showed that energy migration can improve FRET efficiency in both dye-doped silica NPs^[12b] and UCNPs.^[15] Moreover, in conjugated polymers,^[16] this approach enabled 25-100-fold signal amplification, although no single-molecule FRET-based detection were reported. New possibilities appeared with recently introduced giant light-harvesting nanoantenna,^[8a] based on dye-loaded polymeric nanoparticles.^[17] In this nanomaterial, dyes (R18, Scheme 1) are loaded into polymer matrix at high concentration using bulky hydrophobic counterions (F5-TPB) that prevent self-quenching^[18] and enable ultrafast dye-dye energy migration on a time scale $< 30 \text{ fs}$. The obtained 60-nm nanoantenna particle ($\sim 10 R_0$) containing 10,000 energy donors transferred energy to a single acceptor inside the particle, providing unprecedented signal amplification of >1000 -fold. More recently, we functionalized 40 nm nanoantenna with nucleic acids and reported the first DNA-based biosensor featuring exceptional brightness (equivalent of 100 Qdot-605) and 75-fold signal amplification.^[19] However, to achieve efficient FRET in these NPs, 23 acceptor dyes at the particle surface were needed, so that this system was still far from being able to detect single nucleic acid molecules. To the best of our knowledge, no luminescent NPs with a diameter above $2R_0$ ($>10 \text{ nm}$) are capable to undergo efficient FRET (i.e. $>50\%$) to a single acceptor dye at the particle surface.

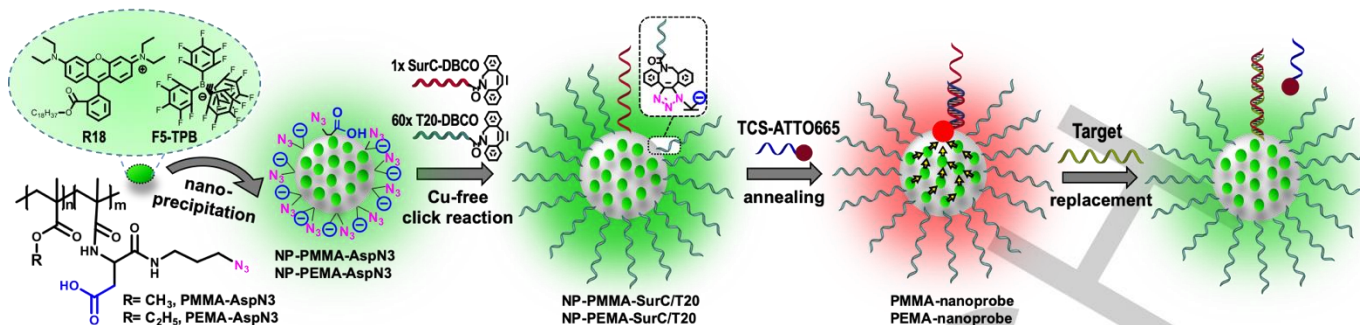
Herein, we overcame the problem of inefficient FRET in nanoparticle-based biosensors and developed a light-harvesting nanoantenna of 20 nm size, encapsulating ~1000 dyes equivalent in brightness to 87 quantum dots (Qdot-605), which undergoes FRET with 51% efficiency to a single acceptor (ATTO665) at the DNA-functionalized surface. This new nanomaterial enabled preparation nanoprobe capable to switch their color in response to a single copy of RNA and DNA molecules and monitor in real-time single hybridization events using a basic epi-fluorescence microscope with ultralow excitation power close to that of ambient sunlight.

Results and Discussion

Development of this single-molecule biosensor requires boosting FRET performance of our dye-loaded NPs. To this end, we need to design a polymer capable to assemble a maximum number of dyes into a particle of optimal small size, while ensuring their efficient emission and excitation energy migration (Scheme 1).

Nina Melnychuk, Sylvie Egloff, Anne Runser, Dr. Andreas Reisch and Dr. Andrey S. Klymchenko*
Laboratoire de Bioimagerie et Pathologies, UMR 7021 CNRS, Faculté de Pharmacie, Université de Strasbourg
74, Route du Rhin, 67401 Illkirch, France
E-mail: andrey.klymchenko@unistra.fr

Supporting information for this article is given via a link at the end of the document.



Scheme 1. Synthesis of the nanoprobe with a single TCS-Acceptor and their response to the target.

Moreover, we need to find a robust FRET acceptor able to collect energy from the whole particle without rapid photobleaching. Then, based on a previously developed DNA-functionalization strategy,^[19] the donor NPs should be modified with only a single FRET acceptor through a nucleic acid sensing unit. In our biosensor, azide-functionalized dye-loaded polymeric NPs are modified with two different oligonucleotide sequences (Scheme 1): (i) excess of non-coding T20 to ensure NPs stability and (ii) a statistically one copy per particle of specific sequence (SurC), encoding a fragment of survivin, an important cancer marker.^[20] The latter is hybridized with a shorter complementary DNA sequence (target competitive sequence, TCS) bearing a corresponding acceptor, which serves in the FRET displacement assay to detect the survivin DNA/RNA target (Scheme 1).

First, we searched for the best FRET acceptor, using previously developed dye-loaded donor NPs based on polymer PMMA-AspN3-1.6% (obtained from PMMA-MA with 1.6% of methacrylic acid).^[19] Among ten tested acceptor dyes (Figure 1A) conjugated to DNA TCS, only positively charged and neutral (zwitterionic) dyes, namely Cy5, Cy5.5, ATTO647N and ATTO665, were found to provide strong FRET signal after hybridization in the DNA nanoprobe. This signal was observed as an intense emission band around 650-750 nm compared to the FRET donor band of R18 dye around 590 nm (Figure 1B and S1). The number of hybridized acceptors per particle was also larger for these dyes (Table S1), probably because their duplexes were more stable than those bearing strongly anionic dyes. Then, we tested the fluorescence response of the obtained four nanoprobe to the target DNA sequence encoding survivin fragment. The three nanoprobe based on Cy5, ATTO647N and ATTO665 showed complete replacement of the acceptor, resulting in loss of the acceptor emission (Figure S2). By contrast, Cy5.5-based acceptor showed residual FRET in the presence of the DNA target, showing that it remains non-specifically bound to the particle (Figure S3). Then, we compared photostability of the four nanoprobe in solution under laser irradiation (Figure S4). Remarkably, nanoprobe built of Cy5 or Cy5.5 dyes showed fast decay of the FRET acceptor signal, expressed as $A/(A+D)$ ratio (Figure S4), whereas the signal from ATTO647N and ATTO665 was far more stable (half-life for ATTO665 and Cy5 was 3500 and 98 s, respectively). The significantly higher photostability of ATTO-based FRET acceptors was also confirmed at a single particle level (half-life for ATTO665 and Cy5 was 128 and 3.7 s, respectively), using fluorescence microscopy of nanoprobe immobilized on the glass surface (Figure 1C, S5, S6). The

observed ~35-fold longer half-life for ATTO665 was an outstanding improvement for the FRET acceptor, and thus it was selected for the single-molecule biosensor design.

The primary approach to improve FRET donor efficiency of the particle is to decrease its size. Our earlier studies showed that smaller polymer NPs can be obtained by increasing the pH during nanoprecipitation^[8a] or increasing the charge on the polymer.^[21] In the first approach, we performed nanoprecipitation of PMMA-AspN3-1.6% at pH 9, which yielded NPs of 30 nm (Figure S7 A-B). However, the obtained DNA-functionalized nanoprobe required >8 acceptors per particle to achieve efficient FRET (Figure S7 C-D), so further decrease in the size was needed. Therefore, we increased the fraction of methacrylic acid units in PMMA-MA to 5 mol%, and further converted it into azide-carboxylate-bearing polymer PMMA-AspN3-5% (Scheme 1). Moreover, to compensate the increase in the fraction of polar carboxylates in the polymer, we replaced its methyl methacrylate unit with more hydrophobic ethyl methacrylate (PEMA-AspN3 polymer, Scheme 1, obtained from PEMA-MA with 1.6% of methacrylic acid). Nanoprecipitation of these polymers yielded dye-loaded NPs of 16 and 18 nm for PMMA-AspN3-5% and PEMA-AspN3, respectively (Figure 2 A-B).

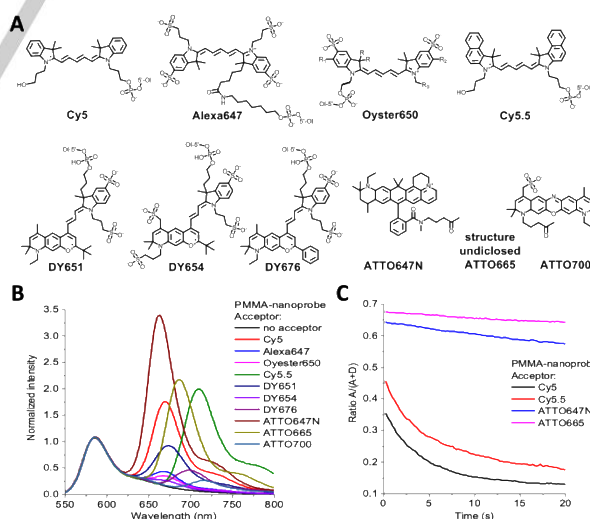


Figure 1. Search for the best FRET acceptor. A) Chemical structure of dyes conjugated with TCS and used as FRET-acceptors. B) Normalized fluorescence spectra of PMMA-nanoprobe (PMMA-AspN3-1.6% polymer) with different acceptors and 30 wt% R18/F5-TPB dye loading. Excitation: 530 nm. C) Photobleaching kinetics of PMMA-nanoprobe formulated with different acceptors, immobilized on the glass surface and measured by microscopy. Excitation: 550 nm; power density: 0.41 W cm⁻².

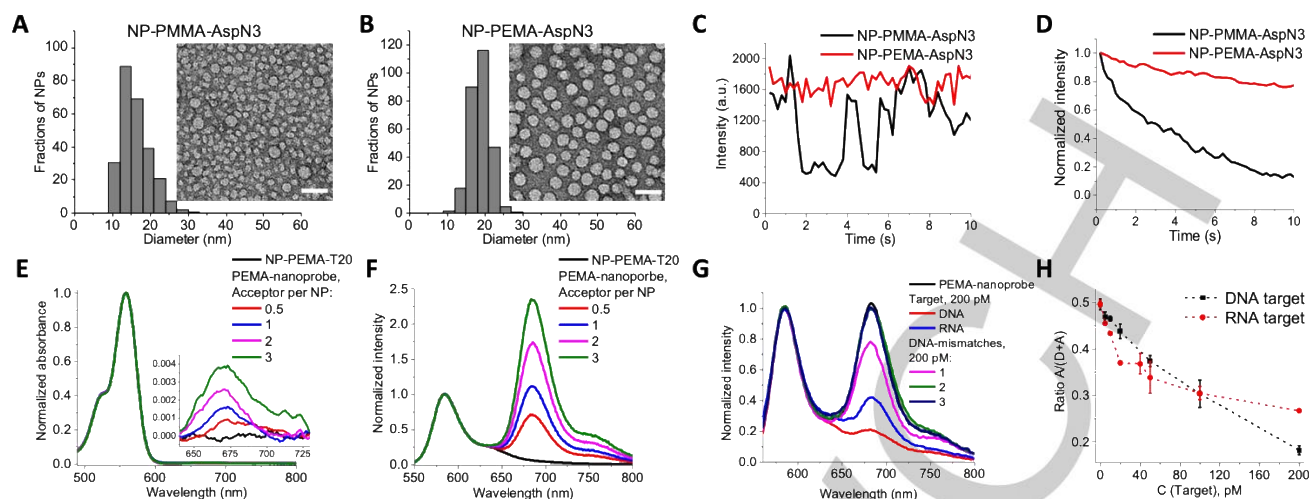


Figure 2. Development and evaluation of FRET nanoprobes. TEM images (scale bar 50 nm) and size distribution statistics for NPs of (A) PMMA-AspN3-5% and (B) PEMA-AspN3 polymers. C) Average intensity traces measured by microscopy for PMMA-AspN3-5% and PEMA-AspN3 NPs loaded with 50 wt% R18/F5-TPB. Excitation: 550 nm; power density: 0.41 W cm^{-2} . D) Example of single-particle intensity traces from PMMA-AspN3-5% and PEMA-AspN3 NPs loaded with 50 wt% R18/F5-TPB. E) Absorbance and F) normalized fluorescence spectra of PEMA-nanoprobes (50 wt% R18/F5-TPB dye) hybridized with 0 (NP-PEMA-T20) and 0.3, 1 and 2 TCS-ATTO665 acceptor. G) Fluorescence response of PEMA-nanoprobe (20 pM of TCS-ATTO665) to survivin DNA and RNA targets (200 pM, 3 h incubation at 20 °C). DNA targets containing 1, 2, and 3 mismatches were tested at the same conditions. H) FRET ratio, $A/(A + D)$, of PEMA-nanoprobes (10 pM of TCS-ATTO665) vs target DNA and RNA concentration (3 h incubation at 20 °C). A and D are the pick intensities of the acceptor (at 665 nm) and the donor (at 580 nm), respectively.

Strikingly, PEMA-AspN3 NPs outdid PMMA-AspN3-5% NPs in all tested properties: (i) better size homogeneity according to TEM (Figure 1 A-B); (ii) higher fluorescence quantum yield; (iii) 2.7-fold higher single-particle brightness and (iv) much lower blinking and higher photostability (Figure 2 C-D, S8, Table S2). Thus, combining higher fraction of carboxylic groups with higher hydrophobicity of PEMA matrix enabled us to prepare very small dye-loaded NPs with drastically improved morphology and optical properties. As the particle brightness and the nanoantenna performance are directly linked to the dye loading, we varied it from 0 to 100 wt% with respect to the PEMA-AspN3 polymer. Even though fluorescence quantum yield remained high for all loadings tested (Table S3), above 50 wt% the NPs showed lower single-particle photostability (Figure S9), probably linked to larger fraction of photo-induced dark states.^[18b] Therefore, we selected 50 wt% as the optimal dye loading. Remarkably, increase in the dye loading till 50 wt% led to >100-fold drop in the fluorescence anisotropy (Figure S10), which suggested strong coupling of closely packed dyes inside NPs and efficient excitation energy migration,^[14, 18a, 18b] required for FRET beyond the Förster radius.^[8a]

Next, in order to prepare the nanoprobes, we functionalized dye-loaded PEMA-AspN3 with oligonucleotides. It was important to increase the concentration of oligonucleotide-DBCO in order to ensure stability of these small DNA-NPs (Figure S11). In the obtained FRET nanoprobes we varied the number of hybridized TCS-ATTO665 acceptors from 0 to 3 (Figure S12) and found that FRET signal was sensitive to the addition of a single acceptor (Figure 2 E-F, S12). Remarkably, the nanoprobe with a single acceptor exhibited extraordinary high FRET efficiency (51%), which implies that 980 donors in the 20-nm particle transfer half of their energy to the surface, which is far beyond the Förster radius (6.65 nm) (Table S3). The nanoprobe also showed high total fluorescence quantum yield (46%), while the amplification of

acceptor emission (antenna effect) was 208 ± 17 . This outstanding performance was highly reproducible in 5 independent preparations (Table S4). The obtained nanoprobes showed strong ratiometric response to the target survivin-encoding DNA and RNA sequences, where the target detection was associated with the loss of FRET signal (Figure 2G, S13). At 10-pM concentration, the nanoprobe exhibited the limit of detection of 2 pM for both DNA and RNA in solution (Figure 2H), the value limited by slow oligonucleotide hybridization at these low concentrations. Incubation of the nanoprobe with target DNA containing 1, 2 and 3 mismatches revealed high sequence specificity of the probe (Figure 2G).

Then, our DNA-functionalized NPs were studied at the single-particle level. We immobilized PEMA-AspN3 NPs bearing only T20 on A20-modified glass surface (Figure 3A) and compared them with Qdot-605 under the wide-field microscope. Remarkably, our 20-nm NPs were 87-fold brighter than Qdot-605 measured at the same conditions (Figure 3 A-C, E). This outstanding brightness for such a small particle size is explained by the high QY (52%) of 980 encapsulated rhodamine B derivatives, giving a theoretical brightness (extinction coefficient \times QY) of 5.1×10^7 vs $5.8 \times 10^5 \text{ M}^{-1} \text{ cm}^{-1}$ of Qdot-605.

FRET-based nanoprobes bearing a single acceptor showed emission in both donor (<640 nm) and acceptor (>640 nm) channels, whereas NPs without acceptor showed signal in the donor channel only (Figure 3B). Remarkably, the signal of acceptor excited through the nanoantenna (Acceptor-FRET) was 257 ± 30 -fold stronger than that obtained by direct excitation (Acceptor-direct) (Figure 3D, F). This value matches well the antenna effect measured in solution, indicating that efficient FRET from a thousand of dyes to a single acceptor results in outstanding amplification. To the best of our knowledge, this is the largest antenna effect ever reported for optical biosensors, including those based on plasmonics.

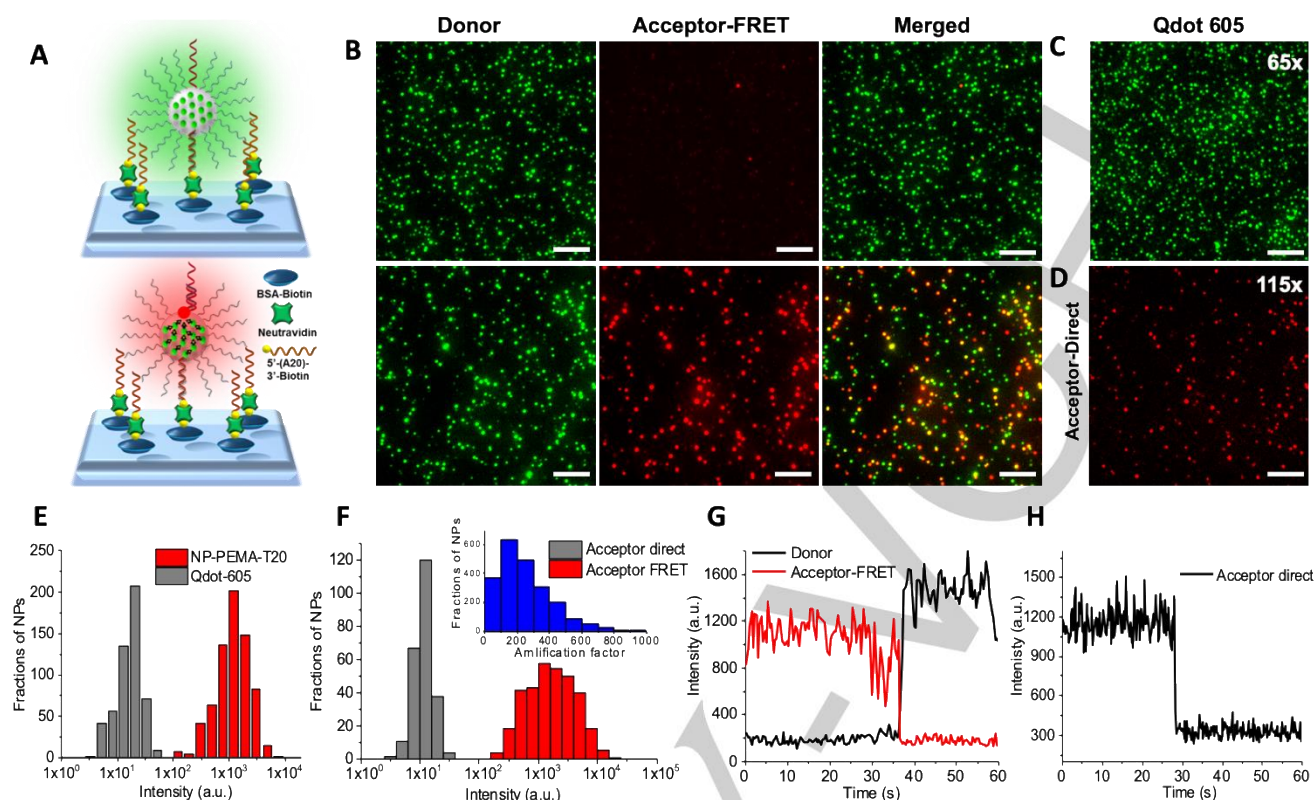


Figure 3. Characterization of nanoprobes at the single particle level. A) Scheme of PEMA-nanoprobe immobilization on a glass surface modified with BSA-biotin, neutravidin, and A20-biotin and B) Wide-field fluorescence microscopy of the immobilized NPs: donor, antenna-amplified acceptor and merged acceptor and donor Without (above) and with (under) TCS-ATTO665. Excitation wavelength was 550 nm with power density 0.24 W cm^{-2} . Signals from Donor and FRET-Acceptor were recorded at <640 and >640 nm, respectively. C) Wide-field fluorescence microscopy of the immobilized Qdot-605 excited at 550nm with power density 15.4 W cm^{-2} . To obtain comparable signals excitation power density for QDot-605 was 65-fold higher than that for PEMA-T20. D) Wide-field fluorescence microscopy of PEMA nanoparticles at direct excitation of acceptor at 640 nm with power density 27.7 W cm^{-2} . Integration time was 400 ms. Histogram of single-particle intensity distribution for E) NP-PEMA-T20 and Qdot-605 and F) acceptor through direct excitation and nanoantenna energy transfer. Smaller graph represents a distribution histogram of amplification of FRET-Acceptor emission (antenna effect) by the nanoprobe at the single-particle level. At least 2000 NPs were analyzed in each case. Examples of single-particle intensity curves of FRET nanoprobe (G) excited at 550 nm with power density 0.24 W cm^{-2} and recorded at donor and acceptor channels and (H) direct excitation of acceptor at 640 nm on TIRF setup with power density 24.7 W cm^{-2} . 50 wt% R18/F5-TPB dye loading was systematically used.

To verify the number of acceptors in our nanoprobe, we analyzed emission traces of the single particles and quantified the number of single-molecule bleaching steps. When excited through nanoantenna (at 550 nm), we estimated that $61 \pm 4\%$ of nanoparticles contained acceptors, among which $48 \pm 5\%$ of nanoprobes demonstrated single bleaching step (Figure 3G, Table S5), corresponding to a single acceptor per nanoprobe. Moreover, $67 \pm 7\%$ of single-step photobleaching events were accompanied by recovery of the donor emission, indicating that in our nanoprobe a single acceptor can switch on/off emission of a thousand of dyes inside NP. Direct excitation of the acceptor in a total internal reflection (TIRF) mode with 640 nm laser (Figure 3H) showed that $52 \pm 4\%$ of acceptors underwent the single bleaching step, confirming that a large fraction of nanoprobes bear single acceptor.

The achieved >250 -fold amplification of acceptor emission by the nanoantenna particles enables single-molecule FRET detection (i.e. single-step bleaching of the acceptor and recovery of the donor) using simple epi-fluorescence microscope setup with very low excitation power density (irradiance) comparable to ambient sunlight (36 mW cm^{-2} , Figure S14). Then, we incubated the immobilized nanoprobes with increasing amounts of DNA target; starting from 1 pM, individual particles switched their emission pseudo-color from red to green and the population of green species increased gradually (Figure S15). At the highest tested

target concentration, all nanoprobes switched their emission to green, showing the decrease in the FRET ratio parameter, $A / (A + D)$ from 0.46 to 0.21 (Figure S16). The gradual switching indicates that the nanoprobe can be used for quantification of the nucleic acid targets. More importantly, as our NPs bear only a single acceptor, the color switch of NPs corresponds to detection of the single nucleic acid molecule, so that we could practically calculate the number of target molecules hybridized with nanoparticles. Therefore, we imaged a given area with immobilized nanoprobes and quantified the number of FRET-positive particles before and after incubation with DNA and RNA targets (Figure 4A). Without the target, no change in the number of FRET-positive nanoprobes was detected, whereas in case of DNA and RNA samples, 1433 ± 87 and 768 ± 24 particles, respectively, switched their color from red to green per $1600 \mu\text{m}^2$ surface area (Figure 4 B-C). This “digital” detection of single-molecule targets correlated with corresponding drop in the average FRET ratio of NPs (Figure 4C, S17). Importantly, our nanoprobe enables detection of DNA/RNA targets with single-molecule sensitivity using basic epi-fluorescence microscope with excitation close to ambient sunlight (36 mW cm^{-2}), something that has not been achieved to date.

Here, the minimal detectable concentration of oligonucleotides is not limited by nanoprobe sensitivity but by the hybridization kinetics.

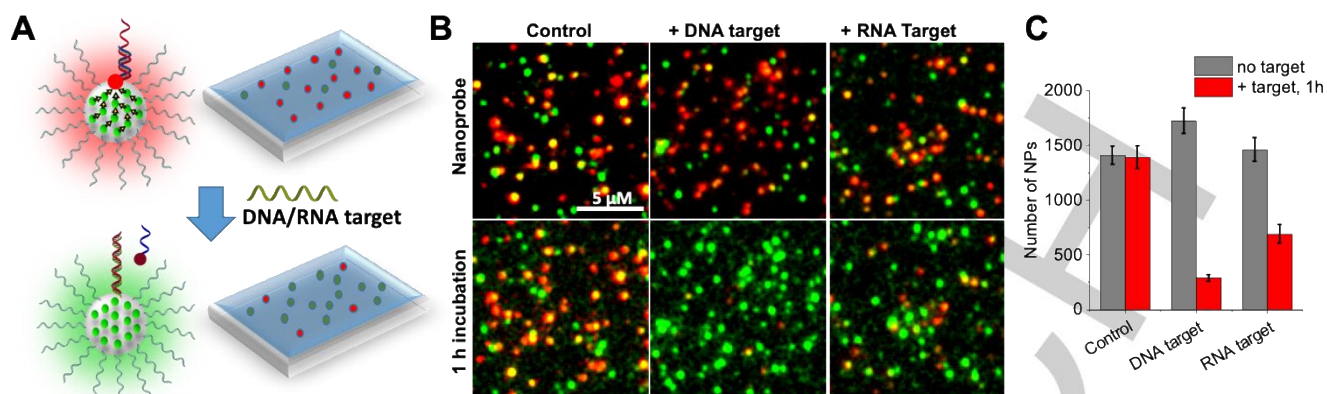


Figure 4. Detection of oligonucleotides with single-molecule sensitivity using PEMA-nanoprobes immobilized on a glass surface. A) Schematic presentation of digital detection of single oligonucleotides. B) Wide-field FRET images (two-color merged) and C) number of FRET-positive nanoprobes without and with 100 pM of DNA and RNA targets. The excitation wavelength was 550 nm with power density 0.036 W cm^{-2} , 60x oil objective. Integration time was 1s.

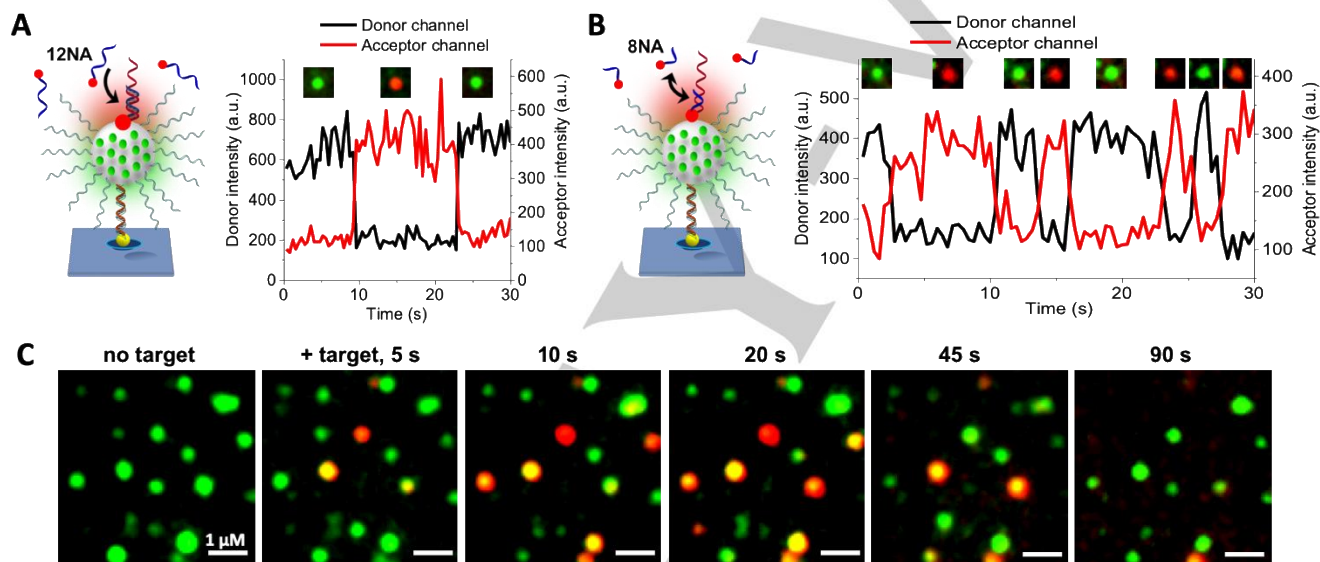


Figure 5. Imaging in real time single hybridization events using PEMA-Surc/T20 immobilized on a glass surface. Schemes of single-molecule irreversible (A) and reversible (B) hybridization of oligonucleotides TCS-ATTO665 of 12 nucleotides (12NA) and 8 nucleotides (8NA), respectively, with NP-PEMA-Surc/T20. Intensity traces of donor (black) and acceptor (red) of a single nanoprobe with addition of TCS-ATTO665 of 12NA (A) and 8NA (B) and corresponding two-color merged images of the same single particle. C) The same experiment as in (A): two-color merged images of a larger area at different times after addition of 50 nM of TCS-ATTO665. The excitation wavelength was 550 nm, 100x oil objective with power density 0.24 W cm^{-2} . Integration time was 400 ms. 50 wt% R18/F5-TPB dye loading was systematically used.

RESEARCH ARTICLE

Finally, we challenged our nanoprobe in another key application: to image in real-time the single hybridization events between two labelled oligonucleotides. In the first experiment, immobilized donor nanoparticle bearing a single capture sequence were treated with TCS-ATTO665 during the imaging (Figure 5A). After addition of TCS-ATTO665, initially green NPs turned into red and then returned back to green (Figure 5C, Video S1). In the intensity traces, the single-step jump of the acceptor emission was accompanied by the drop of the donor one, which corresponded to the single hybridization event. Then, the acceptor dye got bleached which resulted in exactly opposite single-step changes: drop of the acceptor and jump of the donor. In the second experiment, we added shorter (8mer) TCS-ATTO665 (Figure 5B), which was expected to bind reversibly to the target, similar to what is done in DNA-PAINT imaging methods.^[22] Remarkably, we were able to follow a continuous process of binding unbinding in our two color images and the intensity traces, where donor and acceptor signals switched many times in the opposite way (Figure 5B, S18, Video S2). Thus, these two experiments show that, owing to >250-amplification, our light-harvesting nanomaterial enables real-time detection of reversible and irreversible single hybridization processes using a basic imaging setup with ultra-low excitation irradiance.

Conclusion

In conclusion, we developed an organic nanomaterial that breaks the FRET barrier in existing luminescent nanoparticle systems. It is based on a light-harvesting nanoantenna, where ~1000 of strongly coupled rhodamine dyes with 52% fluorescence quantum yield are confined within a 20-nm polymeric particle. The obtained nanoparticle, being as bright as 87 Qdots-605, shows unprecedented 51% FRET efficiency to a single acceptor (ATTO665) hybridized at the DNA-modified particle surface, generating antenna effect (amplification factor) of ~250. To the best of our knowledge, none of reported fluorescent nanoparticles can combine such high brightness and FRET efficiency to a single acceptor at the surface. High loading of bright rhodamine dyes with their bulky counterions (50 wt%) and a specially designed polymer in this nanoantenna ensure short interfluorophore distances with minimal self-quenching that lead to excitation energy migration within 1000 encapsulated dyes and further FRET to a single acceptor beyond the Förster radius with minimal energy losses. Thus, our 20-nm particle is an efficient FRET donor, like a small dye molecule, but it is ~1000-fold brighter. Our DNA-functionalized nanoantenna particles enabled unprecedented FRET-based detection of single copies of short DNA and RNA as well as monitoring single oligonucleotide hybridization events by a simple epi-fluorescence microscope at ultra-low excitation irradiance (36 mW cm⁻²), close to ambient sunlight. For comparison, conventional single-molecule detection techniques would require in this case >1000-fold higher excitation irradiance, TIRF microscopy and minimized detection volumes to achieve good signal-to-noise ratio.^[1a, 3] The developed nanomaterials will drastically simplify single-molecule detection and open a route to FRET assays for ultrasensitive detection of biomolecular markers, especially microRNA, mRNA and DNA,

which are present in biological samples at very low concentrations.^[23]

Acknowledgements

This work was supported by the European Research Council ERC Consolidator grant BrightSens 648525. We thank Corinne Crucifix from the FRISBI platform for her help with the electron microscopy.

Keywords: light-harvesting nanoantenna • fluorescent nanoparticles • Förster resonance energy transfer • single-molecule detection • nucleic acids biosensor

- [1] a) B. A. Flusberg, D. R. Webster, J. H. Lee, K. J. Travers, E. C. Olivares, T. A. Clark, J. Koriach, S. W. Turner, *Nat. Methods* **2010**, *7*, 461; b) J. Clarke, H. C. Wu, L. Jayasinghe, A. Patel, S. Reid, H. Bayley, *Nat. Nanotechnol.* **2009**, *4*, 265; c) R. K. Neely, P. Dedecker, J. I. Hotta, G. Urbanaviciute, S. Klimasauskas, J. Hofkens, *Chem. Sci.* **2010**, *1*, 453; d) K. Jo, D. M. Dhingra, T. Odijk, J. J. de Pablo, M. D. Graham, R. Runnheim, D. Forrest, D. C. Schwartz, *Proc. Natl. Acad. Sci. U. S. A.* **2007**, *104*, 2673; e) L. A. Neely, S. Patel, J. Garver, M. Gallo, M. Hackett, S. McLaughlin, M. Nadel, J. Harris, S. Gullans, J. Rooke, *Nat. Methods* **2006**, *3*, 41; f) M. D. Baaske, M. R. Foreman, F. Vollmer, *Nat. Nanotechnol.* **2014**, *9*, 933; g) B. Hornblower, A. Coombs, R. D. Whitaker, A. Kolomeisky, S. J. Picone, A. Meller, M. Akeson, *Nat. Methods* **2007**, *4*, 315; h) J. D. Spitzberg, A. Zrehen, X. F. van Kooten, A. Meller, *Adv. Mater.* **2019**, *31*, 1900422.
- [2] a) L. D. Lavis, R. T. Raines, *ACS Chem. Biol.* **2014**, *9*, 855; b) G. T. Dempsey, J. C. Vaughan, K. H. Chen, M. Bates, X. W. Zhuang, *Nat. Methods* **2011**, *8*, 1027.
- [3] a) M. J. Levene, J. Koriach, S. W. Turner, M. Foquet, H. G. Craighead, W. W. Webb, *Science* **2003**, *299*, 682; b) G. P. Acuna, F. M. Möller, P. Holzmeister, S. Beater, B. Lalkens, P. Tinnefeld, *Science* **2012**, *338*, 506; c) M. Sauer, J. Hofkens, J. Enderlein, *Handbook of Fluorescence Spectroscopy and Imaging: From Ensemble to Single Molecules*, Wiley-VCH, **2011**.
- [4] a) K. Aslan, I. Gryczynski, J. Malicka, E. Matveeva, J. R. Lakowicz, C. D. Geddes, *Curr. Opin. Biotechnol.* **2005**, *16*, 55; b) Y. Wang, B. Liu, A. Mikhailovsky, G. C. Bazan, *Adv. Mater.* **2010**, *22*, 656; c) A. G. Brolo, *Nat. Photonics* **2012**, *6*, 709; d) F. Zang, Z. Su, L. Zhou, K. Konduru, G. Kaplan, S. Y. Chou, *Adv. Mater.* **2019**, *31*, 1902331.
- [5] A. Puchkova, C. Vietz, E. Pibiri, B. Wunsch, M. S. Paz, G. P. Acuna, P. Tinnefeld, *Nano Lett.* **2015**, *15*, 8354.
- [6] S. E. Ochmann, C. Vietz, K. Trofymchuk, G. P. Acuna, B. Lalkens, P. Tinnefeld, *Anal. Chem.* **2017**, *89*, 13000.
- [7] a) P. D. Howes, R. Chandrawati, M. M. Stevens, *Science* **2014**, *346*, 1247390; b) O. S. Wolfbeis, *Chem. Soc. Rev.* **2015**, *44*, 4743.
- [8] a) K. Trofymchuk, A. Reisch, P. Didier, F. Fras, P. Gilliot, Y. Mely, A. S. Klymchenko, *Nat. Photonics* **2017**, *11*, 657; b) F. J. Hofmann, M. I. Bodnarchuk, L. Protesescu, M. V. Koyalenko, J. M. Lupton, J. Vogelsang, *J. Phys. Chem. Lett.* **2019**, *10*, 1055; c) C. Q. Li, J. Zhang, S. Y. Zhang, Y. Zhao, *Angew. Chem.-Int. Edit.* **2019**, *58*, 1643; d) J. Su, T. Fukaminato, J. P. Placial, T. Onodera, R. Suzuki, H. Oikawa, A. Brosseau, F. Brisset, R. Pansu, K. Nakatani, R. Metivier, *Angew. Chem. Int. Ed.* **2016**, *55*, 3662.
- [9] K. E. Sapsford, L. Berti, I. L. Medintz, *Angew. Chem. Int. Ed.* **2006**, *45*, 4562.
- [10] a) N. Hildebrandt, C. M. Spillmann, W. R. Algar, T. Pons, M. H. Stewart, E. Oh, K. Susumu, S. A. Diaz, J. B. Delehanty, I. L. Medintz, *Chem. Rev.* **2017**, *117*, 536; b) I. L. Medintz, A. R. Clapp, H. Mattoussi, E. R. Goldman, B. Fisher, J. M. Mauro, *Nat. Mater.* **2003**, *2*, 630; c) C. Y. Zhang, H. C. Yeh, M. T. Kuroki, T. H. Wang, *Nat. Mater.* **2005**, *4*, 826.
- [11] a) O. Dukhno, F. Przybilla, M. Collot, A. Klymchenko, V. Pivovarenko, M. Buchner, V. Muhr, T. Hirsch, Y. Mely, *Nanoscale* **2017**, *9*, 11994; b) M.

RESEARCH ARTICLE

- D. Wisser, S. Fischer, C. Siefe, A. P. Alivisatos, A. Salleo, J. A. Dionne, *Nano Lett.* **2018**, *18*, 2689.
- [12] a) S. Bonacchi, D. Genovese, R. Juris, M. Montalti, L. Prodi, E. Rampazzo, N. Zaccheroni, *Angew. Chem. Int. Ed.* **2011**, *50*, 4056; b) D. Genovese, E. Rampazzo, S. Bonacchi, M. Montalti, N. Zaccheroni, L. Prodi, *Nanoscale* **2014**, *6*, 3022.
- [13] a) S. Kundu, A. Patra, *Chem. Rev.* **2017**, *117*, 712; b) J. J. Li, Y. Chen, J. Yu, N. Cheng, Y. Liu, *Adv. Mater.* **2017**, *29*, 1701905; c) S. Guo, Y. Song, Y. He, X.-Y. Hu, L. Wang, *Angew. Chem. Int. Ed.* **2018**, *57*, 3163; d) L. Xu, Z. Wang, R. Wang, L. Wang, X. He, H. Jiang, H. Tang, D. Cao, B. Z. Tang, *Angew. Chem. Int. Ed.* **2019**, *0*.
- [14] R. Camacho, D. Tauber, I. C. Scheblykin, *Adv. Mater.* **2019**, *31*, 30.
- [15] R. Deng, J. Wang, R. Chen, W. Huang, X. Liu, *J. Am. Chem. Soc.* **2016**, *138*, 15972.
- [16] a) W. B. Wu, G. C. Bazan, B. Liu, *Chem* **2017**, *2*, 760; b) Y. S. Wang, B. Liu, *Chem. Commun.* **2007**, 3553; c) B. S. Gaylord, A. J. Heeger, G. C. Bazan, *Proc. Natl. Acad. Sci. U. S. A.* **2002**, *99*, 10954; d) S. W. Thomas, G. D. Joly, T. M. Swager, *Chem. Rev.* **2007**, *107*, 1339; e) S. Rochat, T. M. Swager, *ACS Appl. Mater. Interfaces* **2013**, *5*, 4488; f) Y. Jiang, J. McNeill, *Chem. Rev.* **2017**, *117*, 838; g) S. Wang, G. C. Bazan, *Adv. Mater.* **2003**, *15*, 1425.
- [17] A. Reisch, A. S. Klymchenko, *Small* **2016**, *12*, 1968.
- [18] a) A. Reisch, P. Didier, L. Richert, S. Oncul, Y. Arntz, Y. Mely, A. S. Klymchenko, *Nat. Commun.* **2014**, *5*, 4089; b) A. Reisch, K. Trofymchuk, A. Runser, G. Fleith, M. Rawiso, A. S. Klymchenko, *ACS Appl. Mater. Interfaces* **2017**, *9*, 43030; c) B. Andreiuk, A. Reisch, E. Bernhardt, A. S. Klymchenko, *Chem. Asian. J.* **2019**, *14*, 836; d) B. Andreiuk, A. Reisch, M. Lindecker, G. Follain, N. Peyrieras, J. G. Goetz, A. S. Klymchenko, *Small* **2017**, *13*, 1701582.
- [19] N. Melnychuk, A. S. Klymchenko, *J. Am. Chem. Soc.* **2018**, *140*, 10856.
- [20] A. E. Prigodich, D. S. Seferos, M. D. Massich, D. A. Giljohann, B. C. Lane, C. A. Mirkin, *Acs Nano* **2009**, *3*, 2147.
- [21] A. Reisch, D. Heimbürger, P. Ernst, A. Runser, P. Didier, D. Dujardin, A. S. Klymchenko, *Adv. Funct. Mater.* **2018**, *28*.
- [22] R. Jungmann, M. S. Avendano, J. B. Woehrstein, M. J. Dai, W. M. Shih, P. Yin, *Nat. Methods* **2014**, *11*, 313.
- [23] A. B. Chinen, C. M. Guan, J. R. Ferrer, S. N. Barnaby, T. J. Merkel, C. A. Mirkin, *Chem. Rev.* **2015**, *115*,

Supporting Information

Light-harvesting nanoparticle probes for FRET-based detection of oligonucleotides with single-molecule sensitivity

Nina Melnychuk, Sylvie Egloff, Anne Runser, Andreas Reisch and Andrey S. Klymchenko*

Materials

Chemical compounds: Poly (methyl methacrylate-co-methacrylic acid) (PMMA-MA, 1.6% methacrylic acid, $M_n \sim 15000$, $M_w \sim 34000$), 3-chloropropanamine hydrochloride (98%), rhodamine B octadecyl ester perchlorate (>98.0%), lithium tetrakis (pentafluorophenyl)borate ethyl etherate, N,N-dimethylformamide (anhydrous, 98%), N,N-Diisopropylethylamine ($\geq 99\%$), acetonitrile (anhydrous, 99.8%), dichloromethane (anhydrous, $\geq 99.8\%$), 1-Hydroxybenzotriazole ($\geq 97\%$), BSA-biotin, Amicon Centrifugal filters (0.5mL, 100kD) were purchased from Sigma-Aldrich. Citric acid monohydrate ($\geq 99.5\%$), sodium azide (99%), sodium iodide ($\geq 99.5\%$) and trifluoroacetic acid (99%) were purchased from Alfa Aesar. Fmoc-Asp(OtBu)-OH was purchased from Activotec. HBTU was purchased from ChemPep Inc. Neutravidin, LabTek chambers (Borosilicate cover glass, eight wells), QDot® 605 Streptavidin Conjugate (QDot605), RNAsecure™ RNase Inactivation Reagent (invitrogen) were purchased from ThermoFisher Scientific. Sodium phosphate monobasic (>99.0%, Sigma-Aldrich) and sodium phosphate dibasic dihydrate (>99.0%, Sigma-Aldrich) were used to prepare 20 mM phosphate buffers. Sodium tetraborate decahydrate (>99.0%, Sigma-Aldrich) was used to prepare borate buffer at and pH was adjusted with 0.1M hydrochloride acid. For saline buffer sodium chloride ($\geq 99\%$, Sigma Aldrich) 30 mM and magnesium chloride ($\geq 98\%$, Sigma Aldrich) 12 mM was added to 20 mM phosphate buffer and pH was adjusted with sodium hydroxide 1N solution. Milli-Q water (Millipore) was used in all experiments. For immobilization protocol PBS (without Ca^{2+} and Mg^{2+}) was purchased from Lonza.

Nucleic acids sequences: Lyophilized single strand DNA and RNA sequences were purchased from IBA GmbH, dissolved in Milli-Q water, aliquoted and stored at $-20\text{ }^\circ\text{C}$ for further experiments. The oligonucleotide sequences used in this study are shown below.

DNA:

SurC-DBCO, 5'-CCC AGC CTT CCA GCT CCT TGA - (DBCO)-3'.

T20-DBCO, 5'-TTT TTT TTT TTT TTT TTT TT-(DBCO)-3'.

A20-Biotin, 5'-(BIO)-AAA AAA AAA AAA AAA AAA AA-3'.

TCS-acceptor, 5'-(acceptor)-TCA AGG AGC TGG-3'. As acceptors were used next dyes: Cy5, Alexa-647, Oyster-650, Cy5.5, DY651, DY654, DY676, ATTO647N, ATTO665, ATTO700.

8NA-TCS-ATTO665, 5'-(ATTO665)-TCA AGG AG.

Target-DNA, 5'-CAA GGA GCT GGA AGG CTG GG-3'; single mismatch, 5'-CAA GCA GCT GGA AGG CTG GG-3'; two mismatches, 5'-CAA GCA GCT GGA AGC CTG GG-3'; three mismatches, 5'-CAA GCA GCT CGA AGC CTG GG-3'.

RNA:

Target-RNA, 5'-CAA GGA GCU GGA AGG CUG GG-3'.

Experimental Procedures

Nanoparticle Preparation.

Protocol for NPs, obtained by nanoprecipitation at pH 7.4: 100 μL of the polymer solution in acetonitrile (2 mg mL^{-1} with 30 wt% R18/F5-TPB relative to the polymer) were then added quickly using a micropipette to 900 μL the same buffer under shaking with Thermomixer (1,100 rpm). Then, the residues of acetonitrile were evaporated.

Protocol for NPs, obtained by nanoprecipitation at pH 9: 50 μL of the polymer solution in acetonitrile (2 mg mL^{-1} containing R18/F5-TPB at 20, 30, 50, 70 or 100 wt% relative to the polymer) were added quickly using a micropipette to 450 μL of 10 mM borate buffer, pH 9 at $21\text{ }^\circ\text{C}$ under shaking (Thermomixer comfort, Eppendorf, 1100 rpm). While continues mixing 500 μL of 20 mM phosphate buffer,

SUPPORTING INFORMATION

pH 6 were added. Then, the residues of acetonitrile were evaporated. The particle solution was then 2-fold diluted with the 20 mM of phosphate buffer, pH 7.4.

General protocol for nanoprobe synthesis.

Aliquots of DNA were added to 200 μ L of nanoparticles. The reaction was mixed and kept overnight at 40 °C in Thermomixer without shaking protected from light. Then the reaction was cooled down to room temperature. For annealing with TCS-acceptor, the aliquot of TCS-acceptor in ratio 1:1 with SurC-DBCO was added and mixture was heated to 70 °C in water bath for 3 min. To complete hybridization the reaction was cooled down to room temperature and kept in the dark for 2 h. Then the mixture was diluted with 20 mM phosphate buffer containing 12 mM MgCl₂ and 30 mM NaCl to 4 mL and purified by centrifugation using centrifuge filters (Amicon, 0.5ml, 100kD) on 1000 g at 20 °C for 2 min. The procedure of centrifugation was repeated 5 times to remove the non-reacted oligonucleotides. The obtained nanoprobe in volume of 1 mL were kept in the dark at 4 °C.

Detection in solution.

The PEMA-nanoprobe was diluted in 20 mM phosphate buffer containing 30 mM NaCl and 12 mM MgCl₂ (in case of RNA-target the buffer additional contained 1x RNAsecure™) to a desired concentration (corresponding to TCS-ATTO665) and aliquot of target oligonucleotide was added. The mixture (200 μ L) was kept at 20 °C in Thermomixer without shaking protected from light. Before measurements the mixture was 3-fold diluted with a same buffer.

Detection on surfaces.

300 μ L of the buffer was mixed with aliquot of the target oligonucleotide and then the mixture was added to the LabTek chamber with immobilized nanoprobe. The mixture was kept in the dark at the room temperature for 6 h incubation before measurements. In case of detection by imaging of the same area of nanoparticles, first the PEMA-nanoprobe was imaged with 200 μ L of the same buffer (in case of RNA the buffer contained 1x RNAsecure™) and then 200 μ L of nucleic acid target were added in order to obtain 100 pM final concentration. After 1 hour of incubation at the room temperature the same zone of nanoparticle was imaged.

Nanoparticle characterization.

Dynamic light scattering (DLS) measurements were performed on a Zetasizer Nano series DTS 1060 (Malvern Instruments S.A.). The Zetasizer software provided with standard cumulates and size distribution by volume analysis was used to characterize nanoparticles by DLS. For the data analysis, the following parameters were used: for the solvent (water) – temperature 25 °C, refractive index RI 1.33, and viscosity 0.8872 cP. Nanoparticles were assumed to be all homogenous and spherical in shape. Absorption spectra were recorded on a Cary 4000 scan UV-visible spectrophotometer (Varian). Excitation, emission spectra and anisotropy were recorded on FS5 Spectrofluorometer (Edinburg Instruments). For standard recording of fluorescence spectra, the excitation wavelength was set to 530 nm. The fluorescence spectra were corrected for detector response and lamp fluctuations. Quantum yields of donor dye in NPs were calculated using Rhodamine 101 in methanol as a reference (QY = 1.0) with an absorbance of 0.01 at 530 nm. QYs of the acceptor were measured using DiD in methanol (QY = 0.33) as a reference. To calculate FRET efficiency based on fluorescence spectra, a classical equation was used: $E_{FRET} = 1 - \frac{I_{D-A}}{I_D}$, where I_D is the donor maximum intensity and I_{D-A} is the maximum intensity of the donor in the presence of the acceptor. The overlap integral $J(\lambda)$ was calculated using the FluorTools software.^[1] The Förster distance was calculated by:

$$R_0 = 0.211 \left[\frac{k^2 Q_D J(\lambda)}{n^4} \right]^{1/6}$$

Amplification factor of the acceptor emission (antenna effect, AE) was expressed as the ratio of the maximal excitation intensity of the donor to that of the acceptor with correction from the emission of the donor dyes at 690 nm for CY5 and 700 nm for ATTO665:

$$AE = \frac{I_{D-FRET}^{ex} - I_D^{ex} * \frac{I_{D-FRET}^{em}}{I_D^{em}}}{I_{A-FRET}^{ex} - I_A^{ex}}$$

Where I_{D-FRET}^{ex} and I_{A-FRET}^{ex} are the maximal excitation intensities of donor and acceptor in nanoprobe, respectively; I_D^{ex} and I_A^{ex} are the excitation intensities at the wavelengths of excitation maximum of donor and acceptor in nanoparticle-T20; I_{D-FRET}^{em} and I_D^{em} maximum emission intensity of donor for nanoprobe and nanoparticle-T20, respectively.

Photobleaching of nanoparticles in solution.

Photobleaching experiments were performed on a home-build setup. The cuvette holder (CHV100) with SMA905 Fiber Adapter was purchased from ThorLab. For sample excitation, we used the module of a 532 nm diode laser (Oxxius) guided through the fiber optics and passed through optical beam expander (BE50M, ThorLabs). The cuvette height was adjusted so that sample volume of 100 μ L was fully irradiated. To get rid of laser radiation at 532, the single Noch filter 532 nm (Chroma) was installed. For the fluorescence signal detection OceanOptics QE Pro modular spectrometer was used. The fluorescence signal was further processed by an OceanView Software.

Transmission electron microscopy (TEM).

Carbon-coated copper-rhodium electron microscopy grids with a 300 mesh (Euromedex, France) were surface treated with a glow discharge in amylamine atmosphere (0.45 mbar, 4 – 4.5 mA, 22 s) in an Elmo glow discharge system (Cordouan Technologies, France). Then, 5 μ L of the solution of NPs at 0.04 g/L were deposited onto the grids and left for 2 min. The grids were then treated for 1 min with a 2% uranyl acetate solution for staining. They were observed with a Philips CM120 transmission electron microscope equipped with

SUPPORTING INFORMATION

a LaB6 filament and operating at 100 kV. Areas covered with nanoparticles of interest were recorded at different magnifications on a Peltier cooled CCD camera (Model 794, Gatan, Pleasanton, CA). Image analysis was performed using the Fiji software.

Fluorescence Microscopy

Immobilization protocol for non-functionalized nanoparticles. The 300 μL of 1M KOH aqueous solution was added in the LabTek chamber. After 20 mins the chamber was washed 3 times with $\sim 300 \mu\text{L}$ of MQ-water. Then 200 μL of 1 mg/mL PEI solution in TRIS buffer pH 7.4 was added. After 20 mins the chamber was washed with 300 μL of MQ-water and left with 300 μL of MQ-water for 15 mins. Then the chamber was washed 2 times with 300 μL of MQ-water and 2 times with 300 μL of 20 mM phosphate buffer. The 250 μL of nanoparticle solution with proper concentration to achieve desired density was deposit on the plate and left for 20 mins. Then the chamber was rinsed 3 times with 20 mM phosphate buffer and measurements were performed with a layer of the same buffer ($\sim 300 \mu\text{L}$) above the surface.

Immobilization protocol for DNA-functionalized nanoparticles and QDot605. Immobilization in LabTek chamber was performed according to previously described protocol.^[2] The LabTek chamber was washed 3 times with PBS followed by incubation with 200 μL of BSA-Biotin (0.5 mg mL^{-1} in PBS) for 5 min. Then, BSA-biotin solution was removed, and the chamber was washed 3 times with 500 μL of PBS. In case of nanoparticles immobilization, the chamber was incubated with 200 μL of neutravidin solution (0.5 mg mL^{-1} in PBS) for 5 min and washed 3 times with 500 μL of PBS. Then the chamber was incubated with 200 μL of 1 μM solution of A20-biotin in PBS for 5 min and washed 1 time with PBS and 2 times with 20 mM phosphate buffer containing 12 mM MgCl_2 and 30 mM NaCl. Then nanoprobe solution was deposited with proper concentration to achieve desired density and incubated for 1 hour at room temperature in the dark. Before measurements the chamber was washed 2 times with 20 mM phosphate buffer containing 12 mM MgCl_2 and 30 mM NaCl and covered with 200 μL of the same buffer. In case of QDot605 immobilization, QDot605 Streptavidin Conjugate (ThermoFisher Scientific) was diluted to 100 pM concentration in PBS and 300 μL was added to the chamber. After 1 h of incubation, the chamber was washed 3 times with 500 μL of PBS and filled with 200 μL of PBS.

Single-particle measurements were performed in the epi-fluorescence mode using Nikon Ti-E inverted microscope with a 100x objective (Apo TIRF, oil, NA 1.49, Nikon) and a CFI Plan Apo 60x oil (NA = 1.4) objective. The excitation was provided by light emitting diodes (SpectraX, Lumencor) at 550 and a 640 nm.

In case of non-functionalized nanoparticles (NP-PEMA-AspN3 and NP-PMMA-AspN3-5%) the power density used at 550 nm was 0.4 W cm^{-2} . In case of PEMA-nanoprobe, the power density used at 550 nm was 0.24 W cm^{-2} (100x objective) and 0.036 W cm^{-2} (60x objective). For direct excitation of acceptor (ATTO665), the 640-nm light was used with a power density of 27.62 W cm^{-2} . Also, direct excitation of ATTO665 was done in a TIRF (Total Internal Reflection Fluorescence) setup using a 642 nm diode laser (Oxxius) with power density set to 24.69 W cm^{-2} .

The fluorescence signal was recorded with a Hamamatsu Orca Flash 4 camera. The exposure time was set to 200 ms (PMMA-nanoprobe-1.6%) or 400 ms (PEMA-nanoprobe) per image frame. In case of two-color image detection, corresponding to Donor (R18/F5-TPB) and Acceptor (Cy5 or ATTO665) signals, W-VIEW GEMINI image splitting system (Hamamatsu) was used with dichroic 640 nm (Semrock FF640-FDi01-25x36).

Comparison of single-particle brightness of PEMA-nanoprobe vs QDot605 was performed using the same experimental setup. The excitation of nanoantenna particles and QDot605 were achieved using 550-nm light with power density of 0.24 W cm^{-2} and 15.35 W cm^{-2} correspondently.

The detection of target via illumination the same area of PEMA-nanoprobes before and after 1 hour of incubation with a target was done using the same experimental setup with 60x objective using 550-nm light with power density of 0.036 W cm^{-2} . The images were made with the exposure time of 1s.

Single-particle analysis was performed using the Fiji software. Particle locations were detected through a Fiji routine applied to a projection (maximum intensity) of all obtained frames per experiment. After the automatic background subtraction, the mean intensities of circular regions of interest with a diameter of 8 pixels around the found particle locations were then measured. In order to calculate the FRET response $A/(A+D)$ average of intensity of NPs was obtained base on the first 3 frames for each channel. At least three image sequences (245 pixel \times 245 pixel) per condition were analysed with, on average, 500-1000 particles per sample.

The fluorescence intensity in photons (P – input photon) was calculated for sCMOS camera as:

$$P = \frac{CF \times (I_{output} - I_{dark})}{\frac{Q(\lambda)}{100}}$$

where CF is the conversion factor (according to manufactures CF=0.48), I_{output} and I_{dark} are the output signal with and without illumination, respectively. $Q(\lambda)$ is a conversion efficiency of photons to electrons in % (provided by manufactures). To calculate the total emitted photons per NP-acceptor, value $(I_{output} - I_{dark})$ collected on acceptor channel was integrated over the on-time (time before photobleaching), that gave the total detected photons before the photobleaching.

The amplification factor of the acceptor emission at the single particle level was determined using:

$$AF = \frac{I_A^{550nm}}{I_A^{640nm}} \times \frac{p^{640nm}}{p^{550nm}}$$

R Where I_A^{550nm} and I_A^{640nm} are mean intensities of acceptors under excitation at 550 and 640 nm, respectively, and p^{640nm} and p^{550nm} are laser powers at corresponding wavelengths. The amplification factor indicates how many folds the emission increases when the dye is excited via nanoantenna vs direct dye excitation.

SUPPORTING INFORMATION

Chemical synthesis

NMR spectra were recorded at 20°C on Bruker Avance III 400MHz spectrometer and chemical shifts were reported as delta scale in ppm relative to CHCl₃ (δ = 7.26 ppm) for ¹H NMR and CDCl₃ (δ = 77.16 ppm) for ¹³C NMR. Mass spectra were obtained using an Agilent Q-TOF 6520 mass spectrometer.

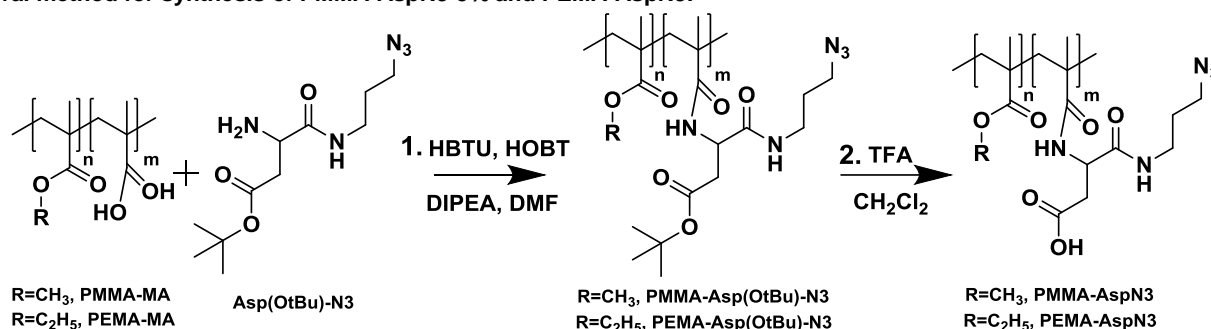
Rhodamine B octadecyl ester trakis(penta-fluorophenyl)borate (R18/F5-TPB) was synthesized by ion exchange and purified by column chromatography as described previously.^[3]

Linker Asp(OtBu)N3 was synthesized by coupling of Fmoc-Asp(OtBu)-OH with a 3-chloropropanamine, followed by azide substitution and Fmoc removal as described previously.REF

PMMA-AspN3-1.6% polymer was obtained by coupling of PMMA-MA (1.6% methacrylic acid, Mn ~15000, Mw ~34000) with Asp(OtBu)N3 and further Boc-protecting group removal as described previously.^[4]

Poly (methyl methacrylate-co-methacrylic acid), PMMA-MA (5% of methacrylic acid) and Poly (ethyl methacrylate-co-methacrylic acid), PEMA-MA (5% of methacrylic acid) were synthesized through free radical polymerization and purified via precipitation in methanol/water mixtures as described elsewhere.^[5]

General method for synthesis of PMMA-AspN3-5% and PEMA-AspN3:



1. The PMMA-MA or PEMA-MA (1 eq of COOH groups) was dissolved in anhydrous N,N-dimethylformamide. To this solution HBTU (3 eq), HOBT (4 eq) and N,N-diisopropylethylamine (10 eq) was added. The mixture was stirred for 15 min and after Asp(OtBu)-N3 or Asp(OtBu)3-N3 (3 eq) was added. The reaction was stirred overnight at room temperature under argon. The solvent was evaporated under reduced pressure and residue was dissolved in minimum of acetonitrile and precipitated with methanol. The precipitate was washed with methanol, redissolved in acetonitrile and reprecipitated twice in methanol. After drying under a vacuum, product was obtained as a white solid.

PMMA-Asp(OtBu)-N3 (5% of initial methacrylic acid) – yield 45%. ¹H NMR (400 MHz, CDCl₃) δ , ppm: 0.84 (br s, 2 H), 1.02 (br s, 1 H), 1.21 (br s, 0.24 H), 1.34 - 1.53 (m, 0.29 H), 1.76 - 2.04 (m, 2 H), 2.10 - 2.32 (m, 1 H), 3.60 (br s, 3 H).

PEMA-Asp(OtBu)-N3 (5% of initial methacrylic acid) – yield 50%. ¹H NMR (400 MHz, CDCl₃) δ , ppm: 0.88 (br s, 2 H) 1.04 (br s, 1 H), 1.27 (s, 3 H), 1.45 (br s, 0.47 H), 1.59 (br s, 1 H), 1.83 (br s, 1 H), 1.93 (br s, 0.72 H), 2.01 (br s, 0.44 H), 4.04 (br s, 2 H).

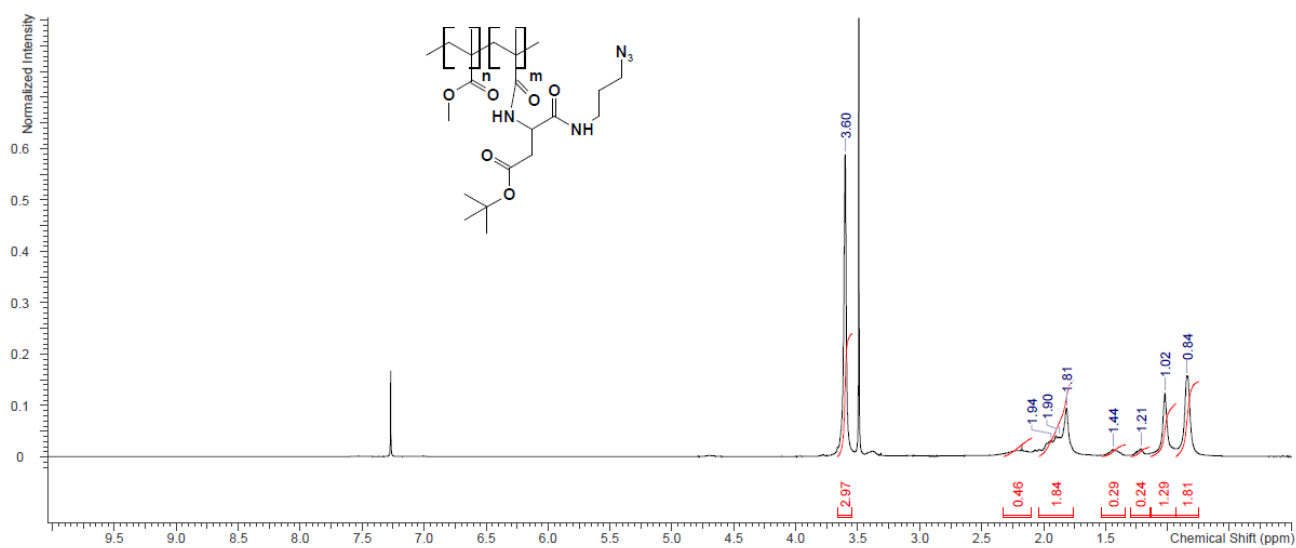
2. Polymer obtained in a previous step was dissolved in anhydrous dichloromethane (~ 5 mL) and 2 mL of trifluoroacetic acid was added. The mixture was stirred for 3 h. Then solvents were evaporated under reduced pressure. Acetonitrile was added to the residue and evaporation was repeated several times until the absence of the trifluoroacetic acid. Then the product was precipitated in methanol and filtrated. After drying under vacuum, the product was obtained as a white solid.

PMMA-AspN3-5% (5% of initial methacrylic acid) – yield 60%. ¹H NMR (400 MHz, CDCl₃) δ , ppm: 0.75 - 0.93 (m, 2 H), 1.02 (br s, 1 H), 1.21 (br s, 0.29 H), 1.45 (br s, 0.33 H), 1.81 (br s, 0.81 H), 1.84 - 2.05 (m, 1 H), 3.60 (br s, 3 H).

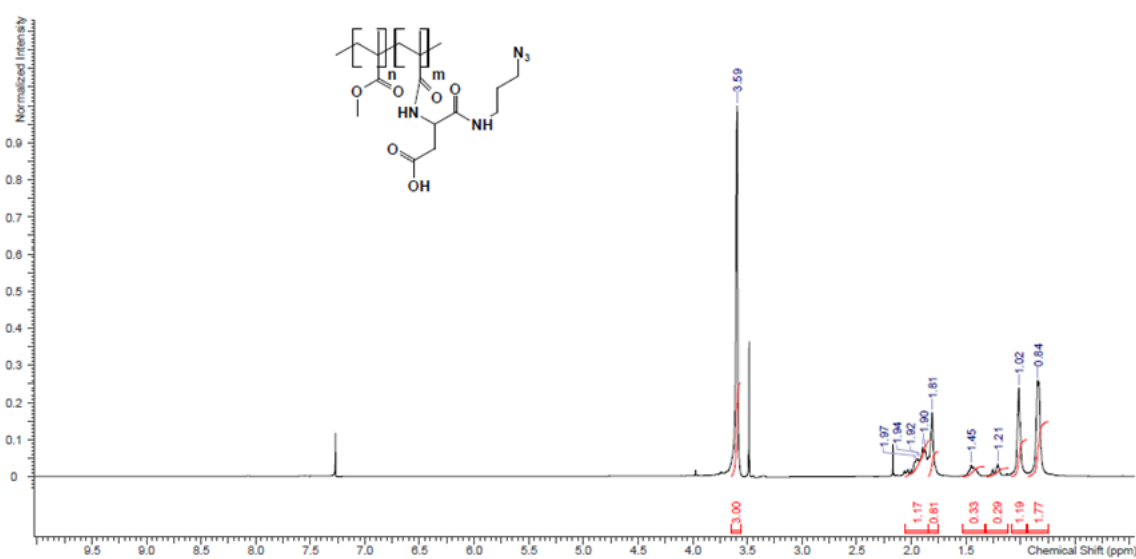
PEMA-AspN3 (5% of initial methacrylic acid) – yield 70%. ¹H NMR (400 MHz, CDCl₃) δ , ppm: 0.83 - 1.10 (m, 2 H), 0.96 - 1.12 (m, 1 H), 1.20 - 1.34 (br s, 3 H), 1.35 - 1.63 (m, 0.47 H), 1.83 (br s, 1 H), 1.93 (br s, 0.72 H), 1.97 - 2.23 (m, 0.44 H), 4.04 (br s, 2 H).

SUPPORTING INFORMATION

NMR spectra

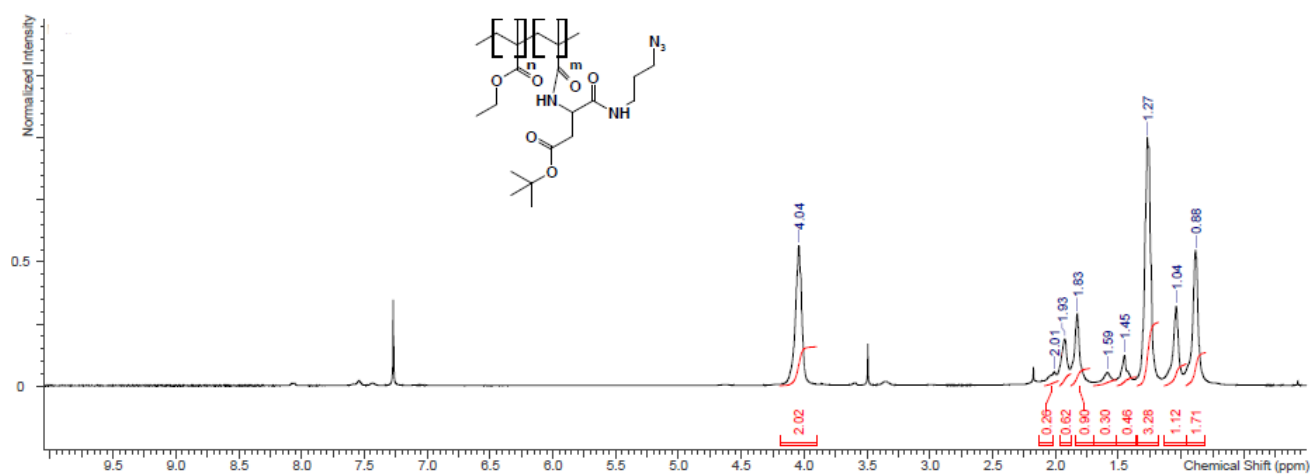


¹H NMR spectrum of PMMA-Asp(OtBu)-N3 (5% of initial methacrylic acid).

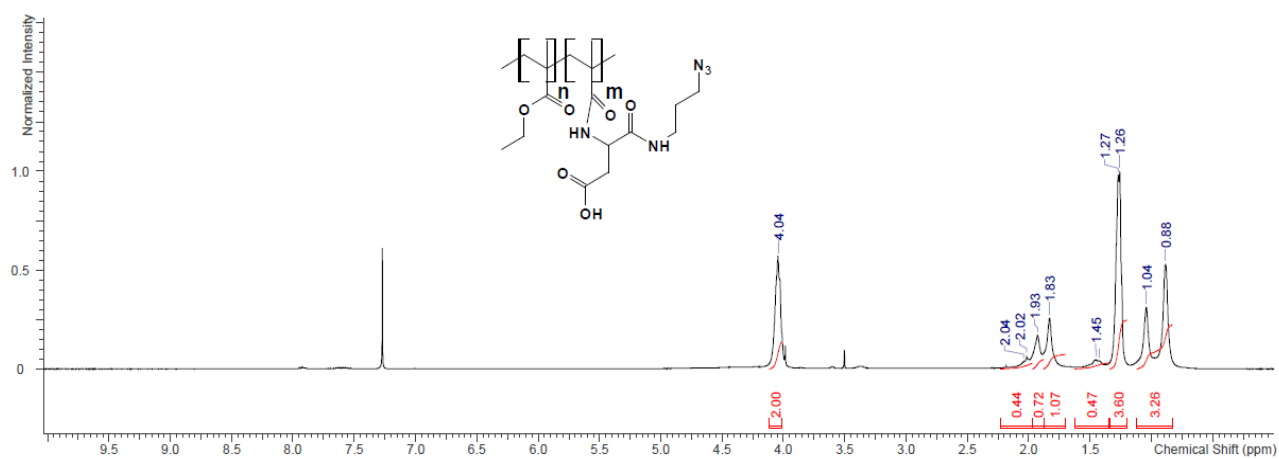


¹H NMR spectrum of PMMA-AspN3-5% (5% of initial methacrylic acid).

SUPPORTING INFORMATION



¹H NMR spectrum of PEMA-Asp(OtBu)-N3 (5% of initial methacrylic acid).



¹H NMR spectrum of PEMA-AspN3 (5% of initial methacrylic acid).

Supporting Figures

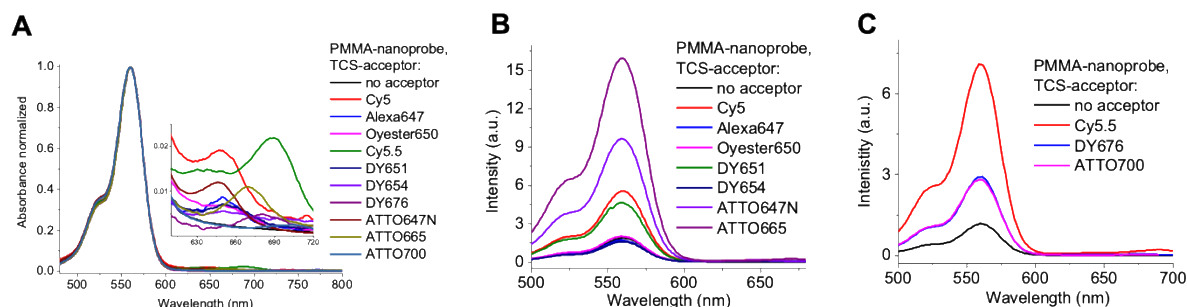


Figure S1. Search for the best FRET acceptor. A) Absorbance spectra and C-D) fluorescence excitation spectra of PMMA-nanoprobes (PMMA-AspN3-1.6% polymer) with ten different FRET acceptors. Emission wavelength was 690 nm (C) and 710 nm (D). R18/F5-TPB loading was 30 wt%.

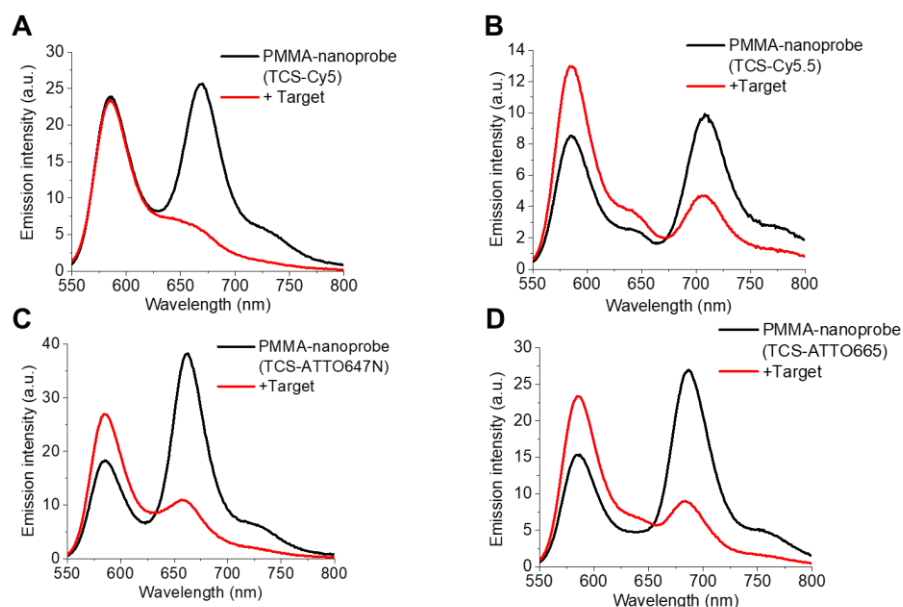


Figure S2. Response of PMMA-nanoprobes (PMMA-AspN3-1.6% polymer) formulated with four different TCS-acceptors to the DNA target. Emission spectra of PMMA-nanoprobe (TCS-Acceptor, 200 pM) formulated with A) Cy5, B) Cy5.5, C) ATTO647N, D) ATTO665 after incubation for 2 h without and with 1 nM of DNA target at the room temperature. Excitation wavelength was 550 nm. R18/F5-TPB loading was 30 wt%.

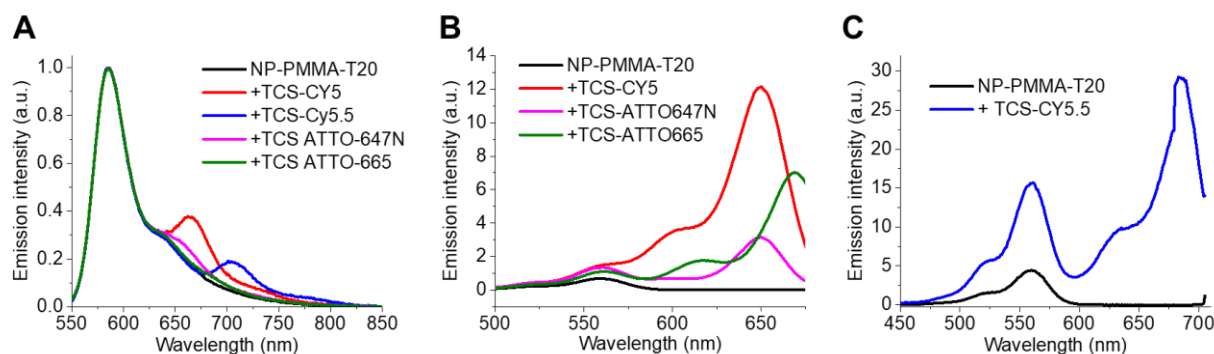


Figure S3. Non-specific interaction of different TCS-acceptors with NP-PMMA-T20 (PMMA-AspN3-1.6% polymer). A) Fluorescence emission spectra of NP-PMMA-T20 after 24 h incubation at the room temperature without and with 50 nM of TCS-Cy5, TCS-ATTO647N, TCS-ATTO665 and TCS-Cy5.5. Excitation wavelength was 550 nm. B) Fluorescence excitation spectra of NP-PMMA-T20 after 24 h incubation at the room temperature without and with 50 nM of TCS-Cy5, TCS-ATTO647N, TCS-ATTO665 at emission wavelength 690 nm and C) NP-PMMA-T20 without and with TCS-Cy5.5 at emission wavelength 710 nm. R18/F5-TPB loading was 30 wt%.

SUPPORTING INFORMATION

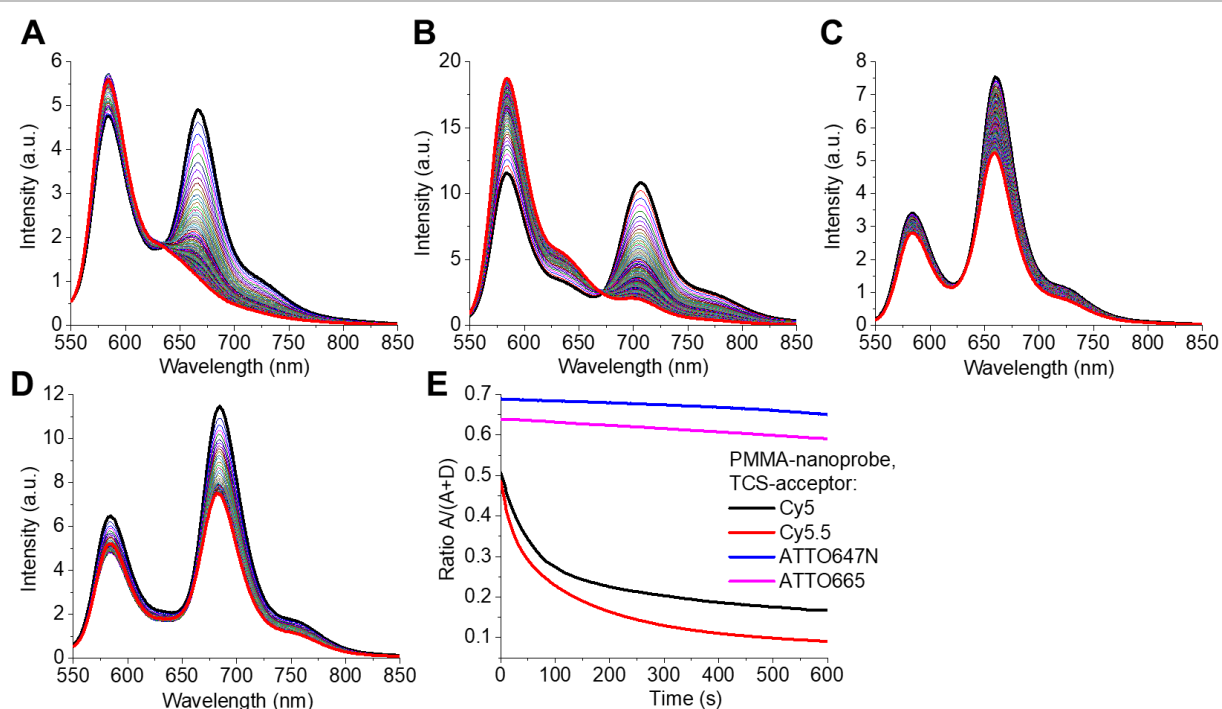


Figure S4. Photobleaching of PMMA-nanoprobe (PMMA-AspN3-1.6% polymer) formulated with four different TCS-acceptors in solution. Fluorescence spectra of PMMA-nanoprobe (TCS-Acceptor, 100 μM): A) Cy5, B) Cy5.5, C) ATTO647N, D) ATTO665 measured during 10 min of irradiation at 532 nm with excitation power density 80 mW cm^{-2} (exposure time 200 ms, 5 scan to average spectrum). E) Photobleaching curves of nanoprobe formulated with TCS-Cy5, TCS-Cy5.5, ATTO647N and ATTO665. R18/F5-TPB loading was 30 wt%.

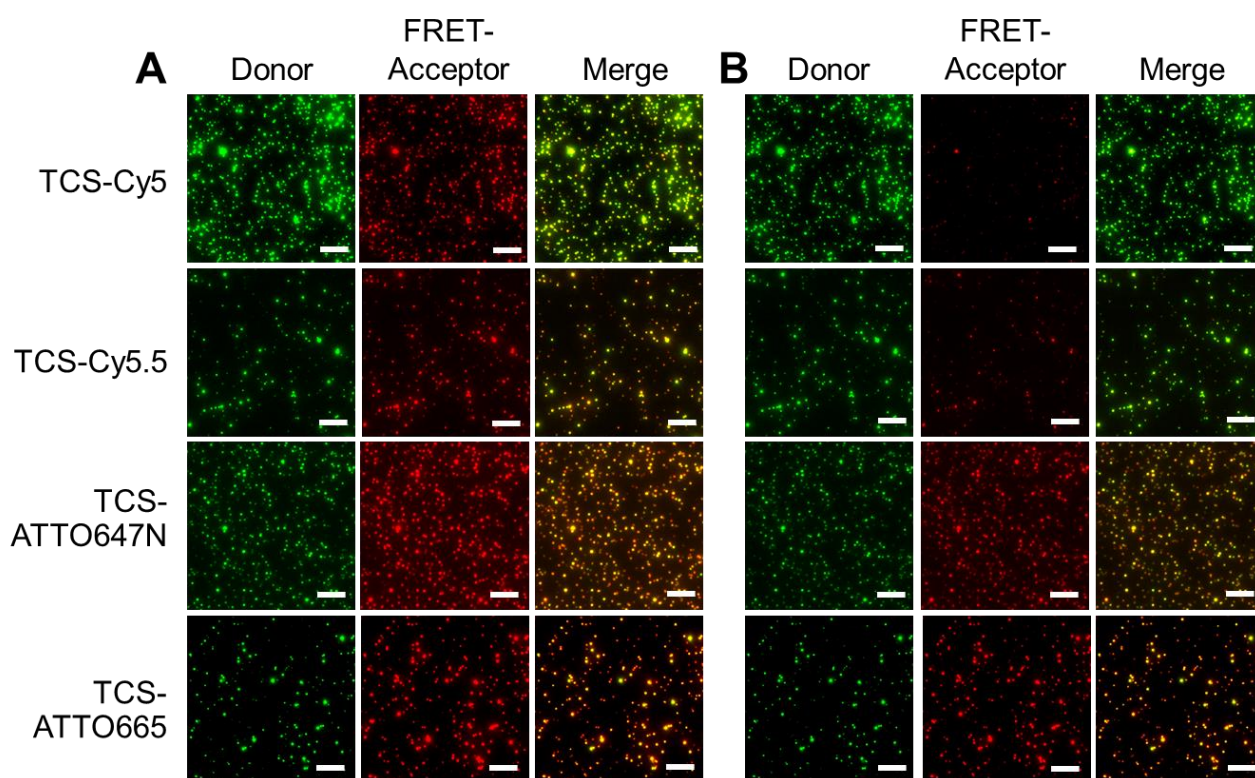


Figure S5. Photostability of PMMA-nanoprobe (PMMA-AspN3-1.6% polymer) formulated with four different TCS-acceptors at a single particle level. Wide-field FRET images (donor channel, acceptor channels and overlay) of PMMA-nanoprobe formulated with TCS-Cy5, TCS-Cy5.5, TCS-ATTO647N and ATTO665 A) before illumination and B) after 20 s of illumination. The excitation wavelength was at 550 nm with 0.54 W cm^{-2} power density. Signals from the donor and the acceptor were recorded at <640 and >640 nm, respectively. All channels are represented at the same intensity scale. Scale bar, 5 μm .

SUPPORTING INFORMATION

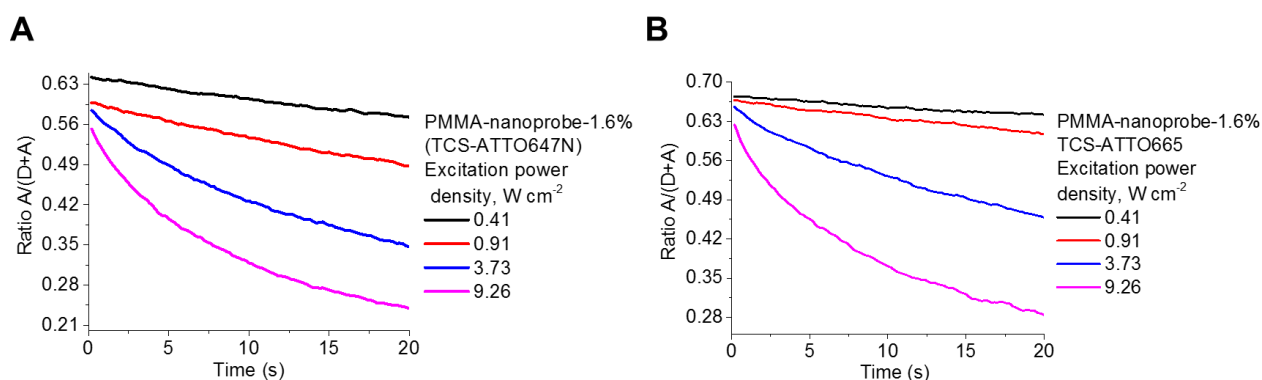


Figure S6. Photostability of PMMA-nanoprobe (PMMA-AspN3-1.6% polymer) formulated with TCS-ATTO647N and TCS-ATTO665 at the single particle level excited with higher power. Curves of relative FRET efficiency $A/(D+A)$ during 20 s of excitation at 550 nm of A) PMMA-nanoprobe (TCS-ATTO647N) and B) PMMA-nanoprobe (TCS-ATTO665) with power density of 0.41, 0.91, 3.73 and 9.26 $W\ cm^{-2}$. Signals from the donor and the acceptor were recorded at <640 and >640 nm, respectively. A and D are the integrated densities of the signal from individual particles recorded at the acceptor and the donor channels, respectively.

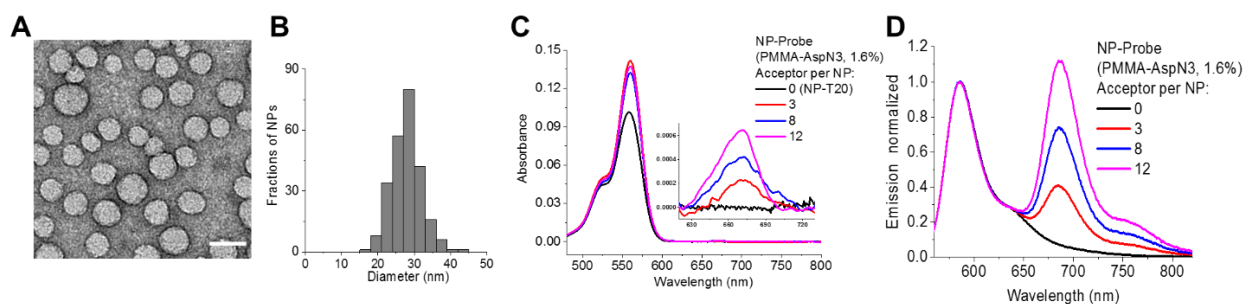


Figure S7. Formulation of PMMA-nanoprobe (PMMA-AspN3-1.6% polymer) at higher pH. A) TEM image (scale bar: 50 nm) and B) Size-distribution diagram of NP-PMMA-AspN3 formulated at pH 9. C) Absorption spectra and D) normalized fluorescence spectra of PMMA-nanoprobe-1.6% without and with 3, 8 and 12 TCS-ATTO665 per NP. Excitation wavelength was 530 nm. R18/F5-TPB loading was 30 wt%.

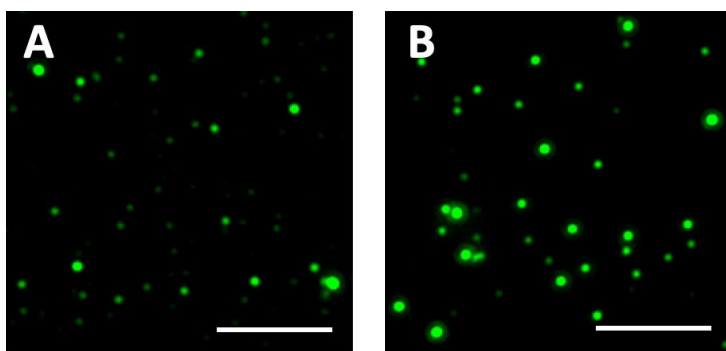


Figure S8. Wide-field microscopy images of immobilized nanoparticles based on A) PMMA-AspN3-5% and B) PEMA-AspN3 polymers. The excitation was at 550 nm with excitation power density 0.41 $W\ cm^{-2}$. Integration time was 200 ms. Scale bar 5 μm . R18/F5-TPB loading was 30 wt%.

SUPPORTING INFORMATION

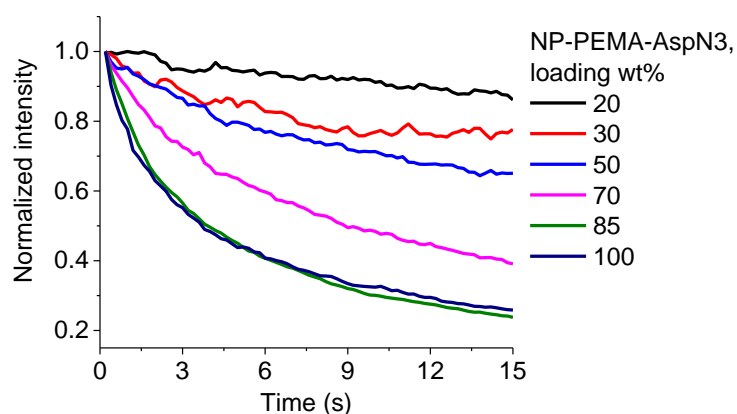


Figure S9. Average intensity curves of NP-PEMA-AspN3 at a single particle level at different loading of R18/F5-TPB dye. The excitation wavelength was at 550 nm with 0.4 W cm^{-2} power density. Intensity is an average integrated density of nanoparticles.

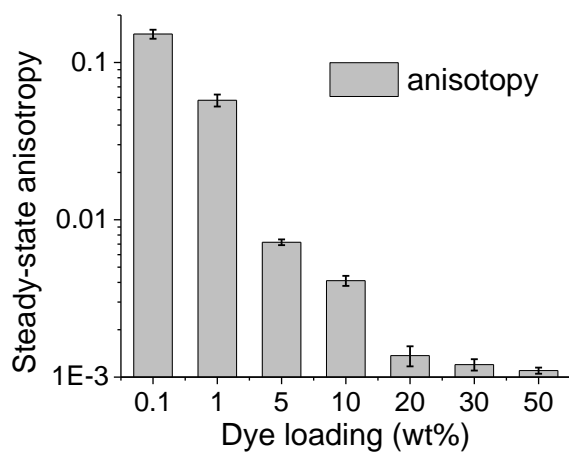


Figure S10. Steady-state fluorescence anisotropy of PEMA-AspN3 NPs as a function of R18/F5-TPB dye loading.

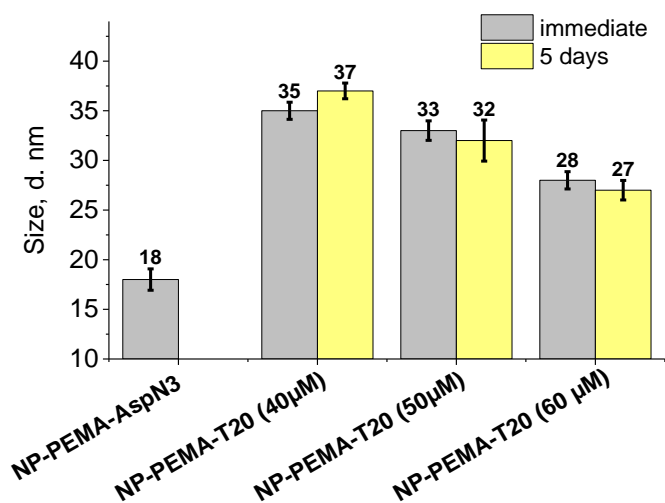


Figure S11. Size by DLS of NP-PEMA-AspN3 functionalized with increasing amount of T20 DNA (40 μM , 50 μM and 60 μM of T20 DNA were added to the reaction mixtures). The DLS was measured immediately after purification and after 5 days of storage in the dark at 4 $^{\circ}\text{C}$. R18/F5-TPB loading was 50 wt%.

SUPPORTING INFORMATION

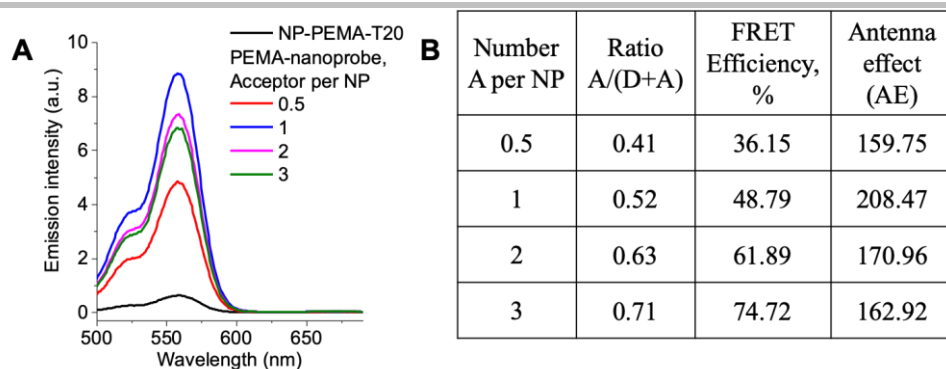


Figure S12. Characterization of PEMA-nanoprobes with different amount of acceptors. A) Fluorescence excitation spectra of PEMA-nanoprobes with increasing amount of acceptors (TCS-ATTO665). R18/F5-TPB loading was 50 wt%. Emission wavelength was 690 nm. B) Characterization of PEMA-nanoprobes with increasing amount of acceptors.

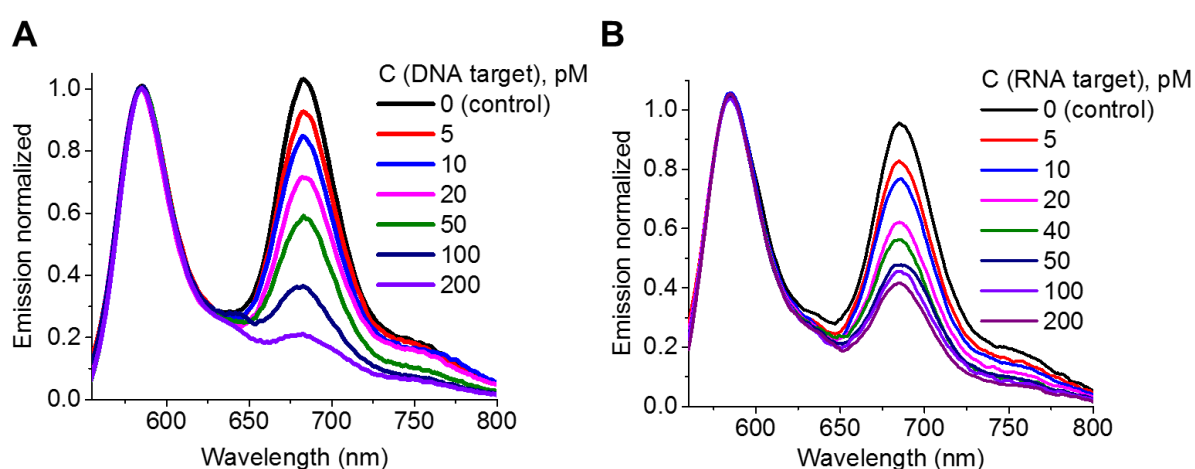


Figure S13. Response of PEMA-nanoprobe to DNA and RNA target in the solution. Fluorescence spectra of PEMA-nanoprobes incubated for 6 h at 20 °C with increasing amount of A) DNA target and B) RNA target. Excitation wavelength was 530 nm.

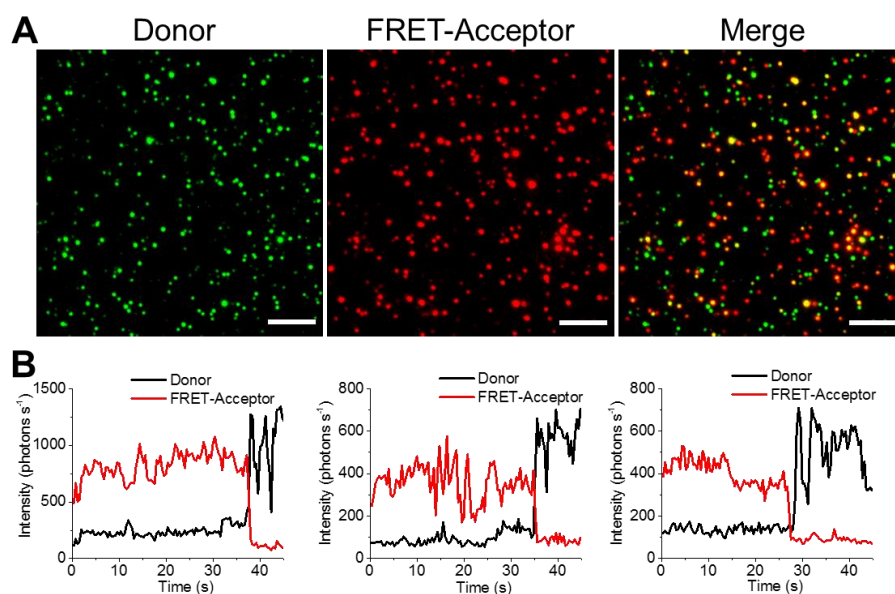


Figure S14. Single-molecule detection in PEMA-nanoprobes at excitation conditions close to ambient light. A) Wide-field FRET images of PEMA-nanoprobes (donor channel, acceptor channels and overlay) and B) Intensity traces of donor and FRET-acceptor. The excitation wavelength was 550 nm, 60x oil objective with power density 0.036 W cm⁻². Integration time was 400 ms. Scale bar, 5 μm

SUPPORTING INFORMATION

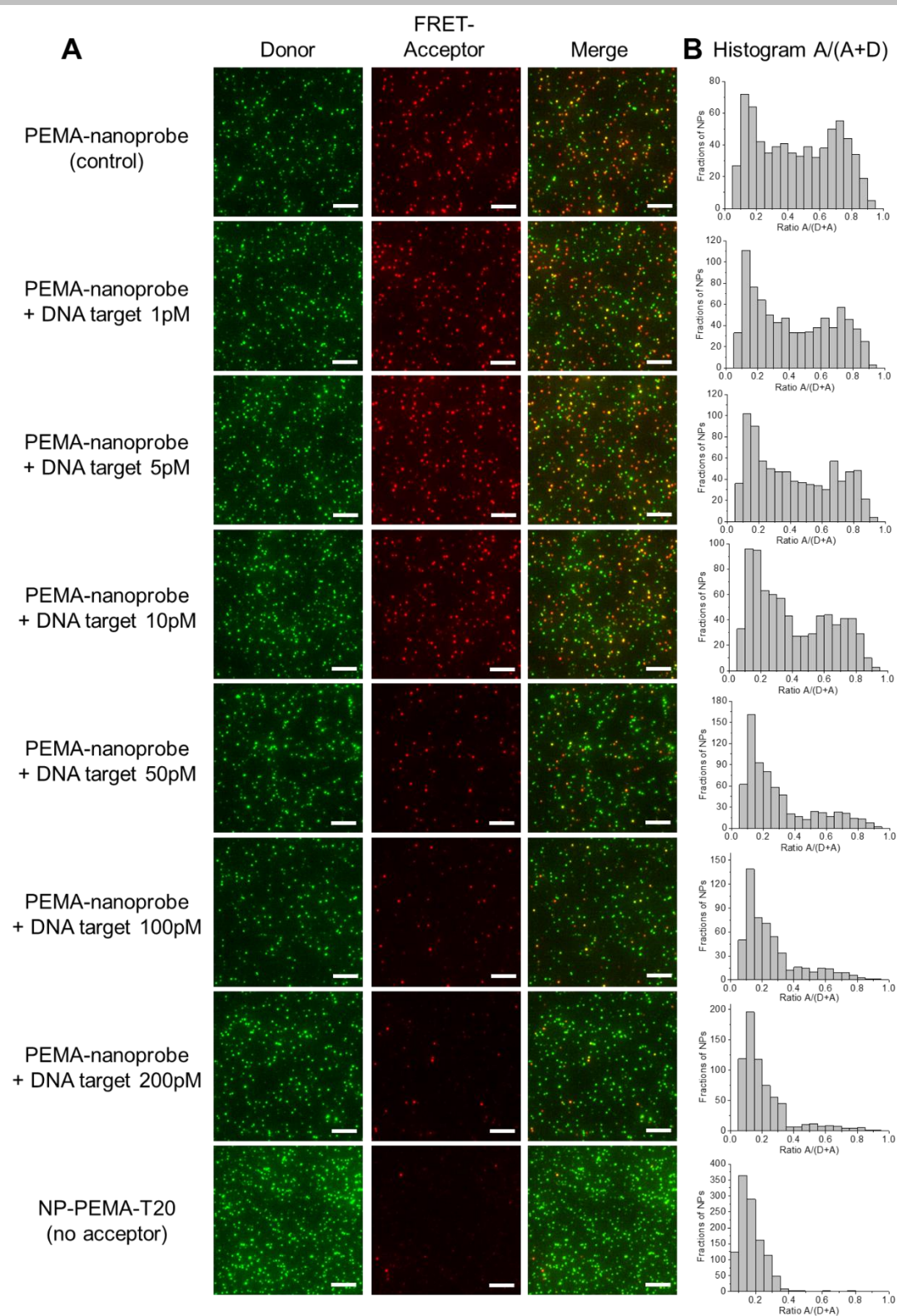


Figure S15. Response of PEMA-nanoprobe to survivin DNA target at the single particle level. A) Wide-field fluorescence microscopy images of the immobilized PEMA-nanoprobe B) and corresponding histograms of relative FRET efficiency, $A/(A + D)$ after 6h incubation at room temperature with different concentrations of survivin DNA target. Excitation wavelength was 550 nm with power density 0.24 W cm^{-2} . Integration time was 400 ms. Signals from Donor and FRET-Acceptor were recorded at <640 and >640 nm, respectively. Both donor and acceptor channels are presented at the same intensity. Scale bar, 5 μM .

SUPPORTING INFORMATION

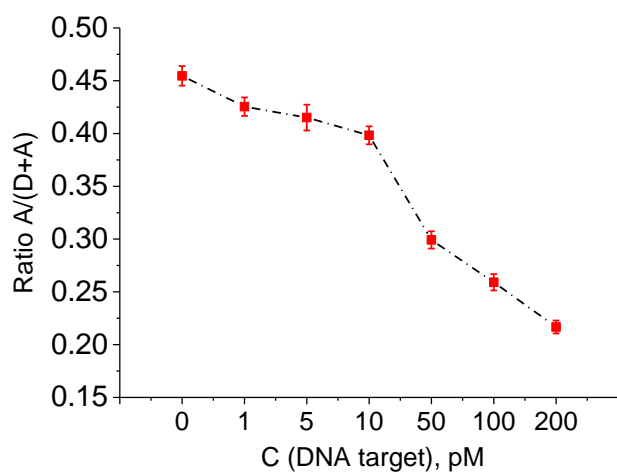


Figure S16. Ratiometric response of PEMA-nanoprobes at the single particle level with increasing DNA target concentration.

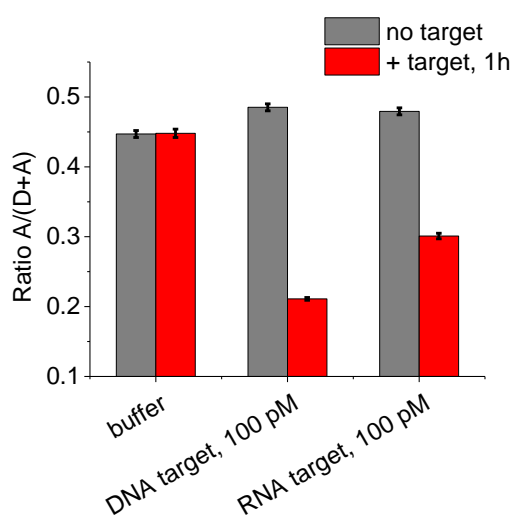


Figure S17. Ratiometric response of PEMA-nanoprobes without and with 100 pM of DNA and RNA targets. The excitation wavelength was 550 nm, 60x oil objective with power density 0.036 W cm^{-2} . Integration time was 1s.

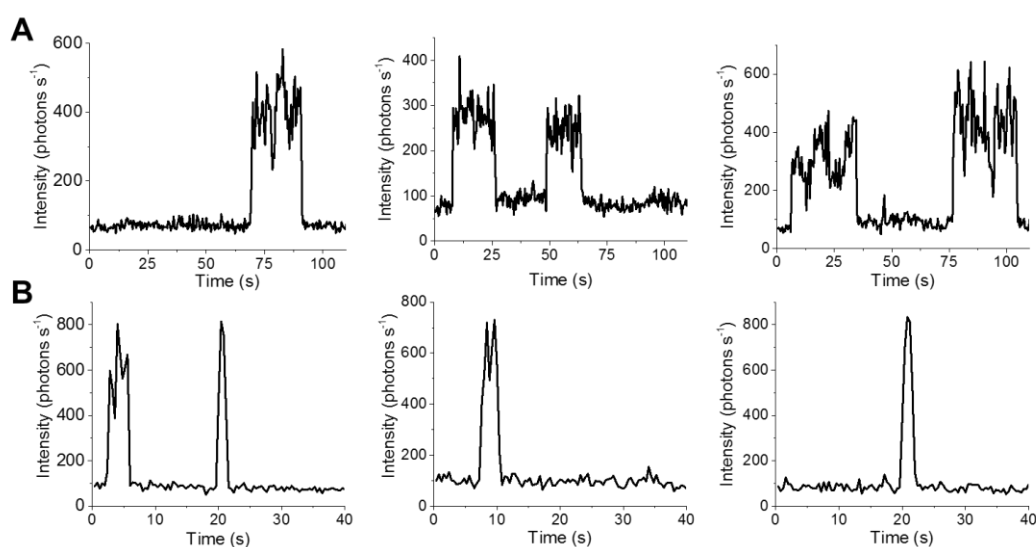


Figure S18. FRET-acceptor traces during imaging of NP-PEMA-SurC/T20 A) containing 3 capture sequences per NP while addition of 100 nM of TCS-ATTO665 (12NA) in PB with 12 mM of MgCl_2 and 30mM NaCl and B) containing 1 capture sequence per NP while addition of 250 nM of TCS-ATTO665 containing 8 NA in PBS.

SUPPORTING INFORMATION

Supporting Tables

Table S1. Number of acceptors per nanoparticle and their FRET ratio A/(A+D) for PMMA-nanoprobes (PMMA-AspN3-1.6% polymer) with different acceptors.

TCS-Acceptor	Number per nanoparticle	Ratio A/(D+A)
Cy5 (650)	20	0.64
Alexa (650)	6.6	0.30
Oyster (650)	6.9	0.26
Cy5.5	33	0.67
DY651	9.7	0.48
DY654	4.7	0.20
DY676	6.1	0.31
ATTO647N	19	0.77
ATTO665	18	0.68
ATTO700	9.2	0.21

Table S2. Comparison of NPs made of PEMA-AspN3, PMMA-AspN3-5% or PMMA-AspN3-1.6% polymers with 30 wt% loading of RhB/F5-TPB.

NP, with loading of RhB/F5-TPB 30 %wt	Size by TEM, d. nm	Size by DLS, d. nm	QY ^[a] , %	Number of dyes per NP ^[b]	Average photon count rate per nanoparticle ^[c]
NP-PEMA-AspN3	18	17.2±0.5	54	401	3570
NP-PMMA-AspN3-5%	15	15.6±0.5	31	232	1350
NP-PMMA-AspN3-1.6%	28	30.8±1.1	38	1510	5650

[a] Rh101 in methanol was used as a standard. [b] Calculated from diameter of nanoparticle. [c] Average number of photons collected from single nanoparticle during 600 ms of acquisition time. Calculated average from ~200 NPs.

Table S3. Formulation of NP-PEMA-AspN3 with different loadings of RhB-C15/F5-TPB.

Loading, % wt	Size, d. nm	QY ^[a] , %	J, ^[b] M ⁻¹ cm ⁻¹ nm ⁴	R, ^[c] nm
20	16.6 ± 0.9	60.0	5.03E+15	6.82
30	17.9 ± 0.7	53.6	5.08E+15	6.69
50	18.6 ± 0.4	52.2	5.00E+15	6.65
70	18.9 ± 0.4	49.3	4.99E+15	6.58
85	22.1 ± 1.3	39.4	4.90E+15	6.32
100	25.9 ± 0.7	39.8	5.02E+15	6.34

[a] As a standard, Rh101 in methanol was used. [b] J is an overlap integral, calculated using the FluorTools software.^[1] [c] R is the Förster radius.

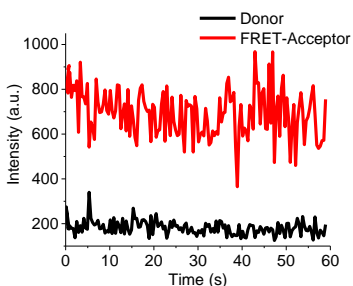
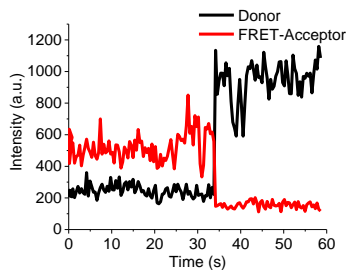
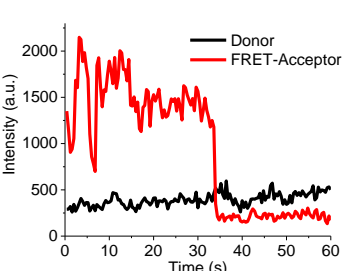
SUPPORTING INFORMATION

Table S4. Composition, light-harvesting and spectroscopic properties of PEMA-nanoprobes prepared with a single acceptor. ^[a]

Preparation	Ratio A/D from Absorbance	Acceptors per NP	Antenna effect	Ratio A/(D+A) from Fluorescence	QY ^[b] , %	FRET efficiency, %
1	558	1.76	193	0.480	43	51
2	573	1.71	220	0.486	47	48
3	548	1.79	190	0.536	53	47
4	567	1.73	225	0.484	38	53
5	584	1.68	214	0.501	52	58
Average, STD	566 ± 14	1.73 ± 0.04	209±16	0.497±0.023	46±6	51±4

[a] For Acceptors per NP calculation, the 980 Donors in NP with a size of 20 nm was used. [b] As a standard, Rh101 in methanol was used.

Table S5. Behavior of PEMA-nanoprobes at the single-particle level. ^[a]

Observation		Size by DLS, d. nm	Percentage ^[b]	
Photobleaching of acceptor was not observed			52±6%	
Single step photobleaching	with turn on of the donor emission		67±7%	
	without turn on of the donor emission		48±5%	33±4%

[a] Analysed 3 independent preparations. Statistics from at least 500 nanoparticle per image. [b] Obtained results demonstrates that at least 61±4% contain an acceptor and at least 48% of all FRET NPs contain single acceptor (demonstrates bleaching step).

References

- [1] <http://www.fluortools.com/software/ae>.
- [2] J. J. Schmied, M. Raab, C. Forthmann, E. Pibiri, B. Wunsch, T. Dammeyer, P. Tinnefeld, *Nat. Protoc.* 2014, 9, 1367.
- [3] A. Reisch, P. Didier, L. Richert, S. Oncul, Y. Arntz, Y. Mely, A. S. Klymchenko, *Nat. Commun.* 2014, 5, 4089.
- [4] N. Melnychuk, A. S. Klymchenko, *J. Am. Chem. Soc.* 2018, 140, 10856.
- [5] V. Rosiuk, A. Runser, A. Klymchenko, A. Reisch, *Langmuir* 2019, 35, 7009.

PART 3. CONCLUSIONS AND PERSPECTIVES

The objective of my PhD thesis was to develop an approach for the functionalization of polymeric dye-loaded nanoparticles with oligonucleotides and apply them for amplified detection of nucleic acids.

In the first part of my work, we investigated two principle approaches that lead to surface functionalization of the dye-loaded polymer nanoparticles: pre-functionalization of polymer with a ligand prior to nanoparticle formulation and post-functionalization of nanoparticles surface after nanoparticles are formed. To attach covalently ligand to the polymer, the polymers with azide groups were synthesized based on commercial PMMA-MA and hydrophilic Sulfo-Cy5(DBCO) was used as a ligand, which acted as a FRET-acceptor, while nanoparticle was a FRET-donor. Copper-free click reaction was performed in both cases of coupling the polymers and a Sulfo-Cy5(DBCO) in organic solvent and coupling the nanoparticles and a Sulfo-Cy5(DBCO) in a buffer. Obtained results demonstrated that the presence of a charged group between the polymer chain and an azide group is absolutely necessary to expose the functional azide group or fluorescent ligand at the nanoparticle surface during the nanoprecipitation. Moreover, different number of charged groups per azide is necessary for each of these two approaches. Indeed, one charged group is favorable for the post-functionalization, because the reactivity of these nanoparticles with DBCO-bearing ligand is higher. On the other hand, three charged groups are required to completely pull out the fluorescent ligand during the nanoprecipitation in the pre-functionalization approach. Based on these results, the sensor of the reduction environment was developed, and its performance was demonstrated in cells. Finally, it was concluded, that due to the solubility issues the only way to attach oligonucleotides to dye-loaded polymer nanoparticle is the post-functionalization approach where biomolecules are coupled with nanoparticles in a buffer.

In the second part of my work, we developed a nanoprobe based on light-harvesting nanoantenna for ultrasensitive detection of nucleic acids. As a target sequence for probe design, we chose a fragment encoding cancer marker survivin. In the nanoprobe design, nanoparticle is modified at the surface with capture oligonucleotide complementary to a nucleic acid target (SurC), which is hybridized with a short target-competitive sequence bearing FRET acceptor Cy5 (TCS-Cy5), so that acceptor is localized close to nanoparticles surface, which ensures good FRET efficiency. In the presence of the target nucleic acid, TCS-Cy5 is replaced and FRET is blocked. This way upon target nucleic acid detection nanoparticles changes its color from red to green. To fulfill the design, we developed a method for surface modification of dye-loaded polymer nanoparticles and obtained a nanoprobe with $\sim 23 \pm 3$ capture sequences per nanoparticle able to distinguish the hybridization of 3-5 TCS-Cy5 by producing clear detectable

change in dual emission of nanoprobe. As a result, we established the nanoprobe with amplification of nucleic acid detection, where a few molecular recognition events can control the emission of 3200 donor dyes inside the nanoantenna. Finally, we have demonstrated their capability for sequence-specific detection of nucleic acids targets in the presence of proteins and mixtures of non-specific nucleic acids in solution and on the glass surface at the single-particle level.

In the third part of my work, we aimed to reach the sensitivity of the nanoprobe to the level of single hybridization. To accomplish this, a number of improvements in the nanoprobe design were made. First, the acceptor with better photostability was absolutely needed. A screening of nanoprobe formulation was performed with 10 different dyes from 3 families: Cy, DY and ATTO with different polarities and emission wavelengths. We discovered that only positively or neutrally charged acceptors are suitable for nanoprobe formulation. Then we compared their photostability and found that dyes from ATTO family are far more photostable than initially used Cy5. ATTO665 was chosen due to its photostability and better spectral separation which is favorable for the ratiometric detection. Second, we designed functionalized nanoparticles of smaller size using a more hydrophobic polymer (PEMA-MA), which allowed us to obtain an improved brightness and photostability of donor nanoparticle. By formulation of nanoprobe using PEMA as a polymer matrix and ATTO665 as a FRET-acceptor, we obtained a system with a statistically single acceptor per NP. This newly designed nanoprobe exhibits extraordinary results: both high fluorescence quantum yield (46%) and high FRET efficiency (51%) through the distance beyond the Förster radius (6.4 nm vs 20 nm particle size). The presence of a single acceptor was confirmed by observation of the single-step switch on/off of acceptor/donor emission at the single-particle level. The amplification of acceptor emission (antenna effect) was 257 ± 40 at the single-particle level. This way, the redesigned nanoprobe showed capacity to detect a single hybridization event by switching on/off energy transfer from thousands of dyes inside the nanoantenna to a single acceptor at the excitation power equivalent to ambient sunlight. This has opened a new way for “digital” detection of oligonucleotide targets just by counting green/red nanoparticles at the single-particle level and lowered down the limit of detection down to a single hybridization event. The remaining limitation of this system is the kinetics of hybridization, which is slow at low target concentrations.

Finally, we demonstrated the direct imaging of a single hybridization event under the epifluorescence microscope. By adding TCS-ATTO665 during the imaging process we were able to follow a single hybridization event by a change in the color of nanoparticle from green to red, which was supported by a single step intensity trace. Moreover, by changing the length of TCS-ATTO665 from 12 to 8 nucleic acids we were able to distinguish irreversible and reversible binding. In the first case the hybridization was followed by acceptor bleaching, so the acceptor

emission was longer observed, while in the second case we observed multiple short acceptor emission spikes, corresponding to reversible single hybridization events.

During the three years of my work, I reached the aims of my thesis. We have developed an approach for the functionalization of dye-loaded polymeric nanoparticles with oligonucleotides and established a platform for amplified detection of nucleic acids. Moreover, such unprecedented properties of nanoprobe allowed us to follow single hybridization events comparable to ambient sunlight excitation conditions.

The important remaining problem of the developed detection assay is the slow hybridization kinetics at ultralow concentrations of both target nucleic acids and nanoprobe, which controls the limit of detection. Therefore, the detection assay should be improved to address this problem. Also, an approach of the synthesis and purification of nanoprobe bearing a single capture sequence is an important challenge to be addressed. Indeed, the elimination of nanoparticles without acceptor will improve the homogeneity of a nanoprobe signal at the single-particle level.

The further step of this project is a validation of assays for the detection of biologically relevant targets, like messenger RNA and microRNA in biological samples, such as cell lysates, fixed and live cells. New nanoprobe should be designed for important nucleic acids cancer markers. Moreover, nanoprobe of different colors should be developed, which will open a possibility of multiplex detection of RNA and DNA targets simultaneously.

The developed surface chemistry could be also applied for attachment of proteins (antibodies) to the surface of dye-loaded polymer nanoparticles. This would create new hybrid materials that are of interest in targeted bioimaging and biosensing.

The ultimate goal of this research is the development of the kits for rapid and effective point-of-care diagnostics of cancer and other diseases.

PART 4. MATERIALS AND METHODS

4.1 Materials

All starting materials and solvents for chemical synthesis were purchased from Alfa Aesar, SigmaAldrich, Iris Biotech, Lumiprobe or TCI Europe and used as received. BSA-biotin, deoxyribonucleic acid sodium salt from calf thymus (Type I, fibers), Albumin bovine serum (Fraction V, minimum 96%, lyophilized powder), Amicon Centrifugal filters (0.5mL, 100K) were purchased from Sigma-Aldrich. Neutravidin, LabTek chambers (Borosilicate cover glass, eight wells), QD605 Streptavidin Conjugate, RNAsecure™ RNase Inactivation Reagent (Invitrogen), OptiMEM (Gibco®) and FBS (Gibco®) were purchased from ThermoFisher Scientific. Illustra NAP Columns (prepacked with Sephadex G-25 DNA Grade) and PD10 desalting columns (prepacked with Sephadex G-25) were purchased from GE Healthcare. Human Serum was purchased from the hospital and supernatant was stored at -20 °C.

Sodium phosphate monobasic (>99.0%, Sigma-Aldrich) and sodium phosphate dibasic dihydrate (>99.0%, Sigma- Aldrich) were used to prepare 20 mM phosphate buffers. Sodium tetraborate decahydrate (>99.0%, Sigma- Aldrich) was used to prepare borate buffer at and pH was adjusted with 0.1M hydrochloride acid. For saline buffer sodium chloride (≥99%, Sigma Aldrich) 30 mM and magnesium chloride (≥98%, Sigma Aldrich) 12 mM was added to 20 mM phosphate buffer and pH was adjusted with sodium hydroxide 1N solution. Milli-Q water (Millipore) was used in all experiments. For immobilization protocol PBS (without Ca²⁺ and Mg²⁺) was purchased from Lonza.

Nucleic acids sequences:

Lyophilized single-strand DNA and RNA sequences were purchased from IBA GmbH, dissolved in Milli-Q water, aliquoted and stored at -20 °C for further experiments. The oligonucleotide sequences used in this study are shown below.

DNA:

SurC-DBCO, 5'-CCC AGC CTT CCA GCT CCT TGA - (DBCO)-3';

T20-DBCO, 5'-TTT TTT TTT TTT TTT TTT TT-(DBCO)-3';

A20-Biotin, 5'-(BIO)-AAA AAA AAA AAA AAA AAA AA-3'

TCS-acceptor, 5'-(label)-TCA AGG AGC TGG-3'; As labels were used next dyes: Cy5, Alexa-647, Oyster-650, Cy5.5, DY651, DY654, DY676, ATTO647N, ATTO665, ATTO700.

8NA-TCS-ATTO665, 5'-(ATTO665)-TCA AGG AG.

Target-DNA, 5'-CAA GGA GCT GGA AGG CTG GG-3'; single mismatch, 5'-CAA GCA GCT GGA AGG CTG GG-3'; two mismatches, 5'-CAA GCA GCT GGA AGC CTG GG-3'; three mismatches, 5'-CAA GCA GCT CGA AGC CTG GG-3'.

RNA: Target-RNA, 5'-CAA GGA GCU GGA AGG CUG GG-3'.

4.2 Methods

Nanoparticle Preparation

Protocol for diluted NPs: 50 μL of the polymer solution in acetonitrile (1 mg mL^{-1} containing R18/F5-TPB at 20 or 30 wt% relative to the polymer) was added quickly using a micropipette to 450 μL of 20 mM phosphate buffer, pH 7.4 at 21 °C under shaking (Thermomixer comfort, Eppendorf, 1100 rpm). The particle solution was then quickly diluted 5-fold with the same buffer.

Protocol for concentrated NPs: 100 μL of the polymer solution in acetonitrile (2 mg mL^{-1} with 30 wt% R18/F5-TPB relative to the polymer) were then added quickly using a micropipette to 900 μL the same buffer under shaking with Thermomixer (1,100 rpm). Then, the residues of acetonitrile were evaporated.

Protocol for concentrated NPs, obtained by nanoprecipitation at pH9: 50 μL of the polymer solution in acetonitrile (2 mg mL^{-1} containing R18/F5-TPB at 20, 30, 50, 70 or 100 wt% relative to the polymer) was added quickly using a micropipette to 450 μL of 10 mM borate buffer, pH 9 at 21 °C under shaking (Thermomixer comfort, Eppendorf, 1100 rpm). While continues mixing 500 μL of 20 mM phosphate buffer, pH 6 was added. Then, the residues of acetonitrile were evaporated. The particle solution was then 2-fold diluted with the 20mM of phosphate buffer, pH 7.4.

Protocol for reaction and purification of NPs with Sulfo-Cy5(DBCO)

An aliquot of Sulfo-Cy5(DBCO) was added to the 1 mL of nanoparticles in 20mM phosphate buffer, pH 7.4 to reach the desired concentration. The mixture was incubated overnight in the dark at room temperature. The size-exclusion column (PD10 desalting columns prepacked with Sephadex G-25) was washed with 10 mL of 20 mM phosphate buffer and the reaction mixture was deposited on a column. Then NPs were eluted with 4 mL of buffer and colored fractions with volume 1 mL were collected. The concentration of nanoparticles was verified by absorbance spectra.

General protocol for nanoprobe synthesis

Aliquots of DNA were added to 200 μL or 300 μL of nanoparticles. The reaction was mixed and kept overnight at 40 °C in Thermomixer without shaking protected from light. Then the reaction was cooled down to room temperature. For annealing with TCS-target, the aliquot of TCS-target in ratio 1:1 with SurC-DBCO was added and the mixture was heated to 70 °C in a water bath for 3 min. To complete hybridization the reaction was cooled down to room temperature and kept in the dark for 2 h. Then the mixture was diluted with 20 mM phosphate buffer containing 12 mM MgCl_2 and 30 mM NaCl to 4 mL and purified by centrifugation using centrifuge filters (Amicon, 0.5ml, 100k) on 1000 g at 20 °C for 2 min. The procedure of

centrifugation was repeated 5 times to remove the non-reacted oligonucleotides. The obtained NP-probes in volume of 1 mL were kept in the dark at 4 °C.

Detection of survivin nucleic acid target

Detection in solution with the NP-Probe: the NP-Probe was diluted in 20 mM phosphate buffer containing 30 mM NaCl and 12 mM MgCl₂ to the desired concentration (corresponding to TCS-Cy5) and aliquot of target oligonucleotide was added. Before measurements, the mixture was incubated in the dark at 4 °C for 20h. For NA detection in different biological media, the PBS and OptiMEM were adjusted to 12 mM MgCl₂ concentrations and further used for sample preparations. BSA was diluted to 0.5 mg/mL concentration in PBS. The deoxyribonucleic acid sodium salt from calf thymus (CT-DNA) was dissolved to a concentration of 2 mg/mL in water and kept overnight at 4 °C for complete dissolution. Then, it was heated for 3 min at 90 °C followed by rapid transfer into an ice bath. For measurements, it was diluted to a concentration of 10 µg/mL in PBS. Fetal bovine serum (FBS) and Human Serum were heat-inactivated by exposing them for 30 min to 56 °C before they were used. After that, the FBS and Human Serum were diluted to 10% concentration in OptiMEM. For measurements in solution the NP-Probe was diluted in the corresponding media and the target oligonucleotide was added. Before the measurements were made, the mixtures of NP-Probe with and without target oligonucleotide were incubated in the dark at 4 °C for a given time.

Detection in solution with PEMA-nanoprobe: the PEMA-nanoprobe was diluted in 20 mM phosphate buffer containing 30 mM NaCl and 12 mM MgCl₂ (in case of RNA-target the buffer additional contained 1x RNA-secure) to a desired concentration (corresponding to TCS-ATTO665) and aliquot of target oligonucleotide was added. The mixture (200 µL) was kept at 20°C in Thermomixer without shaking protected from light. Before measurements, the mixture was 3-fold diluted with the same buffer.

Detection on surfaces with the NP-Probe: 300 µL of the buffer or media was mixed with an aliquot of the target oligonucleotide and then the mixture was added to the LabTek chamber with immobilized NP-Probes (for preparation, see below). The mixture was kept in the dark at room temperature for 1 and 4 h incubation or at 4 °C for 20h incubation before measurements.

Detection on surfaces with the PEMA-nanoprobe: 300 µL of the buffer was mixed with an aliquot of the target oligonucleotide and then the mixture was added to the LabTek chamber with immobilized nanoprobe (for preparation, see below). The mixture was kept in the dark at room temperature for 6 h incubation before measurements. In case of detection by imaging of the same area of nanoparticles, first the PEMA-nanoprobe was imaged with 200µL of the same buffer (in case of RNA the buffer contained 1x RNA-secure) and then 200µL of nucleic acid target were added in order to obtain 100 pM final concentration. After 1 hour of incubation at the room temperature the same zone of nanoparticle were imaged.

Molecular Probe Preparation

To 120 μL of 20 mM phosphate buffer containing 50 mM NaCl and 1 mM of EDTA was added 30 μL of SurC-DBCO (400 μM stock in water) and 50 μL of Sulfo-Cyanine3 azide (2 mM stock in water). The mixture was left overnight under shaking (Thermomixer comfort, Eppendorf, 400 rpm) at room temperature. Then, the mixture was purified using disposable columns pre-packed with Sephadex G-25 DNA Grade (Illustra NAP Columns, GE Healthcare) and 20 mM phosphate buffer as eluent. The fractions were collected in 50 μL volumes and the conjugate formation was verified by absorption and fluorescence emission spectra. The 10 μM of the conjugate was further mixed with 10 μM of TCS-Cy5 and the mixture was heated for 70 $^{\circ}\text{C}$ in a water bath for 3 mins. Finally, it was cooled down to room temperature and kept in the dark for 2 hours before the experiments.

Nanoparticle characterization

Dynamic light scattering (DLS) measurements were performed on a Zetasizer Nano series DTS 1060 (Malvern Instruments S.A.). The Zetasizer software provided with standard cumulates and size distribution by volume analysis was used to characterize nanoparticles by DLS. For the data analysis, the following parameters were used: for the solvent (water) – temperature 25 $^{\circ}\text{C}$, refractive index RI 1.33, and viscosity 0.8872 cP. Nanoparticles were assumed to be all homogenous and spherical in shape. Absorption spectra were recorded on a Cary 4000 scan UV-visible spectrophotometer (Varian), excitation and emission spectra were recorded on a FluoroMax-4 spectrofluorometer (Horiba Jobin Yvon) and FS5 Spectrofluorometer (Edinburg Instruments). For standard recording of fluorescence spectra, the excitation wavelength was set to 530 nm. The fluorescence spectra were corrected for detector response and lamp fluctuations. Measurements of fluorescence anisotropy was performed at 20 $^{\circ}\text{C}$ with a Fluorolog spectrofluorometer (Horiba Jobin Yvon). To measure the anisotropy value of Cy5 the excitation wavelength was 640 nm and the emission wavelength was 665 nm. Quantum yields of donor dye in NPs were calculated using Rhodamine 101 in methanol as a reference (QY = 1.0) with an absorbance of 0.01 at 530 nm. QY of the acceptor was measured using DiD in methanol (QY = 0.33) as a reference. To calculate FRET efficiency based on fluorescence spectra, a classical equation was used: $E_{\text{FRET}} = 1 - \frac{I_{D-A}}{I_D}$, where I_D is the donor maximum intensity and I_{D-A} is the maximum intensity of the donor in the presence of the acceptor. The overlap integral $J(\lambda)$ was calculated using the FluorTools software.¹⁶⁰ The Förster distance was calculated by:

$$R_0 = 0.211 \left[\frac{k^2 Q_D J(\lambda)}{n^4} \right]^{1/6}$$

Amplification factor of the acceptor emission (antenna effect, AE) was expressed as the ratio of the maximal excitation intensity of the donor to that of the acceptor with a correction from the emission of the donor dyes at 690 nm for CY5 and 700 nm for ATTO665:

$$AE = \frac{I_{D-FRET}^{ex} - I_D^{ex} * \frac{I_{D-FRET}^{em}}{I_D^{em}}}{I_{A-FRET}^{ex} - I_A^{ex}}$$

Where I_{D-FRET}^{ex} and I_{A-FRET}^{ex} are the maximal excitation intensities of donor and acceptor in nanoprobe, respectively; I_D^{ex} and I_A^{ex} are the excitation intensities at the wavelengths of excitation maximum of donor and acceptor in nanoprobe-SurC-T20; I_{D-FRET}^{em} and I_D^{em} maximum emission intensity of donor for nanoprobe and nanoprobe-SurC-T20, respectively.

Photobleaching of nanoparticles in solution

For photobleaching experiments were acquired on a home-build setup. The cuvette holder (CHV100) with SMA905 Fiber Adapter was purchased from ThorLab. For sample excitation, we used the module of a 532 nm diode laser (Oxxius) guided through the fiber optics and passed through optical beam expander (BE50M, ThorLabs). The cuvette height was adjusted so that the sample volume of 100 μ L was fully irradiated. The get rid of laser radiation at 532, the single Noch filter 532 nm (Chroma) was installed. For the fluorescence signal detection, OceanOptics QE Pro modular spectrometer was used. The fluorescence signal was further processed by an OceanView Software.

Transmission electron microscopy (TEM)

Carbon-coated copper-rhodium electron microscopy grids with a 300 mesh (Euromedex, France) were surface treated with a glow discharge in amylamine atmosphere (0.45 mbar, 4 – 4.5 mA, 22 s) in an Elmo glow discharge system (Cordouan Technologies, France). Then, 5 μ L of the solution of NPs at 0.04 g/L were deposited onto the grids and left for 2 min. The grids were then treated for 1 min with a 2% uranyl acetate solution for staining. They were observed with a Philips CM120 transmission electron microscope equipped with a LaB6 filament and operating at 100 kV. Areas covered with nanoparticles of interest were recorded at different magnifications on a Peltier cooled CCD camera (Model 794, Gatan, Pleasanton, CA). Image analysis was performed using the Fiji software.

Fluorescence Microscopy

Immobilization protocol for non-functionalized nanoparticles. The 300 μ L of 1M KOH aqueous solution was added to the LabTek chamber. After 20 mins the chamber was washed 3 times with ~300 μ L of MQ-water. Then 200 μ L of 1 mg/mL PEI solution in TRIS buffer pH 7.4 was added. After 20 mins the chamber was washed with 300 μ L of MQ-water and left with 300 μ L of MQ-water for 15 mins. Then the chamber was washed 2 times with 300 μ L of MQ-water and 2

times with 300 μL of 20 mM phosphate buffer. The 250 μL of nanoparticle solution with proper concentration to achieve the desired density was deposited on the plate and left for 20 mins. Then the chamber was rinsed 3 times with 20 mM phosphate buffer and measurements were performed with a layer of the same buffer ($\sim 300\mu\text{L}$) above the surface.

Immobilization protocol for DNA-functionalized nanoparticles and QD605. Immobilization in LabTek chamber was performed according to previously described protocol.¹⁵⁹ The LabTek chamber was washed 3 times with PBS followed by incubation with 200 μL of BSA-Biotin (0.5 mg mL^{-1} in PBS) for 5 min. Then, BSA-biotin solution was removed, and the chamber was washed 3 times with 500 μL of PBS. In case of nanoparticles immobilization, the chamber was incubated with 200 μL of neutravidin solution (0.5 mg mL^{-1} in PBS) for 5 min and washed 3 times with 500 μL of PBS. Then the chamber was incubated with 200 μL of 1 μM solution of A20-biotin in PBS for 5 min and washed 1 time with PBS and 2 times with 20 mM phosphate buffer containing 12 mM MgCl_2 and NaCl 30mM. Then, the nanoprobe solution was deposited with proper concentration to achieve the desired density and incubated for 1 hour at room temperature in the dark. Before measurements, the chamber was washed 2 times with 20 mM phosphate buffer containing 12 mM MgCl_2 and 30 mM NaCl and covered with 200 μL of the same buffer. In case of QD605 immobilization, QD605 Streptavidin Conjugate (ThermoFisher Scientific) was diluted to 100 pM concentration in PBS and 300 μL was added to the chamber. After 1 h of incubation, the chamber was washed 3 times with 500 μL of PBS and filled with 200 μL of PBS.

Single-particle measurements were performed in the epi-fluorescence mode using Nikon Ti-E inverted microscope with a 100x objective (Apo TIRF, oil, NA 1.49, Nikon) and a CFI Plan Apo 60x oil (NA = 1.4) objective. The excitation was provided by light-emitting diodes (SpectraX, Lumencor) at 550 and a 640 nm.

In case of NP-Probe, PEMA-AspN3 and PMMA-AspN3, the power density used at 550 nm was 0.4 W cm^{-2} . In case of PEMA-nanoprobe to 0.24 W cm^{-2} (100x objective) and 0.036 W cm^{-2} (60x objective). For direct excitation of acceptor Cy5 in case of NP-Probe, the 640-nm light was used with a power density of 20 W cm^{-2} . For direct excitation of acceptor ATTO665 in case of PEMA-nanoprobe, the 640-nm light was used with a power density of 27.62 W cm^{-2} . Also, direct excitation of ATTO665 was done in a TIRF (Total Internal Reflection Fluorescence) setup using a 642 nm diode laser (Oxxius) with power density set to 24.69 W cm^{-2} .

The fluorescence signal was recorded with a Hamamatsu Orca Flash 4 camera. The exposure time was set to 200 ms (NP-Probe) or 400 ms (PEMA-nanoprobe) per image frame. In case of two-color image detection, corresponding to Donor (R18/F5-TPB) and Acceptor (Cy5 or ATTO665) signals, W-VIEW GEMINI image splitting system (Hamamatsu) was used with dichroic 640 nm (Semrock FF640-FDi01-25x36).

A comparison of single-particle brightness of our NPs vs QD605 was done using the same experimental setup. In case of NP-Probe, the excitation of nanoantenna particles was done using 550-nm light with a power density of 0.56 W cm^{-2} , whereas QD605 were excited by 470-nm light with a power density of 14 W cm^{-2} . In case of PEMA-nanoprobe, excitation of nanoantenna particles and QD605 were done using 550-nm light with a power density of 0.24 W cm^{-2} and 15.35 W cm^{-2} correspondently.

The detection of the nucleic acid target via illumination of the same area of PEMA-nanoprobes before and after 1 hour of incubation with a target was done using the same experimental setup with 60x objective using 550-nm light with power density of 0.036 W cm^{-2} . The images were made with the exposure time of 1 s.

Single-particle analysis was performed using the Fiji software. Particle locations were detected through a Fiji routine applied to a projection (maximum intensity) of all obtained frames per experiment. After the automatic background subtraction, the mean intensities of circular regions of interest with a diameter of 8 pixels around the found particle locations were then measured. In order to calculate the FRET response $A/(A+D)$ average of intensity of NPs was obtained base on the first 3 frames for each channel. At least three image sequences (245 pixel \times 245 pixel) per condition were analyzed with, on average, 500-1000 particles per sample.

The fluorescence intensity in photons (P – input photon) was calculated for sCMOS camera as:

$$P = \frac{CF \times (I_{output} - I_{dark})}{\frac{Q(\lambda)}{100}}$$

where CF is the conversion factor (according to manufactures CF=0.48), I_{output} and I_{dark} are the output signal with and without illumination, respectively. $Q(\lambda)$ is a conversion efficiency of photons to electrons in % (provided by manufactures). To calculate the total emitted photons per NP-acceptor, value $(I_{output} - I_{dark})$ collected on acceptor channel was integrated over the on-time (time before photobleaching), which gave the total detected photons before the photobleaching.

The amplification factor of the acceptor emission at the single-particle level was determined using:

$$AF = \frac{I_A^{550nm}}{I_A^{640nm}} \times \frac{p^{640nm}}{p^{550nm}}$$

Where I_A^{550nm} and I_A^{640nm} are mean intensities of acceptors under excitation at 550 and 640 nm, respectively, and p^{640nm} and p^{550nm} are laser powers at corresponding wavelengths. The amplification factor indicates how many folds the emission increases when the dye is excited via nanoantenna vs direct dye excitation.

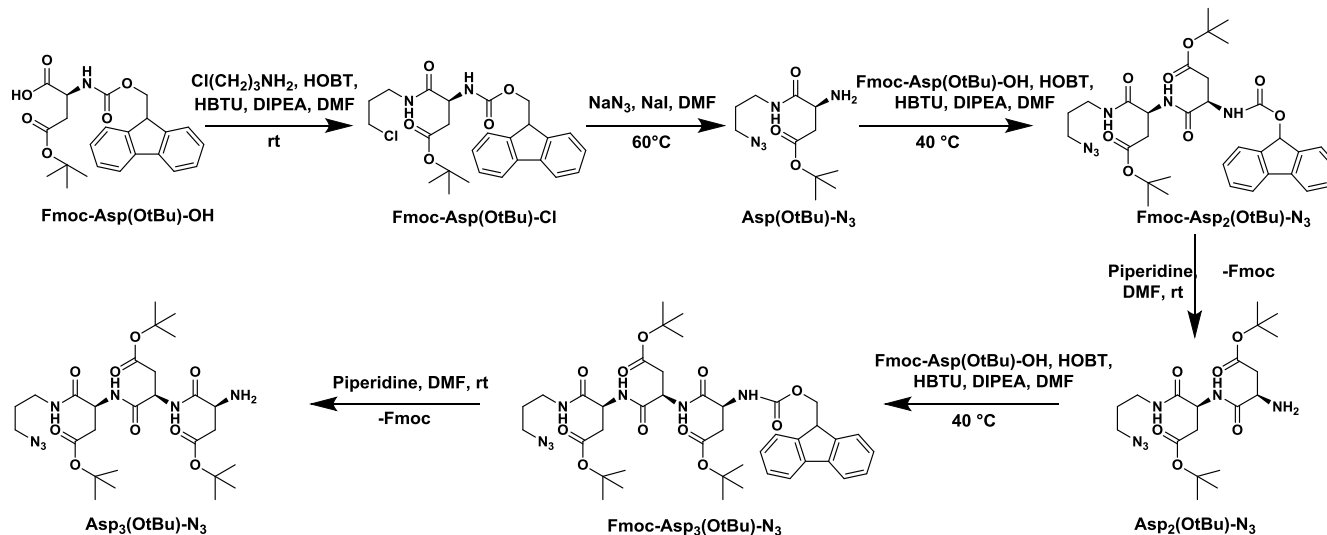
Cellular experiments

HeLa cells (ATCC[®] CCL-2) were grown in Dulbecco's modified Eagle's medium (DMEM, Gibco-Invitrogen), supplemented with 10% fetal bovine serum (FBS, Lonza) and 1% antibiotic solution (penicillin–streptomycin, Gibco-Invitrogen), at 37°C in a humidified atmosphere containing 5% CO₂. Cells were seeded onto a chambered coverglass (IBiDi) at a density of 5×10^4 cells per well 24 h before the microscopy measurement. For imaging, the culture medium was removed and the attached cells were washed with Opti-MEM (Gibco-Invitrogen). Next, freshly prepared FRET NPs (loaded with 20 wt% of donor and 120 eq. of acceptor) were diluted 30 times in Opti-MEM and incubated for 20 mins at room temperature and for 3 h at 37°C. Before imaging, cells were washed with Opti-MEM. Imaging was performed in the epi-fluorescence mode using Nikon Ti-E inverted microscope with a CFI Plan Apo 60x oil (NA = 1.4) objective. The excitation was provided by diode laser (Oxxius) at 532 nm. The fluorescence signal was recorded with a Hamamatsu Orca Flash 4 camera. The exposure time was set to 100 ms per image frame. For two-color image detection, corresponding to Donor (R18/F5-TPB) and Acceptor (Cy5) signals, W-VIEW GEMINI image splitting system (Hamamatsu) was used with dichroic 640 nm (Semrock FF640-FDi01-25x36). Image analysis was performed using Fiji software.

4.3 Chemical synthesis

NMR spectra were recorded at 20°C on Bruker Avance III 400MHz spectrometer and chemical shifts were reported as delta scale in ppm relative to CHCl₃ ($\delta = 7.26$ ppm) for ¹H NMR and CDCl₃ ($\delta = 77.16$ ppm) for ¹³C NMR. Mass spectra were obtained using an Agilent Q-TOF 6520 mass spectrometer.

Synthesis of linkers



Tert-butyl 3-[(3-chloropropyl) carbamoyl]-3-[[[(9H-fluoren-9-ylmethoxy)carbonyl]amino] propanoate (Fmoc-Asp(OtBu)-Cl) – Fmoc-Asp(OtBu)-OH (1 eq, 6 mmol, 2.47 g), HBTU (1.2 eq, 7.2 mmol, 2.73 g) and HOBt (1.3 eq, 7.8 mmol, 1.05 g) were dissolved in 30 mL of anhydrous N,N-dimethylformamide. After complete dissolution the N,N-diisopropylethylamine (3 eq, 18 mmol, 2.97 mL) was added to the stirring mixture under argon at room temperature and after 15 min 3-chloropropanamine hydrochloride (1 eq, 6 mmol, 0.78 g) was added. The reaction was stirred for 24 h and completion of the reaction was checked by TLC (DCM/MeOH: 98/2). The solvent was evaporated under reduced pressure, the residue was diluted with water and precipitate was collected. The crude product was washed with solution of citric acid, followed by solution of sodium bicarbonate. After the crude product was purified by column chromatography (DCM/MeOH 98/2), the product was obtained as pale-yellow solid (2.3 g, 80% yield). ¹H NMR (400 MHz, CDCl₃) δ, ppm: 1.46 (s, 9 H), 1.98 (quin, 2 H), 2.60 (dd, 1 H), 2.95 (br d, 1 H), 3.45 (m, 2 H), 3.56 (br t, 2 H), 4.23 (m, 1 H), 4.36 - 4.60 (m, 3 H), 5.93 (br s, 1 H), 6.59 (br s, 1 H), 7.27 - 7.36 (m, 2 H), 7.42 (t, 2 H), 7.60 (d, 2 H), 7.78 (d, 2 H). ¹³C NMR (101 MHz, CDCl₃) δ, ppm: 28.00, 31.92, 37.07, 37.35, 42.16, 47.13, 51.12, 67.07, 81.88, 120.01, 124.93, 127.01, 127.05, 127.74, 141.28, 143.58, 143.63, 156.02, 170.71, 171.20. . HR/LC/MS for C₂₆H₃₁ClN₂O₅ m/z (M+) calc 487.19943, found 487.19706.

Tert-butyl 3-amino-4-((3-azidopropyl)amino)-4-oxobutanoate Asp(OtBu)-N3 – Fmoc-Asp(OtBu)-Cl (1 eq, 3 mmol, 1.5 g), sodium azide (5 eq, 15.4 mmol, 1 g) and sodium iodide (1 eq, 3 mmol, 0.47 g) were dissolved in anhydrous N,N-dimethylformamide (20 mL) and stirred under Ar overnight at 60 °C. Then, the solvent was evaporated, the residue was extracted with water/DCM and washed twice with brine. The crude product was purified by column chromatography (DCM/MeOH 94/6). By LCMS and NMR was observed Fmoc deprotected Asp(OtBu)-N3 as pale-yellow oil (460 mg, 55% yield). ¹H NMR (400 MHz, CDCl₃) δ, ppm: 1.46 (s, 9 H), 1.65 (m, 2 H), 1.81 (quin, 2 H) 2.57 (dd, 1 H) 2.8 - 2.85 (m, 1 H) 3.29 - 3.44 (m, 4 H) 3.63 (dd, 1 H), 7.57 (br s, 1 H). ¹³C NMR (101 MHz, CDCl₃) δ ppm 28.08, 28.89, 36.65, 40.52, 49.20, 52.02, 81.15, 171.24, 173.71. HR/LC/MS for C₁₁H₂₁N₅O₃ m/z (M+) calc 272.17226, found 272.17153.

tert-butyl 3-(((9H-fluoren-9-yl)oxy)carbonyl)amino)-4-((-1-((3-azidopropyl)amino)-4-(tert-butoxy)-1,4-dioxobutan-2-yl)amino)-4-oxobutanoate (Fmoc-Asp2(OtBu)-N3) – Fmoc-Asp(OtBu)-OH (1 eq, 1.07 mmol, 440 mg), HBTU (1.3 eq, 1.39 mmol, 528 mg) and HOBt (1.5 eq, 1.6 mmol, 217 mg) were dissolved in DMF (15 mL). Then DIPEA (2 eq, 2.14 mmol, 0.35 mL) was added and the mixture was stirred for 15 min. Then Asp(OtBu)-N3 (1.2 eq, 1.28 mmol, 350 mg) was added. The reaction was stirred for 24 h at room temperature. Then solvent was evaporated and the product was extracted with water/DCM, washed with brine. The crude product was purified by column chromatography (DCM/MeOH: 97/3). The product was obtained

as pale-yellow oil (530mg 74% yield). ^1H NMR (400 MHz, CDCl_3) δ , ppm: 1.41 - 1.49 (m, 18 H), 1.76 - 1.83 (m, 2 H), 2.54 (dd, 1 H), 2.70 - 2.92 (m, 2 H), 3.06 (br s, 1 H), 3.32 (tt, 4 H), 4.12 - 4.34 (m, 1 H), 4.43 (br d, 3 H), 4.58 - 4.77 (m, 1 H), 5.77 (br d, 1 H), 7.09 (br s, 1 H), 7.26 - 7.37 (m, 2 H), 7.38 - 7.45 (m, 2 H), 7.52 (br s, 1 H), 7.60 (br d, 2 H), 7.78 (d, 2 H). ^{13}C NMR (101 MHz, CDCl_3) δ , ppm: 27.95, 28.05, 28.72, 36.29, 36.98, 37.38, 47.08, 48.93, 49.54, 51.98, 67.51, 81.92, 82.35, 120.06, 125.02, 127.16, 127.83, 141.33, 143.69, 156.15, 170.13, 170.35, 170.91, 171.53. HR/LC/MS for $\text{C}_{33}\text{H}_{44}\text{N}_6\text{O}_8$ m/z (M^+) calc 664.32206, found 664.32152.

Tert-butyl 3-amino-4-((-1-((3-azidopropyl)amino)-4-(tert-butoxy)-1,4-dioxobutan-2-yl)amino)-4-oxobutanoate (Asp2(OtBu)-N3) – Fmoc-Asp2(OtBu)-N3 (0.45 mmol, 300 mg) was dissolved in DMF (7 mL) and piperidine (2 mL) was added. The reaction was mixed for 2 hours. Then, the solvent was evaporated, the product was extracted with water/DCM and washed twice with brine. The crude product was purified by column chromatography (DCM/MeOH: 92/8). The product was obtained as pale oil (180 mg, 90% yield). ^1H NMR (400 MHz, CDCl_3) δ , ppm: 1.45 (s, 18 H), 1.67 (br s, 2 H), 1.78 (quin, 2 H), 2.53 - 2.70 (m, 2 H), 2.82 (dd, 1 H), 2.95 (dd, 1 H), 3.24 - 3.42 (m, 4 H), 3.61 (t, 1 H), 4.58 - 4.76 (m, 1 H), 5.30 (s, 1 H), 6.96 (br s, 1 H), 8.12 (br s, 1 H). ^{13}C NMR (101 MHz, CDCl_3) δ , ppm: 28.04, 28.08, 28.73, 36.60, 36.98, 40.53, 49.05, 49.49, 52.20, 53.42, 81.47, 81.63, 170.55, 171.18, 171.20, 174.12. HR/LC/MS for $\text{C}_{19}\text{H}_{36}\text{N}_6\text{O}_6$ m/z (M^+) calc 442.25398, found 442.25347.

Tert-butyl 11-((3-azidopropyl)carbamoyl)-5,8-bis(2-(tert-butoxy)-2-oxoethyl)-1-(9H-fluoren-9-yl)-3,6,9-trioxo-2-oxa-4,7,10-triazatridecan-13-oate (Fmoc-Asp3(OtBu)-N3) – Fmoc-Asp(OtBu)-OH (1 eq, 0.27 mmol, 112 mg), HBTU (1.3eq, 0.35 mmol, 133 mg) and HOBT (1.5 eq, 0.4 mmol, 55 mg) were dissolved in DMF (7 mL), then DIPEA (2 eq, 0.54 mmol, 0.09mL) was added and the mixture was stirred for 15 min. Then Asp2(OtBu)-N3 (1 eq, 0.27 mmol, 120 mg) was added and the reaction was stirred for 24 h at room temperature under argon. Then DMF was evaporated and the product was extracted with water/DCM, washed twice with brine. The crude product was purified by column chromatography (DCM/MeOH: 97/3). The product was obtained as pale-yellow oil (203 mg, 90% yield). ^1H NMR (400 MHz, CDCl_3) δ , ppm: 1.41 - 1.48 (m, 27 H), 1.70 - 1.83 (m, 2 H), 2.63-2.92 (m, 6 H), 3.21 - 3.41 (m, 4 H), 4.25 (br t, 1 H), 4.44 (br d, 2 H), 4.47 - 4.56 (m, 1 H), 4.57 - 4.75 (m, 2 H), 5.89 (br s, 1 H) 7.03 (br s, 1 H) 7.31 - 7.37 (m, 2 H) 7.37 - 7.52 (m, 4 H) 7.60 (br d, 2 H) 7.78 (d, 2 H). ^{13}C NMR (101 MHz, CDCl_3) δ , ppm: 28.00, 28.05, 28.70, 36.31, 36.90, 47.09, 48.89, 49.83, 50.49, 51.60, 67.51, 81.64, 82.29, 120.06, 125.02, 127.13, 127.82, 141.33, 143.60, 143.70, 169.92, 170.19, 170.85, 170.99, 171.03, 171.19. HR/LC/MS for $\text{C}_{42}\text{H}_{57}\text{N}_7\text{O}_{11}$ m/z (M^+) calc 834.41161, found 834.41109.

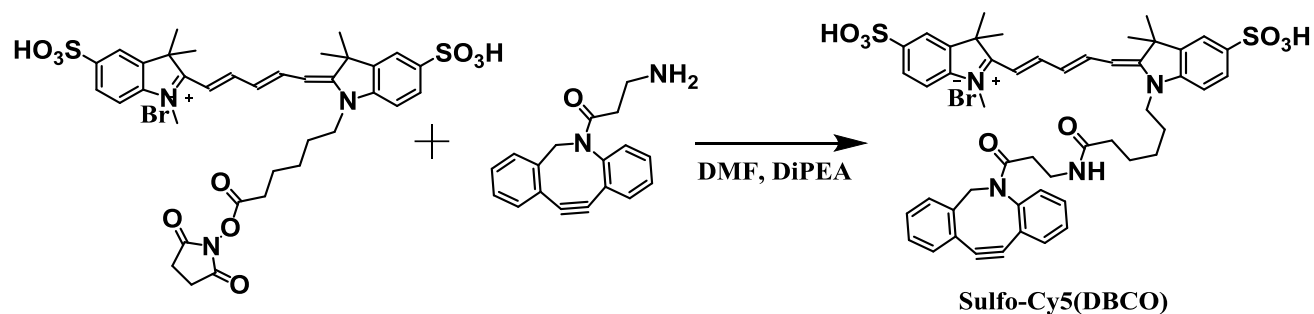
tert-butyl 3-amino-4-((-1-((-1-((3-azidopropyl)amino)-4-(tert-butoxy)-1,4-dioxobutan-2-yl)amino)-4-(tert-butoxy)-1,4-dioxobutan-2-yl)amino)-4-oxobutanoate (Asp3(OtBu)-N3) – Fmoc-Asp3(OtBu)-N3 (0.18 mmol, 150 mg) was dissolved in DMF (5 mL). Then piperidine (2

mL) was added and the reaction was mixed for 2 hours. The mixture was evaporated and the product was extracted with water/DCM, washed twice with brine. The crude product was purified by column chromatography (DCM/MeOH: 95/5). The product was obtained as pale oil (80mg, 73% yield). ^1H NMR (400 MHz, CDCl_3) δ , ppm: 1.41 - 1.47 (m, 27 H), 1.69 - 1.83 (m, 4 H), 2.53 - 2.64 (m, 2 H), 2.73 - 2.88 (m, 3 H), 3.03 (dd, 1 H), 3.19 - 3.41 (m, 4 H), 3.68 (br m, 1 H), 4.56 - 4.69 (m, 2 H), 7.09 (br s, 1 H), 7.52 (br s, 1 H), 8.25 (br s, 1 H). ^{13}C NMR (101 MHz, CDCl_3) δ , ppm: 28.02, 28.09, 28.69, 36.74, 36.90, 40.22, 48.90, 49.63, 50.32, 52.06, 81.44, 81.78, 82.02, 170.20, 170.43, 170.69, 170.93, 171.60, 174.53. HR/LC/MS for $\text{C}_{27}\text{H}_{47}\text{N}_7\text{O}_9$ m/z (M^+) calc 613.34353, found 613.34202.

Synthesis of dyes

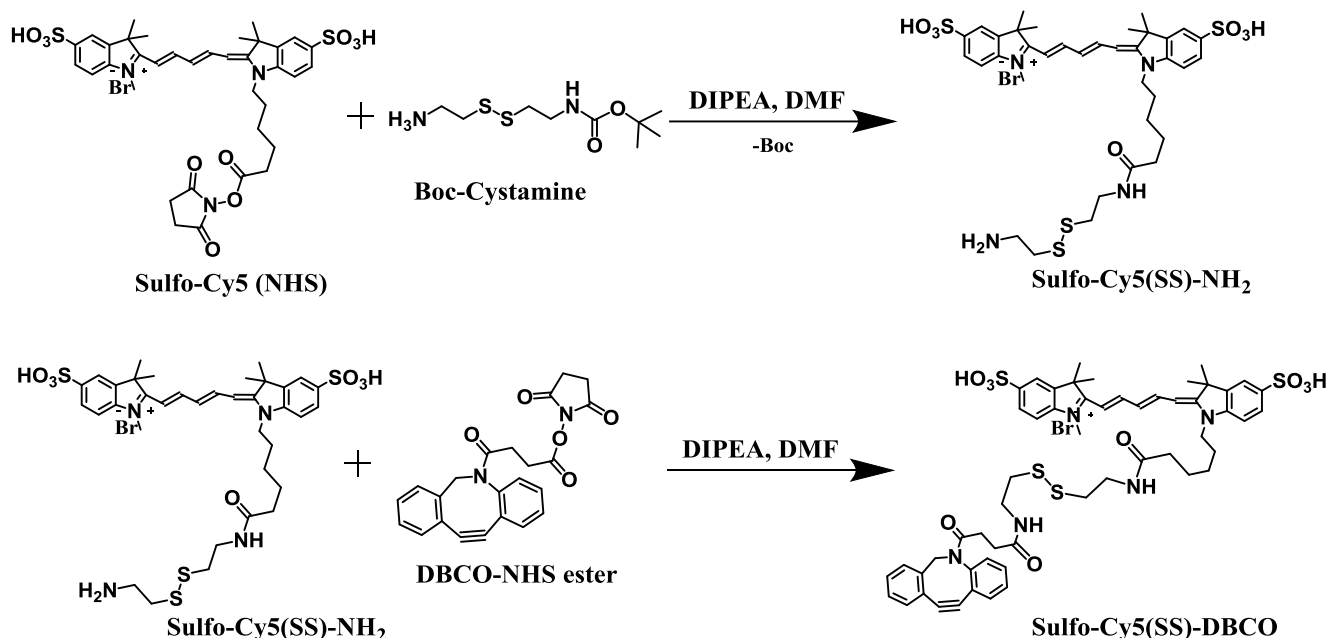
Rhodamine B octadecyl ester trakis(penta-fluorophenyl)borate (R18/F5-TPB) was synthesized by ion exchange and purified by column chromatography as described previously.³¹

Synthesis of the Sulfo-Cy5(DBCO).



Sulfo-Cy5-NHS ester (1 eq, 0.0055 mmol, 4.3 mg) and azadibenzocyclooctyne-amine (2 eq, 0.011 mmol, 3 mg) were dissolved in DMF (150 μL), then DIPEA (4 eq, 0.022 mmol, 3.7 μL) was added and the mixture was stirred overnight at room temperature. The solvent was evaporated. The product was extracted with water/DCM and washed twice with brine. The crude product was purified by preparative TLC (DCM/MeOH: 80/20). The product was obtained as dark blue solid – 3.3 mg, 64% yield. HPLC/MS for $\text{C}_{50}\text{H}_{53}\text{N}_4\text{O}_8\text{S}_2$ m/z (M^+) calc 901.329, found 901.210.

Synthesis of the Sulfo-Cy5(SS)DBCO.



Sulfo-Cy5(SS)-NH₂. To a solution of Sulfo-Cy5(NHS) (1 eq, 6.4 μ mol, 5 mg) in anhydrous N,N-dimethylformamide (0.25 mL) was added diisopropylethylamine (4 eq, 25.71 μ mol, 4.25 μ L) and Boc-Cystamine (1.8 eq, 11.57 μ mol, 2.92 mg) and stirred at room temperature for 12 h. The solvents were evaporated under reduced pressure and the crude product was purified by using preparative silica gel TLC (CH₂Cl₂/MeOH: 7/3). The obtained product from the preparative TLC was found to be Boc deprotected probably due to the acidic condition rendered by silica gel at higher methanol content. Yield: 3.51 mg, 67%. ¹H NMR (400 MHz, MeOD) δ , ppm: 8.31 (br t, 2H), 7.89 (s, 4H), 7.32 (t, 2H), 6.68 (t, 1H), 6.33 (d, 2H), 4.14 (br t, 2H), 3.65 (s, 3H), 3.42 (t, 2H), 3.12 (t, 2H), 2.86 (t, 2H), 2.72 (t, 2H), 2.19 (t, 2H), 1.84 (br s, 2H), 1.76 (s, 12H), 1.69 (t, 2H), 1.60 (br s, 2H). HRMS (ESI): calcd for C₃₆H₄₇N₄O₇S₄ (M-1) 775.2328, found: 775.2334.

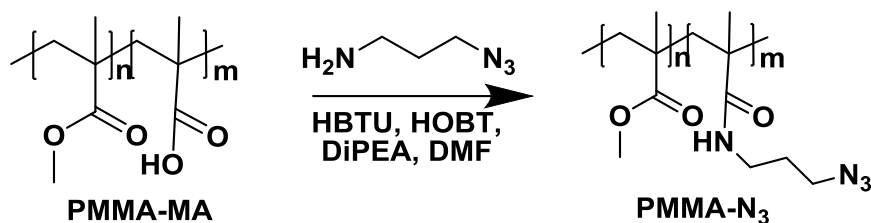
Sulfo-Cy5(SS)-DBCO. To a solution of Sulfo-Cy5(SS)-NH₂ (1 eq, 2.45 μ mol, 2.0 mg) in anhydrous N,N-dimethylformamide (120 μ L) was added diisopropylethylamine (6 eq, 14.72 μ mol, 2.4 μ L) and DBCO-NHS ester (1.8 eq, 4.42 μ mol, 1.78 mg) and stirred for 16 h at room temperature. The solvents were evaporated under reduced pressure and the crude product was purified by using preparative silica gel TLC (CH₂Cl₂/MeOH: 8/2) to obtain pure Sulfo-Cy5(SS)-DBCO (1.57 mg, 58% yield). HRMS (ESI): calcd for C₅₅H₆₀N₅O₉S₄ (M) 1062.3274, found: 1062.3263.

Synthesis of polymers

Poly (methyl methacrylate-co-methacrylic acid) (PMMA-MA), 5% methacrylic acid and Poly (ethyl methacrylate-co-methacrylic acid) (PEMA-MA), 5% methacrylic acid were synthesized through free radical polymerization and purified via reprecipitation in methanol/water as

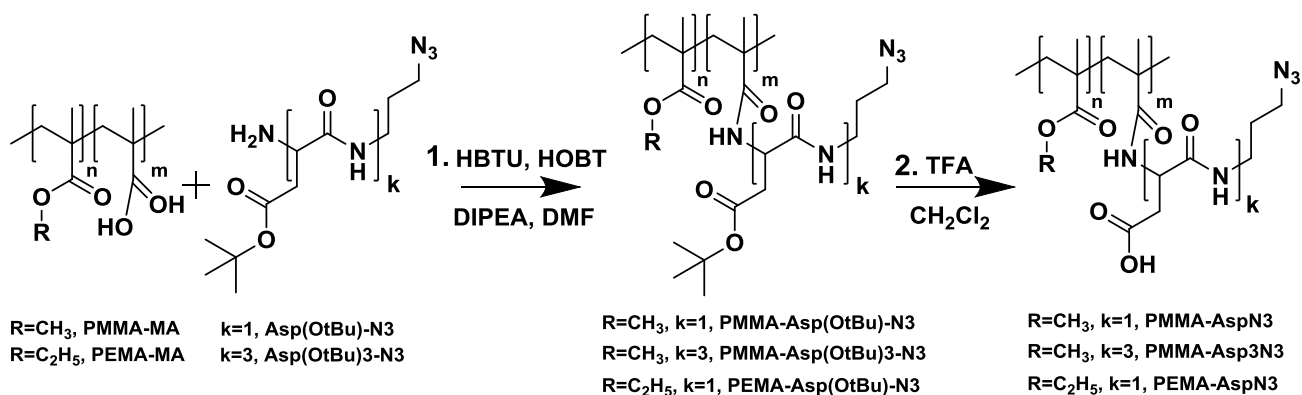
described elsewhere.¹⁶¹ Poly (methyl methacrylate-co-methacrylic acid) (PMMA-MA), 1.6% methacrylic acid, Mn ~15000, Mw ~34000) was purchased from Sigma-Aldrich.

Synthesis of modified PMMA and PEMA polymers.



PMMA-N3. The PMMA-MA (1eq of COOH groups, 0.03 mmol, 250 mg) was dissolved in anhydrous N,N-dimethylformamide (5 ml). To this solution HBTU (3 eq, 0.098 mmol, 38 mg), HOBT (3.3 eq, 0.109 mmol, 15 mg) and N,N-diisopropylethylamine (10eq, 0.33mmol, 0.054mL) was added. The mixture was stirred for 15 min and after 3-azido-1-propamine (3eq, 0.098 mmol, 10mg) was added. The reaction was stirred overnight at room temperature under argon. The solvent was evaporated under reduced pressure and residue was dissolved in a minimum of acetonitrile and precipitate with methanol. The precipitate was washed with methanol, redissolved in acetonitrile and reprecipitated twice in methanol. After drying under a vacuum, product was obtained as a white solid – 130 mg, yield 52%. ¹H NMR (400 MHz, CDCl₃) δ, ppm: 0.84 (br s, 2 H), 1.02 (br s, 1 H), 1.19 - 1.28 (m, 0.31 H), 1.44 (m, 0.29 H), 1.79 - 2.07 (m, 2 H), 3.60 (br s, 3 H).

General method for PMMA-AspN3 (1.6% and 5% of copolymer), PMMA-Asp3N3 (1.6% of copolymer) and PEMA-AspN3 (5% of copolymer) synthesis.



1. The PMMA-MA or PEMA-MA (1 eq of COOH groups) was dissolved in anhydrous N,N-dimethylformamide. To this solution HBTU (3 eq), HOBT (4 eq) and N,N-diisopropylethylamine (10 eq) were added. The mixture was stirred for 15 min and after Asp(OtBu)-N₃ or Asp(OtBu)3-N₃ (3 eq) was added. The reaction was stirred overnight at room temperature under argon. The solvent was evaporated under reduced pressure and residue was dissolved in a minimum of acetonitrile and precipitated with methanol. The precipitate was washed with methanol,

redissolved in acetonitrile and reprecipitated twice in methanol. After drying under a vacuum, a product was obtained as a white solid.

PMMA-Asp(OtBu)-N3 (1.6% of copolymer) – yield 55%. $^1\text{H NMR}$ (400 MHz, CDCl_3) δ , ppm: 0.85 (br s, 2 H), 1.02 (br s, 1 H), 1.18 - 1.29 (m, 0.31 H), 1.46 (br s, 0.29 H), 1.65 (br s, 1H), 1.74 - 2.11 (m, 2 H), 3.60 (br s, 3 H).

PMMA-Asp(OtBu)-N3 (5% of copolymer) – yield 45%. $^1\text{H NMR}$ (400 MHz, CDCl_3) δ , ppm: 0.84 (br s, 2 H), 1.02 (br s, 1 H), 1.21 (br s, 0.24 H), 1.34 - 1.53 (m, 0.29 H), 1.76 - 2.04 (m, 2 H), 2.10 - 2.32 (m, 1 H), 3.60 (br s, 3 H).

PMMA-Asp(OtBu)3-N3 (1.6% of copolymer) – yield 60%. $^1\text{H NMR}$ (400 MHz, CDCl_3) δ , ppm: 0.85 (s, 1.55 H), 1.02 (s, 1.12 H), 1.17 - 1.31 (m, 0.33 H), 1.44 (m, 0.33 H), 1.62 (br s, 0.12 H), 1.72 - 2.22 (m, 1.82 H), 3.60 (br s, 3 H).

PEMA-Asp(OtBu)-N3 (5% of copolymer) – yield 50%. $^1\text{H NMR}$ (400 MHz, CDCl_3) δ , ppm: 0.88 (br s, 2 H) 1.04 (br s, 1 H), 1.27 (s, 3 H), 1.45 (br s, 0.47 H), 1.59 (br s, 1 H), 1.83 (br s, 1 H), 1.93 (br s, 0.72 H), 2.01 (br s, 0.44 H), 4.04 (br s, 2 H).

2. The polymer obtained in a previous step was dissolved in anhydrous dichloromethane (~ 5 mL) and 2 mL of trifluoroacetic acid was added. The mixture was stirred for 3 h. Then solvents were evaporated under reduced pressure. Acetonitrile was added to the residue and evaporation was repeated several times until the absence of the trifluoroacetic acid. Then the product was precipitated in methanol and filtrated. After drying under vacuum, the product was obtained as a white solid.

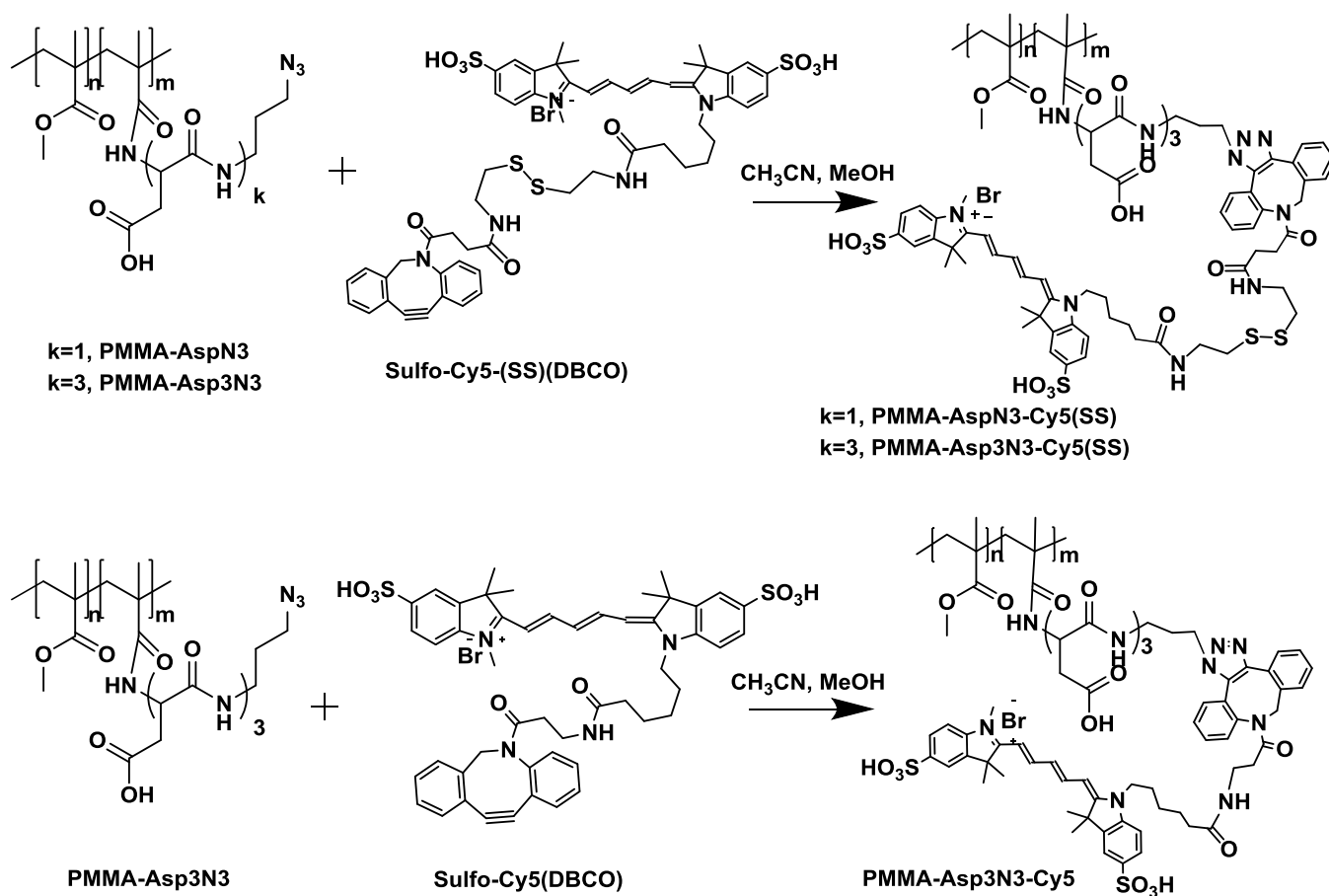
PMMA-AspN3 (1.6% of copolymer) – yield 80%. $^1\text{H NMR}$ (400 MHz, CDCl_3) δ , ppm: 0.78 - 1.11 (m, 2 H), 0.94 - 1.11 (m, 1 H), 1.24 (br s, 0.30 H), 1.45 (br s, 0.37 H), 1.72 - 2.15 (m, 2 H), 3.60 (br s, 3 H).

PMMA-AspN3 (5% of copolymer) – yield 60%. $^1\text{H NMR}$ (400 MHz, CDCl_3) δ , ppm: 0.75 - 0.93 (m, 2 H), 1.02 (br s, 1 H), 1.21 (br s, 0.29 H), 1.45 (br s, 0.33 H), 1.81 (br s, 0.81 H), 1.84 - 2.05 (m, 1 H), 3.60 (br s, 3 H).

PMMA-Asp3N3 (1.6% of copolymer) – yield 73%. $^1\text{H NMR}$ (400 MHz, CDCl_3) δ , ppm: 0.85 (s, 1.63 H), 1.03 (s, 1.23 H), 1.21-1.25 (m, 0.26 H), 1.37 - 1.52 (m, 0.28 H), 1.77 - 2.26 (m, 1.92 H), 3.61 (br s, 2 H).

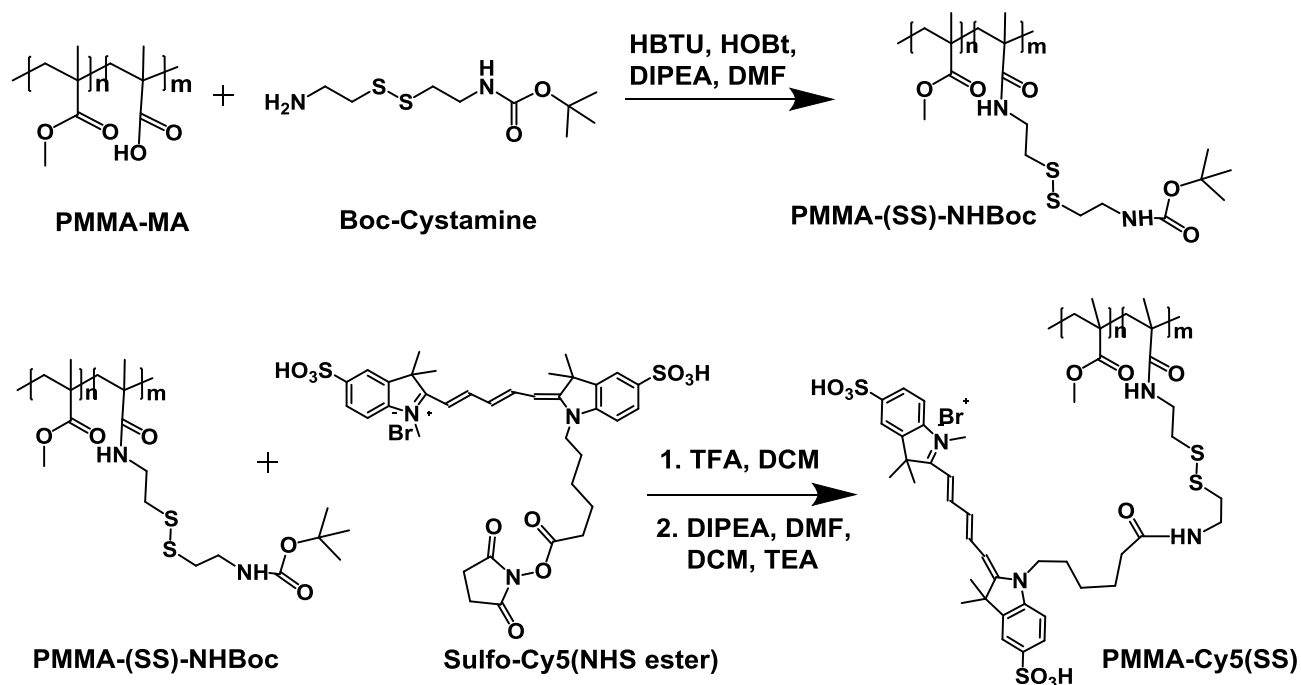
PEMA-AspN3 (5% of copolymer) – yield 70%. $^1\text{H NMR}$ (400 MHz, CDCl_3) δ , ppm: 0.83 - 1.10 (m, 2 H), 0.96 - 1.12 (m, 1 H), 1.20 - 1.34 (br s, 3 H), 1.35 - 1.63 (m, 0.47 H), 1.83 (br s, 1 H), 1.93 (br s, 0.72 H), 1.97 - 2.23 (m, 0.44 H), 4.04 (br s, 2 H).

General method for PMMA-AspN3-Cy5(SS), PMMA-Asp3N3-Cy5(SS) and PMMA-Asp3N3-Cy5 synthesis.



PMMA-AspN3 or PMMA-Asp3N3 (1 eq of COOH groups) was dissolved in anhydrous CH₃CN and Sulfo-Cy5(DBCO) (4 eq) was dissolved in MeOH. Two components were mixed and kept under vortex for 18 h at 40 °C. After the reaction was complete, the solvents were evaporated under reduced pressure and residue was dissolved in CH₂Cl₂:MeOH (1:1). The crude product was purified on a size-exclusion LH20 column using CH₂Cl₂:MeOH (1:1) as eluent.

For all resulting polymers PMMA-AspN3-Cy5(SS), PMMA-Asp3N3-Cy5(SS) and PMMA-Asp3N3-Cy5, the product was insufficient to obtain ¹H NMR spectra with any useful information. But in each case two distinct blue-colored bands observed in LH20 column indicating the existence of unreacted dye and dye coupled with a polymer. The first fraction corresponding to the dye-polymer couple was washed with methanol, which resulted in colorless supernatant. This demonstrates the reaction between dye and polymer and the absence of any unreacted non-specifically bound free dye.

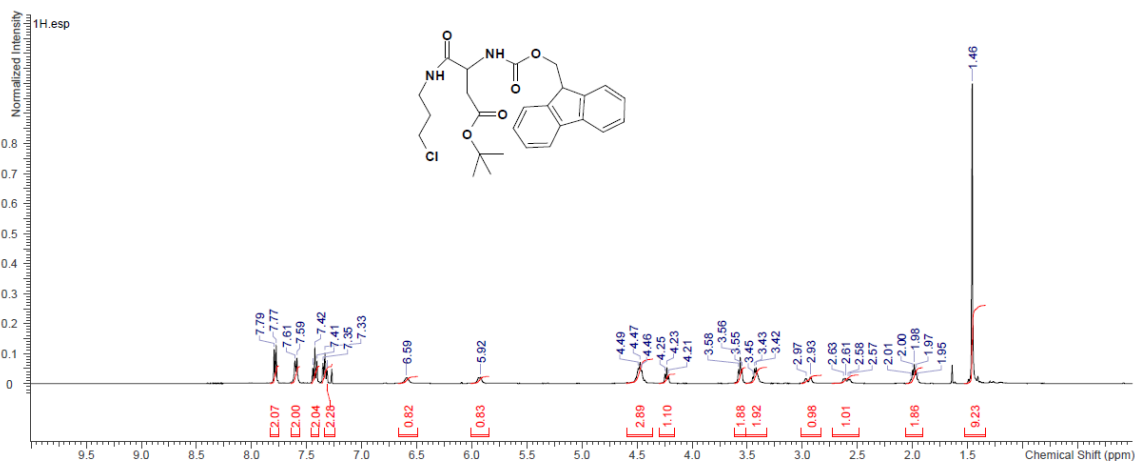
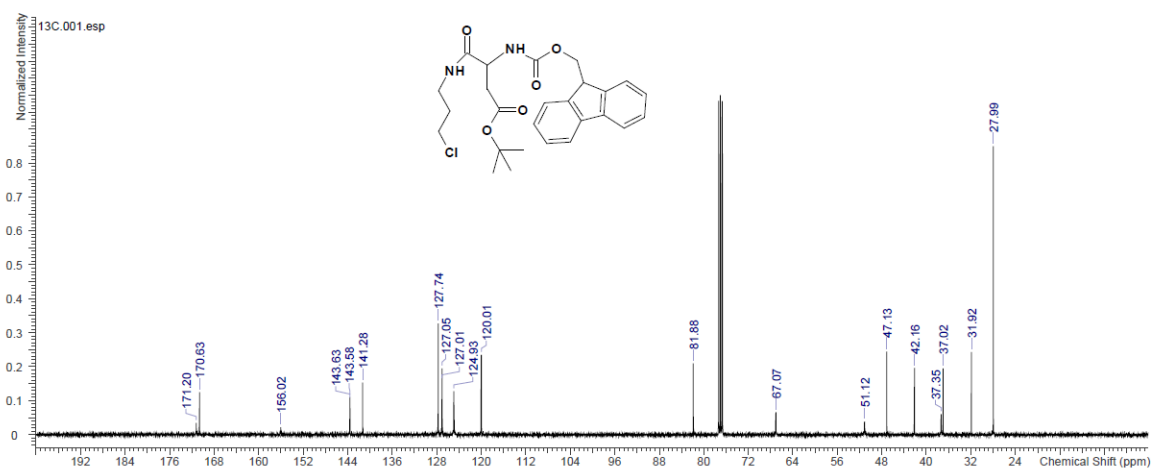
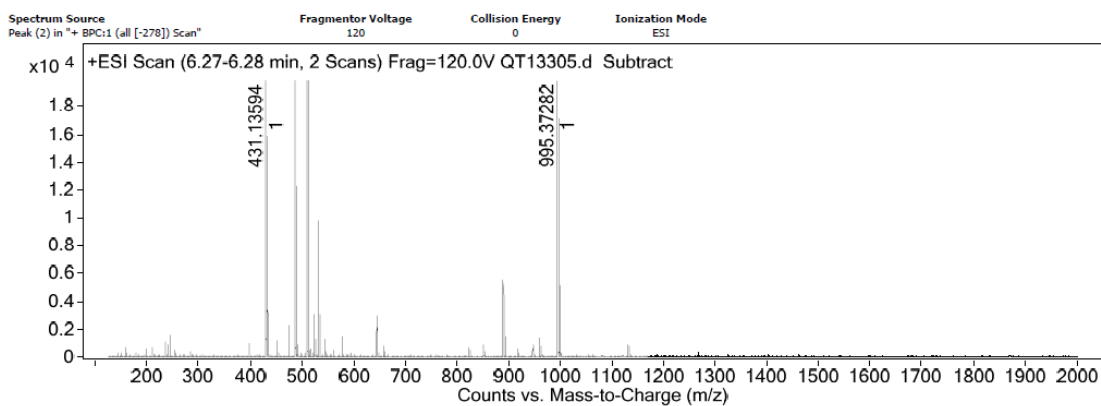
Synthesis of the PMMA-Cy5(SS).

PMMA-(SS)-NHBoc. 50 mg of PMMA-MA (3.33 μmol , 1 eq. of COOH groups) was dissolved in anhydrous N,N-dimethylformamide (0.5 mL). To this solution N,N-diisopropylethylamine (10 eq, 33.3 μmol , 5.5 μL), HOBT (4 eq, 13.3 μmol , 1.80 mg) and HBTU (3 eq, 10.0 μmol , 3.79 mg) were added. Then Boc-Cystamine (3 eq, 10.0 μmol , 2.5 mg) in 0.5 mL of anhydrous dichloromethane was added to the reaction mixture and stirred for 18 h at room temperature. The solvent was evaporated under reduced pressure and residue was dissolved in a minimum of acetonitrile and precipitated with methanol. The precipitate was washed with methanol, redissolved in acetonitrile and reprecipitated twice in methanol. After drying under a vacuum, PMMA-(SS)-NHBoc was obtained as a white solid (26.9 mg, yield 53%). ^1H NMR (400 MHz, CDCl_3) δ , ppm: 3.60 (br s, 3 H), 3.04 (br s, 0.05 H), 2.78 (br s, 0.05 H), 2.07 - 1.81 (m, 2 H), 1.43 (br s, 0.29 H), 1.31 - 1.21 (m, 0.45 H), 1.01 (br s, 1 H), 0.84 (br s, 2 H). (Degree of modification was 77%, calculated from CH_2 signal in NMR spectra).

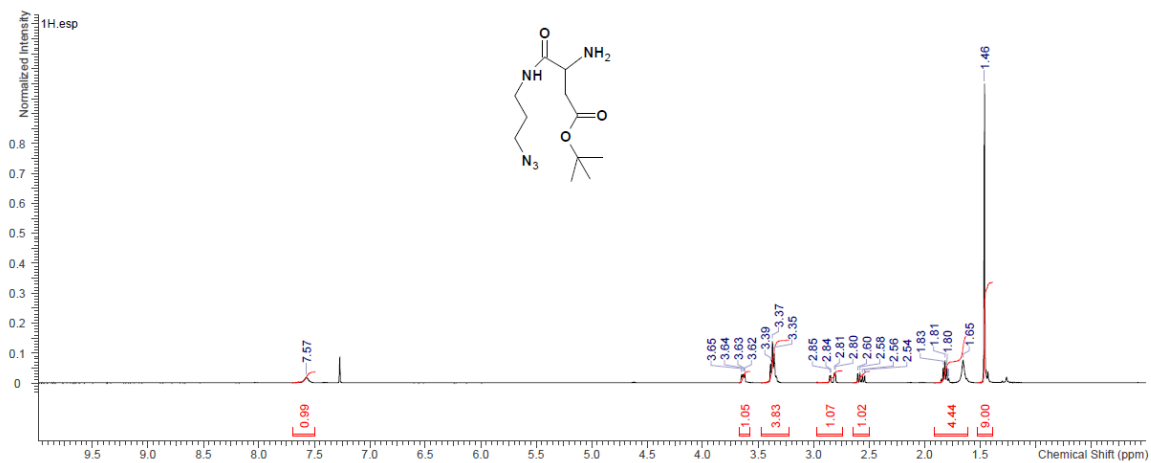
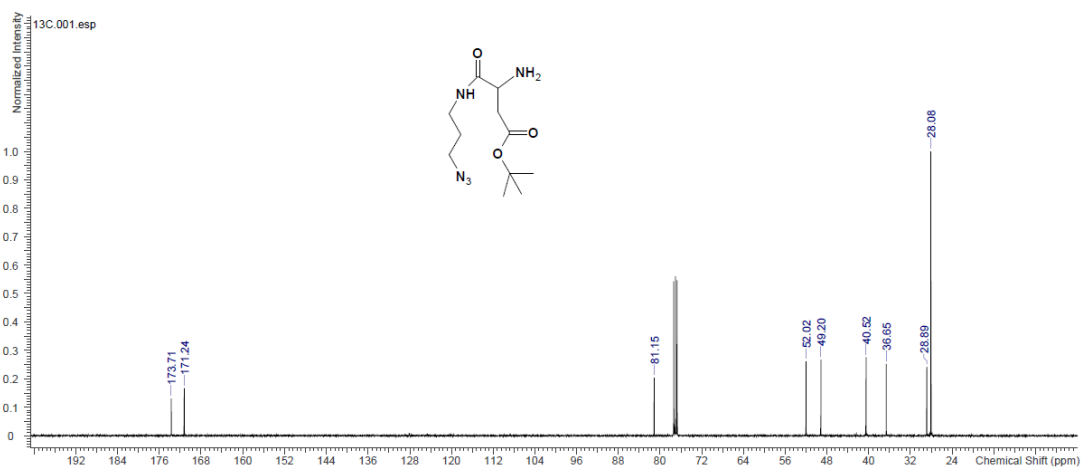
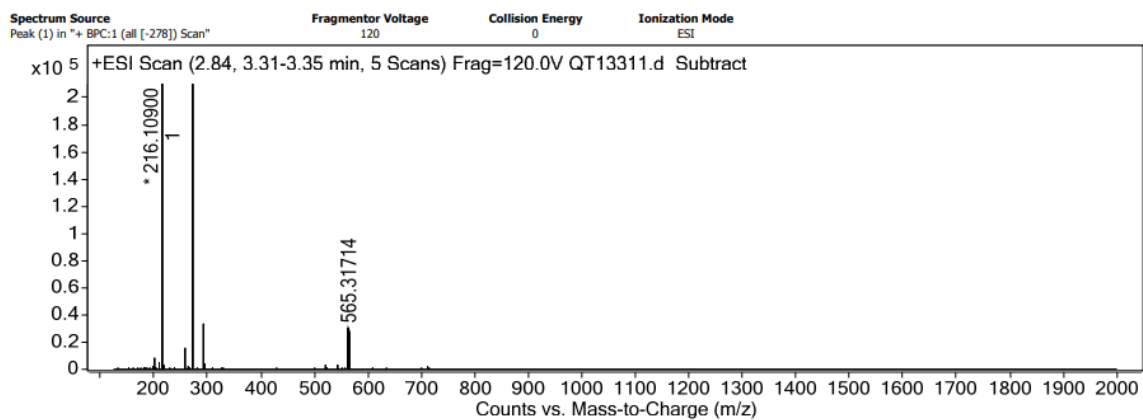
PMMA-Cy5(SS). To a solution of PMMA-(SS)-NHBoc (1 eq of modified copolymer groups, 0.52 μmol , 8 mg) in anhydrous dichloromethane (50 μL) was added trifluoroacetic acid (25 μL) and stirred at room temperature for 3 h. The solvent was removed from the reaction mixture by rotary evaporation. Acetonitrile was added to the residue and evaporation was repeated several times until the absence of the trifluoroacetic acid. The obtained solid was dissolved in anhydrous N,N-dimethylformamide (30 μL) and diisopropylethylamine (14 eq, 7.34 μmol , 1.2 μL) were added to neutralize the amine-TFA salt formed after Boc-deprotection. To this reaction mixture was added a solution of Sulfo-Cy5(NHS ester) (3 eq, 1.57 μmol , 1.22 mg) in anhydrous DCM (30 μL) and

triethylamine (17 eq, 8.92 μmol , 1.24 μL) and stirred for 16 h at room temperature. The solvent was evaporated under reduced pressure and residue was dissolved in a minimum of acetonitrile and precipitated with methanol as described above to get PMMA-Cy5(SS) (6.1 mg, yield 74%). ^1H NMR (400 MHz, CDCl_3) δ , ppm: 7.99 (br s, 0.02H), 7.10 (br s, 0.01 H), 6.14 (br s, 0.03 H), 3.60 (br s, 3 H), 3.49 (s, 0.09 H), 3.12 (br s, 0.03 H), 3.02 (br s, 0.03 H), 2.79 (br s, 0.06H), 2.07 - 1.81 (m, 2 H), 1.42 (br s, 0.30 H), 1.25 - 1.20 (m, 0.38 H), 1.02 (br s, 1 H), 0.84 (br s, 2 H).

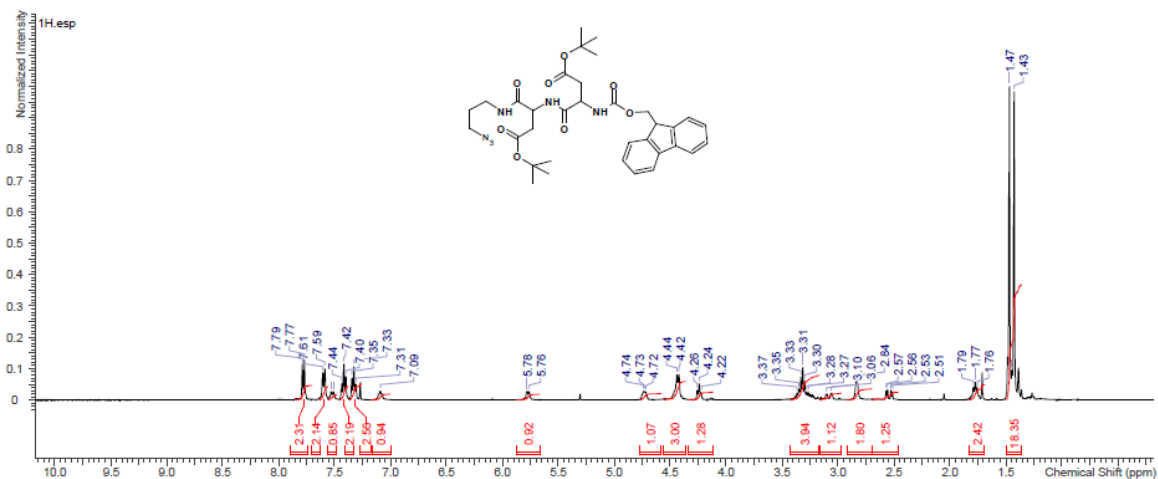
NMR and mass spectra

¹H NMR spectrum of Fmoc-Asp(OtBu)-Cl.¹³C NMR spectrum of Fmoc-Asp(OtBu)-Cl.

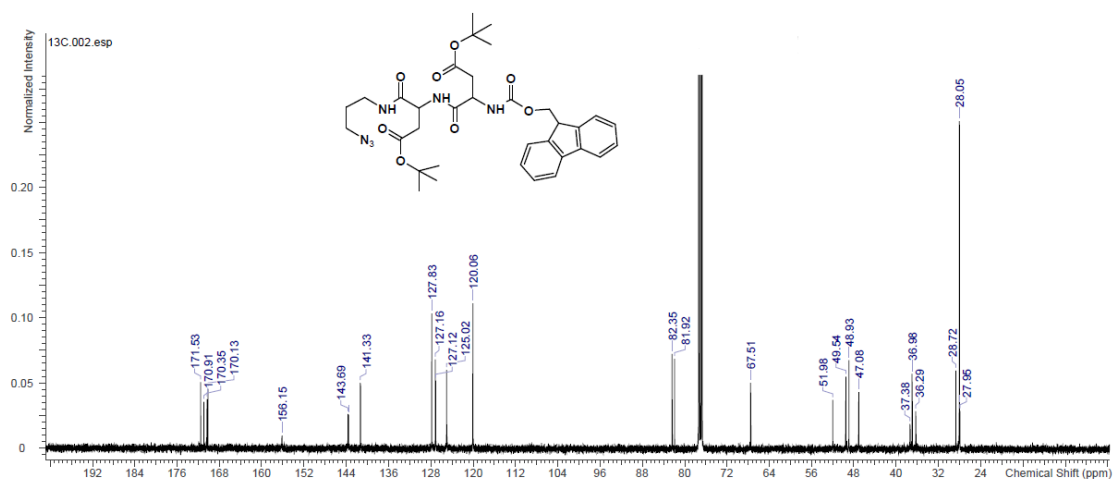
HPLS/MS of Fmoc-Asp(OtBu)-Cl.

¹H NMR spectrum of Asp(OtBu)-N3.¹³C NMR spectrum of Asp(OtBu)-N3.

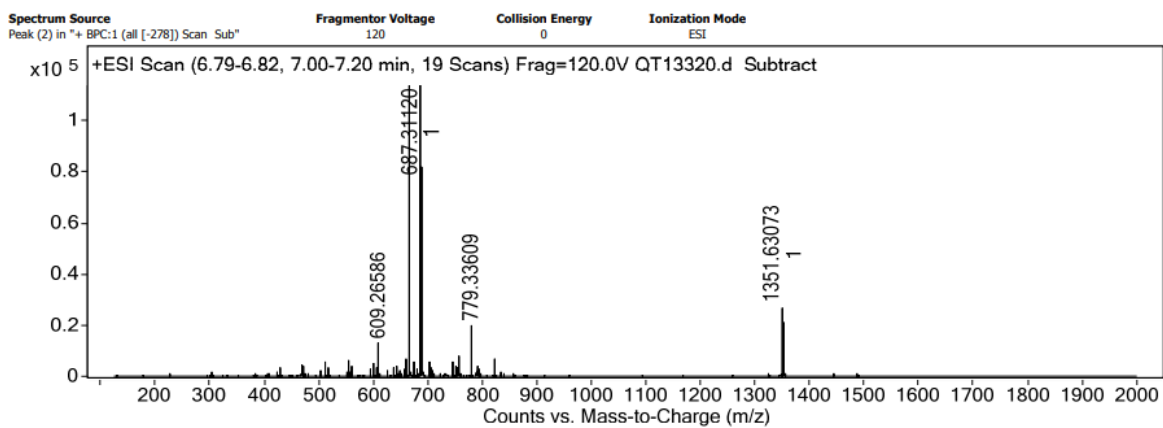
HPLS/MS spectrum of Asp(OtBu)-N3



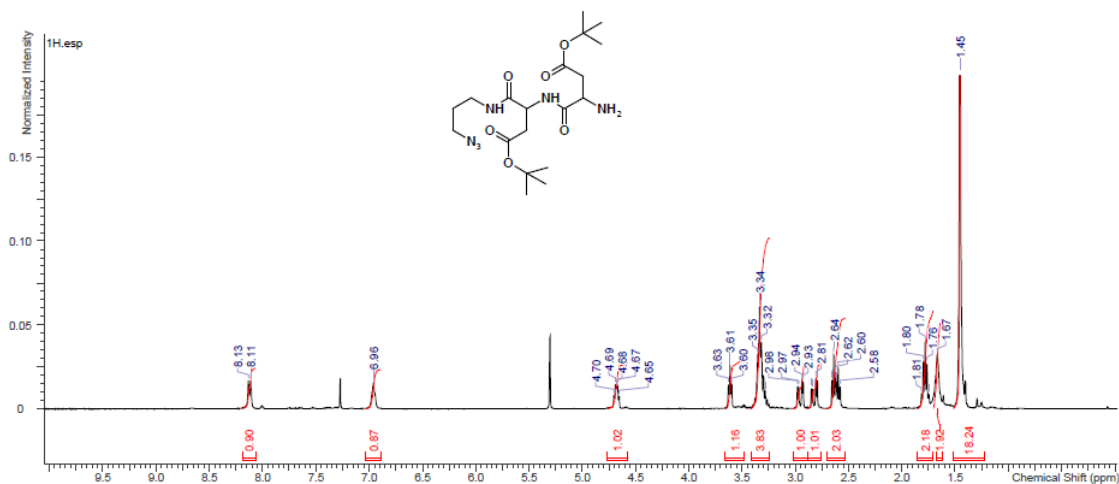
¹H NMR spectrum of Fmoc-Asp(OtBu)₂-N₃.



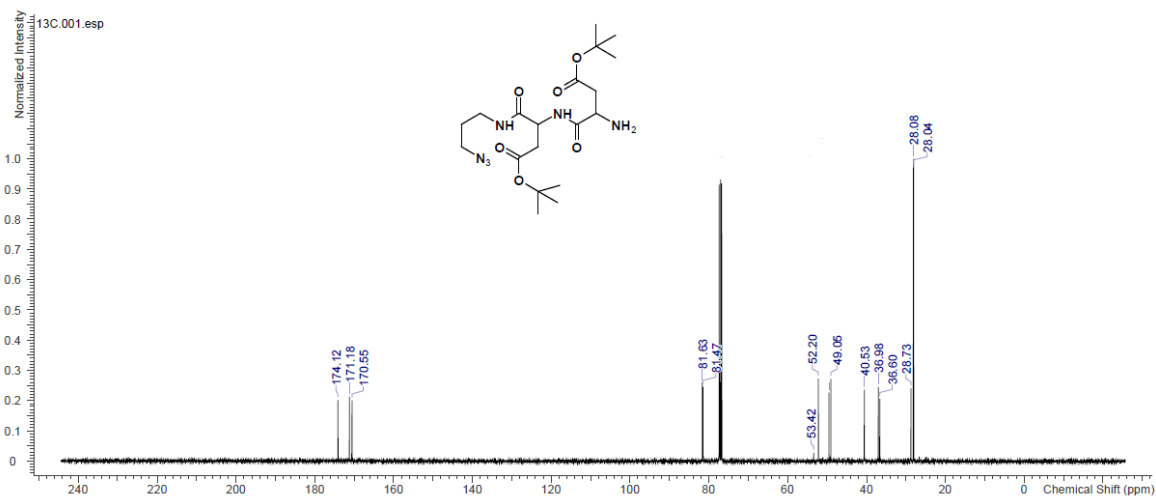
¹³C NMR spectrum of Fmoc-Asp(OtBu)₂-N₃.



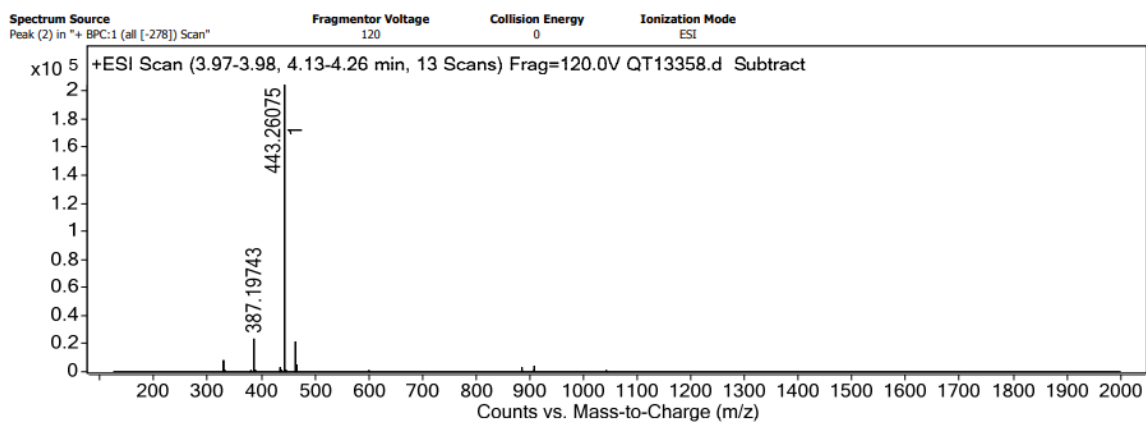
HPLS/MS of Fmoc-Asp(OtBu)₂-N₃.



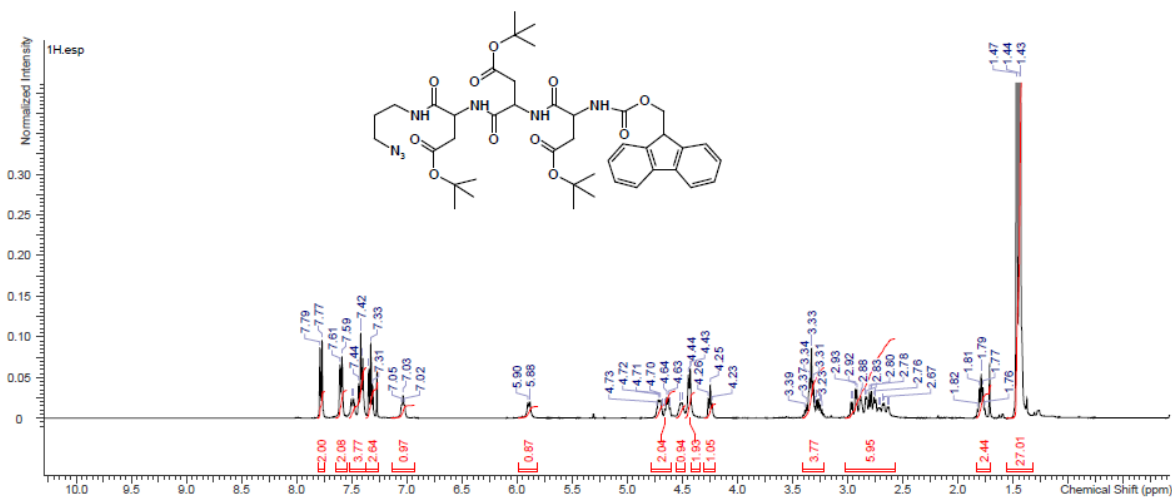
¹H NMR spectrum of Asp(OtBu)2-N3.



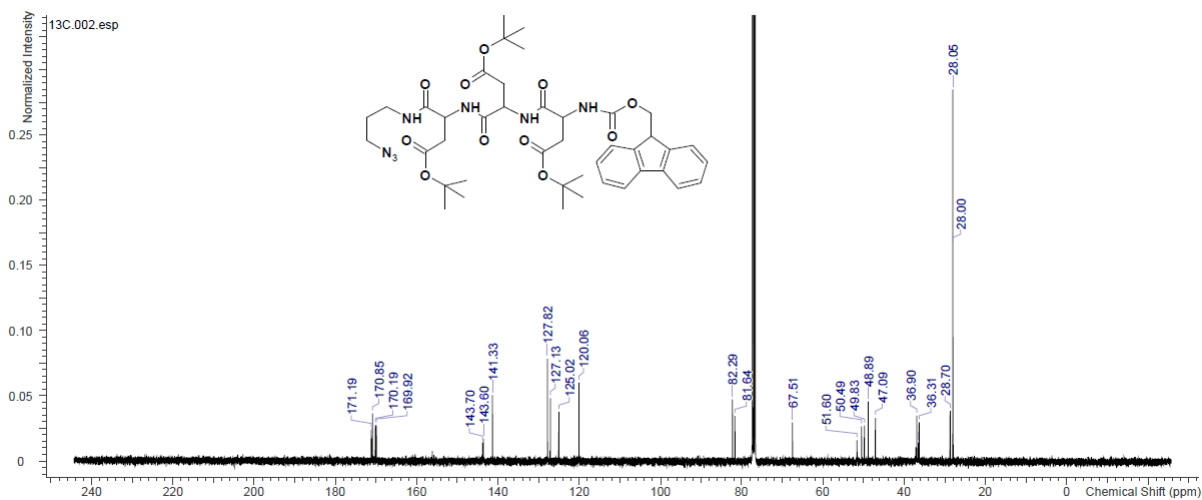
¹³C NMR spectrum of Asp(OtBu)2-N3.



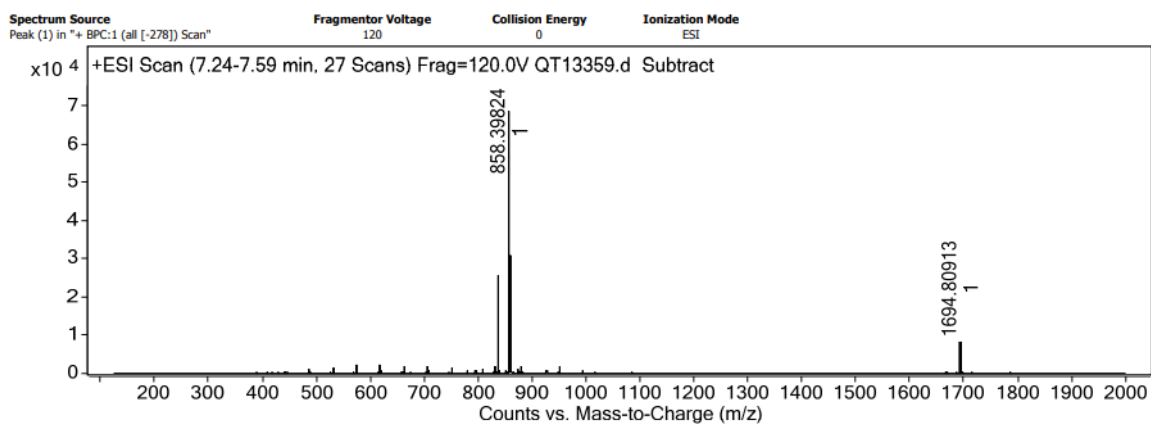
HPLS/MS of Asp(OtBu)2-N3.



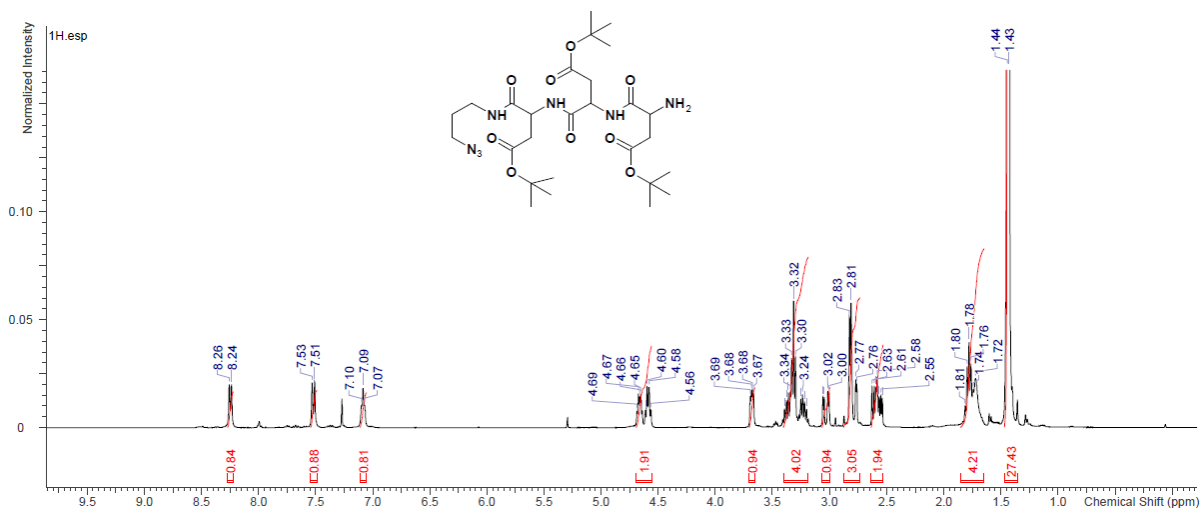
¹H NMR spectrum of Fmoc-Asp(OtBu)₃-N₃.



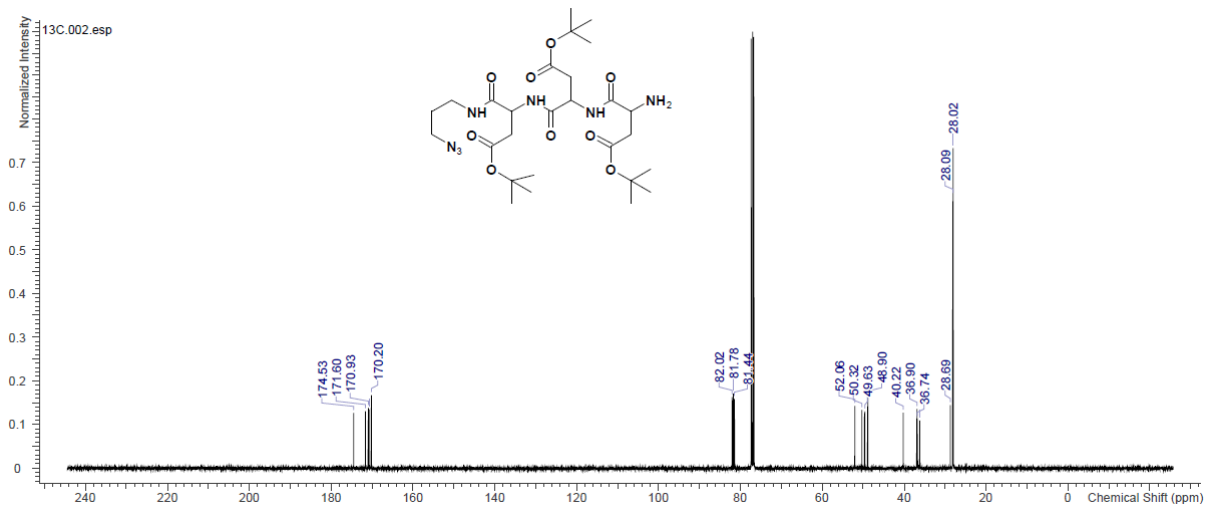
¹³C NMR spectrum of Fmoc-Asp(OtBu)₃-N₃.



HPLS/MS of Fmoc-Asp(OtBu)₃-N₃.

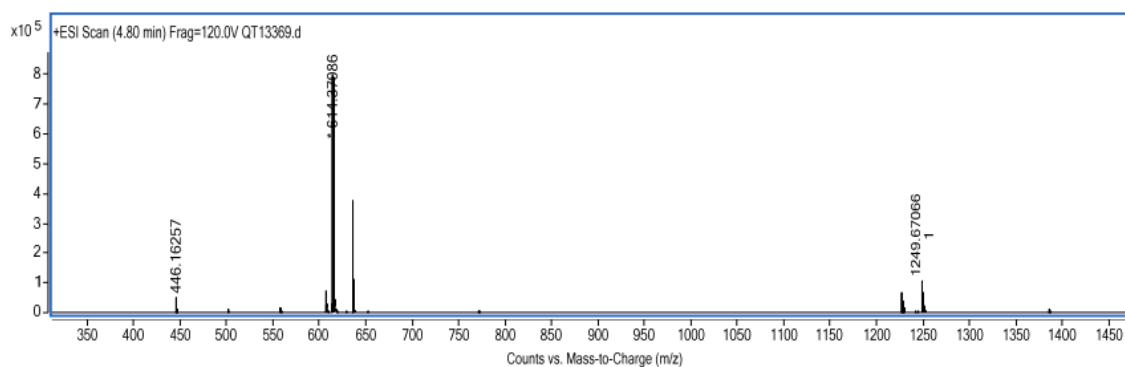


¹H NMR spectrum of Asp(OtBu)₃-N₃.

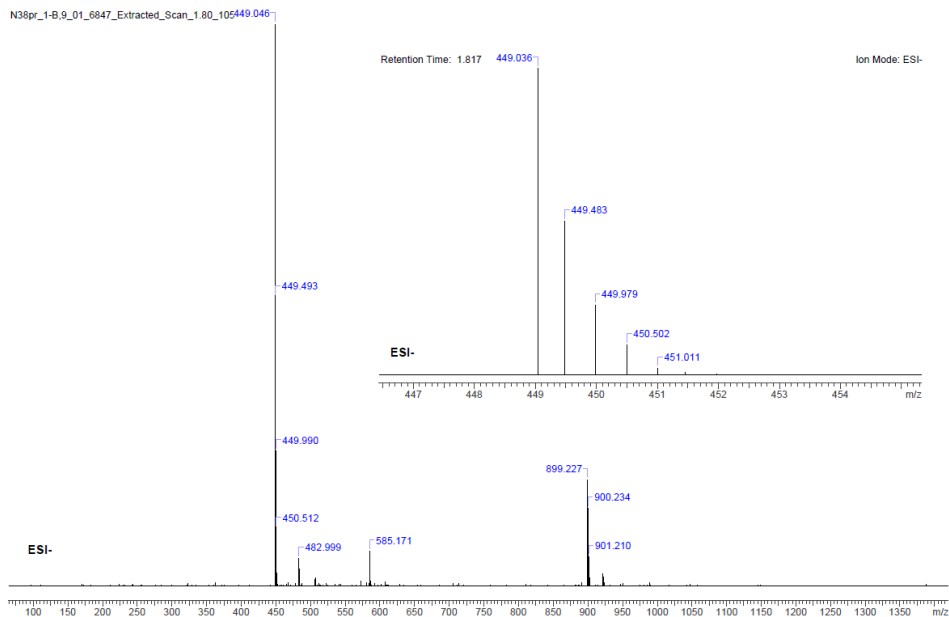


¹³C NMR spectrum of Asp(OtBu)₃-N₃.

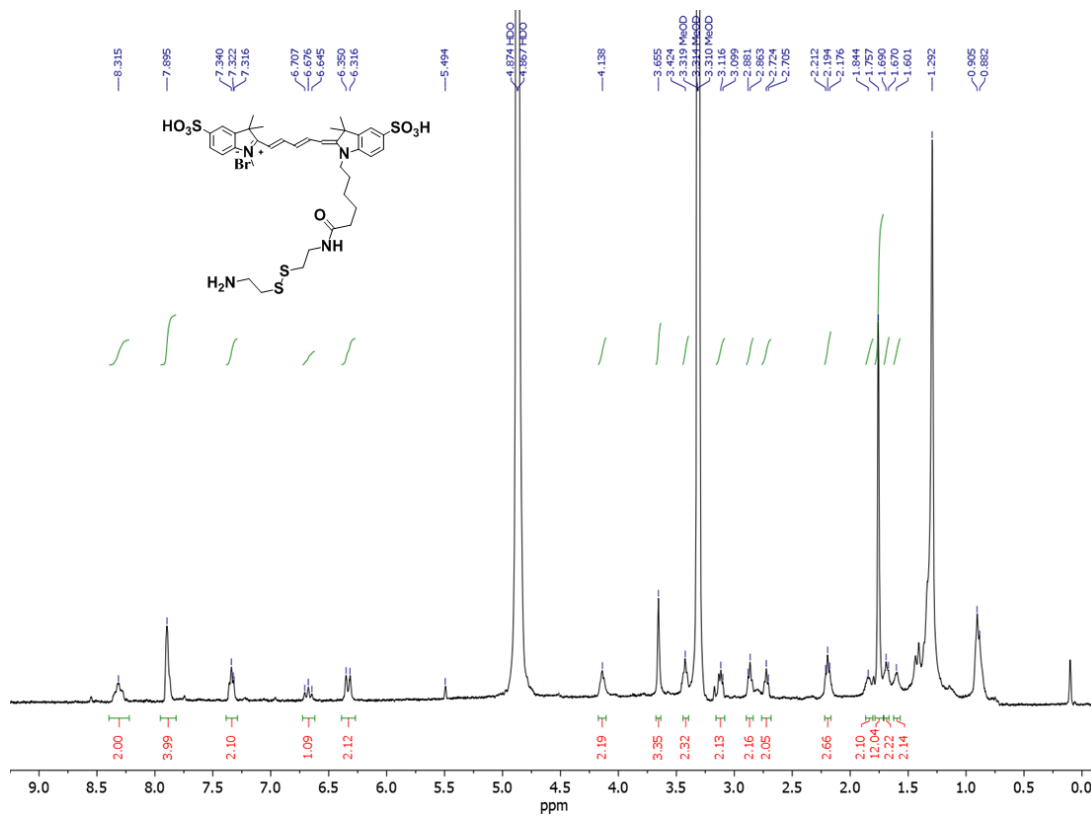
Spectrum Source Peak (5) in "+ BPC:1 (all [-278]) Scan Sub"
Fragmentor Voltage 120
Collision Energy 0
Ionization Mode ESI



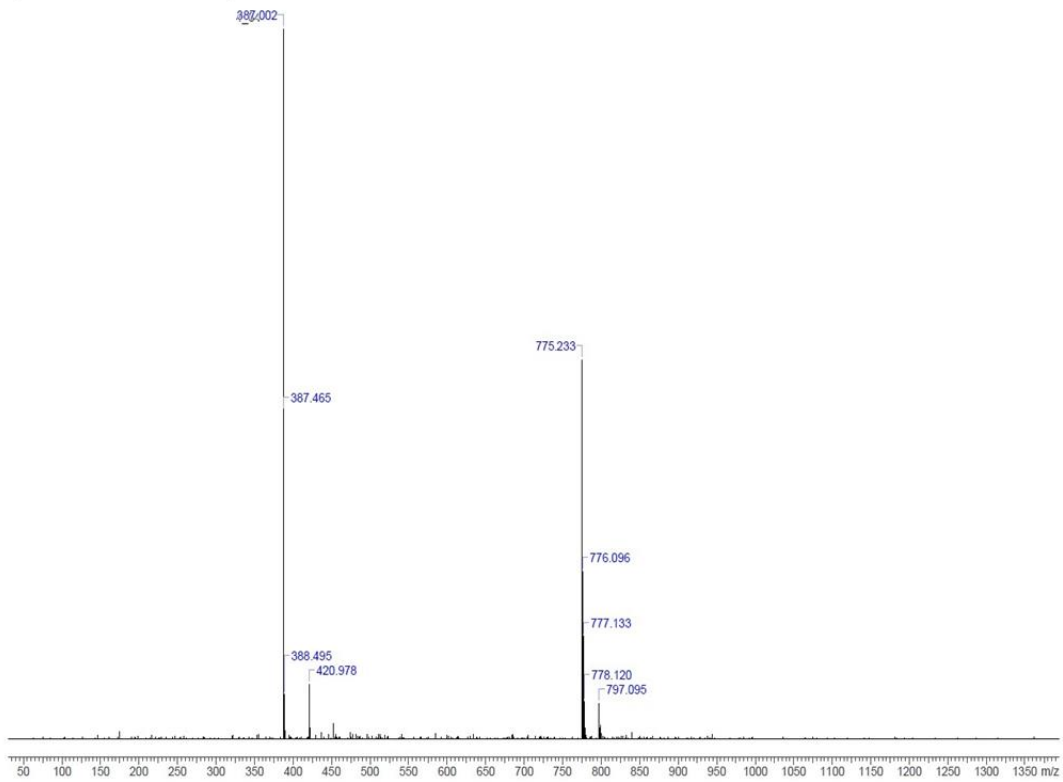
HPLS/MS of Asp(OtBu)₃-N₃.



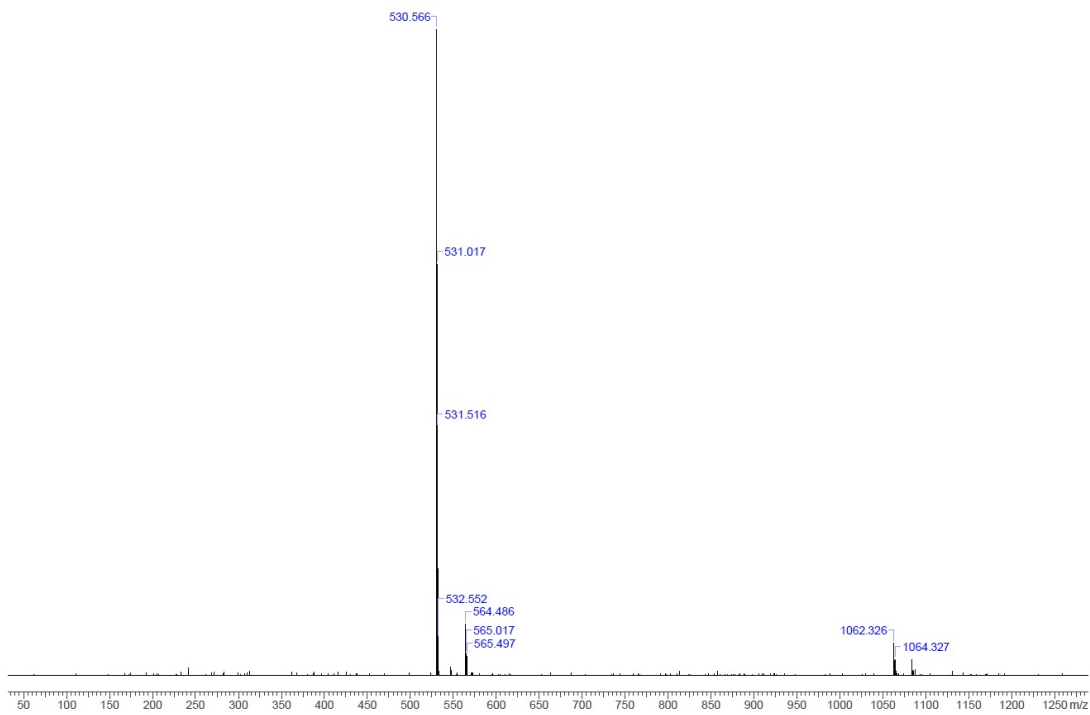
HPLC/MS of Sulfo-Cy5(DBCO).



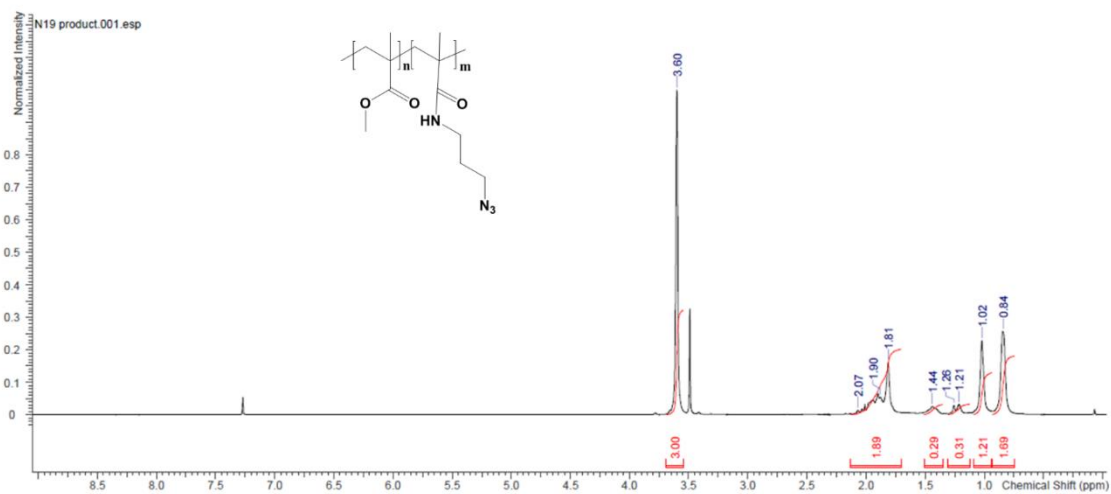
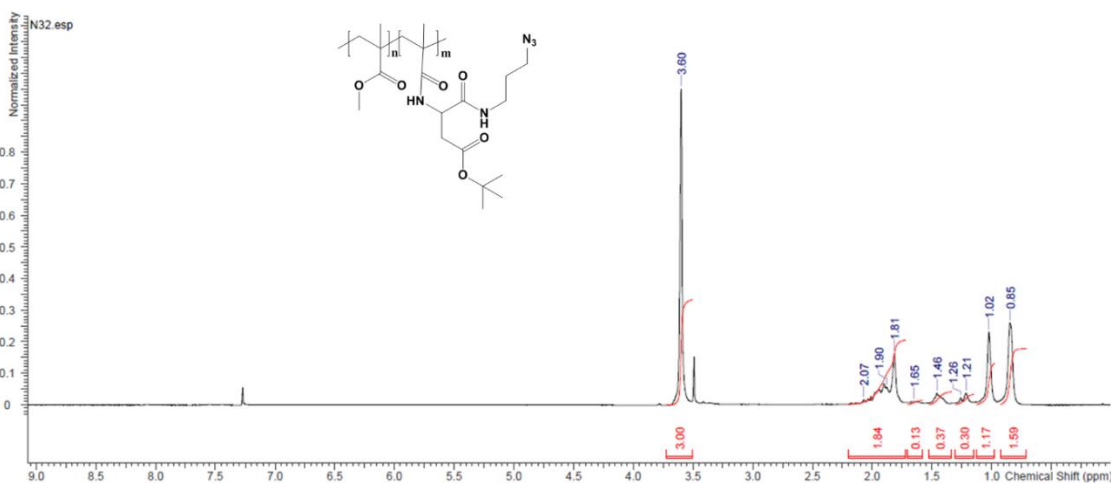
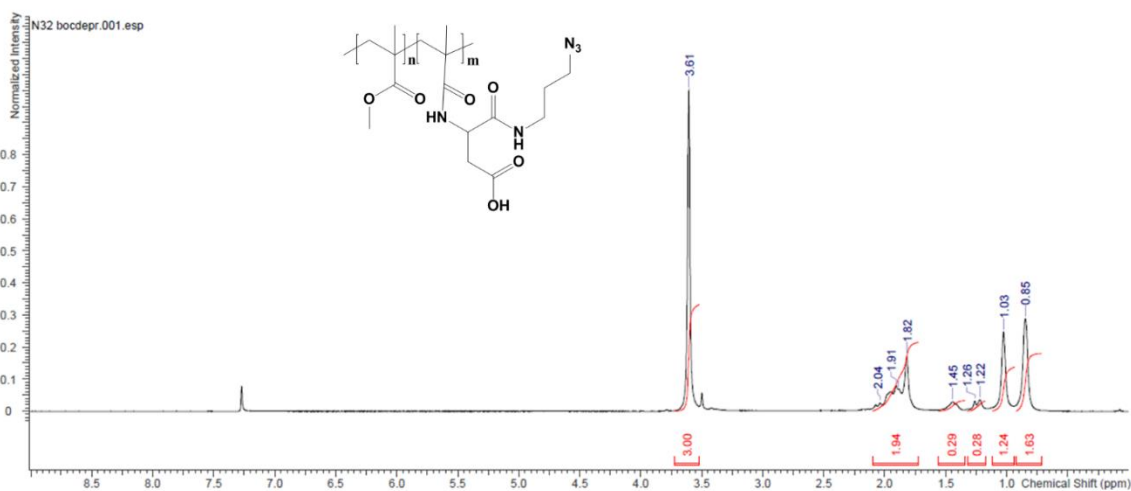
¹H NMR spectrum of Sulfo-Cy5(SS)-NH₂.

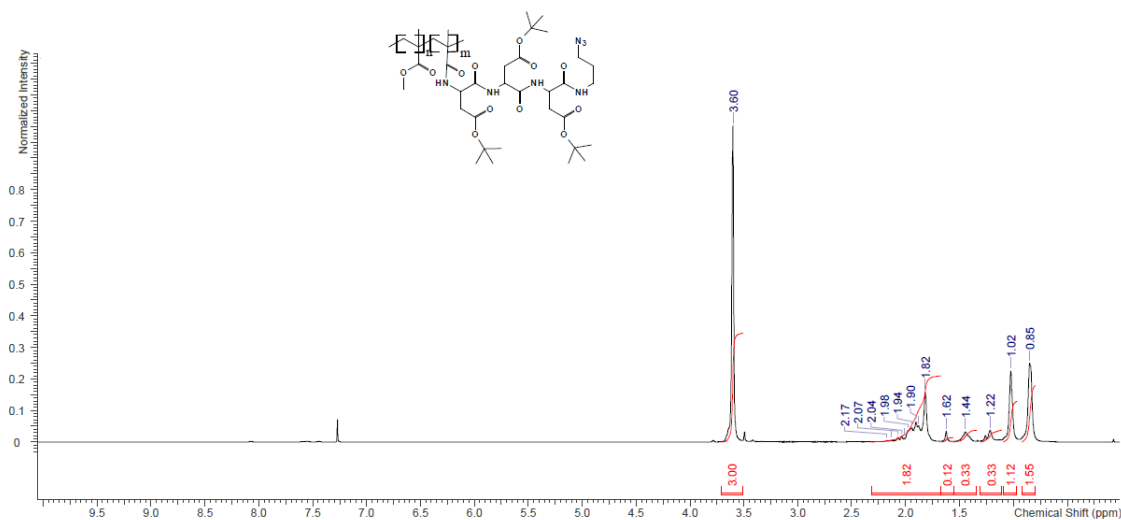
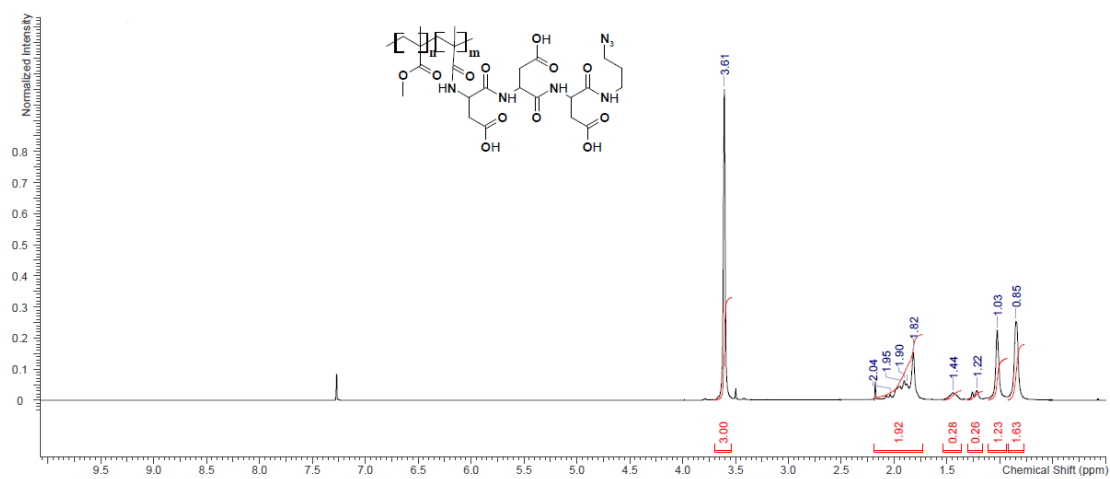


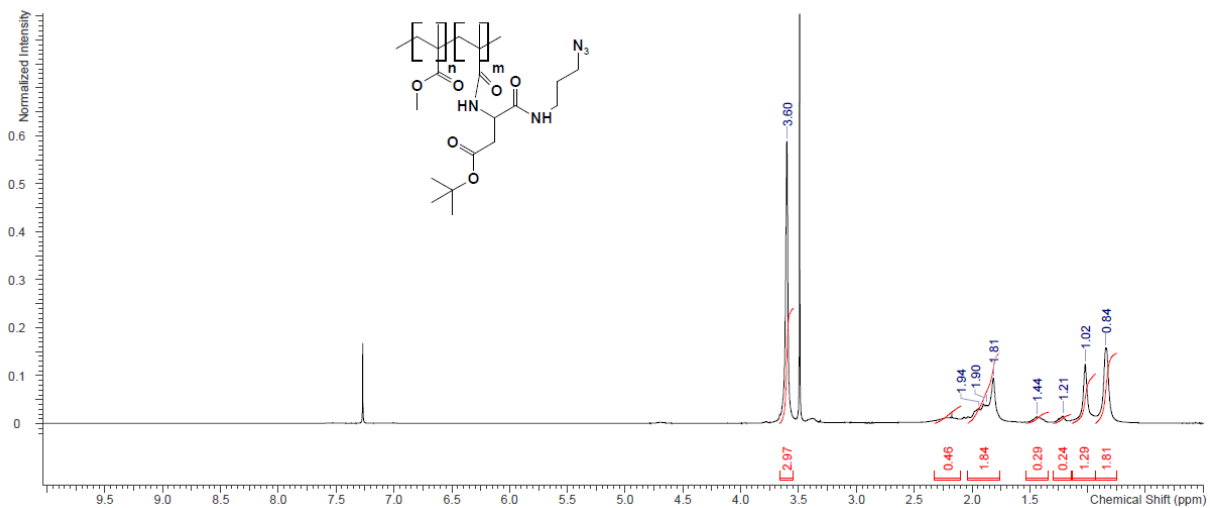
HPLS/MS of Sulfo-Cy5(SS)-NH₂.



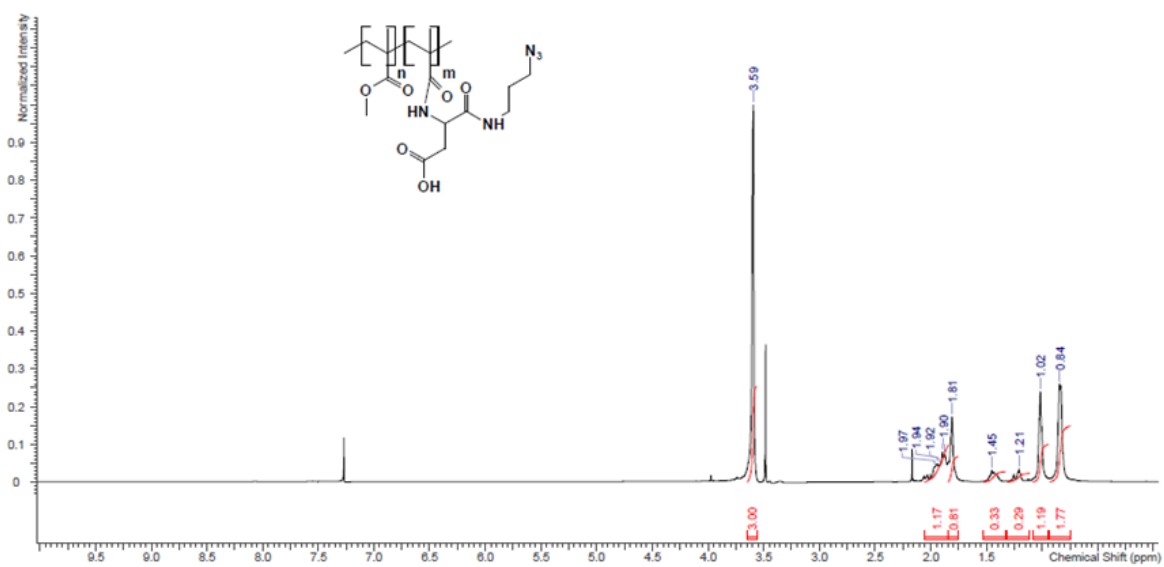
HPLS/MS of Sulfo-Cy5(SS)-DBCO.

 ^1H NMR spectrum of PMMA-N3 (1.6% of copolymer). ^1H NMR spectrum of PMMA-Asp(OtBu)-N3 (1.6% of copolymer).

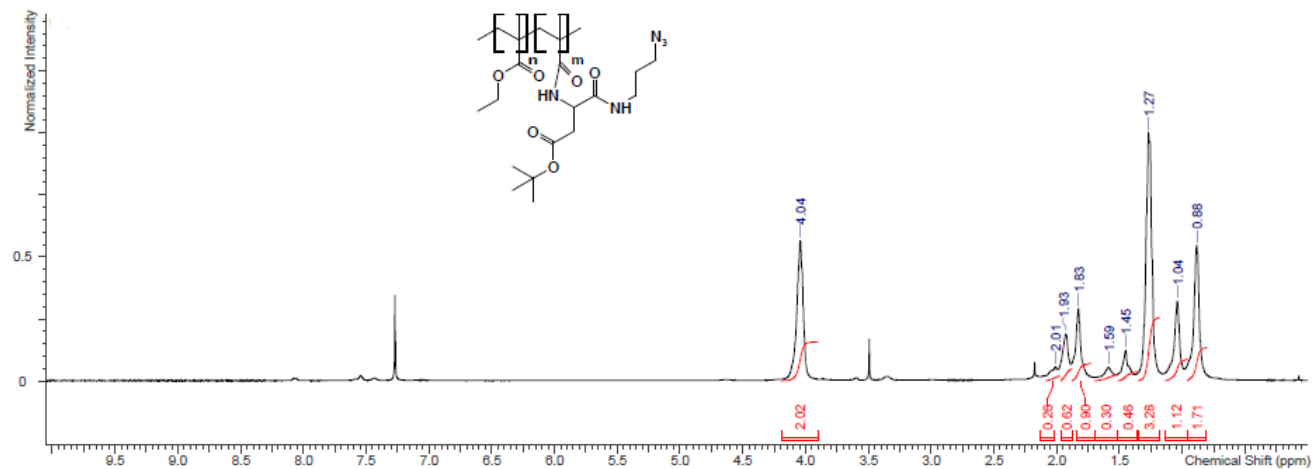
^1H NMR spectrum of PMMA-AspN3 (1.6% of copolymer). ^1H NMR spectrum of PMMA-Asp(OtBu)3-N3 (1.6% of copolymer). ^1H NMR spectrum of PMMA-Asp3-N3 (1.6% of copolymer).



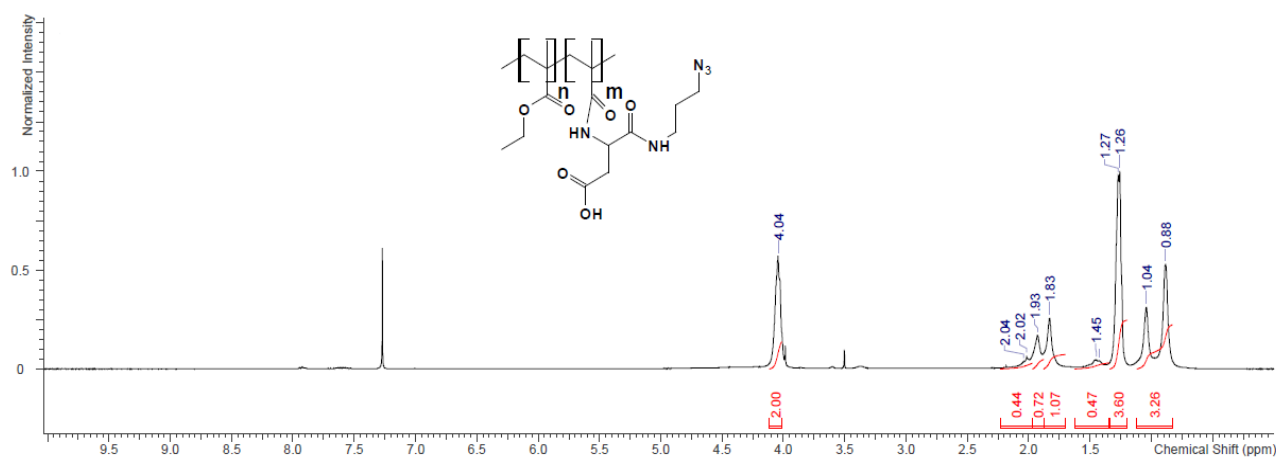
^1H NMR spectrum of PMMA-Asp(OtBu)-N3 (5% of copolymer).



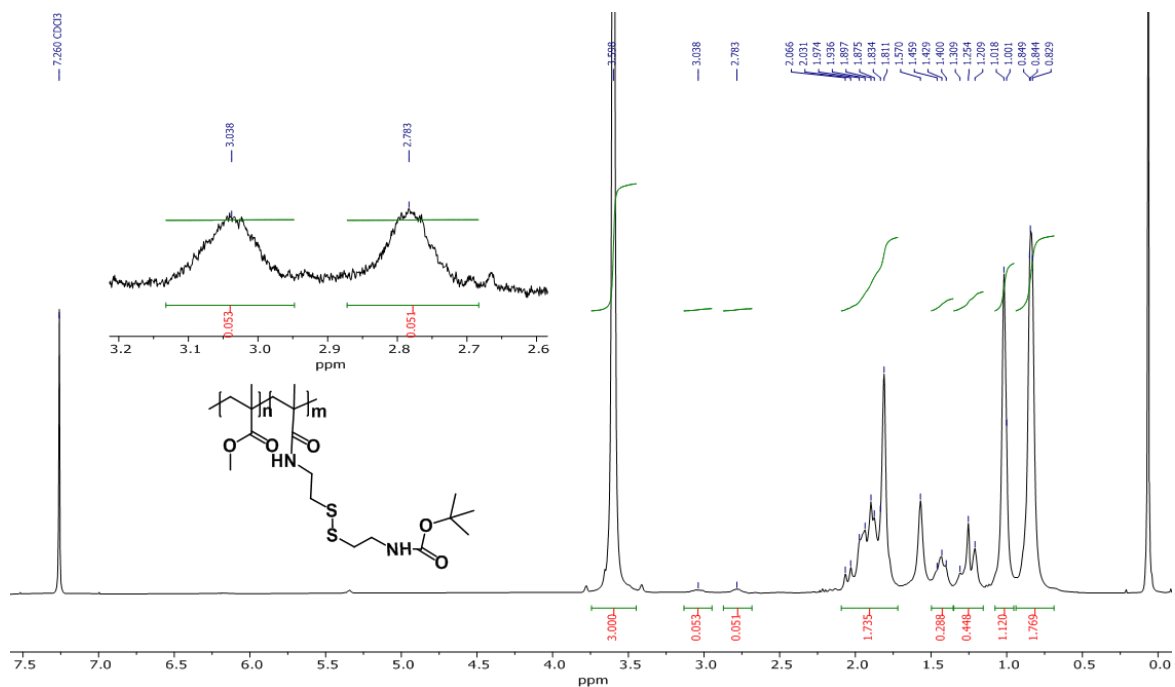
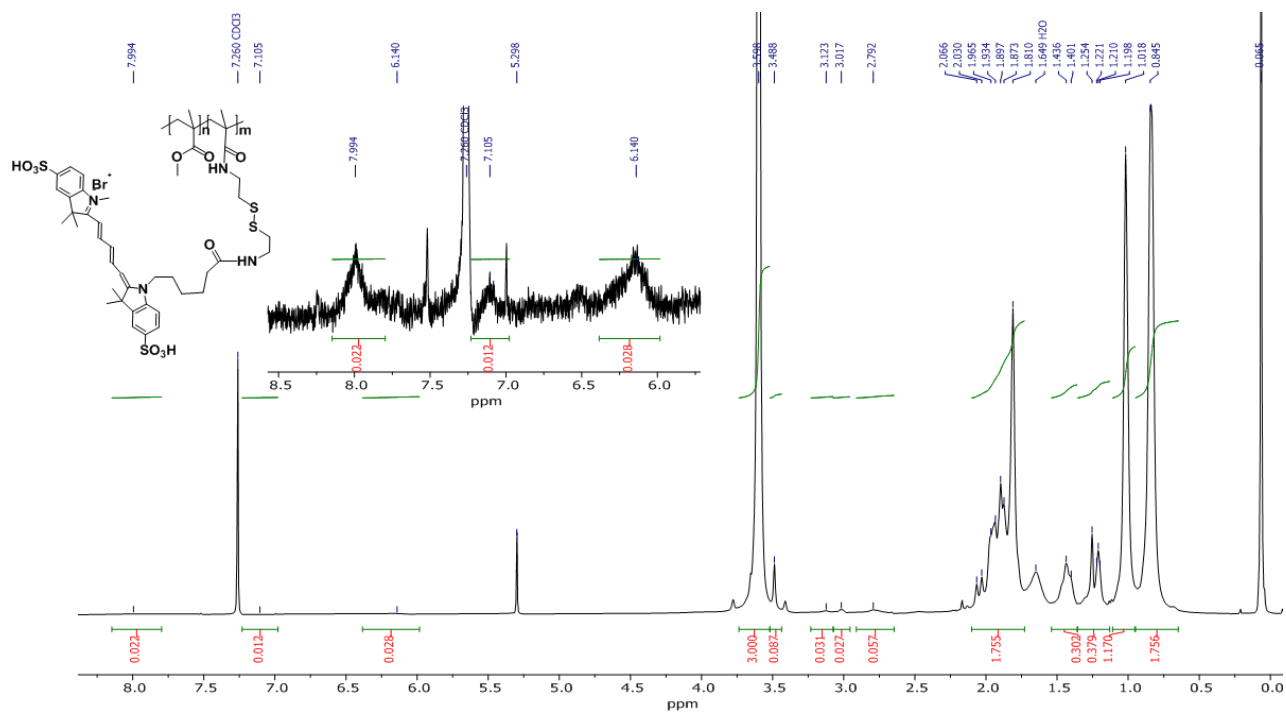
^1H NMR spectrum of PMMA-AspN3 (5% of copolymer).



¹H NMR spectrum of PEMA-Asp(OtBu)-N3 (5% of copolymer).



¹H NMR spectrum of PEMA-AspN3 (5% of copolymer).

¹H NMR spectrum of PMMA-(SS)-NHBoc.¹H NMR spectrum of PMMA-Cy5(SS).

RESUME DE LA THESE EN FRANÇAIS

1. Introduction

Le principal défi en matière de détection par fluorescence de petites concentrations de biomolécules consiste à avoir suffisamment de signal, ce qui s'avère généralement difficile avec des sondes moléculaires classiques.³³ Nous présentons ici une technique d'amplification permettant de convertir un unique phénomène de reconnaissance moléculaire en une réponse de centaines de molécules.³⁷ Un tel procédé est particulièrement important pour les acides nucléiques, pour lesquels une multiplication moléculaire, telle que la PCR et sa variante RT-PCR, est actuellement nécessaire pour détecter les très faibles concentrations d'ADN et d'ARN. Ces méthodes présentent des inconvénients compte tenu de leur reproductibilité et elles nécessitent des mélanges complexes de réactifs, un équipement sophistiqué et du personnel qualifié.⁴⁵

Dans ce but, notre groupe a développé des nanoparticules (NPs) polymères ultra-brillantes dopées en fluorophores, qui se caractérisent par une petite taille contrôlée et une luminosité exceptionnelle car elles encapsulent >1000 fluorophores par particule.³¹ Nous avons constaté que ces nanoparticules fonctionnent comme des nano-antennes captant la lumière, capables d'amplifier >1000 fois par rapport à la fluorescence d'un fluorophore unique, ce qui nous a permis de détecter pour la première fois une molécule unique dans des conditions d'excitation comparable à la lumière ambiante.⁶⁸ Pour convertir de telles nanoparticules en nano-sondes pour biomolécules, leur surface doit pouvoir être fonctionnalisée afin de fixer une molécule capteur dont les cibles les plus importantes en recherche biologique et en diagnostic médical sont les acides nucléiques.¹⁵⁵

Les objectifs de ma thèse sont de développer des stratégies de fonctionnalisation de telles particules polymères de nano-antennes avec des oligonucléotides et de convertir ainsi ces nanoparticules en nano-sondes ultrasensibles, pouvant répondre à une hybridation unique avec une molécule d'acide nucléique cible par un changement de leur couleur d'émission.

Pour atteindre ces objectifs, le plan de travail de la thèse comprends trois étapes principales: i) concevoir et synthétiser de petites nanoparticules à forte teneur en fluorophores, pourvues en groupes réactifs à leur surface pour des modifications ultérieures; ii) développer des nano-sondes pour les acides nucléiques, basées sur une approche "*nanoflare*" modifiée. Dans ce cas, les nanoparticules seront des donneurs de FRET et devront être modifiées avec des oligonucléotides, tandis qu'un oligonucléotide sera marqué par un fluorophore accepteur de FRET; iii) développer un système pour lequel les nanoparticules changeront de couleur d'émission en réponse à un oligonucléotide cible et l'appliquer à la détection des acides nucléiques cibles dans les lysats cellulaires.

2. Résultats et discussions

La première tâche de ma thèse a consisté à développer des nanoparticules pourvues de groupes fonctionnels à leur surface. Nous avons choisi comme base le polymère PMMA-MA, car il donne de petites nanoparticules et a démontré une encapsulation efficace des fluorophores, sans fuite.¹³² Pour y fixer des groupes fonctionnels, nous avons mis au point des *linkers* trifonctionnels contenant (i) un carboxyle comme groupe chargé; (ii) un azide pour une réaction ultérieure et (iii) un groupe amino pour la conjugaison avec le polymère (Fig. 1A). Comme synthon, nous avons choisi l'acide aspartique bi-protégé, couramment utilisé pour la synthèse peptidique en phase solide: Fmoc-Asp(OtBu)-OH. La fonction carboxylique a été modifiée avec la 3-chloropropylamine, puis l'atome chlore a été remplacé par un groupement azide. Après déprotection du Fmoc, nous avons obtenu le premier *linker* Asp(OtBu)-N₃. Puis, nous l'avons couplé avec deux autres Fmoc-Asp(OtBu)-OH et nous avons obtenu le deuxième *linker* Asp₃(OtBu)-N₃. Chaque *linker* a été couplé à PMMA-MA via une liaison amide (Fig. 1B). Enfin, le groupe tert-butyle a été éliminé, donnant *in fine* deux types de polymères: PMMA-AspN₃ et PMMA-Asp₃N₃.

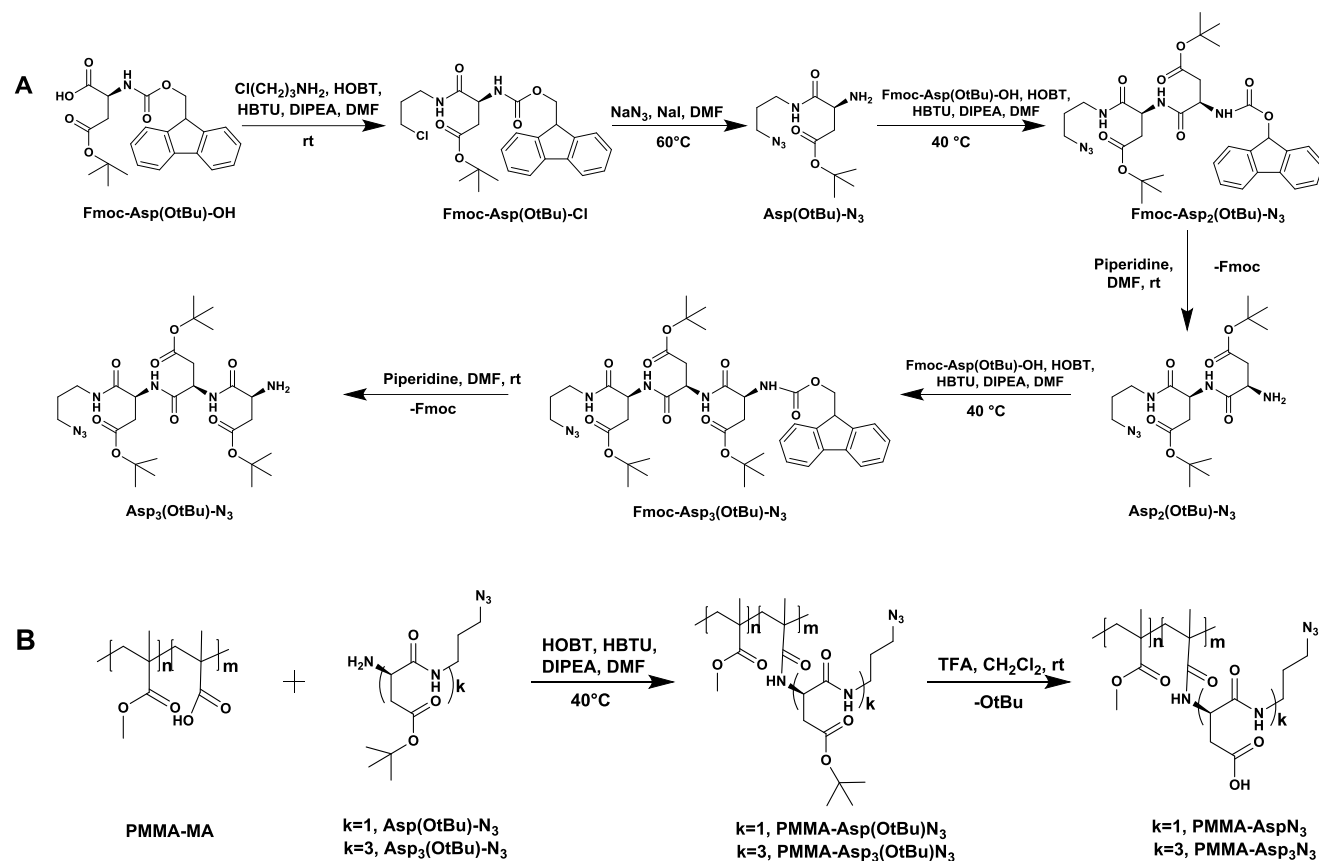


Fig.1. Schéma de synthèse A) *linkers* à trois fonctions Asp(OtBu)-N₃ et Asp₃(OtBu)-N₃ et B) polymères fonctionnalisés PMMA-AspN₃ et PMMA-Asp₃N₃.

Les nanoparticules ont été obtenues par nano-précipitation des polymères correspondants en solution dans l'acétonitrile avec un fluorophore (R18/F5-TPB) dans un tampon pH 7.4. La taille, la forme et la polydispersité des NPs ont été étudiées par DLS et TEM. (Fig. 2A-B) Afin de vérifier la présence de groupes azides à la surface, nous avons fait réagir les nanoparticules avec le Sulfo-Cy5(DBCO), qui est un accepteur de FRET. Nous avons étudié la cinétique de la réaction en suivant l'apparition du signal de FRET et nous avons montré que NP-AspN₃ réagissait beaucoup plus rapidement et efficacement que NP-Asp₃N₃. Pour prouver que le Sulfo-Cy5(DBCO) est fixé à la surface par liaison chimique, nous avons purifié le mélange réactionnel. Ceci a révélé que NP-AspN₃ était ~ 5 fois plus réactif avec le Sulfo-Cy5(DBCO) comparé à NP-Asp₃N₃ (Fig. 2C-F), ce qui fait de NP-AspN₃ le candidat idéal pour la fonctionnalisation des oligonucléotides. Sur la base de ces travaux, une publication est en préparation.

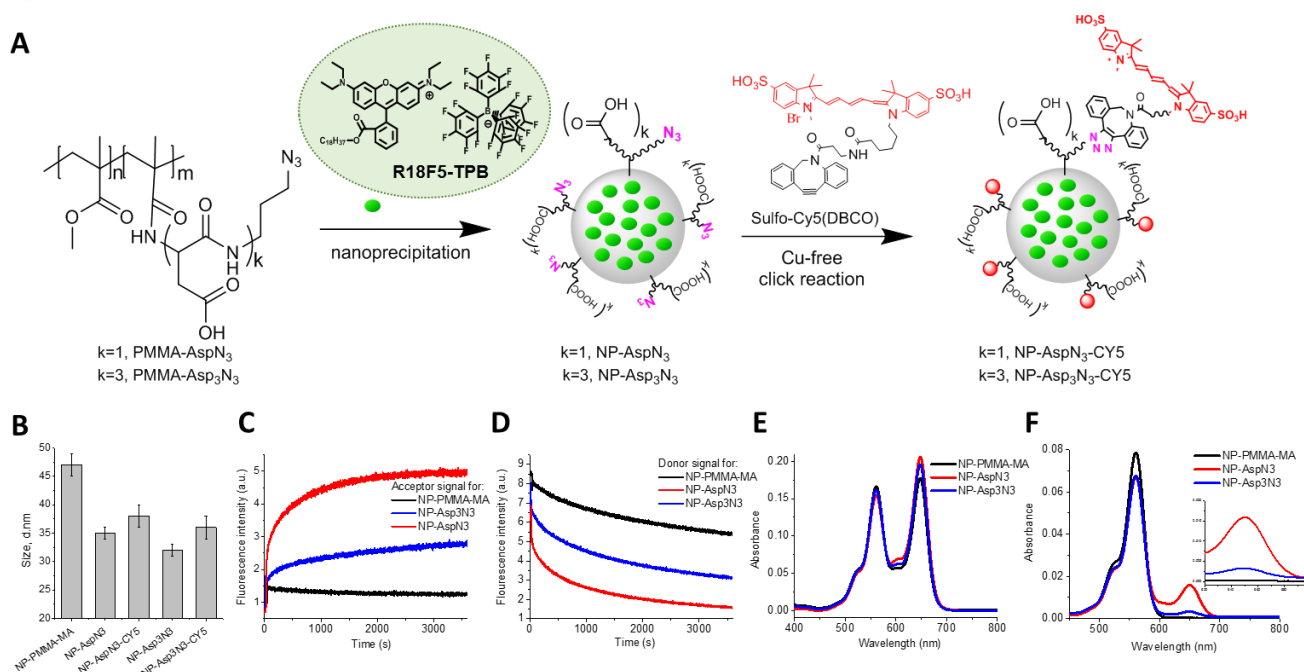


Fig.2. A) Formulation de nanoparticules et réaction ultérieure avec le sulfo-Cy5 (DBCO), B) taille par DLS, C) Cinétique de réaction de NP-PMMA-MA, NP-AspN₃ et NP-Asp₃N₃, suivie par émission de l'accepteur à 655 nm et D) du donneur à 584 nm. E) Spectres d'absorption de NP-PMMA-MA, NP-AspN₃ et NP-Asp₃N₃ après addition de 2 μM de Sulfo-Cy5 (DBCO) et F) après purification sur colonne d'exclusion stérique PD-10.

Nous avons proposé une conception de nano-sondes (Fig. 3) pour laquelle une nanoparticule de polymère est dopée en fluorophores (donneur FRET) et modifiée à sa surface avec un oligonucléotide complémentaire d'un fragment d'acide nucléique codant pour la survivine, un marqueur du cancer (SurC). SurC est hybridé avec une courte séquence cible-compétitive portant l'accepteur FRET Cy5 (TCS-Cy5), afin que l'accepteur soit localisé près de la surface des nanoparticules, garantissant ainsi une bonne efficacité du FRET. Ensuite, l'acide nucléique

cible déplace les accepteurs TCS-Cy5 et bloque le FRET, de sorte que la nano-sonde émette dans le vert. La combinaison de ces deux séquences d'oligonucléotides a été proposée à l'origine par Mirkin et ses collaborateurs dans *Nanoflares*, basés sur des NPs d'or.⁹⁵

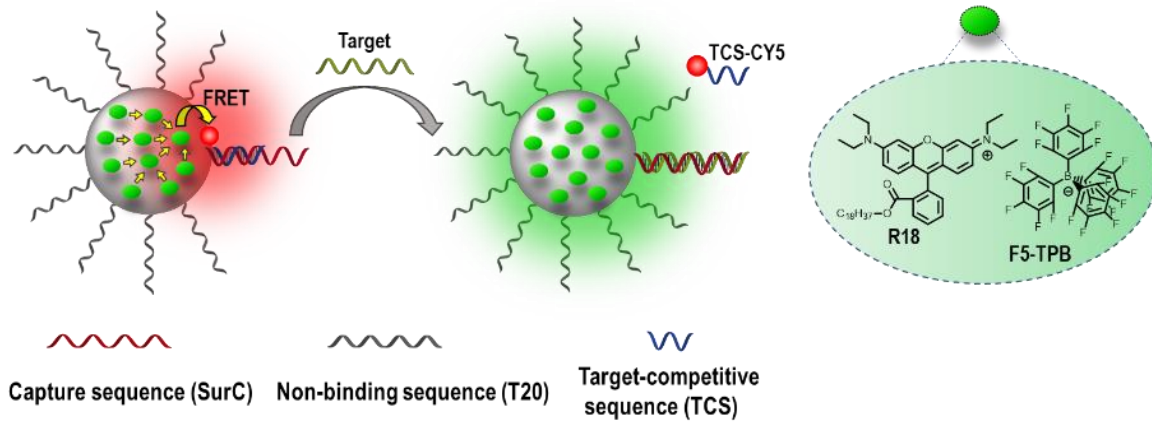


Fig.3. Conception de nano-antennes pour la détection amplifiée d'acides nucléiques.

Afin de synthétiser la nano-sonde, nous avons greffé des oligonucléotides sur le NP-Asp-N₃ concentré via une réaction avec des oligonucléotides SurC-DBCO et T20-DBCO porteurs de DBCO, suivis d'une hybridation avec un oligonucléotide plus court portant l'accepteur FRET TCS-Cy5 (Fig. 4A). La séquence non codante T20 a été nécessaire pour assurer la stabilité et la sensibilité de la nano-sonde dans un tampon PBS contenant 12 mM de Mg²⁺ nécessaire pour la stabilisation du duplex (Fig. 4B). Un greffage réussi des oligonucléotides a démontré la présence du signal de Cy5 dans les spectres d'absorption après purification ($\sim 23 \pm 3$ par NP) et l'apparition de la bande de FRET dans les spectres d'émission (Fig. 4C). La puissance de cette approche par amplification obtenue par nano-antennes a été démontrée par comparaison avec une sonde FRET moléculaire (Cy3-SurC / TCS-Cy5), pour laquelle SurC, conjugué avec le fluorophore Cy3, a été hybridé avec TCS-Cy5. Pour la même concentration d'accepteur (1 nM de TCS-Cy5), le signal de notre nano-sonde est plus de 100 fois supérieure à celui de la sonde moléculaire (Fig. 4D). TCS-Cy5 a été hybridé avec des NPs modifiés par SurC à différents rapports pour démontrer que l'hybridation de 3 à 5 TCS-Cy5 par particule produit une modification clairement détectable de l'émission duale de la nano-sonde, indiquant que seul un nombre limité des phénomènes de reconnaissance moléculaire sont à même de contrôler l'émission des ~ 3200 fluorophores donneurs présents dans les nano-antennes (Fig. 4E). Cette sensibilité des sondes basées sur les nano-antennes vis-à-vis d'un faible taux d'hybridation, associée à une forte amplification du signal, revêt une importance fondamentale pour la détection d'acides nucléiques cibles.

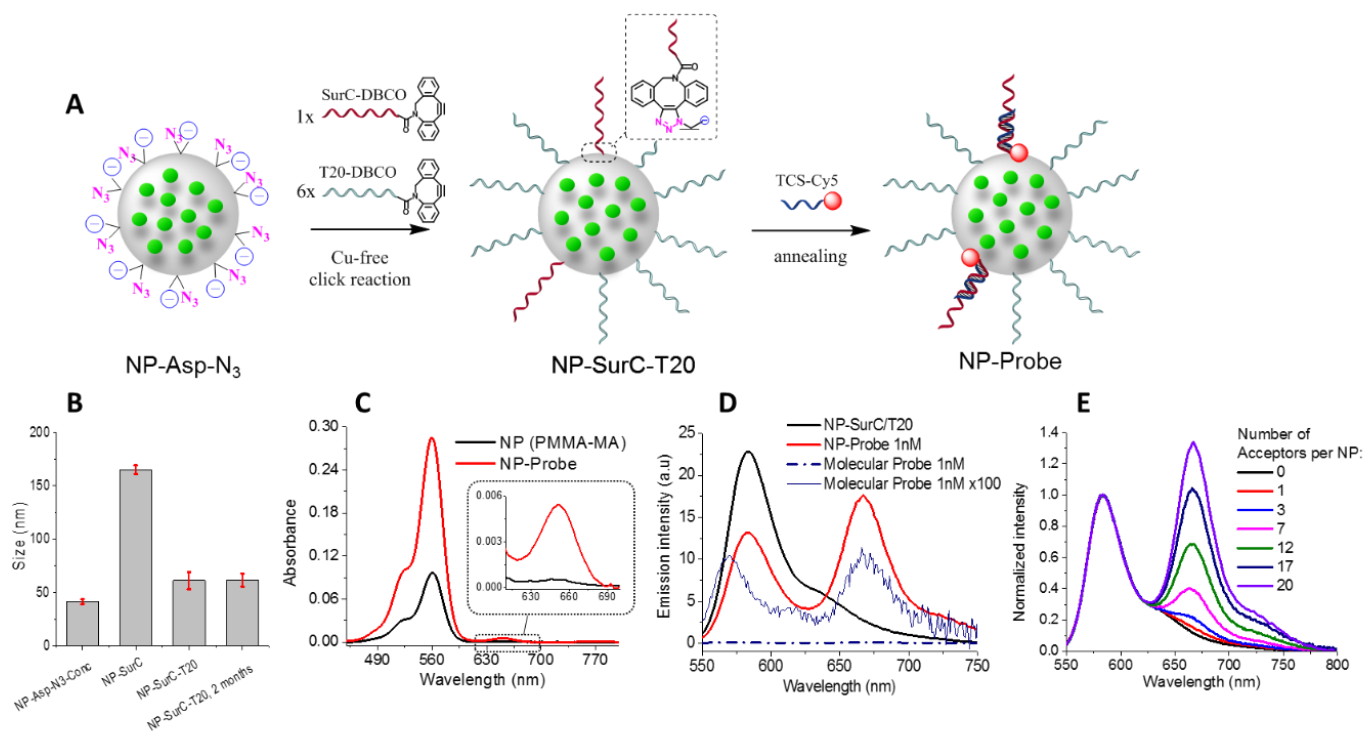


Fig.4. A) Schéma de synthèse de la nano-sonde, B) Taille par DLS de NP-AspN₃ concentrée, NP-SurC et NP-SurC-T20 (en dernier, stable après 2 mois de stockage). C) Spectres d'absorption du témoin (PMMA-MA) et de la nano-sonde après réaction avec SurC-DBCO et T20-DBCO, suivi d'une hybridation avec TCS-Cy5, puis purification, D) Spectres d'émission de fluorescence de NP-SurC/T20, nano-sonde à 1 nM de TCS-Cy5 et sonde moléculaire à 1 nM de TCS-Cy5 (conditions expérimentales et X100). E) Spectres de fluorescence normalisés de NP-SurC-T20 avec un nombre différent de TCS-Cy5 hybridé par particule.

En présence de l'acide nucléique cible (ADN ou ARN) codant pour la survivine, la nano-sonde perd le signal FRET à 670 nm, contrairement à l'échantillon témoin sans la cible. Une incubation supplémentaire de la nano-sonde avec un mésappariement de l'ADN cible démontre une bonne spécificité de séquence (Fig. 5A). Nous avons estimé la limite de détection à 5 pM en solution et démontré la stabilité de la nano-sonde dans différents milieux biologiques (Fig. 5B-C). Le test final pour la nano-sonde a été de déterminer sa performance au niveau de la particule unique. La microscopie à fluorescence de ces NPs immobilisées sur une surface de verre¹⁵⁹ a montré l'homogénéité de leur intensité de fluorescence (Fig. 5D), environ 100 fois plus forte que celle de QD605. L'incubation avec différentes concentration cibles de survivine a montré que la nano-sonde est fonctionnelle au niveau de la particule unique dans différents milieux biologiques avec une limite de détection de 0.25 pM (Fig. 5E-F).

En conclusion de cette partie, nous avons développé une méthodologie de fonctionnalisation chimique des nanoparticules polymères dopées en fluorophores avec des acides nucléiques. Les sondes obtenues ont montré des propriétés sans précédent, telles qu'une luminosité élevée, une amplification de la détection d'acide nucléique pour laquelle un FRET provenant d'environ

3000 donneurs à l'intérieur de NPs a été transféré avec succès à quelques accepteurs (environ 20) situés en surface. Ainsi, nous avons développé un système ultrabrillant pour la détection amplifiée d'acides nucléiques basée sur le FRET. Ces résultats ont récemment été publiés (Melnychuk et Klymchenko, J. Am. Chem. Soc., 2018, 140, 10856–65).

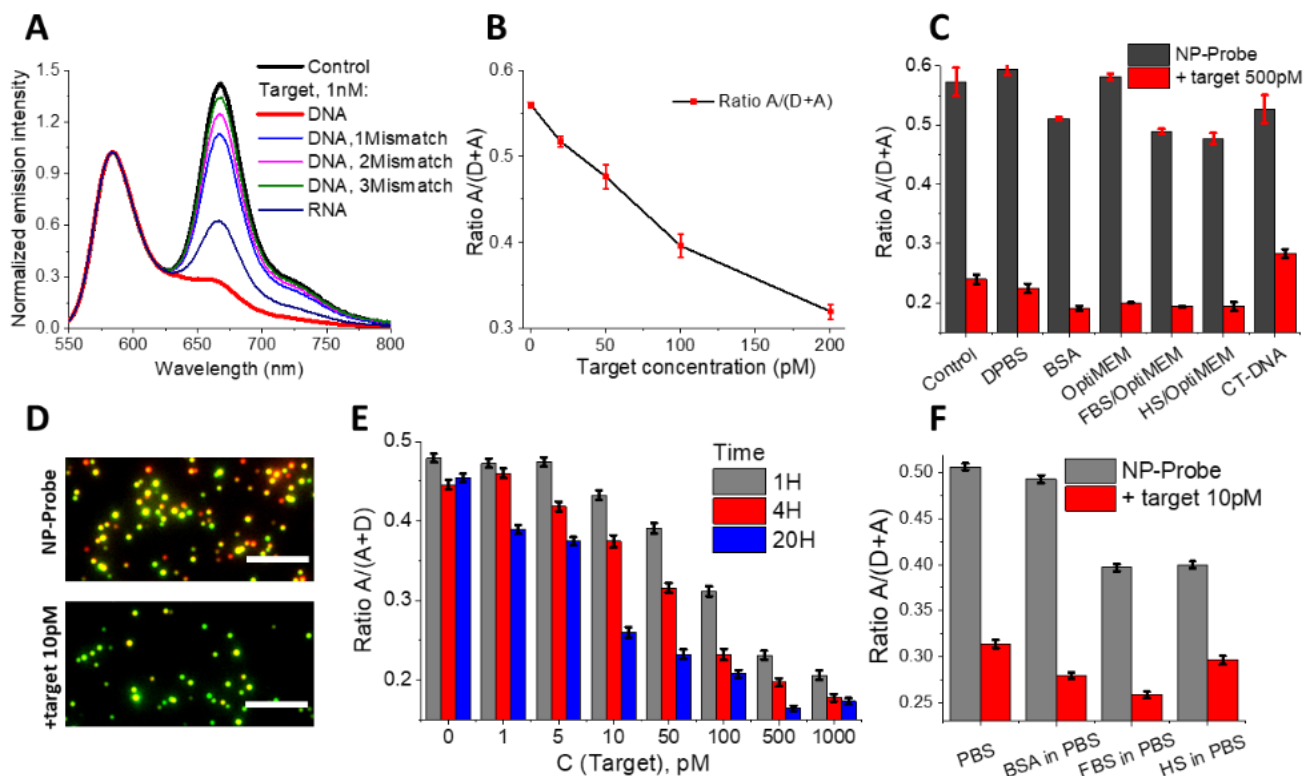


Fig.5. A) spectres d'émission de fluorescence de la nano-sonde après incubation avec un ADN et un ARN cibles et des ADN cibles contenant 1, 2 et 3 mésappariements; B) réponse FRET $A/(D + A)$ de la nano-sonde après incubation avec différentes quantités d'ADN cible et C) avec 500 pM d'ADN cible dans différents milieux biologiques, D) images du remplacement d'ADN cible à 10 pM au niveau de la particule unique, E) réponse ratiométrique de la nano-sonde immobilisée à différentes concentrations d'ADN cible pour trois temps d'incubation différents, F) réponses à l'ADN cible de la nano-sonde à 10 pM après 20 h d'incubations à 4 °C dans différents milieux biologiques.

Malgré l'excellente performance du test de détection d'acide nucléique obtenu à partir de ces nano-antennes, notre objectif ultime a été de développer un système permettant à une hybridation unique à la surface de la nanoparticule d'activer/désactiver le transfert d'énergie à partir de milliers de fluorophores à l'intérieur des nano-antennes. Cependant, pour obtenir une telle nano-sonde, nous avons dû la reconcevoir, en particulier le couple particule donneuse et fluorophore accepteur. En effet, le fluorophore accepteur Cy5 d'origine est apparu avoir une médiocre photo-stabilité au niveau de la particule unique lorsque des milliers de fluorophores transféraient leur énergie à 23 accepteurs. Afin de trouver un système photostable, ce qui est une nécessité absolue pour une nano-sonde basée sur un accepteur unique, nous avons effectué un criblage d'accepteurs potentiels pour notre approche (Fig. 6A). Nous avons contrôlé

3 familles de fluorophores: cyanine, DY et ATTO présentant différentes polarités et longueurs d'onde d'émission. Les nano-sondes avec 10 accepteurs différents ont été synthétisées et nous avons découvert que seuls les accepteurs chargés positivement ou neutres conviennent aux formulations des nano-sondes (Fig. 6B-C). Ensuite, nous avons comparé la photo-stabilité des fluorophores des familles ATTO et cyanine au niveau de la particule unique et nous avons trouvé que ATTO647N et ATTO665 sont beaucoup plus photostables que les fluorophores Cy5 ou Cy5.5 (Fig. 6D). Pour remplacer Cy5, nous avons donc choisi le fluorophore ATTO665 en raison de sa photo-stabilité exceptionnelle et de sa meilleure résolution spectrale afin d'améliorer la détection.

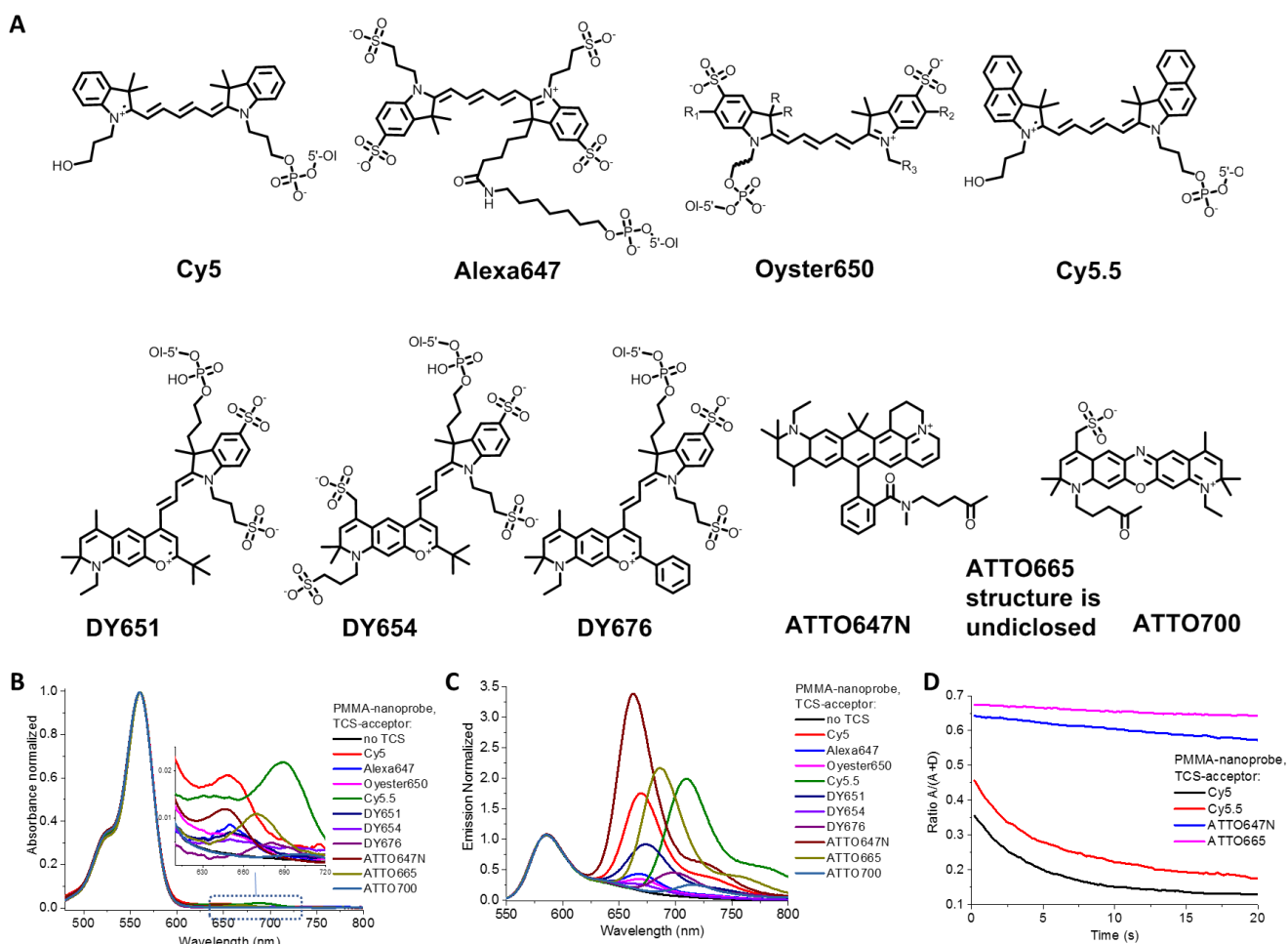


Fig.6. Criblage d'accepteurs dans les NPs polymères (PMMA-AspN₃) chargées en fluorophores et fonctionnalisées par un oligonucléotide. A) structures chimiques des accepteurs testés; B) spectres d'absorption et C) spectres d'émission de fluorescence de nano-sondes avec ces accepteurs; D) cinétique du rapport A/(A + D) lors de l'excitation de la nano-sonde au niveau de la particule unique à 550 nm avec 0.548 W/cm².

Nos précédents résultats ont démontré qu'une nano-antenne de 40 nm peut distinguer 3 à 5 phénomènes d'hybridation à sa surface. Nous avons donc cherché à réduire la taille de la nano-

antenne. Dans ce but, nous avons effectué la nano-précipitation du polymère PMMA-AspN₃ à un pH plus élevé (pH 9) et avons ainsi formulé des nano-sondes de taille inférieure (32 nm), que nous avons fonctionnalisées avec une quantité inférieure d'accepteur par particule (4). Les résultats obtenus ont montré que l'efficacité du FRET était insuffisante, ainsi une réduction supplémentaire de la taille était encore nécessaire. Nous avons donc synthétisé des polymères PMMA-MA avec une concentration 5% molaire d'acide méthacrylique comparé aux 1.6% du polymère initial, que nous avons modifié avec un linker suivant le protocole précédent (PMMA-AspN₃). Nous avons constaté que les NPs obtenus (PMMA-AspN₃) présentaient une taille nettement plus petite et une excellente efficacité de FRET avec 1-2 accepteurs, mais que leur photo-stabilité était faible. Nous avons alors synthétisé le polymère à base de polyméthacrylate d'éthyle (PEMA) avec 5% molaire d'acide méthacrylique (PEMA-AspN₃) (Fig. 7A). Les NPs obtenues avec ce polymère présentaient une excellente homogénéité de taille à 18 nm (Fig. 7B) et une photo-stabilité nettement améliorée au niveau de la particule unique par rapport aux NPs obtenues à partir de PMMA-AspN₃. Afin d'obtenir de meilleures brillance et amplification du signal de l'accepteur, nous avons augmenté la charge des NPs PEMA-AspN₃ à 50% en poids du fluorophore.

Les nano-sondes formulées avec PEMA-AspN₃, portant des oligonucléotides et statistiquement un unique accepteur ATTO665 (Fig. 7C-D), ont donné des résultats remarquables: à la fois un rendement quantique de fluorescence élevé (46%) et une efficacité de FRET élevée (51%) sur une distance au-delà du rayon de Förster (6.65 nm), ceci avec une amplification de l'émission de l'accepteur (effet d'antenne) de 208 ± 17 . Pour vérifier la présence d'un accepteur unique sur la nano-antenne, nous avons immobilisé ces nanoparticules et analysé leurs tracés par excitation à 550 nm. L'activation/désactivation en une étape du couple accepteur/donneur dans la nanoparticule a mis en évidence sa modification avec un accepteur unique dans au moins 50% des NPs (Fig. 7G). La présence d'un accepteur unique dans ces nano-sondes a été confirmée par l'analyse des tracés d'émission de l'accepteur par son excitation directe par laser à 640 nm (Fig. 7H). En outre, l'effet d'antenne au niveau de la particule unique est de 257 ± 30 (Fig. 7E-F). En utilisant ces NPs, nous avons pu détecter de façon spectaculaire un seul oligonucléotide hybridé, marqué avec l'accepteur, dans des conditions d'excitation comparable à la lumière ambiante.

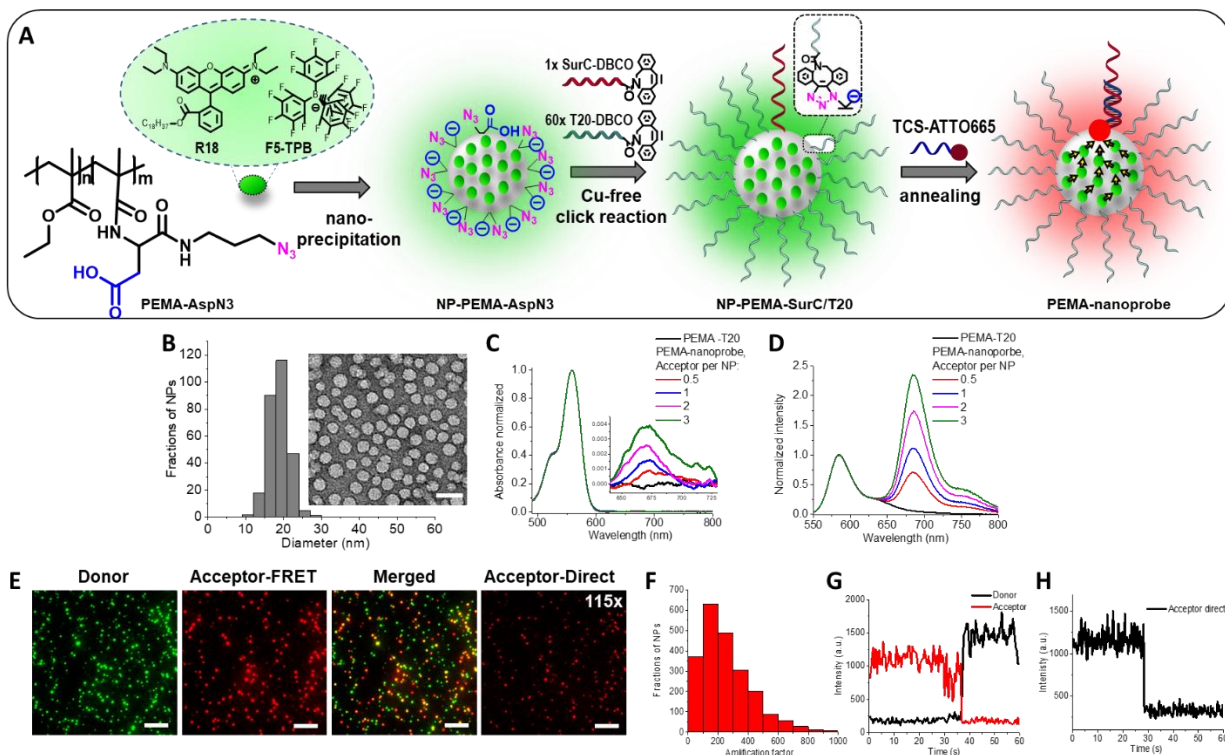


Fig.7. A) Schéma de synthèse de nano-sondes à base de PEMA; B) image TEM et statistique de distribution en taille de nano-sonde PEMA; C) Spectres d'absorption et D) spectres de fluorescence normalisés de nano-sonde PEMA avec différentes quantités de TCS-ATTO665 hybridé par particule; E) Images en microscopie de fluorescence à champ large de la nano-sonde au niveau du donneur (FRET-donneur), de l'accepteur amplifié par antenne (FRET-accepteur), de la fusion des canaux FRET-accepteur et donneur (à la même échelle d'intensité) et de l'accepteur (excitation directe à 640 nm). F) Amplification de l'émission de FRET-accepteur (effet d'antenne) par la nano-sonde au niveau de la particule unique, présenté sous forme d'histogramme de distribution. L'analyse a porté sur au moins 2500 NPs. G) Tracé représentatif de l'intensité d'une seule particule pour le donneur et l'accepteur excités à 550 nm et H) de l'accepteur excité à 640 nm.

Le système obtenu apporte une nouvelle voie pour la détection numérisée des acides nucléiques (Fig. 8A). Étant donné qu'un unique phénomène d'hybridation peut changer la couleur d'une nanoparticule, cela signifie qu'une seule molécule d'acide nucléique correspond à une seule nanoparticule. Nous avons procédé à l'imagerie de ces mêmes nano-sondes immobilisées dans des conditions de lumière ambiante avant et après incubation avec des ADN et ARN cibles pendant une heure à température ambiante. Ainsi, en suivant l'hybridation d'une seule particule, nous avons pratiquement pu calculer le nombre d'acides nucléiques cibles attachés aux nanoparticules, d'où une limite de détection au niveau d'une hybridation unique (Fig. 8B).

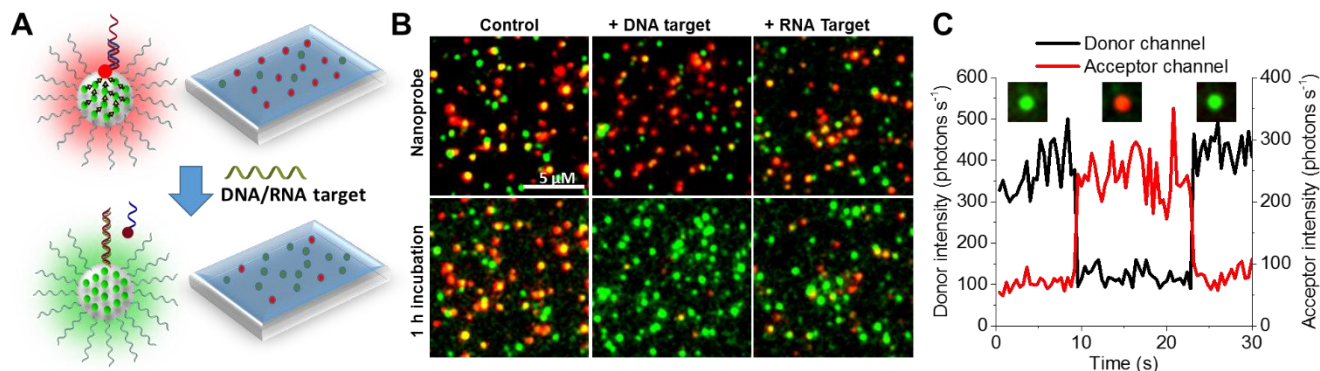


Fig.8. A) Concept de détection numérisée d'une cible à molécule unique ; B) Images de la nano-sonde avant et après une heure d'incubation avec un tampon (témoin), 100 pM d'ADN et ARN cibles ; C) Images fusionnées bicolores (donneur + accepteur) représentatives d'une seule particule (au-dessus) et tracés de l'intensité du donneur et de l'accepteur lors de l'imagerie de nano-sondes en présence de 10 nM de TCS-ATTO665.

Le test final a consisté en l'imagerie directe du processus pour un unique phénomène d'hybridation sous microscope. Au cours de l'imagerie, nous avons ajouté le TCS-ATTO665 et par enregistrement du signal de l'accepteur, nous avons pu suivre l'hybridation directe d'un seul oligonucléotide. Le tracé d'intensité en une étape a prouvé la mise en évidence d'accepteurs uniques, suivie du photoblanchissement de l'accepteur unique à la surface de la nanoparticule (Fig. 8C). Cette capacité exceptionnelle de la nano-antenne que nous avons développée à transférer l'énergie d'un millier de donneurs à un seul accepteur a permis l'observation directe, sans précédent, de l'hybridation d'un oligonucléotide unique au microscope dans des conditions de lumière ambiante. Globalement, grâce à une conception rationnelle de la nano-sonde, l'objectif principal de ma thèse a été atteint: les NPs développés ont permis la détection de molécules uniques d'acides nucléiques. Une publication sur ce travail est en préparation.

3. Conclusion générale

Au cours des trois années de mon travail de thèse, j'ai développé une approche pour fonctionnaliser des nanoparticules de polymères, dopées en fluorophores, avec des acides nucléiques et ainsi créer des nano-sondes pour la détection amplifiée des acides nucléiques. J'ai démontré leur capacité à détecter spécifiquement des séquences d'acides nucléiques cibles en présence de protéines et de mélanges d'acides nucléiques non spécifiques en solution et sur surface de verre, au niveau de la particule unique. Ainsi, pour parvenir à une sensibilité de telles nano-sondes au niveau d'une hybridation unique, j'ai apporté un certain nombre d'améliorations à leur conception. Tout d'abord, en testant 10 fluorophores différents, des accepteurs beaucoup plus photostables ont été trouvés, basés sur la famille ATTO. Ensuite, j'ai conçu des nanoparticules fonctionnalisées de plus petite taille en utilisant un polymère plus hydrophobe (PEMA), ce qui a permis d'obtenir une brillance et une photo-stabilité nettement améliorées. Les

nano-sondes ainsi nouvellement conçues ont montré leur capacité à détecter un seul phénomène d'hybridation en activant/désactivant le transfert d'énergie de milliers de fluorophores à l'intérieur de la nano-antenne à un accepteur unique. Ce travail apporte une nouvelle voie pour la détection numérisée d'oligonucléotides cibles simplement en comptant les nanoparticules vertes et rouges au niveau de la particule unique. Enfin, ces nouvelles nano-sondes ont permis la première observation d'un phénomène unique d'hybridation en commutant la couleur des nanoparticules au microscope dans des conditions d'excitation comparable à la lumière ambiante.

Sur la base des excellentes performances de ce système, les étapes suivantes de ce projet devraient être la détection des ARN messagers et des micro-ARN dans les cellules et leurs lysats, ainsi que la mise au point de kits de détection des différents acides nucléiques marqueurs de cancers.

REFERENCES

1. Jameson, D. M. *Introduction to Fluorescence*. (CRC Press, 2014).
2. Lakowicz, J. R. *Principles of Fluorescence Spectroscopy*. (Springer, 2006).
3. Valeur, B. *Molecular Fluorescence. Principles and Applications*. (Wiley, 2001).
4. Lavis, L. D. & Raines, R. T. Bright ideas for chemical biology-supplement. *ACS Chem. Biol.* **3**, 142–55 (2008).
5. Fu, Y. & Finney, N. S. Small-molecule fluorescent probes and their design. *RSC Adv.* **8**, 29051–29061 (2018).
6. Klymchenko, A. S. Solvatochromic and Fluorogenic Dyes as Environment-Sensitive Probes: Design and Biological Applications. *Acc. Chem. Res.* **50**, 366–375 (2017).
7. Demchenko, A. P. *Introduction to fluorescence sensing*. (Springer, 2009).
8. Medintz, I. & Hildebrandt, N. *FRET – Förster Resonance Energy Transfer From Theory to Applications*. (Wiley-VCH, 2014).
9. Chen, B. *et al.* Energy transfer-based biodetection using optical nanomaterials. *J. Mater. Chem. B* **6**, 2924–2944 (2018).
10. Hildebrandt, N. *et al.* Energy transfer with semiconductor quantum dot bioconjugates: A versatile platform for biosensing, energy harvesting, and other developing applications. *Chem. Rev.* **117**, 536–711 (2017).
11. Liu, Z., Lavis, L. D. & Betzig, E. Imaging Live-Cell Dynamics and Structure at the Single-Molecule Level. *Mol. Cell* **58**, 644–659 (2015).
12. Elson, E. L. Fluorescence correlation spectroscopy: Past, present, future. *Biophys. J.* **101**, 2855–2870 (2011).
13. Wöll, D. Fluorescence correlation spectroscopy in polymer science. *RSC Adv.* **4**, 2447–2465 (2014).
14. Coelho, M., Maghelli, N. & Tolić-Nørrelykke, I. M. Single-molecule imaging in vivo: The dancing building blocks of the cell. *Integr. Biol.* **5**, 748–758 (2013).
15. Von Diezmann, A., Shechtman, Y. & Moerner, W. E. Three-Dimensional Localization of Single Molecules for Super-Resolution Imaging and Single-Particle Tracking. *Chem. Rev.* **117**, 7244–7275 (2017).
16. Axelrod, D. Cell-substrate contacts illuminated by total internal reflection fluorescence. *J. Cell Biol.* **89**, 141–145 (1981).
17. Moerner, W. E. & Fromm, D. P. Methods of single-molecule fluorescence spectroscopy and microscopy. *Rev. Sci. Instrum.* **74**, 3597–3619 (2003).
18. Kondo, T., Chen, W. J. & Schlau-Cohen, G. S. Single-molecule fluorescence spectroscopy of photosynthetic systems. *Chem. Rev.* **117**, 860–898 (2017).
19. Betzig, E. *et al.* Imaging intracellular fluorescent proteins at nanometer resolution. *Science (80-.)*. **313**, 1642–1645 (2006).
20. Rust, M. J., Bates, M. & Zhuang, X. Sub-diffraction-limit imaging by stochastic optical reconstruction microscopy (STORM). *Nat. Methods* **7**, 2006 (2006).
21. Vanden Bout, D. A. *et al.* Discrete intensity jumps and intramolecular electronic energy transfer in the spectroscopy of single conjugated polymer molecules. *Science (80-.)*. **277**, 1074–1077 (1997).
22. Zhang, H. U. I., Shu, D. A. N., Huang, F. & Guo, P. Instrumentation and metrology for single RNA counting in biological complexes or nanoparticles by a single-molecule dual-view system. *RNA* **13**, 1793–1802 (2007).
23. Hellenkamp, B. *et al.* Precision and accuracy of single-molecule FRET measurements—a multi-laboratory benchmark study. *Nat. Methods* **15**, 669–676 (2018).
24. Sasmal, D. K., Pulido, L. E., Kasal, S. & Huang, J. Single-molecule fluorescence resonance energy transfer in molecular biology. *Nanomaterials* **8**, 19928–19944 (2016).
25. Roy, R., Hohng, S. & Ha, T. A practical guide to single-molecule FRET. *Nat. Methods* **5**, 507–16 (2008).

26. Gust, A. *et al.* A Starting Point for Fluorescence-Based Single-Molecule Measurements in Biomolecular Research. *Molecules* **19**, 15824–15865 (2014).
27. Jin, D., Xi, P., Wang, B., Zhang, L. & Oijen, A. M. Van. Nanoparticles for super-resolution microscopy and single-molecule tracking. *Nat. Methods* **15**, 415–423 (2018).
28. Wegner, K. D. & Hildebrandt, N. Quantum dots: Bright and versatile in vitro and in vivo fluorescence imaging biosensors. *Chem. Soc. Rev.* **44**, 4792–4834 (2015).
29. Zhang, R. *et al.* Two-photon 3D fiona of individual quantum dots in an aqueous environment. *Nano Lett.* **11**, 4074–4078 (2011).
30. He, H. *et al.* High-Density Super-Resolution Localization Imaging with Blinking Carbon Dots. *Anal. Chem.* **89**, 11831–11838 (2017).
31. Reisch, A. *et al.* Collective fluorescence switching of counterion-assembled dyes in polymer nanoparticles. *Nat. Commun.* **5**, 4089 (2014).
32. Fang, X. *et al.* Multicolor Photo-Crosslinkable AIEgens toward Compact Nanodots for Subcellular Imaging and STED Nanoscopy. *Small* **13**, 1–7 (2017).
33. Wolfbeis, O. S. An overview of nanoparticles commonly used in fluorescent bioimaging. *Chem. Soc. Rev.* **44**, 4743–4768 (2015).
34. Goggins, S. & Frost, C. G. Approaches towards molecular amplification for sensing. *Analyst* **141**, 3157–3218 (2016).
35. Van Amerongen, H. & Croce, R. Light harvesting in photosystem II. *Photosynth. Res.* **116**, 251–263 (2013).
36. Scholes, G. D., Fleming, G. R., Olaya-Castro, A. & Van Grondelle, R. Lessons from nature about solar light harvesting. *Nat. Chem.* **3**, 763–774 (2011).
37. Scrimin, P. & Prins, L. J. Sensing through signal amplification. *Chem. Soc. Rev. Chem. Soc. Rev.* **40**, 4488–4505 (2011).
38. Abolhasan, R., Mehdizadeh, A., Rashidi, M. R., Aghebati-Maleki, L. & Yousefi, M. Application of hairpin DNA-based biosensors with various signal amplification strategies in clinical diagnosis. *Biosens. Bioelectron.* **129**, 164–174 (2019).
39. Nam, J. M., Thaxton, C. S. & Mirkin, C. A. Nanoparticle-based bio-bar codes for the ultrasensitive detection of proteins. *Science (80-.).* **301**, 1884–1886 (2003).
40. Song, Y. *Advances in DNA Detection. KTH Royal Institute of Technology* (2014).
41. Li, J., Macdonald, J. & Von Stetten, F. Review: a comprehensive summary of a decade development of the recombinase polymerase amplification. *Analyst* **144**, 31–67 (2019).
42. Wong, M. L. & Medrano, J. F. Real-time PCR for mRNA quantitation. *Biotechniques* **39**, 75–85 (2005).
43. Gill, P. & Ghaemi, A. Nucleic acid isothermal amplification technologies - A review. *Nucleosides, Nucleotides and Nucleic Acids* **27**, 224–243 (2008).
44. Dirks, R. M. & Pierce, N. A. Triggered amplification by hybridization chain reaction. *PNAS* **101**, 15275–15278 (2004).
45. Nolan, T., Hands, R. E. & Bustin, S. A. Quantification of mRNA using real-time RT-PCR. *Nat. Protoc.* **1**, 1559–1582 (2006).
46. Bachman, J. *Reverse-Transcription PCR (RT-PCR). Methods in Enzymology* **530**, (Academic Press, 2013).
47. Chen, H. L. *et al.* Nucleic acid amplification-based methods for microRNA detection. *Anal. Methods* **7**, 2258–2263 (2015).
48. Butier, J. M. *PCR Amplification: Capabilities and Cautions. Advanced Topics in Forensic DNA Typing: Methodology* (Elsevier, 2012). doi:10.1016/B978-0-12-374513-2.00004-X
49. Kaur, H. & Shorie, M. Nanomaterial based aptasensors for clinical and environmental diagnostic applications. *Nanoscale Adv.* **1**, 2123–2138 (2019).
50. Zhu, Z. *et al.* Plasmon-Enhanced Fluorescence in Coupled Nanostructures and Applications in DNA Detection. *ACS Appl. Bio Mater* **1**, 118–124 (2019).
51. Park, J. E., Kim, J. & Nam, J. M. Emerging plasmonic nanostructures for controlling and enhancing

- photoluminescence. *Chem. Sci.* **8**, 4696–4704 (2017).
52. Zhou, C. *et al.* Signal amplification strategies for DNA-based surface plasmon resonance biosensors. *Biosens. Bioelectron.* **117**, 678–689 (2018).
 53. Punj, D. *et al.* A plasmonic ‘antenna-in-box’ platform for enhanced single-molecule analysis at micromolar concentrations. *Nat. Nanotechnol.* **8**, 512–516 (2013).
 54. Kinkhabwala, A. *et al.* Large single-molecule fluorescence enhancements produced by a bowtie nanoantenna. *Nat. Photonics* **3**, 654–657 (2009).
 55. Punj, D. *et al.* Self-Assembled Nanoparticle Dimer Antennas for Plasmonic-Enhanced Single-Molecule Fluorescence Detection at Micromolar Concentrations. *ACS Photonics* **2**, 1099–1107 (2015).
 56. G. P. Acuna, F. M. Möller, P. Holzmeister, S. Beater, B. Lalkens, Tinnefeld, P. Fluorescence Enhancement at Docking Sites of DNA-Directed Self-Assembled Nanoantennas. *Science (80-.)*. **338**, 506–511 (2012).
 57. Ochmann, S. E. *et al.* Optical Nanoantenna for Single Molecule-Based Detection of Zika Virus Nucleic Acids without Molecular Multiplication. *Anal. Chem.* **89**, 13000–13007 (2017).
 58. Lu, L., Qian, Y., Wang, L., Ma, K. & Zhang, Y. Metal-enhanced fluorescence-based core-shell Ag@SiO₂ nanoflakes for affinity biosensing via target-induced structure switching of aptamer. *ACS Appl. Mater. Interfaces* **6**, 1944–1950 (2014).
 59. Govorov, A. O., Lee, J. & Kotov, N. A. Theory of plasmon-enhanced Förster energy transfer in optically excited semiconductor and metal nanoparticles. *Phys. Rev. B - Condens. Matter Mater. Phys.* **76**, 1–16 (2007).
 60. Zhang, J., Fu, Y. & Lakowicz, J. R. Enhanced Förster resonance energy transfer (FRET) on a single metal particle. *J. Phys. Chem. C* **111**, 50–56 (2007).
 61. Li, M., Cushing, S. K. & Wu, N. Plasmon-enhanced optical sensors: A review. *Analyst* **140**, 386–406 (2015).
 62. Zhao, T., Li, T. & Liu, Y. Silver nanoparticle plasmonic enhanced Förster resonance energy transfer (FRET) imaging of protein-specific sialylation on the cell surface. *Nanoscale* **9**, 9841–9847 (2017).
 63. Lunz, M. *et al.* Surface plasmon enhanced energy transfer between donor and acceptor CdTe nanocrystal quantum dot monolayers. *Nano Lett.* **11**, 3341–3345 (2011).
 64. L. Viger, M., Brouard, D. & Boudreau, D. Plasmon-enhanced resonance energy transfer from a conjugated polymer to fluorescent multilayer core-shell nanoparticles: A photophysical study. *J. Phys. Chem. C* **115**, 2974–2981 (2011).
 65. Hu, J. *et al.* Combining gold nanoparticle antennas with single-molecule fluorescence resonance energy transfer (smFRET) to study DNA hairpin dynamics. *Nanoscale* **10**, 6611–6619 (2018).
 66. Lee, J. H., Cho, H. Y., Choi, H. K., Lee, J. Y. & Choi, J. W. Application of gold nanoparticle to plasmonic biosensors. *Int. J. Mol. Sci.* **19**, (2018).
 67. Kundu, S. & Patra, A. Nanoscale strategies for light harvesting. *Chem. Rev.* **117**, 712–757 (2017).
 68. Trofymchuk, K. *et al.* Giant light-harvesting nanoantenna for single-molecule detection in ambient light. *Nat. Photonics* **11**, 657–663 (2017).
 69. Abd-El-Aziz, A. S., Abdelghani, A. A., Wagner, B. D. & Bissessur, R. Advances in Light-Emitting Dendrimers. *Macromol. Rapid Commun.* **40**, 58–61 (2019).
 70. Wang, H. *et al.* Integrating dye-intercalated DNA dendrimers with electrospun nanofibers: A new fluorescent sensing platform for nucleic acids, proteins, and cells. *J. Mater. Chem. B* **3**, 3541–3547 (2015).
 71. Divsar, F. & Ju, H. Electrochemiluminescence detection of near single DNA molecules by using quantum dots-dendrimer nanocomposites for signal amplification. *Chem. Commun.* **47**, 9879–9881 (2011).
 72. Xu, Z. *et al.* Broad-Spectrum Tunable Photoluminescent Nanomaterials Constructed from a Modular Light-Harvesting Platform Based on Macrocyclic Amphiphiles. *Adv. Mater.* **28**, 7666–7671 (2016).
 73. Algar, W. R., Hildebrandt, N., Vogel, S. S. & Medintz, I. L. FRET as a biomolecular research tool

- understanding its potential while avoiding pitfalls. *Nat. Methods* **16**, 815–829 (2019).
74. Teunissen, A. J. P., Pérez-Medina, C., Meijerink, A. & Mulder, W. J. M. Investigating supramolecular systems using Förster resonance energy transfer. *Chem. Soc. Rev.* **47**, 7027–7044 (2018).
 75. Hochreiter, B., Garcia, A. P. & Schmid, J. A. Fluorescent proteins as genetically encoded FRET biosensors in life sciences. *Sensors* **15**, 26281–26314 (2015).
 76. Sapsford, K. E., Berti, L. & Medintz, I. L. Materials for fluorescence resonance energy transfer analysis: Beyond traditional donor-acceptor combinations. *Angew. Chemie - Int. Ed.* **45**, 4562–4588 (2006).
 77. Su, Q., Feng, W., Yang, D. & Li, F. Resonance energy transfer in upconversion nanoplatforms for selective biodetection. *Acc. Chem. Res.* **50**, 32–40 (2017).
 78. Shi, J., Tian, F., Lyu, J. & Yang, M. Nanoparticle based fluorescence resonance energy transfer (FRET) for biosensing applications. *J. Mater. Chem. B* **3**, 6989–7005 (2015).
 79. Kim, D., Shin, K., Kwon, S. G. & Hyeon, T. Synthesis and Biomedical Applications of Multifunctional Nanoparticles. *Adv. Mater.* **30**, 1802309 (2018).
 80. Medintz, I. L., Uyeda, H. T., Goldman, E. R. & Mattoussi, H. Quantum dot bioconjugates for imaging, labelling and sensing. *Nat. Mater.* **4**, 435–446 (2005).
 81. Chou, K. F. & Dennis, A. M. Förster resonance energy transfer between quantum dot donors and quantum dot acceptors. *Sensors* **15**, 13288–13325 (2015).
 82. Qiu, X. & Hildebrandt, N. Rapid and Multiplexed MicroRNA Diagnostic Assay Using Quantum Dot-Based Förster Resonance Energy Transfer. *ACS Nano* **9**, 8449–8457 (2015).
 83. Medintz, I. L. *et al.* Self-assembled nanoscale biosensors based on quantum dot FRET donors. *Nat. Mater.* **2**, 630–638 (2003).
 84. Samanta, A. & Medintz, I. L. Nanoparticles and DNA - a powerful and growing functional combination in bionanotechnology. *Nanoscale* **8**, 9037–9095 (2016).
 85. Su, S. *et al.* DNA-conjugated quantum dot nanoprobe for high-sensitivity fluorescent detection of DNA and micro-RNA. *ACS Appl. Mater. Interfaces* **6**, 1152–1157 (2014).
 86. Zhang, C. Y., Yeh, H. C., Kuroki, M. T. & Wang, T. H. Single-quantum-dot-based DNA nanosensor. *Nat. Mater.* **4**, 826–831 (2005).
 87. Qiu, X. *et al.* Multiplexed Nucleic Acid Hybridization Assays Using Single-FRET-Pair Distance-Tuning. *Small* **13**, 1–6 (2017).
 88. Chen, Z. *et al.* Versatile synthesis strategy for carboxylic acid-functionalized upconverting nanophosphors as biological labels. *J. Am. Chem. Soc.* **130**, 3023–3029 (2008).
 89. Xu, S. *et al.* NaYF₄:Yb,Tm nanocrystals and TiO₂ inverse opal composite films: A novel device for upconversion enhancement and solid-based sensing of avidin. *Nanoscale* **6**, 5859–5870 (2014).
 90. Laurenti, M. *et al.* Enhancement of the Upconversion Emission by Visible-to-Near-Infrared Fluorescent Graphene Quantum Dots for miRNA Detection. *ACS Appl. Mater. Interfaces* **8**, 12644–12651 (2016).
 91. Yang, Y., Zhong, S., Wang, K. & Huang, J. Gold nanoparticle based fluorescent oligonucleotide probes for imaging and therapy in living systems. *Analyst* **144**, 1052–1072 (2019).
 92. Seferos, D. S., Giljohann, D. A., Hill, H. D., Prigodich, A. E. & Mirkin, C. A. Nano-Flares: Probes for Transfection and mRNA Detection in Living Cells. *J. Am. Chem. Soc.* **129**, 15477–15479 (2007).
 93. Prigodich, A. E. *et al.* Nano-flares for mRNA Regulation and Detection. *ACS Nano* **3**, 2147–2152 (2009).
 94. Samanta, D., Ebrahimi, S. B. & Mirkin, C. A. Nucleic-Acid Structures as Intracellular Probes for Live Cells. *Adv. Mater.* 1901743 (2019). doi:10.1002/adma.201901743
 95. Prigodich, A. E. *et al.* Multiplexed Nanoflares: mRNA Detection in Live Cells. *Anal. Chem.* **84**, 2062–2066 (2012).
 96. Yang, Y. *et al.* FRET Nanoflares for Intracellular mRNA Detection: Avoiding False Positive Signals and Minimizing Effects of System Fluctuations. *J. Am. Chem. Soc.* **137**, 8340–3 (2015).

97. Wu, W., Bazan, G. C. & Liu, B. Conjugated-Polymer-Amplified Sensing, Imaging, and Therapy. *Chem* **2**, 760–790 (2017).
98. Donus Tuncel, D. & Demir, H. V. Conjugated polymer nanoparticles. *Nanoscale* **2**, 484–494 (2010).
99. Reisch, A. & Klymchenko, A. S. Fluorescent Polymer Nanoparticles Based on Dyes: Seeking Brighter Tools for Bioimaging. *Small* **12**, 1968–1992 (2016).
100. Chan, Y. H. *et al.* Development of ultrabright semiconducting polymer dots for ratiometric pH sensing. *Anal. Chem.* **83**, 1448–1455 (2011).
101. Frausto, F. & Thomas, S. W. Ratiometric Singlet Oxygen Detection in Water Using Acene-Doped Conjugated Polymer Nanoparticles. *ACS Appl. Mater. Interfaces* **9**, 15768–15775 (2017).
102. Rochat, S. & Swager, T. M. Conjugated Amplifying Polymers for Optical Sensing Applications. *ACS Appl. Mater. Interfaces* **5**, 4488–4502 (2013).
103. Gaylord, B. S., Heeger, A. J. & Bazan, G. C. DNA detection using water-soluble conjugated polymers and peptide nucleic acid probes. *PNAS* **99**, 10954–10957 (2002).
104. Doré, K. *et al.* Fluorescent Polymeric Transducer for the Rapid, Simple, and Specific Detection of Nucleic Acids at the Zeptomole Level. *J. Am. Chem. Soc.* **126**, 4240–4244 (2004).
105. Bao, B. *et al.* Conjugated Polymer Nanoparticles for Label-Free and Bioconjugate-Recognized DNA Sensing in Serum. *Adv. Sci.* **2**, 2–7 (2015).
106. Brouard, D., Ratelle, O., Bracamonte, A. G., St-Louis, M. & Boudreau, D. Direct molecular detection of SRY gene from unamplified genomic DNA by metal-enhanced fluorescence and FRET. *Anal. Methods* **5**, 6896–6899 (2013).
107. Wang, Y. & Liu, B. Silica nanoparticle assisted DNA assays for optical signal amplification of conjugated polymer based fluorescent sensors. *ChemComm* 3553–3555 (2007). doi:10.1039/b705936a
108. Battistelli, G., Cantelli, A., Guidetti, G., Manzi, J. & Montalti, M. Ultra-bright and stimuli-responsive fluorescent nanoparticles for bioimaging. *Wiley Interdiscip. Rev. Nanomedicine Nanobiotechnology* **8**, 139–150 (2016).
109. Montalti, M., Prodi, L., Rampazzo, E. & Zaccheroni, N. Dye-doped silica nanoparticles as luminescent organized systems for nanomedicine. *Chem. Soc. Rev.* **43**, 4243–4268 (2014).
110. Genovese, D. *et al.* Energy transfer processes in dye-doped nanostructures yield cooperative and versatile fluorescent probes. *Nanoscale* **6**, 3022–3036 (2014).
111. Rampazzo, E. *et al.* A versatile strategy for signal amplification based on core/shell silica nanoparticles. *Chem. - A Eur. J.* **17**, 13429–13432 (2011).
112. Gao, F. *et al.* A DNA hybridization detection based on fluorescence resonance energy transfer between dye-doped core-shell silica nanoparticles and gold nanoparticles. *Analyst* **136**, 3973–3980 (2011).
113. Mao, D. & Ding, D. AIE Nanoparticles for in Vitro and in Vivo Imaging. in *Aggregation-Induced Emission: Materials and Applications* **2**, 217–243 (2016).
114. Mei, J., Leung, N. L. C., Kwok, R. T. K., Lam, J. W. Y. & Tang, B. Z. Aggregation-Induced Emission: Together We Shine, United We Soar! *Chem. Rev.* **115**, 11718–11940 (2015).
115. Chen, Y., Lam, J. W. Y., Kwok, R. T. K., Liu, B. & Tang, B. Z. Aggregation-induced emission: Fundamental understanding and future developments. *Mater. Horizons* **6**, 428–433 (2019).
116. Li, K. & Liu, B. Polymer-encapsulated organic nanoparticles for fluorescence and photoacoustic imaging. *Chem. Soc. Rev.* **43**, 6570–6597 (2014).
117. Geng, J. *et al.* Near-infrared fluorescence amplified organic nanoparticles with aggregation-induced emission characteristics for in vivo imaging. *Nanoscale* **6**, 939–945 (2014).
118. Wu, W. C. *et al.* Enhancement of aggregation-induced emission in dye-encapsulating polymeric micelles for bioimaging. *Adv. Funct. Mater.* **20**, 1413–1423 (2010).
119. Li, J. J., Chen, Y., Yu, J., Cheng, N. & Liu, Y. A Supramolecular Artificial Light-Harvesting System with an Ultrahigh Antenna Effect. *Adv. Mater.* **29**, 1–5 (2017).
120. Guo, S., Song, Y., He, Y., Hu, X. Y. & Wang, L. Highly Efficient Artificial Light-Harvesting Systems

- Constructed in Aqueous Solution Based on Supramolecular Self-Assembly. *Angew. Chemie - Int. Ed.* **57**, 3163–3167 (2018).
121. Li, C., Zhang, J., Zhang, S. & Zhao, Y. Efficient Light-Harvesting Systems with Tunable Emission through Controlled Precipitation in Confined Nanospace. *Angew. Chemie - Int. Ed.* **58**, 1643–1647 (2019).
 122. Xu, L. *et al.* AEE Conjugated Polymeric Supramolecular Network: an Efficient Light-Harvesting System with Ultrahigh Antenna Effect. *Angew. Chemie Int. Ed.* (2019). doi:10.1002/anie.201907678
 123. Li, K. & Liu, B. Polymer-encapsulated organic nanoparticles for fluorescence and photoacoustic imaging. *Chem. Soc. Rev.* **43**, 6570–6597 (2014).
 124. Peng, H. S. & Chiu, D. T. Soft fluorescent nanomaterials for biological and biomedical imaging. *Chem. Soc. Rev.* **44**, 4699–4722 (2015).
 125. Wagh, A. *et al.* Polymeric nanoparticles with sequential and multiple FRET cascade mechanisms for multicolor and multiplexed imaging. *Small* **9**, 2129–2139 (2013).
 126. Wang, Z. *et al.* Color-tunable AIE-active conjugated polymer nanoparticles as drug carriers for self-indicating cancer therapy: Via intramolecular FRET mechanism. *Polym. Chem.* **9**, 3205–3214 (2018).
 127. Canfarotta, F., Whitcombe, M. J. & Piletsky, S. A. Polymeric nanoparticles for optical sensing. *Biotechnol. Adv.* **31**, 1585–1599 (2013).
 128. Valanne, A., Malmi, P., Appelblom, H., Niemelä, P. & Soukka, T. A dual-step fluorescence resonance energy transfer-based quenching assay for screening of caspase-3 inhibitors. *Anal. Biochem.* **375**, 71–81 (2008).
 129. Bhattacharyya, S., Jana, B. & Patra, A. Multichromophoric organic molecules encapsulated in polymer nanoparticles for artificial light harvesting. *ChemPhysChem* **16**, 796–804 (2015).
 130. Su, J. *et al.* Giant Amplification of Photoswitching by a Few Photons in Fluorescent Photochromic Organic Nanoparticles. *Angew. Chemie - Int. Ed.* **55**, 3662–3666 (2016).
 131. Frigoli, M., Ouadahi, K. & Larpent, C. A cascade FRET-mediated ratiometric sensor for Cu²⁺ ions based on dual fluorescent ligand-coated polymer nanoparticles. *Chem. - A Eur. J.* **15**, 8319–8330 (2009).
 132. Reisch, A., Runser, A., Arntz, Y., Mély, Y. & Klymchenko, A. S. Charge-Controlled Nanoprecipitation as a Modular Approach to Ultrasmall Polymer Nanocarriers: Making Bright and Stable Nanoparticles. *ACS Nano* **9**, 5104–5116 (2015).
 133. Reisch, A. *et al.* Protein-Sized Dye-Loaded Polymer Nanoparticles for Free Particle Diffusion in Cytosol. *Adv. Funct. Mater.* **28**, 1–10 (2018).
 134. Andreiuk, B. *et al.* Fluorescent Polymer Nanoparticles for Cell Barcoding In Vitro and In Vivo. *Small* **13**, 1701582 (2017).
 135. Biju, V. Chemical modifications and bioconjugate reactions of nanomaterials for sensing, imaging, drug delivery and therapy. *Chem. Soc. Rev.* **43**, 744–764 (2014).
 136. Sapsford, K. E. *et al.* Functionalizing nanoparticles with biological molecules: Developing chemistries that facilitate nanotechnology. *Chem. Rev.* **113**, 1904–2074 (2013).
 137. Guerrini, L., Alvarez-Puebla, R. & Pazos-Perez, N. Surface Modifications of Nanoparticles for Stability in Biological Fluids. *Materials (Basel)*. **11**, 1154 (2018).
 138. Ali, A. S. *et al.* Layer-by-layer electrostatic entrapment of protein molecules on superparamagnetic nanoparticle: A new strategy to enhance adsorption capacity and maintain biological activity. *J. Phys. Chem. C* **113**, 15260–15265 (2009).
 139. Conde, J. *et al.* Design of multifunctional gold nanoparticles for in vitro and in vivo gene silencing. *ACS Nano* **6**, 8316–8324 (2012).
 140. Wilchek, M., Bayer, E. A. & Livnah, O. Essentials of biorecognition: The (strept)avidin-biotin system as a model for protein-protein and protein-ligand interaction. *Immunol. Lett.* **103**, 27–32 (2006).
 141. Pulkkinen, M. *et al.* Three-step tumor targeting of paclitaxel using biotinylated PLA-PEG nanoparticles and avidin-biotin technology: Formulation development and in vitro anticancer

- activity. *Eur. J. Pharm. Biopharm.* **70**, 66–74 (2008).
142. Sletten, E. M., Bertozzi, C. R., Bertozzi, C. R. & Sletten, E. M. Bioorthogonal Chemistry: Fishing for Selectivity in a Sea of Functionality. *Angew. Chem. Int. Ed* **48**, 6974–6998 (2009).
 143. Cserep, G. B., Herner, A. & Kele, P. Bioorthogonal fluorescent labels: A review on combined forces. *Methods Appl. Fluoresc.* **3**, 042001 (2015).
 144. Rostovtsev, V. V., Green, L. G., Fokin, V. V. & Sharpless, K. B. A stepwise Huisgen cycloaddition process: Copper(I)-catalyzed regioselective ‘ligation’ of azides and terminal alkynes. *Angew. Chemie - Int. Ed.* **41**, 2596–2599 (2002).
 145. Baskin, J. M. & Bertozzi, C. R. Bioorthogonal click chemistry: Covalent labeling in living systems. *QSAR Comb. Sci.* **26**, 1211–1219 (2007).
 146. Jewett, J. C. & Bertozzi, C. R. Cu-free click cycloaddition reactions in chemical biology. *Chem. Soc. Rev.* **39**, 1272 (2010).
 147. Ning, X., Guo, J., Wolfert, M. A. & Boons, G. J. Visualizing metabolically labeled glycoconjugates of living cells by copper-free and fast Huisgen cycloadditions. *Angew. Chemie - Int. Ed.* **47**, 2253–2255 (2008).
 148. Kwak, M. & Herrmann, A. Nucleic acid/organic polymer hybrid materials: Synthesis, superstructures, and applications. *Angew. Chemie - Int. Ed.* **49**, 8574–8587 (2010).
 149. Yang, C. J., Pinto, M., Schanze, K. & Tan, W. Direct synthesis of an oligonucleotide-poly(phenylene ethynylene) conjugate with a precise one-to-one molecular ratio. *Angew. Chemie - Int. Ed.* **44**, 2572–2576 (2005).
 150. Wilks, T. R. & O'Reilly, R. K. Efficient DNA–Polymer Coupling in Organic Solvents: A Survey of Amide Coupling, Thiol–Ene and Tetrazine–Norbornene Chemistries Applied to Conjugation of Poly(N-Isopropylacrylamide). *Sci. Rep.* **6**, 39192 (2016).
 151. Alemdaroglu, F. E., Ding, K., Berger, R. & Herrmann, A. DNA-templated synthesis in three dimensions: Introducing a micellar scaffold for organic reactions. *Angew. Chemie - Int. Ed.* **45**, 4206–4210 (2006).
 152. Li, Z., Zhang, Y., Fullhart, P. & Mirkin, C. A. Reversible and Chemically Programmable Micelle Assembly with DNA Block-Copolymer Amphiphiles. doi:10.1021/nl049628o
 153. Banga, R. J. *et al.* Drug-Loaded Polymeric Spherical Nucleic Acids: Enhancing Colloidal Stability and Cellular Uptake of Polymeric Nanoparticles through DNA Surface-Functionalization. *Biomacromolecules* **18**, 483–489 (2017).
 154. Zhu, S., Xing, H., Gordiichuk, P., Park, J. & Mirkin, C. A. PLGA Spherical Nucleic Acids. *Adv. Mater.* **30**, 1–6 (2018).
 155. Tagit, O. & Hildebrandt, N. Fluorescence Sensing of Circulating Diagnostic Biomarkers Using Molecular Probes and Nanoparticles. *ACS Sensors* **2**, 13–45 (2017).
 156. Yang, J., Chen, H., Vlahov, I. R., Cheng, J. X. & Low, P. S. Evaluation of disulfide reduction during receptor-mediated endocytosis by using FRET imaging. *Proc. Natl. Acad. Sci. U. S. A.* **103**, 13872–13877 (2006).
 157. Niko, Y., Arntz, Y., Mely, Y., Konishi, G. I. & Klymchenko, A. S. Disassembly-Driven Fluorescence Turn-on of Polymerized Micelles by Reductive Stimuli in Living Cells. *Chem. - A Eur. J.* **20**, 16473–16477 (2014).
 158. Garg, H., Suri, P., Gupta, J. C., Talwar, G. P. & Dubey, S. Survivin: a unique target for tumor therapy. *Cancer Cell Int.* **16**, 49 (2016).
 159. Schmied, J. J. *et al.* DNA origami–based standards for quantitative fluorescence microscopy. *Nat. Protoc.* **9**, 1367–1391 (2014).
 160. <http://www.fluortools.com/software/ae>.
 161. Rosiuk, V., Runser, A., Klymchenko, A. & Reisch, A. Controlling Size and Fluorescence of Dye-Loaded Polymer Nanoparticles through Polymer Design. *Langmuir* **35**, 7009–7017 (2019).

LIST OF PUBLICATIONS

1. N. Melnychuk, P. Ashokumar, A. S. Klymchenko. Investigation of methods that lead to surface functionalized dye-loaded polymeric nanoparticles. (to be submitted)
2. N. Melnychuk, R. Rodik, P. Ashokumar, A. S. Klymchenko. Protein-Sized Fluorogenic Micelles: Design and Imaging Applications. (in preparation)
3. N. Melnychuk, S. Egloff, A. Runser, A. Reisch and A. S. Klymchenko. Light-harvesting nanoparticle probes for FRET-based detection of oligonucleotides with single-molecule sensitivity. (submitted)
4. Nina Melnychuk & Andrey S. Klymchenko. DNA-Functionalized Dye-Loaded Polymeric Nanoparticles: Ultrabright FRET Platform for Amplified Detection of Nucleic Acids. *J. Am. Chem. Soc.* 2018, 140, 10856-65. DOI: 10.1021/jacs.8b05840
5. Andrey Klymchenko, Nina Melnychuk and Andreas Reisch. OLIGONUCLEOTIDE-FUNCTIONALIZED HYDROPHOBIC POLYMER NANOPARTICLES. European patent application number WO2019EP55847.
6. O. Zamotaiev, V. Shvadchak, T. Sych, N. Melnychuk, D. Yushchenko, Y. Mely, V. Pivovarenko. "Environment-Sensitive Quinolone Demonstrating Long-Lived Fluorescence and Unusually Slow Excited-State Intramolecular Proton Transfer Kinetics" *MAF*, 2016, Vol.4, No.3, 034004. DOI: 10.1088/2050-6120/4/3/034004
7. A.Yu. Mandzhulo, N. A. Melnychuk, V. N. Fetyukhin, and M. V. Vovk. Synthesis of 4'-Alkyl-8-azaspiro[bicyclo[3.2.1]octane-3,2'-morpholin]-5'-ones. *Russian Journal of Organic Chemistry*, 2016, Vol. 52, No. 1, pp. 87-91. DOI: 10.1134/S1070428016010164

LIST OF CONFERENCES

Oral presentations

1. Nina Melnychuk, Sylvie Egloff, Anne Runser, Andreas Reisch and Andrey S. Klymchenko. Fluorescent polymeric nanoparticles for ultrasensitive detection of nucleic acid cancer markers. C'NANO 2018, The Nanoscience Meeting. Toulon, France, 11-13 December 2018.
2. Nina Melnychuk, Andrey S. Klymchenko. Organic nanoantenna for amplified fluorescence detection of nucleic acids. Les journées du campus d'Illkirch (JCI-2018). Illkirch, France, 15-16 May 2018.

Poster presentations

3. Nina Melnychuk, Sylvie Egloff, Anne Runser, Andreas Reisch and Andrey S. Klymchenko. Light-harvesting polymeric nanoparticles for amplified detection of nucleic acid cancer markers. World Congress on Light and Life, ESP-IUPB 2019. Barcelona, Spain, 25-30 August 2019.
4. Nina Melnychuk, Andreas Reisch and Andrey S. Klymchenko. Nanomedicine in Strasbourg. (Fluorescent nanoparticles for biosensing and point of care diagnostics – *Flash talk*). 11th European and Global Summit for Clinical Nanomedicine, Targeted Delivery and Precision Medicine (CLINAM). Basel, Switzerland, 2-5 September 2018.
5. Nina Melnychuk, Sylvie Egloff, Anne Runser, Andreas Reisch and Andrey S. Klymchenko. Biosensors based on fluorescent organic nanoparticles for ultrasensitive detection of nucleic acid cancer markers. International Meeting on Optical Biosensors. Ghent, Belgium, 15-17 November 2018.
6. N. Melnychuk, I.Shulov, R. Rodik, P. Ashokumar, Y. Arntz, A. Reisch, V. Kalchenko, A. Klymchenko. Protein-Sized Fluorogenic Micelles: Design and Imaging Applications. 15th Conference on Methods and Applications in Fluorescence (MAF 2017), Bruges, Belgium, 10-13 September 2017
7. I.Shulov, N. Melnychuk, R. Rodik, P. Ashokumar, Y. Arntz, A. Reisch, V. Kalchenko, A. Klymchenko. Protein-Sized Fluorogenic Micelles: Design and Imaging Applications. The 28th International Conference on Photochemistry (ICP 2017), Strasbourg, France, 16-21 July 2017

Synthèse de nanoparticules organiques fluorescentes pour la détection de biomolécules

Résumé

La détection à de très faibles concentrations de biomolécules est un défi en raison de la luminosité limitée des sondes moléculaires fluorescentes. Le but de mon projet de thèse est de fonctionnaliser des nanoparticules polymères (NP) ultra-brillantes dopées de fluorophores avec des oligonucléotides et d'obtenir des nano-sondes pour les acides nucléiques. Nous avons constaté que les NP avec un groupement azide bien orienté peuvent être facilement fonctionnalisées avec l'ADN par le biais d'une réaction de type «click» sans cuivre. Les NP fonctionnalisées par l'ADN ont été ensuite converties en biocapteurs grâce au transfert d'énergie de résonance de type Förster (FRET), fournissant une réponse ratiométrique de fluorescence amplifiée vers la cible ADN/ARN en solution et au niveau particulaire. Enfin, nous avons mis au point des nano-sondes radicalement améliorées permettant de détecter un seul événement d'hybridation en activant / désactivant le FRET de milliers de colorants de la particule de nanoantenne jusqu'à un accepteur unique. Les nano-sondes obtenues constituent une nouvelle plate-forme puissante pour la détection de biomarqueurs du cancer.

Mots-clés : nanoparticules polymères fluorescentes, nanoparticules fonctionnalisées par l'ADN, nano-antennes captant la lumière, biocapteur, nano-sonde.

Résumé en anglais

The detection of ultralow concentrations of biomolecules is challenging because of limited brightness of fluorescent molecular probes. The aim of my PhD project is to functionalize ultrabright dye-loaded polymeric nanoparticles (NPs) with oligonucleotides and obtain nanoprobes for nucleic acids. We found that NPs with efficiently exposed azide group can be readily functionalized with DNA through a Cu-free “click” reaction. DNA-functionalized NPs were then converted into biosensors based on energy transfer (FRET), providing amplified fluorescence ratiometric response to the target DNA/RNA in solution and at the single-particle level. Finally, we made drastically improved nanoprobes that enabled detecting a single hybridization event by switching on/off FRET from thousands of dyes in the nanoantenna particle to a single acceptor. The obtained nanoprobes constitute a new powerful platform for detection of cancer biomarkers.

Keywords: fluorescent polymeric nanoparticles, DNA-functionalized nanoparticles, light-harvesting nanoantenna, biosensor, nanoprobe.